# Characterization of phosphorylation-dependent interactions involving neurofibromin 2 (NF2, merlin) isoforms and the Parkinson protein 7 (PARK7, DJ1)

D i s s e r t a t i o n

zur Erlangung des akademischen Grades

d o c t o r  r e r u m  n a t u r a l i u m

(Dr. rer. nat.)

im Fach Biologie

eingereicht an der

Mathematisch-Naturwissenschaftlichen Fakultät I

der Humboldt-Universität zu Berlin

von

Frau Dipl.-Biol. Josephine Maria Worseck

Präsident der Humboldt-Universität zu Berlin:

Prof. Dr. Jan-Hendrik Olbertz

Dekan der Mathematisch-Naturwissenschaftlichen Fakultät I:

Prof. Dr. Andreas Herrmann

Gutachter/innen: 1. Prof. Dr. Christian Spahn

2. Prof. Dr. Erich E. Wanker

3. Prof. Dr. Hans Lehrach

Tag der mündlichen Prüfung: 15. Juni 2012

**Für meine Familie**

*“[...] you can't connect the dots looking forward; you can only connect them looking backwards.*
*So you have to trust that the dots will somehow connect [...]”*
*Steve Jobs*

# Zusammenfassung

Veränderungen in phosphorylierungsabhängigen Signalwegen, Akkumulation von Proteinaggregaten im Gehirn und neuronaler Zelltod sind Neurodegenerationskennzeichen und Indikatoren für überlappende molekulare Mechanismen. Um Einblicke in die involvierten Signalwege zu erhalten, wurde mit Hilfe eines modifizierten Hefe-Zwei-Hybrid (Y2H)-Systems für 71 Proteine, die mit neurologischen Erkrankungen assoziiert sind, proteomweit nach Protein-Protein Interaktionen (PPIs) gesucht. Für 21 dieser Proteine wurden PPIs identifiziert. Das Gesamtnetzwerk besteht aus 79 Proteinen und 90 PPIs von denen 5 phosphorylierungsabhängig sind. Ein Teil dieser PPIs wurde in unabhängigen Interaktionsassays mit einer Validierungsrate von 66 % getestet. Der netzwerkbasierte Versuch verbindet erfolgreich neurologische Erkrankungen untereinander aber auch mit zellulären Prozessen. Ser/Thr-Kinase abhängige PPIs verknüpfen zum Beispiel das Parkinson Protein 7 (PARK7, DJ1) mit den E3 Ligase Komponenten ASB3 und RNF31 (HOIP). Die Funktion dieser Proteine bekräftigt den Zusammenhang zwischen dem Ubiquitin-Proteasom-System und der Parkinson Krankheit (PD). Neurofibromin 2 (NF2, merlin) Isoformen und PARK7 interagieren mit der regulatorischen PI3K Untereinheit p55γ (PIK3R3). Diese PPIs basieren auf Tyr-Kinase Aktivität im modifizierten Y2H System und funktionellen PIK3R3 pTyr-Erkennungsmodulen (SH2 Domänen) in co-IP und Venus PCA Versuchen. Dies verknüpft den PI3K/AKT Überlebenssignalweg mit zwei unterschiedlichen neurologischen Erkrankungsphenotypen: dem PD-assoziierten neuronalen Zelltod und der Neurofibromatose Typ 2-assoziierten Tumorentstehung. Die vergleichende Beobachtung von PIK3R3, AOF2 (KDM1A, LSD1) Interaktionen auf NF2 Isoformlevel offenbart eine Bevorzugung von Isoform 7 bei zytoplasmatischer Lokalisation, wohingegen Isoform 1 PPIs an der Membran lokalisiert sind. Das modifizierungsabhängige und isoformspezifische PPI Netzwerk ermöglicht die Aufstellung neuer Hypothesen zu molekularen Pathomechanismen.

Schlagwörter:

Kinaseabhängige Protein-Protein Interaktionen (PPIs), modifiziertes Hefe-Zwei-Hybrid-System (Y2H), Neurologische Erkrankungen, Interaktionsnetzwerke

# Abstract

Alterations in phosphorylation-dependent signalling pathways, accumulation of aggregated proteins in the brain and neuronal apoptosis are common to neurodegeneration and implicate overlapping molecular mechanism. To gain insight into involved pathways, a modified yeast-two hybrid (Y2H) system was applied to screen 71 proteins associated with neurological disorders in a proteome-wide manner. For 21 of these proteins interactions were identified including 5 phosphorylation-dependent ones. In total, the network connected 79 proteins through 90 protein-protein interactions (PPIs). A fraction of these Y2H PPIs was tested in secondary interaction assays with a validation rate of 66 %. The described network-based approach successfully identified proteins associated with more than one disorder and cellular functions connected to specific disorders. In particular, the network revealed Ser/Thr kinase-dependent PPIs between the Parkinson protein 7 (PARK7, DJ1) and the E3 ligase components ASB3 and RNF31 (HOIP). The function of these proteins further substantiates the established connection between Parkinson's disease (PD) and ubiquitination-mediated proteasome (dis)functions. Neurofibromin 2 (NF2, merlin) isoforms and PARK7 were identified as PI3K regulatory subunit p55γ (PIK3R3) interactors. These PPIs required Tyr kinase coexpression in the modified Y2H system and functional PIK3R3 pTyr-recognition modules (SH2 domains) in co-IP and Venus PCA experiments. This finding implicates the PI3K/AKT survival pathway in PD-associated neuronal apoptosis and Neurofibromatosis type 2-associated tumour formation. Investigation of PIK3R3, AOF2 (KDM1A, LSD1) and EMILIN1 PPIs on NF2 isoform level revealed preferential isoform 7 binding and cytoplasmic or membrane localisation of these PPIs for isoform 7 or 1, respectively. The generated modification-dependent and isoform-specific PPI network triggered many hypotheses on the molecular mechanisms implicated in neurological disorders.



Keywords:

Kinase-dependent protein-protein interactions (PPIs), modified yeast-two hybrid system (Y2H), neurological disorders, PPI network

# Abbreviations

| | |
|---|---|
| aa | Amino acids |
| AKT | V-akt murine thymoma viral oncogene homolog |
| ALD | Alzheimer disease |
| ALS | Amyotrophic Lateral Sclerosis |
| APH | Alkaline phosphatase |
| AP-MS | Affinity purification coupled to mass spectrometry |
| AR | Androgen receptor |
| ATP | Adenosine-5'-triphosphate |
| bp | Base pair |
| cAMP | Cyclic adenosine monophosphate |
| co-IP | Coimmunoprecipitation |
| CoA | Coenzyme A |
| CoREST | Corepressor of REST (RE1-silencing transcription factor) |
| CRL | Cullin-RING-ligase |
| CtBP | C-terminal binding protein |
| DBD | DNA-binding domain |
| DMEM | Dulbecco’s modified eagle’s medium |
| DNA | Deoxyribonucleic acid |
| DPBS | Dulbecco’s phosphate buffered solution |
| ECL | Enhanced chemiluminescence |
| EGF | Epidermal growth factor |
| EMI | Elastin microfibril interface |
| ERM | E for ezrin, R for radixin and M for moesin |
| FBS | Fetal bovine serum |
| FERM | F for four point one protein, E for ezrin, R for radixin and M for moesin |
| GAT | Glutamine amidotransferase |
| gC1q | Globular domain of the q subcomponent of the complement component 1 |
| GTP | Guanosine-5'-triphosphate |
| HD | Huntington disease |
| HDAC | Histone deacetylases |
| HECT | Homologous to E6-AP carboxy terminus |
| HEK | Human embryonic kidney |
| HRP | Horseradish peroxidase |
| HTP | High-throughput |
| IBR | In-between-RING |
| IFs | Intermediate filaments |
| Ig | Immunoglobulin |
| IP | Immunoprecipitation |
| LB | Lysogeny broth |
| LUBAC | Linear ubiquitin chain assembly complex |

| | |
|---|---|
| LUMIER | Luminescence-based mammalian interactome mapping |
| LWBs | Lewy bodies |
| MAPPIT | Mammalian protein-protein interaction trap |
| mRNA | Messenger RNA |
| MTP | Microtiterplate |
| MYTH | Membrane yeast-two hybrid |
| NAPPA | Nucleic acid programmable protein array |
| NCBI | National Centre for Biotechnological information |
| NDs | Neurodegenerative disease/neurodegenerative Erkrankungen |
| NFκB | Nuclear factor kappa-light-chain-enhancer of activated B cells |
| NLS | Nuclear localisation signal |
| NuRD | Mi-2/nucleosome remodeling and deacetylase |
| $OD_{600}$ | Optical density at 600 nm |
| ORF | Open reading frames |
| PA | Protein A |
| PCA | Protein fragment complementation assay |
| PCR | Polymerase chain reaction |
| PD | Parkinson's disease/Parkinson Erkrankung |
| PH | Pleckstrin homology |
| PI3K | Phosphoinositide 3-kinase |
| PIKE-L | Long form of the PI3K-enhancer |
| $PIP_2$ | Phosphatidylinositol 4,5-bisphosphate |
| $PIP_3$ | Phosphatidylinositol 3,4,5-trisphosphate |
| PKA | Protein kinase A |
| PKC | Protein kinase C |
| PLC | Phospholipase C |
| PPIs | Protein-protein interactions/Protein-Protein Interaktionen |
| pSer | Phosphorylated serine |
| PTB | Phosphotyrosine-binding |
| pThr | Phosphorylated threonine |
| PTM | Post-translational modification |
| pTyr | Phosphorylated tyrosine |
| PVDF | Polyvinylidene fluoride |
| RBR | RING-in-between-RING, RING-IBR-RING |
| RING | Really interesting new gene |
| RLU | Relative luciferase units |
| RNA | Ribonucleic acid |
| ROS | Reactive oxygen species |
| RTK | Receptor tyrosine kinase |
| SCA | Spinocerebellar Ataxia 1 |
| SDS | Sodium Dodecyl Sulfate |
| SDS-PAGE | SDS-polyacrylamide gel electrophoresis |

| | |
|---|---|
| SH2 | Src homology 2 |
| SNpc | Substantia nigra pars compacta |
| TBE | Tris/Borate/EDTA |
| TBS | Tris-buffered saline |
| TBST | TBS supplemented with Tween 20 |
| TGF-β | Transforming growth factor-β |
| TNF | Tumour necrosis factor |
| TNFR2 | Tumour necrosis factor receptor 2 |
| Ub | Ubiquitin |
| UBA | Ubiquitin-associated |
| UBL | Ubiquitin-like |
| UPS | Ubiquitin-proteasome system |
| Y2H | Yeast-two hybrid |
| YFP | Yellow fluorescent protein |

**TABLE OF CONTENTS**

# 1 Introduction

## 1.1 Neurological disorders

### 1.1.1 Accumulation of aggregated, misfolded proteins is linked to neurodegenerative disorders

Neurodegenerative diseases (NDs) like Alzheimer disease (ALD), Huntington disease (HD), Parkinson's disease (PD), Amyotrophic Lateral Sclerosis (ALS) and Spinocerebellar Ataxia 1 (SCA) are characterized by progressive neuronal loss and synaptic abnormalities starting later in life leading to decay of various mental and physical skills and premature death. Neurodegenerative diseases have both sporadic and inherited origins with the majority of disease cases being sporadic. Evidences are accumulating that protein misfolding and aggregation are the common reason for sporadic neurodegeneration (Soto, 2003).

In ALD, plaques consisting of amyloid-β protein are extracellularly deposited in the brain parenchyma and around the cerebral vessel vals (Glenner and Wong, 1984) whereas tangles of hyperphosphorylated tau protein build intracellular aggregates (Grundke-Iqbal, et al., 1986). In PD, α-synuclein accumulates into inclusions called Lewy bodies (LWB) in the cytoplasm of neurons located in the substantia nigra pars compacta (SNpc) (Forno, et al., 1996; Spillantini, et al., 1997). In patients with HD, huntingtin mutants containing more than 36 glutamine residues form intranuclear deposits (DiFiglia, 1997). In ALS patients, cell bodies and axons of motor neurons contain aggregates consisting of superoxide dismutase 1 (Bruijn, et al., 1998). This protein aggregates are found mainly in the class of neurons and in the brain region that show degeneration indicating a key role of misfolding and aggregation in neuronal death. The affected brain regions differ between the NDs and explain the different associated clinical symptoms. In ALD cerebral damage leads to dementia, in PD neurodegeneration in the SNpc induces rigidity and tremor, in HD cell death in the striatum results in uncontrolled movement whereas neurodegeneration in the cerebellum provokes ataxia in ALS (Soto, 2003).

Several findings indicate that misfolded or aggregated proteins lead to neurodegeneration (Selkoe, 2004) and are not simply the result of neurodegeneration but the final proof is still missing. Many models have been proposed to explain how misfolding and aggregation could lead to neurodegeneration (Soto, 2003). In the loss-of-function hypothesis misfolding and aggregation leads to protein depletion and the lack of biological activity to neurodegeneration. In contrast the gain-of-function hypothesis argues that misfolded aggregated proteins activate apoptotic signalling pathways, recruit essential cellular factors, form ion channels or induce oxidative stress. In the inflammation model aggregates are thought to cause a chronic inflammatory reaction which leads to neuronal death mediated by activated astroglial cells. Furthermore, it's possible that aggregation of proteins simply overwhelms the quality-control systems of the cell (Meredith, 2005) or affects cell trafficking and synaptic transmission (Kiachopoulos, et al., 2004; Mattson and Sherman, 2003; Welch, 2004).

Protein misfolding and aggregation can be caused by both genetic and environmental factors. During aging environmental factors as oxidative stress, pH, metal ion or protein concentration are changing and lead to age-related protein misfolding (Mrak, et al., 1997; Soto, 2001; Teplow, 1998). Mutations in components of the ubiquitin-proteasome system (UPS) or the chaperone network or the aggregation prone protein itself lead to protein destabilization, misfolding and aggregation at earlier life stages already. With the exception of proteins implicated in polyglutamine diseases, proteins implicated in protein folding disease do not share any sequence or structural homology although they build aggregates with the same β-sheet rich structure (Serpell, et al., 2000;

Sunde, et al., 1997). As the monomeric native proteins are generally composed of unordered structures and α-sheets, large conformational rearrangements have to occur during misfolding and aggregation. Probably, slight conformational changes lead to the exposure of hydrophobic segments which make the protein unstable and prone to oligomerization before stable β-sheet oligomers, protofibrils and finally amyloid-like fibrils are formed. However, until now it is not known if oligomerization depends on misfolded proteins or if oligomerization leads to misfolding or if structural changes induce protein destabilization as prerequisite for oligomerization and complete misfolding. Why the ubiquitously expressed proteins misfold and aggregate only in specific brain regions and which of the described protein species mediates the cell type specific pathomechanisms remains elusive.

The investigation of proteins involved in neurological disorders performed in this study revealed an interaction map that connects the Parkinson protein 7 (PARK7, DJ1) and the Neurofibromatosis type 2-associated tumour suppressor NF2 (merlin, neurofibromin 2) with interesting novel interaction partners. The implication of these proteins in Parkinson's disease (1.1.2) and Neurofibromatosis type 2 (1.1.3) will be discussed in detail in the following chapters.

### 1.1.2 Parkinsonism and Parkinson's disease

Parkinsonism is a neurological syndrome characterized by tremor, hypokinesia, stiffness, postural instability and slowing of movement (Jankovic, 2008). The underlying causes of Parkinsonism are numerous and are used to classify Parkinsonism as primary or secondary (Figure 1).

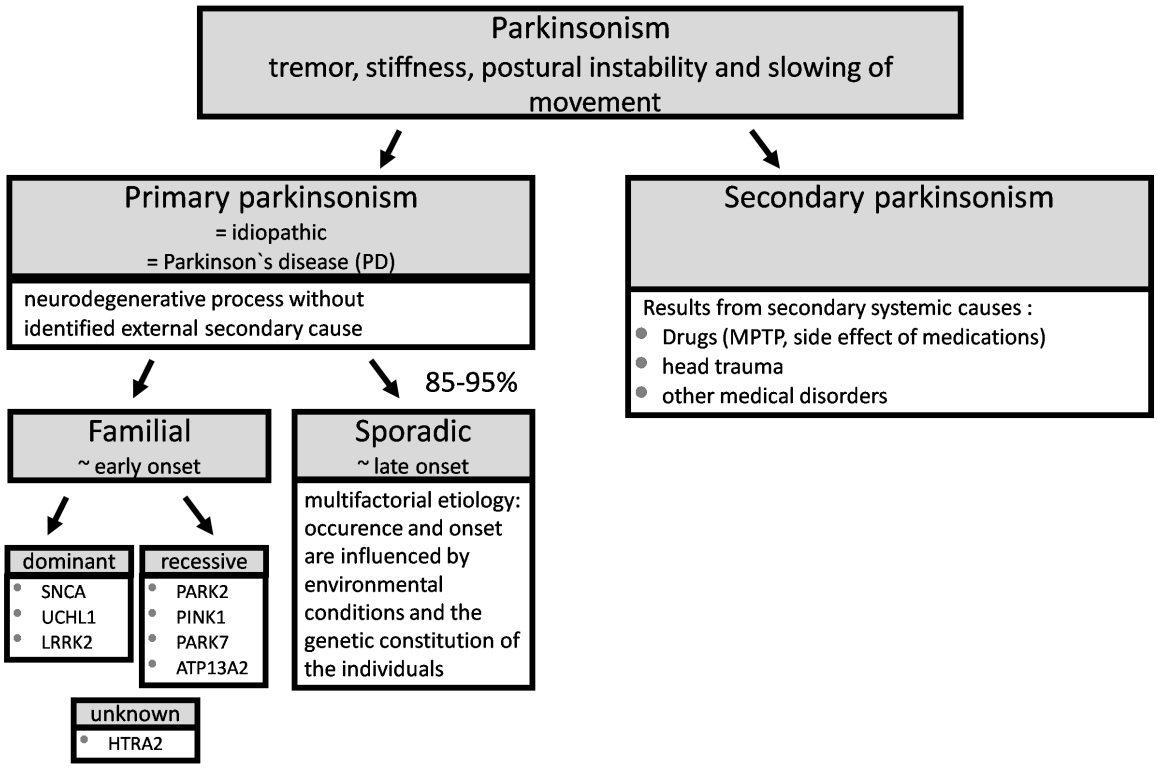


**Figure 1: Definition of primary and secondary Parkinsonism.**

Parkinsonism is a neurological syndrome with numerous underlying causes (see main text for details).

Secondary Parkinsonism can be caused by certain medicines (like antipsychotics, narcotics or anaesthesia drugs), the heroin byproduct MPTP (1-Methyl-4-phenyl-1,2,3,6-tetrahydropyridin), head traumas, exposure to toxins (like carbon monoxide or manganese) and different disorders (like multiple system atrophy) or illnesses (like encephalitis or meningitis) (Christine and Aminoff, 2004; Montastruc, et al., 1994).

*Primary Parkinsonism*. Parkinson's disease is the most common form of parkinsonism and is usually defined as "primary" parkinsonism, which means that no external cause is identified (Samii, et al., 2004). PD is the second most common progressive neurodegenerative disorder, affecting 1-2 % of the population over the age of 65 years (de Rijk, et al., 2000). Most of the PD cases (85-95 %) are sporadic and truly idiopathic (Lesage and Brice, 2009; Papapetropoulos, et al., 2007) whereas for a small fraction internal, genetic causes are identified. Defects in eight genes have been established to cause this “familial” form of PD: α-synuclein (SNCA, PARK1, PARK4), E3 ubiquitin-ligase parkin (PARK2), ubiquitin carboxyl-terminal esterase L1 (UCHL1, PARK5), pten-induced putative kinase 1 (PINK1, PARK6), Parkinson protein 7 (PARK7, DJ1), leucine-rich repeat kinase 2 (LRRK2, PARK8), ATPase type 13A2 (ATP13A2, PARK9), and the HtrA serine peptidase 2 (HTRA2, PARK13) (Thomas and Beal, 2007). Although the identified gene defects explain only a very small fraction of PD cases, they are promoting the understanding of the molecular pathways involved in the sporadic forms of PD as both show the same phenotype.

*Lewy bodies: cause or effect of primary Parkinsonism?* PD brains are pathologically characterized by pronounced loss of dopaminergic neurons in the SNpc and by formation of cytoplasmic inclusions known as Lewy bodies (Dawson and Dawson, 2003; Valente, et al., 2004). LWBs contain poly-ubiquitin-aggregated proteins, including α-synuclein and PARK2 (Betarbet, et al., 2005; Kawahara, et al., 2008; Schlossmacher, et al., 2002) and are absent in PD-patients with homozygous PARK2 deletions (Takahashi, et al., 1994). PD-associated mutant α-synuclein shows increased self-aggregation which results in oligomerization and LWB formation (Conway, et al., 1998). The accumulation of misfolded proteins into cellular aggregates is a common feature of NDs but as in other NDs also in PD the cause-and-effect relationship remains unclear (Goldberg and Lansbury, 2000; Selkoe, 2004). LWBs contain α-synuclein fibrils which are formed in a complex process through one or more discrete intermediate forms. Probably one of these intermediate assembly states is toxic which would also explain the observation that the prevalence of nigral LWBs in postmortem brains is approximately tenfold greater than the prevalence of PD (Goldberg and Lansbury, 2000). However, the mechanism by which abnormal α-synuclein intermediate states may cause dysfunction and death of dopaminergic neurons is unclear.

*Implications of the ubiquitin-proteasome system.* Several attempts have being made to uncover the functional relationship between the eight genes implicated in familial PD and to identify common pathogenic pathways leading to neuronal degeneration in PD. The observation that PARK2 mediates the ubiquitination of α-synuclein (Shimura, et al., 2001) and other LWB proteins (Chung, et al., 2001; Lim, et al., 2005) suggests that their might be a converging pathway. One of the several explanatory hypothesis states that the parkin-mediated polyubiquitination of aggregation-prone proteins and their subsequent proteasomal degradation is impaired in PD. This is further supported by the finding that mutations in PARK2 which impair its E3 ligase activity or its ability to interact with upstream ubiquitin (Ub) conjugating enzymes or substrates are the most common cause of familial PD (Kitada, et al., 1998; Lucking, et al., 2000). Additionally, PARK2 E3 ligase activity was shown to decrease sensitivity to proteasome inhibitors whereas mutant α-synuclein increases this sensitivity by decreasing proteasome function (Petrucelli, et al., 2002). Furthermore, key ubiquitin-proteasome elements are known to be altered in PD post-mortem brains (McNaught, et al., 2003). Additionally, two further PD gene products, namely

PARK7 and PINK1, mediate ubiquitination in complex with PARK2 (Xiong, et al., 2009) and a fourth PD gene product, namely UCHL1, encompasses an ubiquitin ligase/hydrolase activity (Liu, et al., 2002) which clearly links PD pathogenesis to the UPS.

*Phosphorylation targets proteins to the ubiquitin-proteasome pathway.* Degradation of proteins by the ubiquitin system involves the covalent attachment of multiple ubiquitin molecules to the target protein and subsequent degradation of the tagged protein by the 26S proteasome. In an ATP-driven three-step process named ubiquitinylation the C-terminal glycine residue of ubiquitin becomes covalently attached to a substrate protein, which is catalyzed by Ub-activating (E1), Ub-conjugating (E2) and Ub-ligating (E3) enzymes (Hershko and Ciechanover, 1998; Pickart and Eddins, 2004). The over 900 putative human E3 ligases recognize substrates via primary motifs such as the N-terminal residue, over association with ancillary proteins (*e.g.* Hsc or HPV-E6) or following post-translational modification (*e.g.* phosphorylation) (Ciechanover, 1998).

Interestingly, neurodegeneration has been linked to phosphorylation-dependent signalling processes (Kanehisa, et al., 2010; Limviphuvadh, et al., 2007) and PD to ubiquitination-mediated proteasome (dis)functions (Cook and Petrucelli, 2009; Giasson and Lee, 2003; Malkus, et al., 2009). This raises the reasonable suspicion that PD gene products implicated in ubiquitination processes might recognize ubiquitination substrates in a phosphorylation-dependent manner or might themselves be regulated by phosphorylation. To address this question, proteins associated with neurological disorders including five proteins implicated in familial PD were screened with a modified yeast two hybrid (Y2H) system to reveal phosphorylation-dependent interactions. We expected to identify novel substrate proteins or components of the ubiquitination cascade as interaction partners. Indeed, two E3 ligase components were identified as novel PARK7 interaction partners. The implication of PARK7 in Parkinson's disease will be discussed in the following chapter.

#### *1.1.2.1 The PD-associated gene product PARK7 is involved in multiple physiological processes*

Recessive mutations in the PARK7 gene cause familial PD (Bonifati, et al., 2003). Until now seven distinct PARK7 mutations in 15 affected patients have been reported (Cookson, 2010). Some of these mutations impair PARK7 dimerization which leads to protein destabilization and effective knockout (Moore, et al., 2003). This suggests that these PARK7 mutations cause a loss of function. However, some mutations are quite stable and must disrupt an unidentified biological function of PARK7 (Blackinton, et al., 2005). PARK7 is conserved from yeast to human and belongs to the ThiJ/PfpI protein family (Bandyopadhyay and Cookson, 2004), which is in turn a member of the large glutamine amidotransferase (GAT) superfamily (Horvath and Grishin, 2001). ThiJ/PfpI-family members include protein chaperones, catalases, proteases, transcriptional regulators and the ThiJ kinases (Bandyopadhyay and Cookson, 2004). Interestingly, PARK7 affects transcription (Clements, et al., 2006; Taira, et al., 2004), posses chaperone (Shendelman, et al., 2004) and weak protease activity (Koide-Yoshida, et al., 2007; Olzmann, et al., 2004). ThiJ kinase activity has not been detected in human PARK7 and amidotransferase activity has not yet been tested (Wilson, et al., 2003). Additionally, several distinct functions ranging from cellular transformation (Nagakubo, et al., 1997) to oxidative stress response (Guzman, et al., 2011) have been described for PARK7.

*PARK7 contains a functionally important cysteine residue embedded in a Cys-His-Asp/Glu triad.* The crystal structure of human full length PARK7 shows an α/β sandwich structure that is conserved among

ThiJ/PfpI superfamily members and reveals that PARK7 contains an Cys-His-Asp/Glu triad (Tao and Tong, 2003). If this triad consisting of Cys106, His126 and Glu18 (in human PARK7) forms a functional active site and whether it is indeed a catalytic triad remains to be determined. Cys-His-Asp/Glu catalytic triads are responsible for the catalytic activity of related family members including chaperones (Quigley, et al., 2003), proteases (Du, et al., 2000) and several GAT domain containing biosynthetic enzymes (Horvath and Grishin, 2001). The cysteine and glutamine residues of the PARK7 triad are absolutely conserved among all ThiJ/PfpI-family members whereas the histidine residue is only conserved in the PARK7-family which is in agreement with the observation that other family members use the cysteine residues in combination with several distinct His-Asp/Glu pairs for triad formation (Tao and Tong, 2003). The triad cysteine residue is of functional importance for ThiJ/PfpI-family members and is required to protect against oxidative stress in PARK7 (Canet-Aviles, et al., 2004; Meulener, et al., 2006; Taira, et al., 2004). Under oxidative stress, the sulfhydryl group (SH) of this residue reacts with reactive oxygen species (ROS) to cysteine sulfinic acid (Cys-$SO_2H$) (Lee, et al., 2003; Wilson, et al., 2003) and the isoelectric point of PARK7 shifts towards more acidic values (Mitsumoto and Nakagawa, 2001; Mitsumoto, et al., 2001).

*How does PARK7 protect from oxidative stress?* It has been suggested that PARK7 might be protective against oxidative stress because of its function as ROS scavenger (Taira, et al., 2004), its association with the neuroprotective E3 ligase PARK2 under oxidative stress (Moore, et al., 2005), its oxidative stress induced chaperone activity which inhibits α-synuclein aggregation (Shendelman, et al., 2004) or its ability to protect the antioxidant transcriptional master regulator NFE2L2 from ubiquitination and degradation (Clements, et al., 2006). Interestingly, the expression of PARK7 is enhanced under oxidative stress (Kinumi, et al., 2004) and in certain tumours (Kim, et al., 2005) which further supports the hypothesis that PARK7 promotes cell survival. The suggested pathways and mechanisms are, however, numerous and include activation of the proliferative PI3K/AKT pathway (Aleyasin, et al., 2009; Kim, et al., 2005) and altering p53 activity (Shinbo, et al., 2005).

*Why are SNpc dopaminergic neurons specifically affected in PD?* PARK7 deficient mice are viable, fertile and show no major neuronal or anatomical abnormalities but their SNpc dopaminergic neurons show increased vulnerability to oxidative stress causing neurotoxins (Kim, et al., 2005) and the dopamine overflow is markedly reduced (Goldberg, et al., 2005). PARK7 is widely expressed in most tissues (Bonifati, et al., 2003) so it is unclear why particular these neurons are affected in PARK7 deficient mice and in patients bearing a PARK7 loss-of-function mutation. Recently, it has been suggested that $Ca^{2+}$ entry through L-type channels during normal autonomous pacemaking creates this oxidative stress specific to SNpc dopaminergic neurons and it has been shown that PARK7 is protective in this model (Guzman, et al., 2011).

Oxidative stress might activate signalling cascades leading to PARK7 activation and subsequent protection. Conditional PARK7 interactions (*i.e.* phosphorylation-dependent interactions triggered by oxidative stress) could reveal insights into the neuroprotective function of PARK7 in SNpc dopaminergic neurons. Furthermore, the interaction of PARK7 with already characterized proteins allows conclusions on its biological mode of function.

### *1.1.3* Malfunction of NF2 is implicated in Neurofibromatosis type 2

Neurofibromatosis type 2 is an inheritable disorder with an autosomal dominant mode of transmission that affects around 1 in 60,000 individuals (Evans, 2009). Biallelic mutations in the NF2 gene coding for neurofibromin 2 (NF2, merlin, schwannomin) cause sporadic and Neurofibromatosis type 2-associated tumours

of the nervous system (*i.e.* schwannomas, meningiomas, ependymomas and gliomas). Because of the prevalence in sporadic tumours and the predisposition of heterozygous NF2 mutant mice ($NF2^{+/-}$) to develop various tumours NF2 is considered to be a tumour suppressor (McClatchey and Giovannini, 2005; Okada, et al., 2007).

*NF2 structure.* NF2 shares significant sequence homology with proteins of the ERM (Ezrin-Radixin-Moesin) family. The three described family member's ezrin, radixin and moesin crosslink actin filaments with the plasma membrane. NF2 and ERM family members are characterized by a highly conserved N-terminal FERM (four point one, Ezrin, Radixin, Moesin) domain, followed by a coiled-coil domain and a charged C-terminal domain. The globular FERM domain is composed of three subdomains that interact with each other and form a single module (Pearson, et al., 2000). The subdomains have no sequence homology to other protein domains but their structures are homologous to previously described folds. The first subdomain (residues 1-82) resembles a typical ubiquitin fold and is similar to the fold of the Ras-binding domain of Raf, the second subdomain (residues 96-195) is classified as an acyl-CoA binding protein-like fold and the third subdomain (residues 204-297) is structurally similar to the pleckstrin homology (PH), phosphotyrosine-binding (PTB) domain or enabled/VASP (Vasodilator-stimulated phosphoprotein) homology 1 (EVH1) domain (Pearson, et al., 2000).

*NF2 is regulated by posttranslational modifications.* Similar to classical ERM proteins NF2 can switch between an open and a closed conformation by self-association between the FERM and the C-terminal domain. This intramolecular interaction of NF2 is disturbed by phosphorylation of Ser518 by the p21-activated kinases 1 and 2 (Kissil, et al., 2002; Xiao, et al., 2002) and the cAMP-dependent protein kinase PKA (Alfthan, et al., 2004) (Figure 2). The opposing effect is mediated through dephosphorylation of Ser518 by the moesin and myosin phosphatase MYPT-1-PP1δ (Jin, et al., 2006). Interestingly, NF2 has to be in the closed conformation to suppress tumourigenesis (Sherman, et al., 1997). This conformation is disrupted by phosphorylation and many tumour-derived missense mutations (Okada, et al., 2007). Integrin-dependent adhesion to the matrix activates PAK which leads to phosphorylation of Ser518 and accumulation of NF2 in the open conformation which is incapable to block cell cycle progression (Okada, et al., 2005). PAK inhibition through cadherin-mediated cell-cell contacts reverses this effect and stops cell proliferation (Lallemand, et al., 2003; Lallemand, et al., 2009).

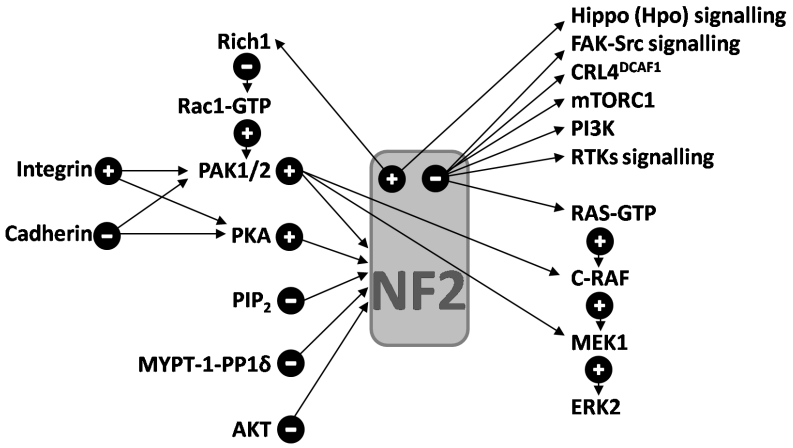


**Figure 2: Overview of upstream and downstream NF2 signalling events.**

NF2 is regulated by posttranslational modifications and implicated in numerous signalling pathways (see main text for details).

Furthermore, in ERM proteins binding to phosphatidylinositol 4,5-bisphosphate ($PIP_2$) is thought to weaken the closed conformation (Barret, et al., 2000) and as these binding sites are conserved and NF2 is known to bind to phosphatidylinositols, $PIP_2$-binding may also play an important role in regulating NF2 function (Okada, et al., 2009). In addition to Ser518, NF2 is phosphorylated by PKA on Ser10, which leads to modulation of the actin cytoskeleton (Laulajainen, et al., 2008). The same residue (Ser10) was also described as AKT phosphorylation site and AKT-dependent phosphorylation was shown to lead to proteasome-mediated degradation (Laulajainen, et al., 2011). AKT-mediated phosphorylation and degradation by ubiquitination was also observed for Thr230 and Ser315, phosphorylation of these residues disturbs the head-to-tail interaction and leads to AKT binding (Tang, et al., 2007). A complex interplay between these phosphorylation sites has been proposed because Ser518 phosphorylation increases Ser10 phosphorylation and Ser315/Thr230 phosphorylation decreases Ser518 phosphorylation (Laulajainen, et al., 2011). A multi-step phosphorylation-dependent conformational change could best explain these results. Probably, growth factor signalling and consequent Ser518 phosphorylation induce a conformational change (Alfthan, et al., 2004; Kissil, et al., 2002; Xiao, et al., 2002) that enables AKT-mediated Ser10/Ser315/Thr230 phosphorylation-dependent degradation of NF2 (Laulajainen, et al., 2011; Tang, et al., 2007).

*NF2 is located to the membrane.* Ezrin, radixin and moesin mediate linkage of cell adhesion receptors to the actin cytoskeleton in the open conformation (Bretscher, et al., 2002). Sequence homology and cortical cytoskeleton localization have led to the assumption that NF2 mediates its tumour suppressor function also at or near the cell membrane by linking transmembrane receptors to the actin cytoskeleton (McClatchey and Fehon, 2009). However, NF2 has to be in its closed non-phosphorylated conformation to suppress tumourigenesis (Bretscher, et al., 2002; Sherman, et al., 1997) and is able to interact with the cortical actin network in this conformation (James, et al., 2001; Shaw, et al., 2001) by using a distinct actin-binding domain than the classical *bona fide* C-terminal actin-binding domain present in other ERM proteins (Huang, et al., 1998). Additionally, interactions with cytoskeletal proteins like paxillin (Fernandez-Valle, et al., 2002), βII spectrin (Scoles, et al., 1998) and other ERM proteins (Gronholm, et al., 1999; Meng, et al., 2000) indirectly link NF2 with the actin cytoskeleton. Furthermore, NF2 associates with transmembrane and scaffolding proteins like CD44 (Sainio, et al., 1997), CD43 (Yonemura, et al., 1998), layilin (Bono, et al., 2005), paranodin (Denisenko-Nehrbass, et al., 2003), β-integrin (Obremski, et al., 1998), NHERF (Murthy, et al., 1998) and syntenin (Jannatipour, et al., 2001) at the plasma membrane. NF2 probably functions at the membrane-cytoskeleton interface to integrate signals from growth factors and adhesion molecules localized at the plasma membrane (McClatchey and Fehon, 2009).

*How does NF2 perform its tumour suppressing function?* In confluent cells NF2 is recruited to cell junctions, enables stable adherens junction formation and inhibits cell proliferation (Curto, et al., 2007; Deguen, et al., 1998; Lallemand, et al., 2003; Yi, et al., 2011). This is probably achieved by downregulating receptor tyrosine kinase (RTK) levels at the cell surface by trafficking (Ammoun, et al., 2008; Lallemand, et al., 2009) or by sequestration into microdomains (Curto, et al., 2007). Downstream of RTKs, NF2 inhibits Ras-mediated activation of the mitogen-activated protein kinase (MAPK) pathway (Ammoun, et al., 2008). Full activation of ERK over the MAPK pathway requires PAK-mediated c-Raf and MEK1 phosphorylation and PAKs are activated by Rac1 (Beeser, et al., 2005). NF2 in closed conformation inhibits this Rac1-induced PAK activation (Okada, et al., 2005) as it releases the Rac1-inhibitor Rich1 from the Angiomotin complex (Yi, et al., 2011). Thus NF2 tumour suppressor function is partially achieved by reduction of mitogenic ERK/MAPK signalling over PAK inhibition. Additionally, NF2 blocks cell proliferation by inhibiting phosphoinositide 3-kinase (PI3K)

through binding to PIKE-L (PI3K-enhancer) (Rong, et al., 2004) and inhibits the mammalian target of rapamycin complex 1 (mTORC1 or the mTOR-raptor complex) but not via the established mechanism of PI3K/AKT inhibition (James, et al., 2009; Lopez-Lago, et al., 2009). Furthermore, NF2 activates the Hippo tumour-suppressor pathway (Zhang, et al., 2010) and inhibits the E3 ubiquitin ligase complex $CRL4^{DCAF1}$ (Li, et al., 2010) which both induces growth arrest. Finally, NF2 inhibits focal adhesion kinase (FAK)-Src signalling which coordinates adhesion dynamics/cell migration and survival signalling by integrating signals from extracellular cues (*e.g.* growth-factor receptors and integrins) and the upstream Src-family kinases (Ammoun, et al., 2008; Jin, et al., 2006; Rong, et al., 2004). The tumour suppressive function of the closed form of NF2 is probably coupled to its inhibitory effect on multiple of these mitogenic signalling pathways.

#### *1.1.3.1 The NF2 isoforms differ in conformation, localisation and function*

The NF2 gene is composed of 17 exons (Bianchi, et al., 1994) and at least ten alternatively spliced versions (isoforms) are expressed in vivo. Isoform 1 lacks exon 16 and encodes a 595 amino acid protein with a predicted molecular mass of 66 kDa (Rouleau, et al., 1993; Trofatter, et al., 1993). Isoform 2 (590 aa) contains the frameshift causing exon 16, which consequently results in premature stop and a shortened protein with different C-terminus (PQAQGRRPICI instead of LTLQSAKSRVAFFEEL) (Bianchi, et al., 1994; Hara, et al., 1994). Isoform 7 (508 aa, 56 kDa) lacks exons 2 and 3 but contains the frameshift causing exon 16. The resulting protein lacks amino acids 39-121 of isoform 1 and 2 and has the same C-terminus as isoform 2.

*The structure regulates conformation, localisation and function of NF2 isoforms.* The NF2 tumour suppressor function is believed to be regulated by self-association between the FERM (residues 302-308) and the C-terminal domain (residues 585-595, KSRVAFFEEL) (Gronholm, et al., 1999; Gutmann, et al., 1999). This intramolecular head-to-tail interaction depends on proper folding of the N-terminal FERM domain which requires self-association of residues 8-121 and 200-302 (Gutmann, et al., 1999). Proper FERM folding and formation of a head-to-tail closed protein are important for localization beneath the plasma membrane, in membrane ruffles and filopodia (Brault, et al., 2001; Gonzalez-Agosti, et al., 1996; Sainio, et al., 1997). Most studies conclude that formation of the closed formation and membrane association are necessary for the growth-suppressing function of NF2. The conclusion, that mutants and isoforms which cannot form an intramolecular head-to-tail interaction cannot localize to the membrane and cannot inhibit cell proliferation is supported by the finding that isoforms lacking the C-terminal domain (*e.g.* isoform 2, isoform 7) are constitutively in an open conformation (Gronholm, et al., 1999) and do not function as tumour suppressor (Sherman, et al., 1997). This is probably explained by distinct interaction and localization patterns.

*NF2 isoforms differ in interaction pattern.* The intramolecular interactions in isoform 1 reduce its actin binding capability which results in decreased effects on actin filament dynamics in comparison to isoform 2 (James, et al., 2001). Furthermore, isoform 1 only binds to ezrin if ezrin is in the open conformation, whereas isoform 2 binds to ezrin regardless of the ezrin conformation (Meng, et al., 2000). The binding of NF2 to the adaptor protein syntenin is also impaired with a C-terminal truncated isoform 1 (which simulates isoform 2) in comparison to the full length protein (Jannatipour, et al., 2001). However, isoform 2 can not reverse abnormal ruffling and cell spreading or restore normal actin organization in NF2-deficient human tumour cells in contrast to isoform 1 (Bashour, et al., 2002).

*NF2 isoforms differ in localization pattern.* Isoforms with deletions in the FERM domain (*e.g.* isoform 7) and resulting improper FERM domain folding show impaired membrane localization (Brault, et al., 2001;

Deguen, et al., 1998; den Bakker, et al., 2000; Koga, et al., 1998; Kressel and Schmucker, 2002). However, also NF2 isoform 1 is not always membrane localized as this isoform shuttles in a cell cycle-dependent manner between the cell membrane, the cytoplasm and the nucleus (Muranen, et al., 2005). Additionally, NF2 isoform 1 in its closed, growth-inhibitory form has been shown to accumulate in the nucleus, where it binds to the cullin-RING ligase complex $CRL4^{DCAF1}$, suppresses its E3 ligase activity and induces growth arrest (Li, et al., 2010). Binding and inhibition are disrupted by mutations in the first subdomain of the FERM domain, which consists of an ubiquitin-like fold (Shimizu, et al., 2002) and could serve as inhibitory pseudosubstrate for the ubiquitin ligase (Li, et al., 2010). Interestingly, deletions in the same subdomain lead to unrestricted entry into the nucleus (Kressel and Schmucker, 2002) which implies a cellular function different to the wild-type protein for naturally occurring splice variants lacking exon 2 (*e.g.* isoform 7).

Collectively, these studies point into the direction that NF2 isoforms differ not only in conformation and subcellular localization but also in molecular function. These functions are modulated by intramolecular and intermolecular interactions. To uncover the complex biological outputs associated with NF2 mutations and NF2 deficiency it is important to investigate these interactions on isoform level and to reveal functional differences between the isoforms. Furthermore, these interactions are known to be regulated by phosphorylation so it would be advantageous to investigate interactions with respect to the signalling status of the cell. The modified Y2H system described here allows the investigation of isoform-specific interaction patterns in absence or presence of several active kinases simultaneously. This could reveal insights into novel regulatory mechanisms.

## 1.2 Mapping of protein-protein interactions

### 1.2.1 Interaction networks

The human genome encodes approximately 22,000 protein encoding genes and roughly 86 % of them undergo alternate splicing to produce two or more distinct isoforms with a minor isoform frequency above 15 % (Wang, et al., 2008). A large fraction of these genes and their resulting protein isoforms are still uncharacterized. To improve the understanding of important physiological and pathological processes, it is necessary to assemble a detailed binary map (if possible) at the isoform level which shows how proteins and pathways connect. The level of complexity is further increased by post-translational modifications (PTMs) which alter the ability of proteins to interact. It is estimated that about 5 % of the human genes encode modifying enzymes that perform more than 200 types of PTMs and target nearly the complete proteome (Hunter, 2007; Mann and Jensen, 2003; Walsh, 2006). The 518 human kinases, for example, were expected to phosphorylate 100,000 sites (Zhang, et al., 2002). Recently the number of phosphorylation sites that might exist in the human proteome has been corrected upwards to more than 500,000 sites (Lemeer and Heck, 2009; Safaei, et al., 2011). The current PhosphoELM data set (version 9.0) contains more than 42,500 non-redundant phosphorylation-sites in more than 11,000 different protein sequences (Dinkel, et al., 2011). Approximately 60 % of these protein sequences are human which corresponds to 25,000 identified human phosphorylation sites and indicates that 75-95 % of the sites remain to be identified. Although PTMs are known to influence protein interactions and although isoforms have differential functions, current interaction maps include only sparse information about modification-dependency and isoform-specificity, which would be necessary to reveal the full complexity of the interactome. Several high-throughput (HTP) techniques have been developed and were applied in order to generate more complete interactomes. However, interaction maps are far from being complete and most of the currently described

unbiased, proteome-wide HTP methods rely on further detailed experimentation to uncover modification-dependency and isoform-specificity.

This study addressed these problems by the application of various HTP techniques able to detect modification-dependent isoform-specific interactions. A modified Y2H system developed in this study was chosen as primary interaction detection method. The resulting modification-dependent, isoform-specific Y2H interactions were further evaluated in luminescence-based HTP co-IP experiments and protein complementation assays (PCA) based on the yellow fluorescent protein (YFP) variant Venus. The following chapters will give a detailed overview of the current HTP interaction detection methods and will discuss their respective advantages and disadvantages.

### 1.2.2 The Y2H system as primary interaction detection method

The Y2H system, originally developed by Stanley Fields (Fields and Song, 1989), is based on the observation that eukaryotic transcription factors have two functionally required but separable domains, one that directs binding to a promoter DNA sequence (DBD) and another that activates transcription (AD). In the Y2H system, these domains are tethered separately to the proteins of interest resulting in DBD and AD fusion proteins designated as bait and prey proteins, respectively. Interaction between the tethered proteins in yeast cells, expressing both hybrid proteins, brings the DBD and AD into proximity and leads to reconstitution of the transcription factor (Figure 3, A). The functional transcription factor activates the expression of one or more reporter genes that enable the selection of yeast cells harbouring an interacting protein pair.

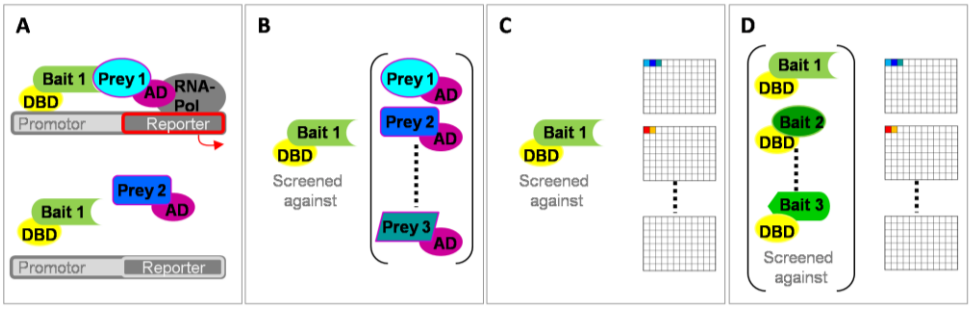


**Figure 3: Y2H system.**

**A,** In the Y2H system the bait proteins are fused to the DNA binding domain (DBD) and the prey proteins to the activation domains (AD) such that interaction between any bait and prey pair reconstitutes a functional transcription factor that drives reporter gene expression.

**B,** the library approach: baits are screened separately against a pool of preys.
**C** and **D**, the matrix approach: bait proteins are screened separately (C) or in a poolwise manner (D) against an ordered array of individually subcloned and characterized prey proteins.

In the last decade the Y2H has been advanced to one of the most powerful methods for screening entire proteomes. HTP Y2H approaches can be differentiated into matrix-based and library-based. In the library approach, the baits are screened separately against a prey pool (the prey library) containing random cDNA fragments or open reading frames (ORFs) (Figure 3, B). Diploid positives are selected based on reporter gene activation and the resulting ability to grow on selective media. In the Y2H library approach interacting prey proteins have to be determined by DNA sequencing. This is circumvented in Y2H matrix screens which use ordered arrays of individually subcloned and characterized prey clones that express a particular prey protein in one well of a plate (Figure 3, C). The bait strains are mated separately with this array of prey strains and diploids expressing an interacting protein pair are identified based on the expression of reporter genes and resulting

growth in a specific plate position. The throughput of the matrix approach can be further enhanced by screening a pool of bait strains against this prey matrix as performed in this study. However, this pooling strategy requires a retest that shows which bait in a pool is interacting with the prey (Worseck, et al., 2012) (Figure 3, D). The major advantage of matrix screens in general is that all protein pairs are tested with equal probability and that these screen can be repeated.

Repetition by performing interaction screens in several replicas is one of the main criteria for obtaining high quality interaction data in Y2H analysis. Further parameters for a stringent Y2H screen include low expression levels of the hybrid proteins and employment of different reporter genes (under distinct promoters) that are completely repressed in the absence of interaction (Worseck, et al., 2012). Furthermore the usage of different Y2H vectors and systems can increase sensitivity and coverage to the same extend as usage of different interaction methods (Chen, et al., 2010; Rajagopala, et al., 2009). The described parameters, the relative low costs and the possibility for automation make HTP Y2H experiments to one of the most powerful tools to generate quality-controlled, proteome-wide, binary PPI maps. Proteome-wide Y2H studies have been used to generate interaction maps for yeast (Ito, et al., 2001; Uetz, et al., 2000), fly (Giot, et al., 2003), worm (Li, et al., 2004) and human (Bandyopadhyay, et al., 2010; Goehler, et al., 2004; Rual, et al., 2005; Stelzl, et al., 2005; Venkatesan, et al., 2009; Vinayagam, et al., 2011; Yu, et al., 2009). Additionally, the Y2H technique is amenable for the investigation of dynamic protein-protein interactions (PPIs) including nitric oxide (NO)-dependent (Matsumoto, et al., 2003) and phosphorylation-dependent PPIs (Cao, et al., 2002; Guo, et al., 2004; Osborne, et al., 1995; Yamada, et al., 2001). Collectively, these facts motivated us to create a modified Y2H version suitable to detect phosphorylation-dependent interactions on a proteome-wide scale.

### 1.2.3 Comparative analysis between large-scale interaction detection methods

Large-scale interaction mapping is until today based on two main technologies: the Y2H system, which detects binary protein interactions and affinity purification coupled with mass spectrometry (AP-MS), which reveals the composition of protein complexes and co-operative binding patterns. AP-MS is based on the principle that the composition of stable protein complexes isolated from cells can be analyzed using mass spectrometry (Poetz, et al., 2009). Epitope-tagging of proteins, tandem affinity purification (TAP), stable transfection of bacterial artificial chromosomes (BACs) expressing tagged proteins (Poser, et al., 2008) and streamlined protocols for the HTP identification of endogenous protein complexes (Malovannaya, et al., 2011; Malovannaya, et al., 2009) facilitated the large-scale analysis, the sensitivity and the specificity of the AP-MS approach (Wilm, 2009).

Y2H and AP-MS have their own set of advantages and disadvantages. The analysis of human protein interactions in the Y2H system provides a foreign environment where modifying enzymes and PTMs are likely to be absent whereas AP-MS enables analysis of proteins and their PTMs in their natural cellular environment (Choudhary and Mann, 2010). However, washing steps in the affinity purification before mass spectrometry remove weak or transiently bound proteins so that only high abundant proteins can be detected whereas the interaction signal is amplified in Y2H screens. AP-MS studies are unbiased as in principle all interaction partners of the protein under investigation could be assayed simultaneously, however, the cellular context influences the interactome and thus under a given cellular context only a part of all potential interactions will be detected. Matrix Y2H screens depend on the coverage of the prey matrix but have the advantage that all interactions are tested with equal probability. Both of these techniques are not suitable for the detection of membrane–protein

interactions and extracellular interactions.

Methods capable of investigating large numbers of membrane–protein interactions are MYTH (membrane yeast-two hybrid) (Stagljar, et al., 1998) and the yeast-adapted dihydrofolate reductase (DHFR) PCA (Tarassov, et al., 2008). AVEXIS (aviditiy-based extracellular interaction screen) is capable to investigate extracellular interactions (Bushell, et al., 2008). Further interaction spaces might be covered by luminescence-based mammalian interactome mapping (LUMIER) (Barrios-Rodiles, et al., 2005), mammalian protein-protein interaction trap (MAPPIT) (Eyckerman, et al., 2001) and nucleic acid programmable protein array (NAPPA) (Ramachandran, et al., 2004), which all have not been employed on a genome-wide scale so far but are amenable to HTP experimentation. PCAs are based on the principle that two non-active reporter fragments assemble non-covalently to the functional reporter if brought into close proximity by two interacting proteins. MAPPIT and MYTH rely on interaction-induced transcription factor activation and subsequent reporter gene transcription whereas LUMIER and NAPPA are based on coimmunoprecipitation of tagged proteins. Comparison of MAPPIT, LUMIER, NAPPA, Y2H and an YFP-based PCA revealed that each of these methods detects a different subset of a well-known reference interaction set, encompassing on average approximately 30 % of the tested gold-standard interactions (Braun, et al., 2009). The detection of approximately 60 % of the reference interactions required the use of all five methods and the observed interaction overlap between the methods was not larger than expected for independent measures. This indicates that sensitivity and interaction map coverage can be increased by combining data obtained with different PPI detection methods (Schwartz, et al., 2009) or with one method in several modifications, as recently observed for multiple Y2H variants (Chen, et al., 2010).

Some of the above mentioned interaction detection strategies are amenable for the investigation of dynamic PPIs including an MAPPIT adoption (heteromeric MAPPIT) for the detection of phosphorylation-dependent PPIs (Lemmens, et al., 2003) and the LUMIER system which can be used to detect transforming growth factor-β (TGF-β) induced interaction dynamics (Barrios-Rodiles, et al., 2005). Furthermore, several PCAs allow the investigation of dynamic PPIs if the interaction-mediated reassembly of the corresponding protein reporter is reversible. Many PCAs based on the reconstitution of enzymatic activity are reversible (Michnick, et al., 2007). For example β-lactamase PCAs have successfully been used to probe dynamic PPIs (Remy, et al., 2007), like the phosphorylation-dependent association between the cAMP response element binding protein (CREB) and CBP (Spotts, et al., 2002). A transcription factor-coupled tobacco etch virus (TEV) protease PCA assay identified several adaptor proteins that interact with the ErbB4 receptor in a phosphorylation-dependent manner upon receptor stimulation (Wehr, et al., 2008). However, while PCAs that are based on reconstitution of the Gaussia (Remy and Michnick, 2006) or Renilla (Stefan, et al., 2007) luciferase are reversible, those based on the reconstitution of fluorescent proteins are not (Kerppola, 2008; Kerppola, 2009). This is a disadvantage if dynamic PPIs should be investigated but a clear advantage if transient PPIs should be detected (Magliery, et al., 2005). Fluorescent complementation techniques generate a visible signal which can be used to determine the subcellular localization of the interacting proteins in intact viable cells including bacteria, yeast, *C. elegans* and mammalian cells (Hu et al., 2002; Cole et al., 2007; Min et al., 2007). Although reconstitution of fluorescent proteins is irreversible, fluorescent PCA-based techniques can reveal some interaction dynamics if the interaction between the fused proteins is inducible. For example an YFP fragment complementation assay showed that the interaction between AKT and Smad3 is induced by insulin in a process inhibited by TGF-β or wortmannin addition, furthermore, TGF-β induced the phosphorylation-dependent interaction between Smad3 and Smad4 and nuclear translocation of this complex (Remy, et al., 2004).

Based on the comparative analysis of the described HTP interaction detection methods and their ability to detect dynamic PPIs we used a refined version of the IP method LUMIER and a PCA based on the YFP variant Venus as secondary interaction assays. The complementary nature of these assays made them attractive for the validation of the obtained modification-dependent, isoform-specific Y2H interactions.

## 1.3 Aims of this study

Neurodegeneration, PTM pathways and common methods suitable for interactome mapping have been discussed in the introductory chapters. Protein interactions are modulated by several PTMs and differ between protein isoforms. Thus, the interactome is conditional with respect to the signalling status of the cell, *e.g.* which isoforms and modifying enzymes are expressed and/or which enzymes are active. Many human disorders result from breakdowns in signal transduction and especially neurodegeneration has been linked to phosphorylation-dependent signalling processes (Kanehisa, et al., 2010; Limviphuvadh, et al., 2007). Evidences are accumulating that protein misfolding and aggregation are the common reason for sporadic neurodegeneration (Soto, 2003), characterized by progressive neuronal loss and synaptic abnormalities. The common ND phenotypes suggest overlapping molecular mechanism. Furthermore, the change in phosphorylation-dependent signalling processes implicates that the phosphorylation status influences the function of ND-related proteins.

The aim of this study was to systematically generate a high quality proteome-wide interaction network to connect proteins involved in distinct neurological disorders. Furthermore we aimed to investigate conditional *i.e.* phosphorylation-dependent and isoform-specific PPIs of these proteins. To realize these aims, a modified Y2H system developed in this study was applied as primary interaction detection method. The screen of 71 proteins (including 24 variants *i.e.* isoforms, fragments, mutants) implicated in neurological disorders against a prey matrix covering over 65 % of the human protein coding genes revealed an interaction map consisting of 90 interactions between 79 proteins. We detected three Ser/Thr kinase-dependent PPIs and two Tyr kinase-dependent PPIs which involved the PD-associated gene product PARK7 (DJ1, Parkinson protein 7) and isoforms of the tumour suppressor NF2 (merlin, neurofibromin 2). These phosphorylation-dependent PPIs and a fraction of the modification-independent Y2H interactions were tested in co-IP and Venus PCA experiments. The two complementary secondary interaction assays validated over 66 % of the tested PPIs and further elucidated their subcellular localization and their modification- and isoform-dependency.

Analysis of high-quality binary protein interaction maps have shown that protein products of genes associated with similar disorders are more likely to interact and have a higher probability to be coexpressed (Goh, et al., 2007), furthermore, they reveal insight into the implicated signal transduction mechanisms (Goehler, et al., 2004; Lim, et al., 2006). With the network-based approach described here, we successfully identified proteins but also cellular functions and processes that are associated with more than one disorder. Specifically, PARK7 and the Neurofibromatosis type 2-associated tumour suppressor NF2 have been shown to interact with the PI3K regulatory subunit p55γ (PIK3R3), which implicates the PI3K/AKT survival pathway in PD-associated neuronal apoptosis and Neurofibromatosis type 2-associated tumour formation, respectively.

The simultaneous investigation of two NF2 isoforms (1 and 7) with three independent interaction detection methods revealed following differences between them: (I) in contrast to isoform 1, isoform 7 was only able to heterodimerize but not to homodimerize in Venus PCA experiments also both of them homodimerized in co-IP experiments, (II) in Venus PCA experiments PIK3R3, AOF2 (KDM1A, LSD1) and EMILIN1 interact with isoform 7 in the cytoplasm whereas the corresponding interactions with isoform 1 (including the homo- and

heterodimers) were detected beneath the membrane, (III) in Y2H and co-IP experiments isoform 7 was the preferred interaction partner for all of these proteins.

Furthermore, the network substantiates the already established connection between PD and ubiquitination-mediated proteasome (dis)functions. Two novel PPIs between the PD-associated gene product PARK7 and the E3 ligase components ASB3 and RNF31 (HOIP) were identified. These interactions are triggered by Ser/Thr phosphorylation and might reveal regulatory mechanisms connecting PD pathogenesis to ASB3- and RNF31-mediated ubiquitination processes.

The approach has the potential to reveal common molecular mechanism(s) involved in neurological disorders and to uncover novel disease modifiers. Network-derived models build the basis for further investigations addressing how cellular processes under neurological disease states might be modulated. Furthermore, conditional interactions, especially modification-dependent ones, could offer new points of actions for drugs against NDs (Fry and Vassilev, 2005; Ozbabacan, et al., 2011; Rudolph, 2007).

# 2 Material and Methods

## 2.1 Material

### 2.1.1 Chemicals

1-Phenylazo-2-naphthol-6,8-disulfonic acid disodium salt (Orange G) (Sigma-Aldrich, Taufkirchen)

4-(2-Hydroxyethyl)-1-piperazineethanesulfonic acid (HEPES) (Sigma-Aldrich, Taufkirchen)

4'6-Diamidino-2-phenylindole (DAPI) (Roth, Karlsruhe)

Acetic acid (Merck, Darmstadt)

Acrylamide/Bisacrylamide 40 % (37,5:1) (Roth, Karlsruhe)

Adenosine-5'-triphosphate (ATP) (Sigma-Aldrich, Taufkirchen)

Agarose (Sigma-Aldrich, Taufkirchen)

Ammonium persulfate (APS) (Merck, Darmstadt)

Ammonium sulfate (Merck, Darmstadt)

Ampicillin trihydrate (Sigma, Deisenhofen)

Bacto agar (BD Biosciences, USA)

Bacto peptone (BD Biosciences, USA)

Bacto tryptone (BD Biosciences, USA)

Bacto yeast extract (BD Biosciences, USA)

Betain (Sigma-Aldrich, Taufkirchen)

Boric acid (Calbiochem part of Merck, Darmstadt)

Bovine serum albumin fraction V (Roche, Mannheim)

Bromphenol blue (Merck, Darmstadt)

Calcium chloride dihydrate (Merck, Darmstadt)

Chloramphenicol (Sigma-Aldrich, Taufkirchen)

Chloroform (Merck, Darmstadt)

Coomassie Brilliant Blue G-250 (Biomol GmbH, Hamburg)

Dipotassium phosphate (Acros organics part of Thermo Fisher Scientific Inc., Geel, Belgium)

Dithiothreitol (DTT) (Roth, Karlsruhe)

D-luciferin sodium lyophilized firefly (Sigma-Aldrich, Taufkirchen)

Dulbecco's modified eagle medium (DMEM+GlutaMAX™-I) (Gibco BRL, Gaithersburg, USA)

Dulbecco's phosphate buffered saline (DPBS) (Gibco BRL, Gaithersburg, USA)

Ethylenediaminetetraacetic acid (EDTA) (Roth, Karlsruhe)

Ethylene glycol tetraacetic acid (EGTA) (Roth, Karlsruhe)

Ethanol (Merck, Darmstadt)

Fetal bovine serum (FBS) (qualified FBS, south american) (Gibco BRL, Gaithersburg, USA)

Glucose monohydrate (Merck, Darmstadt)

Glycerol (Merck, Darmstadt)

Glycine (MP Biochemicals, Aurora, USA)

Glycogen (Roche, Mannheim)

Histidine (Sigma-Aldrich, Taufkirchen)

Isopropanol (Merck, Darmstadt)

Kanamycin sulfate (Sigma-Aldrich, Taufkirchen)

Leucine (Sigma-Aldrich, Taufkirchen)

Lithiumacetate (LiOAc) (Sigma-Aldrich, Taufkirchen)

Magnesium chloride (Roth, Karlsruhe)

Magnesium sulfate (Roth, Karlsruhe)

Methanol (Merck, Darmstadt)

Monopotassium phosphate (Roth, Karlsruhe)

Opti-MEM I (Gibco BRL, Gaithersburg, USA)

Orthophosphoric acid (Alfa Aesar GmbH & Co KG, Karlsruhe)

Paraformaldehyde (PFA) (Roth, Karlsruhe)

Phosphatase inhibitor, cocktail 1-3 (Sigma-Aldrich, Taufkirchen)

Polyethylene glycol (PEG) 3350 (Sigma-Aldrich, Taufkirchen)

Polyethylene glycol (PEG) 8000 (Sigma-Aldrich, Taufkirchen)

Potassium acetate (Merck, Darmstadt)

Potassium chloride (Roth, Karlsruhe)

Protease inhibitor (Roche, Mannheim)

Sodium carbonate (Merck, Darmstadt)

Sodium chloride (Roth, Karlsruhe)

Sodium citrat (Roth, Karlsruhe)

Sodium dihydrogen phosphate (Merck, Darmstadt)

Sodium dodecyl sulfate (SDS) (Roth, Karlsruhe)

Sodium hydrogencarbonate (Merck, Darmstadt)

Sodium hydroxide (Roth, Karlsruhe)

Sorbitol (Sigma-Aldrich, Taufkirchen)

Spectinomycin dihydrochloride pentahydrate (Sigma-Aldrich, Taufkirchen)

Sucrose (Merck, Darmstadt)

SYBR Gold Nucleic Acid Gel Stain (Invitrogen, Darmstadt)

Tetracycline hydrochloride (Sigma-Aldrich, Taufkirchen)

Tetramethylethylenediamine (TEMED) (Invitrogen, Darmstadt)

Tris (hydroxymethyl) aminomethane (Tris Base) (Roth, Karlsruhe)

Tris (hydroxymethyl) aminomethane hydrochloride (Tris HCl) (Sigma-Aldrich, Taufkirchen)

Triton X-100 (Sigma-Aldrich, Taufkirchen)

Tryptophan (Sigma-Aldrich, Taufkirchen)

Tween 20 (Sigma-Aldrich, Taufkirchen)

Uracil (Sigma-Aldrich, Taufkirchen)

Yeast nitrogen base (Difco part of BD Biosciences, USA)

### 2.1.2 Lab ware

NanoDrop ND-1000 (Thermo Fisher Scientific Inc.)
Mini-protean tetra cell electrophoresis system (Bio-Rad Laboratories)
Trans-blot SD semi-dry transfer cell (Bio-Rad Laboratories)
PowerPac universal power supply (Bio-Rad Laboratories)
Sunrise 96 horizontal gel electrophoresis apparatus (Biometra GmbH)
Kby roboter (Cambridge, UK)
BiomekNX (Beckman Coulter GmbH)
Biophotometer plus (Eppendorf AG)
Thermomixer comfort (Eppendorf AG)
Centrifuge 5810 R (Eppendorf AG)
E.A.S.Y 429k digital camera (Herolab GmbH Laborgeräte)
Tetrad PTC-225 thermo cycler (MJ Research Inc.)
Titramax 1000 (Heidolph Instruments GmbH & Co. KG)
Incubator 1000 (Heidolph Instruments GmbH & Co. KG)
Innova44 shaker (New Brunswick Scientific)
InfiniteM200 multimode microplate reader (Tecan Group Ltd.)
96well MTPs, tissue culture test plates (TPP Techno Plastic Products AG, 92096)
96well MTPs, PS, flat bottom, crystal clear (Greiner Bio-One GmbH, 655101)
96well MTPs, PS, flat bottom, TC, µclear, black, sterile, with lid, (Greiner Bio-One GmbH, 655090)
96well MTPs, PS, flat bottom, TC, white, sterile (Greiner Bio-One GmbH, 655073)
96well MTPs, PS, flat bottom, lumnitrac600, high binding, white, sterile (Greiner Bio-One GmbH, 655074)
384well MTPs, PS, flat bottom, clear, sterile, with lid (Greiner Bio-One GmbH, 781186)
Tissue culture flask (TPP Techno Plastic Products AG, 90076)
Omnitrays (Nunc GmbH & Co. KG, 165218)
Agar-plates (241 x 241 x 20) (Nunc GmbH & Co. KG, 240845)
96well PCR plate (Costar part of Corning Incorporated, 6511)
96well deepwell plates (2000 µl/well) (Eppendorf AG, 0030 501.322)
Plastic tape for sealing PCR plates/MTPs
(Costar part of Corning Incorporated, 6524 or Thermo Fisher Scientific Inc., AB-5558)
Sterile breathable sealing films (Aeraseal, Excel Scientific Inc., BS-25)
Polyvinylidene fluoride (PVDF) membrane (Bio-Rad Laboratories, 162-0177)
Nitrocellulose membrane (Bio-Rad Laboratories, 162-0115)
Glass beads, acid-washed <106 µm (Sigma-Aldrich, G4649)
Pin tools with 96 and 384 pins. The steel pins are cylindrical with a diameter of 1.3 mm and the edge of the flat top that is touching the agar is bevelled 45°at 0.2 mm. Sterilize by heating the pins until they glow red. Let them cool in a sterile environment.

### 2.1.3 Enzyme, proteins, DNA, kits

Coenzyme A (CoA) (Sigma-Aldrich, Taufkirchen)

1 Kb Plus DNA ladder (Invitrogen, USA)

Prestained protein ladder, PageRuler™ Plus (Fermentas GmbH, St. Leon-Rot)

Phusion hot start high-fidelity DNA polymerase (Finnzymes, Vantaa)

QIAquick PCR purification kit (Qiagen GmbH, Hilden)

Western lightning plus-ECL (PerkinElmer, Massachusetts)

AttoPhos substrate set (Roche, Mannheim)

Bright-Glo luciferase assay system (Promega, Madison)

QuikChange site-directed mutagenesis kit (Stratagene, Santa Clara)

PfuTurbo DNA polymerase (Stratagene, Santa Clara)

PureYield plasmid midiprep system (Promega, Madison)

QIAprep spin miniprep kit (Qiagen GmbH, Hilden)

dNTP-Mix (Fermentas GmbH, St. Leon-Rot)

Salmon sperm carrier DNA (Sigma-Aldrich, Taufkirchen)

FastDigest Bsp1407I (Fermentas GmbH, St. Leon-Rot)

Trypsin-EDTA (Gibco BRL, Gaithersburg, USA)

Lipofectamine 2000 (Invitrogen, USA)

BP Clonase enzyme mix (Invitrogen, USA)

LR Clonase enzyme mix II (Invitrogen, USA)

Proteinase K solution (Invitrogen, USA)

Zymolase 20T (Seikagaku Corporation)

## 2.1.4 Organisms

### *2.1.4.1 Bacteria strains*

DH10B: F`*mcrA* Δ-(*mrr hsd RMS-mcr BC*) ϕ80d*lacZ*ΔM15 Δ*lacX*74 *deoR recA*1 *araD*139 Δ(*ara leu*)7697 *alU galK* λ⁻ *rpsL endA*1 *nupG* (Invitrogen)

XL1-Blue: *recA*1 *endA*1 *gyrA*96 *thi*-1 *hsdR*17 *supE*44 *relA*1 *lac*⁻ F`[*pro*AB *lac*lqZΔM15 Tn10 ($Tet^r$) (Stratagene)

### *2.1.4.2 Yeast strains*

*L40c* MAT*a:* MAT*a his3Δ200 trp1-901 leu 2-3,112* ade2 lys2-801am can1 *LYS2::(lexAop)*$_4$*-HIS3 URA3::(lexAop)*$_8$*-lacZ*

*L40ccU2* MAT*a:* MAT*a his3Δ200 trp1-901 leu 2-3,112 ade2 lys2*-801am gal4 gal80 cyh2 can1 *LYS2::(lexAop)*$_4$*-HIS3 ura3::(lexAop)*$_8$*-lacZ* (Goehler et al., 2004)

*L40ccα MATα: MATα his3Δ200 trp1-910 leu2-3,112 ade2 GAL4 can1 cyh2 LYS2::(lexAop)*$_4$*-HIS3 URA3::(lexAop)*$_8$*-lacZ* (Goehler et al., 2004)

W303 B124: MATa/MAT*α leu2-3,112 trp1-1 can1-100 ura3-1 ade2-1 his3-11,15 [phi+]* (Markus Ralser, Ralser laboratory, MPI for Molecular Genetics)

### *2.1.4.3 Mammalian cell lines*

The HEK 293 cell line, which we used, is a immortalized line of primary human embryonic kidney (HEK) cells transformed by sheared human adenovirus type 5 (Ad 5) DNA. The HEK 293 cell line is an adherent fibroblastoid cell line growing as monolayer.

## 2.1.5 Media

### *2.1.5.1 E. coli growth medium and medium supplements*

| LB-medium | LB-agar |
|---|---|
| 10 g Bacto tryptone | 10 g Bacto tryptone |
| 5 g Bacto yeast extract | 5 g Bacto yeast extract |
| 10 g NaCl | 10 g NaCl |
| pH 7.2 (with NaOH) | pH 7.2 (with NaOH) |
| ad 1000 ml $H_2O$ | 20 g Bacto agar |
| | ad 1000 ml $H_2O$ |

| SOB-medium | SOC-medium |
|---|---|
| 20 g Bacto tryptone | 99 ml SOB-medium |
| 5 g Bacto yeast extract | 1 ml 20x Glucose |
| 0.5 g NaCl | |
| ad 1000 ml $H_2O$ | |
| ad after autoclaving: | |
| 10 ml 1 M $MgCl_2$ | |
| 10 ml 1 M $MgSO_4$ | |

| 2YT-medium | Transformation and storage solution (TSS) |
|---|---|
| 16 g Bacto tryptone | 85 % LB-medium |
| 10 g Bacto yeast extract | 10 % (w/v) PEG 8000 |
| 5 g NaCl | 5 % DMSO |
| pH 7.2 (with NaOH) | 50 mM $MgCl_2$ |
| ad 1000 ml $H_2O$ | Filter sterilize through a 0.22 µm pore filter |

| Antibiotic stock solutions | Stock concentration | Final concentration |
|---|---|---|
| Ampicillin | 100 mg/ml in $H_2O$ | 100 µg/ml |
| Tetracycline | 12.5 mg/ml in 50% EtOH | 20 µg/ml |
| Kanamycin | 30 mg/ml in $H_2O$ | 15 mg/l |
| Spectinomycin | 25 mg/ml in $H_2O$ | 50 µg/ml |

### *2.1.5.2 S. cerevisiae growth medium and medium supplements*

| 1.25x YPD liquid medium | 1.25x YPD agar |
|---|---|
| 5 g Bacto yeast extract | 5 g Bacto yeast extract |
| 10 g Bacto peptone | 10 g Bacto peptone |
| ad 400 ml $H_2O$ | 10 g Bacto agar |
| | ad 400 ml $H_2O$ |

| 2.5x Yeast liquid medium (NB) | 2.5x Agar |
|---|---|
| 6.7 g Yeast nitrogen base<br>ad 400 ml $H_2O$ | 10 g Bacto agar<br>ad 200 ml $H_2O$ |

| 1.25x Yeast liquid medium (NB) | 1.25x Yeast storage medium (NBG) |
|---|---|
| 3.35 g Yeast nitrogen base<br>ad 400 ml $H_2O$ | 3.35 g Yeast nitrogen base<br>250 ml Glycerol (99 %)<br>29.44 g Betain<br>ad 400 ml $H_2O$ |

| 20x Glucose stock solution |
|---|
| 200 g Glucose monohydrate<br>ad 500 ml $H_2O$ |

| 100x Amino acid stock | Stock concentration | Final concentration |
|---|---|---|
| 100x Leucine | 10 g/L Leucine | 100 mg/L Leucine |
| 100x Histidine | 2 g/L Histidine | 20 mg/L Histidine |
| 100x Uracil | 2 g/L Uracil | 20 mg/L Uracil |
| 100x Tryptophan | 2 g/L Tryptophan | 20 mg/L Tryptophan |

#### *2.1.5.3 Mammalian cell culture medium and medium supplements*

| Cell culture medium |
|---|
| Dulbecco's modified eagle medium (DMEM+GlutaMAX™-I)<br>10 % FBS (fetal bovine serum) |

### 2.1.6 Solutions

#### *2.1.6.1 E. coli and yeast miniprep buffers*

| Buffer P1 | Buffer P2 |
|---|---|
| 50 mM Tris pH 8.0<br>10 mM EDTA pH 8.0<br>add 50 mg/l RNAse A after autoclaving | 200 mM NaOH<br>1 % (w/v) SDS |

| Buffer P3 | Buffer H1 |
|---|---|
| 300 ml 5 M Potassium acetate pH 5.5<br>57.5 ml Acetic acid<br>ad to 500 ml $H_2O$ | 50 µl Zymolase 20T (20mg/ml)<br>940 µl SCE-buffer<br>10 µl 1 M DTT |

| SCE-buffer |
|---|
| 1 M Sorbitol |
| 0.1 M Sodium citrat pH 5.8 |
| 10 mM EDTA pH 8.0 |

### *2.1.6.2 Agarose gel electrophoresis buffers*

| 10x Tris/Borate/EDTA (10x TBE) | 10x Orange G sample buffer |
|---|---|
| 108 g Tris Base | 50 % (w/v) Sucrose |
| 55 g Boric acid | 0.5 % (w/v) Orange G |
| 40 ml 0.5 M EDTA pH 8.0 | |
| pH 8.3 (with HCl) | |
| ad to 1000 ml $H_2O$ | |

### *2.1.6.3 Yeast transformation*

| 10x Tris/EDTA buffer pH 7.5 (10x TE) | Carrier DNA |
|---|---|
| 100 mM Tris pH 7.5 | 5 mg Salmon sperm DNA |
| 10 mM EDTA pH 8.0 | 1 ml 1x TE |

| Mix1 | Mix 2 |
|---|---|
| 1 ml 1 M LiOAc | 6 ml 1 M LiOAc |
| 0.5 ml 10x TE | 6 ml 10x TE |
| 5 ml 2 M Sorbitol | 40 ml 60 % PEG 3350 |
| ad to 10 ml $H_2O$ | ad to 60 ml $H_2O$ |

### *2.1.6.4 SDS polyacrylamide gel electrophoresis buffers*

| 4x SDS gel loading buffer | 10x Electrophoresis buffer |
|---|---|
| 200 mM Tris pH 6,8 | 30.2 g Tris Base |
| 4 % SDS | 144 g Glycine |
| 40 % Glycerine | 10 g SDS |
| 0,4 % Bromphenol blue | ad to 1000 ml with $H_2O$ |
| ad prior to use: | |
| 200 mM DTT | |

### 2.1.6.5 Western blot buffers

| 10x Stock blotting buffer | Transfer buffer |
|---|---|
| 60.4 g Tris Base | 100 ml 10x Stock blotting buffer |
| 288 g Glycine | 200 ml Methanol |
| 3.75 g SDS | ad to 1000 ml with $H_2O$ |
| ad to 1000 ml with $H_2O$ | |

| 10x Tris-buffered saline (TBS) | TBS supplemented with Tween 20 (TBST) |
|---|---|
| 30 g Tris Base | 100 ml 10x TBS |
| 87 g NaCl | 1 ml Tween 20 |
| pH 7.5 (with HCl) | ad to 1000 ml with $H_2O$ |
| ad to 1000 ml with $H_2O$ | |

| Blocking buffer | Coomassie blue stain |
|---|---|
| 100 ml TBST | 500 ml Methanol |
| 5 g BSA (bovine serum albumin fraction V) | 100 ml Acetic acid |
| | 2.5 g Coomassie Brilliant Blue G-250 |
| | ad to 1000 ml with $H_2O$ |

| Destain solution | Blue silver stain |
|---|---|
| 300 ml Methanol | 20 % (v/v) Methanol |
| 100 ml Acetic acid | 10 % (v/v) Orthophosphoric acid |
| ad to 1000 ml with $H_2O$ | 10 % (w/v) Ammonium sulfate |
| | 0.12 % (w/v) Coomassie Brilliant Blue G-250 |

### 2.1.6.6 Co-IP buffers

| Hepes buffer |
|---|
| 50 mM HEPES pH 7.4 |
| 150 mM NaCl |
| 1 mM EDTA |
| 10 % Glycerine |
| 1 % Triton X-100 |
| Protease inhibitor (Roche 11051600) |
| Phosphatase inhibitor for tyrosine protein phosphatases (Sigma P5726) |
| Phosphatase inhibitor for Ser/Thr protein phosphatases (Sigma P2850 or P0044) |

| Luciferase substrate | 0.5 M $K_xPO_4$ pH 8.0 |
|---|---|
| 250 mM Glycylglycine | 9.4 ml 0.5 M $K_2HPO_4$ |
| 150 mM $KxPO_4$ pH 8.0 | 0.6 ml 0.5 M $KH_2PO_4$ |
| 40 mM EGTA | |
| 20 mM ATP | |
| 10 mM DTT | |
| 150 mM $MgSO_4$ | |
| 1 mM CoA | |
| 75 µM Luciferin | |

| 1x TBST II | 1x Carbonate buffer |
|---|---|
| 10 mM Tris Base | 70 mM $NaHCO_3$ |
| 150 mM NaCl | 30 mM $Na_2CO_3$ |
| 0.05 % Tween 20 | |

#### *2.1.6.7 Immunofluorescence buffers*

| 2 % Paraformaldehyde solution |
|---|
| 2 g Paraformaldehyde |
| ad to 100 ml with Dulbecco's phosphate buffered saline |

### 2.1.7 Antibodies

#### *2.1.7.1 Primary antibodies*

| Antisera | Species | Dilution | Source |
|---|---|---|---|
| Anti-V5-APH conjugate | Mouse | 1:5000 | Invitrogen (R96025) |
| Anti-Phospho-(Ser)-PKC Substrate | Rabbit (polyclonal) | 1:2500 | Cell signalling (2261) |
| Anti-Phospho-(Ser/Thr)-AKT Substrate | Rabbit (polyclonal) | 1:2500 | Cell signalling (9611) |

#### *2.1.7.2 Secondary antibodies*

| Antibody | Conjugate | Species | Dilution | Source |
|---|---|---|---|---|
| Anti-rabbit | APH conjugate | Goat | 1:10.000 | Promega (S3731) |
| Anti-goat | HRP conjugate | Rabbit | 1:3000 | Zymed (61-1620) |
| Anti-rabbit | HRP conjugate | Donkey | 1:3000 | GE Healthcare/Amersham (NA934) |

#### 2.1.7.3 Antibodies for 96well co-IP plate coating

| Antibody | Species | Dilution | Source |
|---|---|---|---|
| Sheep gamma globulin | Sheep | 1:1000 | Jackson ImmunoResearch (013-000-002) |
| AffiniPure rabbit anti-sheep IgG | Rabbit | 1:750 | Jackson ImmunoResearch (313-005-003) |

### 2.1.8 Vectors

#### 2.1.8.1 Entry vectors

| pDONR221 | pDONR223 |
|---|---|
| Size: 4762 bp | Size: 5005 bp |
| Sequencing primers M13 forward/M13 reverse | Sequencing primers: M13 forward/M13 reverse |
| Negative selection: ccdB | Negative selection: ccdB |
| Bacterial resistance: Kanamycin | Bacterial resistance: Spectinomycin |
| Reference: Invitrogen | Reference: Invitrogen |

#### 2.1.8.2 Expression vectors for S. cerevisiae

| pBTM116-D9 | pACT4-DM |
|---|---|
| Gateway compatible | Gateway compatible |
| Size: 8176 bp | Size: 9613 bp |
| Promoter/terminator: Truncated ADH | Promoter/terminator: Truncated ADH |
| DNA binding domain: LexA (N-terminal) | Activation domain: GAL4 (N-terminal) |
| Selection marker: Tryptophan (TRP1) | Selection marker: Leucine (LEU2) |
| Bacterial resistance: Tetracycline | Bacterial resistance: Ampicillin |
| Sequencing primers: BTM-5plus/BTM-3min | Sequencing primers: Prey-5p |
| Properties Y2H vector: 2µ plasmid | Properties Y2H vector: 2µ plasmid |
| Reference: Goehler *et al.* (Goehler, et al., 2004) | Reference: Goehler *et al.* (Goehler, et al., 2004) |

| pASZ-CN-DM | pASZ-C-DM |
|---|---|
| Gateway compatible | Gateway compatible |
| Size: 8525 bp | Size: 8459 bp |
| Promoter: *S. cerevisiae* Cup1 promotor | Promoter: *S. cerevisiae* Cup1 promotor |
| Terminator: *S. cerevisiae* CYC1 terminator | Terminator: *S. cerevisiae* CYC1 terminator |
| Nuclear localization sequence (N-terminal) | |
| Selection marker: Adenine (ADE) | Selection marker: Adenine (ADE) |
| Bacterial resistance: Ampicillin | Bacterial resistance: Ampicillin |
| Sequencing primers: CUPSeq-5p/CycT-5m | Sequencing primers: CUPSeq-5p/CycT-5m |
| Properties Y2H vector: ARS-CEN plasmid | Properties Y2H vector: ARS-CEN plasmid |
| Reference: modified from Stotz *et al.* (Stotz and Linder, 1990) | Reference: modified from Stotz *et al.* (Stotz and Linder, 1990) |

### 2.1.8.3 Expression vectors for mammalian cells

| pVEN-F2N-DM | pVEN-F1C-DM |
|---|---|
| Gateway compatible | Gateway compatible |
| Size: 7889 bp | Size: 8092 bp |
| Promoter: Human cytomegalovirus (CMV) | Promoter: Human cytomegalovirus (CMV) |
| Terminator: Bovine growth hormone (BGH) | Terminator: Bovine growth hormone (BGH) |
| Bacterial resistance: Ampicillin | Bacterial resistance: Ampicillin |
| Venus fragment 2 (C-terminal) | Venus fragment 1 (N-terminal) |
| (Nagai, et al., 2002) | (Nagai, et al., 2002) |
| Sequencing primers: T7-for/BGHrev | Sequencing primers: T7-for/BGHrev |
| Reference: Eduard Stefan | Reference: Eduard Stefan |
| (University of Innsbruck) | (University of Innsbruck) |

| pVEN-F2C-DM | pVEN-F1N-DM |
|---|---|
| Gateway compatible | Gateway compatible |
| Size: 7861 bp | Size: 8119 bp |
| Promoter: Human cytomegalovirus (CMV) | Promoter: Human cytomegalovirus (CMV) |
| Terminator: Bovine growth hormone (BGH) | Terminator: Bovine growth hormone (BGH) |
| Bacterial resistance: Ampicillin | Bacterial resistance: Ampicillin |
| Venus fragment 2 (N-terminal) | Venus fragment 1 (C-terminal) |
| (Nagai, et al., 2002) | (Nagai, et al., 2002) |
| Sequencing primers: T7-for/BGHrev | Sequencing primers: T7-for/BGHrev |
| Reference: Eduard Stefan | Reference: Eduard Stefan |
| (University of Innsbruck) | (University of Innsbruck) |

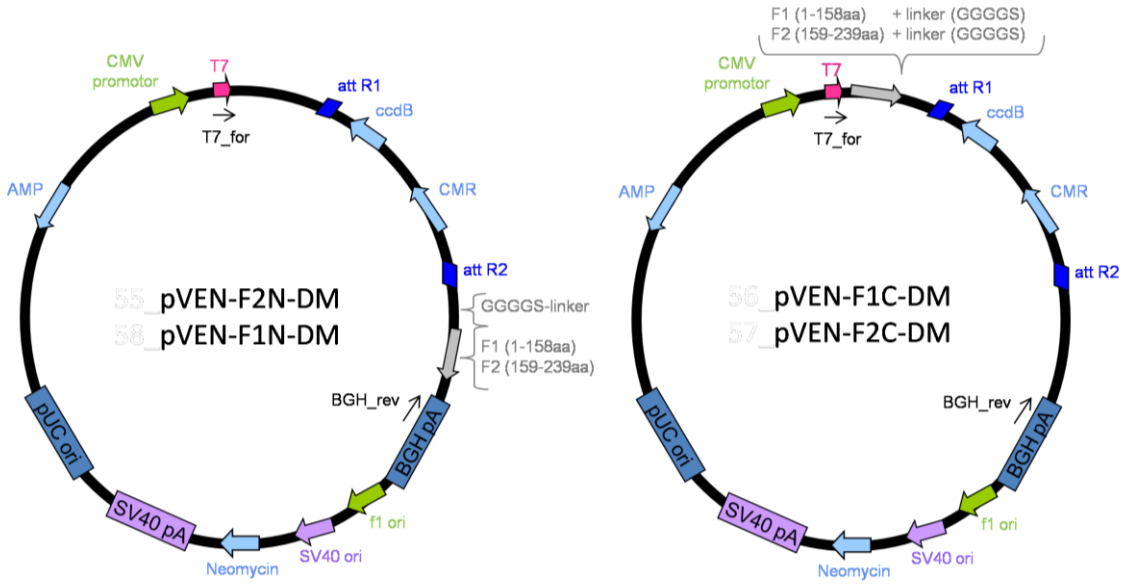


**Figure 4: Features of the Venus PCA expression vectors.**

N-terminal (1-158 aa; F1) and C-terminal (159-239 aa; F2) Venus fragments were inserted into a pcDNA 3.1 expression vector together with a 5-amino-acid linker sequence (Gly-Gly-Gly-Gly-Ser) to create C- or N-terminal Venus fragment fusion proteins, respectively. The resulting four vectors have the following features: cytomegalovirus (CMV) enhancer-promoter for high-level expression in mammalian cells, T7 promotor/priming site (T7) for *in vitro* transcription and sequencing through the insert, two recombination sites (attR1 and attR2) for recombinational cloning of the gene of interest, the chloramphenicol resistance gene (CMR) and the ccdB gene for counter selection, bovine growth hormone polyadenylation signal and transcription termination sequence (BGHpA) for enhanced mRNA stability, f1 origin (f1 ori) for production of single-strand DNA in F plasmid containing *E. coli*, SV40 early polyadenylation signal (SV40 pA), SV40 early promoter and origin (SV40 ori) for expression of the neomycin resistance gene and stable propagation of the plasmid in mammalian hosts expressing the SV40 large T antigen, the neomycin resistance gene for selection of stable cell lines using geneticin, and the ampicillin resistance gene (Amp) and pUC origin (pUC ori) for selection and maintenance in *E. coli.*

| pFireV5-DM | pcDNA3.1PA-D57 |
|---|---|
| Gateway compatible | Gateway compatible |
| Size: 8828 bp | Size: 7646 bp |
| Promoter: Human cytomegalovirus (CMV) | Promoter: Human cytomegalovirus (CMV) |
| Terminator: Bovine growth hormone (BGH) | Terminator: Bovine growth hormone (BGH) |
| V5-Firefly (N-terminal) | Protein A (N-terminal) |
| Bacterial resistance: Ampicillin | Bacterial resistance: Ampicillin |
| Sequencing primers: T7-for/BGHrev | Sequencing primers: T7-for/BGHrev |
| Reference: modified from Palidwor *et al.* | Reference: modified from Palidwor *et al.* |

## 2.1.9 Oligonucleotides

### *2.1.9.1 Oligonucleotides for sequencing*

| Primer | 5′-Sequence-3′ |
|---|---|
| M13 forward | GTAAAACGACGGCCAG |
| M13 reverse | CAGGAAACAGCTATGAC |
| protA-seq5p | CACGATGAAGCCGTGG |
| Fire-seq5p | AAAAGTTGCGCGGAGGAG |
| T7 forward | TAATACGACTCACTATAGGG |
| BGHrev | TAGAAGGCACAGTCGAGG |
| seq.T308 | TGGACAAGGACGGGCAC |
| Prey-5p | CCAAAGCTTCTGAATAAGCC |
| BTM-5plus | TCGTAGATCTTCGTCAGCAG |
| BTM-3min | AGCAACCTGACCTACAGG |
| CUPSeq-5p | CTTGTCTTGTATCAATTGC |
| CycT-5m | GGACCTAGACTTCAGGTTG |

### *2.1.9.2 Oligonucleotides for mutagenesis PCR*

| Primer | 5′-Sequence-3′ |
|---|---|
| AKT1_T308D for | CGGTGCCACCATGAAGGACTTTTGCGGCACACCT |
| AKT1_T308D rev | GCCACGGTGGTACTTCCTGAAAACGCCGTGTGGA |
| AKT1_S473D for | CACTTCCCCCAGTTCGACTACTCGGCCAGCGG |
| AKT1_S473D rev | GTGAAGGGGGTCAAGCTGATGAGCCGGTCGCC |
| AKT1_T308A for | GGTGCCACCATGAAGGCCTTTTGCGGCACAC |
| AKT1_T308A rev | CCACGGTGGTACTTCCGGAAAACGCCGTGTG |
| AKT1_S473A for | CTTCCCCCAGTTCGCCTACTCGGCCAG |
| AKT1_S473A rev | GAAGGGGGTCAAGCGGATGAGCCGGTC |

### *2.1.9.3 Oligonucleotides for two step PCR*

| Primer | 5′-Sequence-3′ |
|---|---|
| uni_attB1 for | GGGGACAAGTTTGTACAAAAAAGCAGGCT |
| uni_attB2 rev | GGGGACCACTTTGTACAAGAAAGCTGGGT |
| PKCZ_attB1 for | AAAAAGCAGGCTTAATGGATGGAATCAAAATCTCTC |
| PKCZ_attB2 rev | AGAAAGCTGGGTCTCACACCGACTCCTCGGTG |
| PKCA_attB1 for | AAAAAGCAGGCTTAAACCTTGACCGAGTGAAACTC |
| PKCA_attB2 rev | AGAAAGCTGGGTCTCATACTGCACTCTGTAAGATG |

### 2.1.10 Databases

Swissprot http://www.ebi.ac.uk/swissprot/

TrEMBL http://www.ebi.ac.uk/TrEMBL/

MINT http://mint.bio.uniroma2.it/mint/

HPRD http://www.hprd.org/

BIND http://www.bind.ca/

Expasy http://us.expasy.org/tools/

MultiAlin http://multalin.toulouse.inra.fr/multalin/

NetworKIN http://networkin.info/version_2_0/search.php

Phosida http://www.phosida.de/

PhosphoELM http://phospho.elm.eu.org/

Phosphosite http://www.phosphosite.org/

NetPhorest http://netphorest.info/

### 2.1.11 Software

VectorNTI Invitrogen

Acess

Cytoscape

yED Graph Editor

## 2.2 Methods

### 2.2.1 Work with *E. coli*

#### *2.2.1.1 Growth and storage of E. coli*

To generate liquid cultures of *E. coli*, the requested amount of LB-medium was inoculated with a single *E. coli* colony and cells were grown for 16-20 hours in a shaker at 37 °C. Depending on the desired storage time different storing methods were applied. Glycerol stocks enabled long-term storage of bacteria and were generated by mixing overnight cultures with 50 % autoclaved glycerol at a ratio of 1:1 prior to freezing and storage at -80 °C. For short-term storage, *E. coli* strains were streaked on LB-plates containing 2 % agar and incubated for 16-20 hours at 37 °C prior to storage at 4 °C. The liquid or solid LB-media contained the appropriate antibiotic if transformed *E. coli* were grown.

#### *2.2.1.2 Preparation of competent E. coli*

##### 2.2.1.2.1 Chemically competent cells

In order to generate chemical-competent DH10B, 20 ml 2YT-medium was inoculated with a single *E. coli* colony freshly grown on LB-agar and cells were grown in a shaker at 37 °C. After 16-20 hours, the overnight culture was used for inoculation of 2000 ml 2YT-medium. Cells were grown in a shaker at 37 °C until an $OD_{600}$ of 0.7-0.8 was reached. At this point the culture was divided into four 500 ml flasks and flasks were centrifuged at 4000 rpm for 15 minutes at 4 °C. After removing the supernatant each pellet was resuspended in 40 ml sterile TSS (Transformation and storage solution). Glycerol stocks were generated by mixing the TSS resuspended pellets with 4 ml 87 % autoclaved glycerol prior to freezing and storage at -80 °C. Chemical-competent DH10B cells generated with this protocol had a transformation efficiency of up to $1x\ 10^5$ cfu/µg.

##### 2.2.1.2.2 Electrocompetent cells

In order to generate electrocompetent DH10B, 50 ml LB-medium were inoculated with a single *E. coli* colony freshly grown on LB-agar and cells were grown in a shaker at 37 °C. After 16-20 hours, 45 ml of the overnight culture were used for inoculation of 1500 ml LB-medium. Cells were grown in a shaker at 37 °C until an $OD_{600}$ of 0.3-0.4 was reached. At this point the culture was divided into six 250 ml flasks and flasks were incubated on ice for 30 minutes. Cells were collected by centrifugation at 3500 rpm for 10 minutes at 4 °C. After removing the supernatant each pellet was resuspended in 100 ml of cold, sterile 15 % glycerol, incubated on ice for 20 minutes, and centrifuged as before. The supernatant was removed and each pellet was gently resuspended in 10 ml of cold, sterile 15 % glycerol, incubated on ice for 20 minutes, and centrifuged again as before. The supernatant was removed and each pellet was gently resuspended in 2 ml of cold, sterile 15 % glycerol to yield the final competent cell suspension, which was aliquoted and stored at -80 °C.

### *2.2.1.3 Transformation of competent cells*

#### *2.2.1.3.1* Chemical transformation of *E. coli*

This protocol was used for 96well format transformation of DHB10 *E. coli* cells with the BP- or LR-reaction mixtures. Competent bacterial cells were thawed on ice and aliquoted into a PCR plate. Typically for a transformation from a BP- or LR-reaction, 2.5 µl of the reaction solution was pipetted into 30 µl cells. The PCR plate was sealed with plastic tape, vortexed softly and incubated on ice for 30 minutes. Following that, the plate was incubated at 42 °C for 90 seconds and returned to ice for a further 5 minutes before 70 µl prewarmed SOC-medium was added. The whole content of the PCR plate wells was than transferred into the corresponding wells of a deepwell plate which were filled with 130 µl prewarmed SOC-medium. The deepwell plate was incubated at 37 °C for 1 hour at 220 rpm before 50 µl from each well were pipetted on selective LB-plates by making rows of drops on the agar. LB-plates were incubated for 16-20 hours at 37 °C. If chemically competent DH10B were used, this protocol yielded colonies for 95-100 % of the BP- or LR-reactions. If no colonies were obtained, the transformation was repeated with the residual BP- or LR-reaction using an electroporation protocol.

#### 2.2.1.3.2 Electroporation of *E. coli*

Competent bacterial cells were thawed on ice and aliquoted in 2 ml microfuge tubes. Typically for a transformation from a BP- or LR-reaction, 1-2 µl of the reaction solution was pipetted into microfuge tubes containing 50 µl cells and an equal volume of sterile 15 % glycerol. The mixture of cells and DNA was transferred into a 0.1 cm gap electroporation cuvette and tapped to the bottom. A Gene Pulser apparatus was used to pulse the sample in the cuvette, generating a pulse with a field strength of 1.7 kV and a time constant of approximately 4-5 msec (25 µF and 200 Ω). Immediately after pulse delivery 200 µl prewarmed SOC-medium was added. The cell suspension was transferred into a sterile 2 ml microfuge tube and incubated at 37 °C for 1 hour at 600 rpm. Following that, 200 µl cell suspension was spread on LB-agar and incubated overnight at 37 °C.

## 2.2.2 Work with *S. cerevisiae*

### *2.2.2.1 Yeast Media preparation*

This section describes the preparation of different media from stock solutions. The media are named after the missing and required amino acids/nucleosides. Amino acids/nucleosides are abbreviated with a single letter as followed: “H” for histidine, “A” for adenine, “U” for uracil, “L” for leucine and “T” for tryptophan. Anabolytes omitted are marked by a minus sign and separated by a slash from the amino acids/nucleosides which are added to the media. The order on both sides of the slash is always HAULT.

*Liquid medium:* 25 ml 20x glucose stock solution and 5 ml of each required 100x amino acid/nucleoside stock solution were added to 400 ml 1.25x NB or 1.25x NBG. The liquid medium was adjusted to a final volume of 500 ml with sterile water.

*Solid medium:* 200 ml of 2.5x NB, 25 ml 20x glucose stock solution and 5 ml of each required 100x amino acid/nucleoside stock solution were added to 200 ml 2.5x agar. Solid medium was adjusted to a final volume of 500 ml with sterile water and dissolved using a microwave. After the medium was cooled down to

60 °C agar, plates were filled with 200 ml medium under a sterile hood.

*YPD liquid medium:* 25 ml 20x glucose stock solution and 5 ml 100x adenine stock solution (optional) were added to 400 ml 1.25x YPD. The YPD liquid medium was adjusted to a final volume of 500 ml with sterile water.

*YPD solid medium:* 25 ml 20x glucose stock solution and 5 ml 100x adenine stock solution (optional) were added to 400 ml 1.25x YPD agar. Solid medium was adjusted to a final volume of 500 ml with sterile water and dissolved using a microwave. After the medium was cooled down to 60 °C agar, plates were filled with 200 ml medium under a sterile hood.

#### *2.2.2.2 Growth and storage of S. cerevisiae*

For Y2H experiments, yeast needed to be grown in and was thus transferred to different liquid and solid media. The yeast was transferred from liquid to solid, solid to liquid, liquid to liquid and solid through liquid to solid (solid-liquid-solid). Instead of a solid to solid transfer, the solid-liquid-solid step was used to dissolve yeast agglomerates and to consequently obtain a better growth selection. Correct growth and storage of yeast is important for successful screening. To generate liquid cultures of yeast; the requested amount of liquid medium was inoculated with yeast colonies and vortexed. Cells were grown for 16-20 hours in a shaker (250 rpm) at 30 °C. Depending on the desired storage time different storing methods were applied. Glycerol stocks enabled long-term storage of yeast and were generated by freezing (-80 °C) overnight cultures grown in NBG medium. These glycerol stocks can be thawed two times only. For short-term storage, yeast strains were streaked on solid medium and incubated for 1-5 days at 30 °C prior to storage at 4 °C. Stored yeast needs to be replicated on agar for an extra generation before starting an Y2H experiment. Generally, untransformed yeast was grown in YPD media and transformed yeast in the appropriate selective media.

#### *2.2.2.3 Transformation of S. cerevisiae*

With this 96well format yeast transformation protocol, the two haploid MATa yeast strains were cotransformed with different combinations of bait and kinase plasmids. The following protocol describes the transformation of eight 96well plates in parallel. Fresh MATa yeast was used for inoculation of 12.5 ml YPDA liquid medium, vortexed and grown in a shaker (250 rpm) at 30 °C. After 16-20 hours, 250 ml YPDA medium was inoculated with the overnight culture to an $OD_{600}$ of 0.10-0.15 prior to further incubation at 30 °C until an $OD_{600}$ of 0.6-0.8 was reached. At this point the culture was divided into five 50 ml screw-cap centrifuge tubes and yeast was harvested by centrifugation for 5 min at 2000 rpm at room temperature. After removing the supernatant each pellet was resuspended in 20 ml sterile 1x TE and pelleted as above. After removing the supernatant the pellets were resuspended in 2000 µl Mix 1, pooled and incubated at room temperature for 10-60 minutes. The yeast suspension was mixed well before 11 µl were transferred into individual wells of a PCR plate containing bait and kinase plasmid and carrier DNA. Typically for a cotransformation, 2.5 µl bait plasmid DNA and 2.5 µl kinase plasmid DNA were mixed with 5 µl 10.5 mg/ml heat denatured salmon testis DNA. One negative control (*i.e.* only carrier DNA) and one positive control (*i.e.* a well-tried vector preparation) were included in each plate. The yeast suspension was mixed with the DNA before 58 µl of Mix 2 were added into each well of the PCR plate. The plate was sealed, mixed and incubated at 30 °C for 30 minutes before 8 µl DMSO were added to each well. The plates were sealed, mixed and incubated at 42 °C for 7 minutes in a thermocycler. Four biological replicas were created by transferring the cells to four selective agar plates. Selection of the transformed yeast

cells required -AT/HUL media because the bait vector (pBTM116-D9) has a tryptophan and the kinase vector (pASZ-C/CN) an adenine selection marker. To allow the growth of transformed yeast colonies, plates were incubated at 30 °C for 3-5 days. Colonies obtained from the transformation were solid-liquid-solid replicated before they were used in an autoactivation or mating experiment.

### 2.2.2.4 Preparation of cell lysates for western blots

Three yeast spots (0.5 cm in diameter) freshly grown on agar were scraped off using an inoculation loop and stirred into microfuge tubes (1.5 ml) containing 30 µl 4x SDS gel loading buffer and an equal volume of acid washed 0.45 µm glass beads. The tubes were vortexed vigorously for 5 minutes and heated at 95 °C for 5 minutes prior to freezing and storage at -80 °C for at least 30 minutes. This vortex-heat-freeze cycle was repeated three times before 7-10 µl were analyzed by SDS-PAGE.

### 2.2.2.5 Autoactivation test

Autoactive baits induce constitutive activation of reporter genes even in the absence of a positive interacting protein conjugated to the Gal4 activation domain. This causes false-positive interactions in Y2H screens and masks interaction signals of other baits in a pooled Y2H screen. In order to identify autoactive bait strains, all four biological replicas were mated with a prey strain carrying a prey plasmid without insert and autoactive baits that grew on -HAULT (SD4) medium were not taken forward into the pooled matrix matings. Typically for an autoactivation assay, liquid -L/HAUT medium was inoculated with a freshly grown prey strain carrying a prey plasmid without insert one day before mating. After vortexing and incubation at 30 °C for 16-20 hours in a shaker (250 rpm) 100-120 µl liquid culture were pipetted into each well of a 96well MTP. Using a pin tool, bait strains freshly grown on selective agar were stirred into the MTPs containing the prey strain without insert. This bait and prey strain mixture was directly stamped onto YPD agar and incubated for 36-44 h at 30 °C. Grown yeast spots were resuspended in -ALT/HU MTPs and transferred to -ALT/HU agar (solid-liquid-solid) to select for diploid yeast. After four nights of incubation at 30 °C diploid yeast was transferred to -HAULT agar (solid-liquid-solid via -ALT/HU MTPs). The colonies were left to grow at 30 °C for 5 days to select for growth reporter gene activity. Bait strains which did not grow on -ALT/HU agar plates as well as those growing on -HAULT agar plates were removed.

### 2.2.2.6 Screening bait pools against a prey matrix

Prey and bait strains were solid-liquid-solid replicated (in 384- or 96well format, respectively) three to four days before they were used in matrix mating experiments. One day before mating, bait strains freshly grown on selective agar were stirred into 96well MTPs containing 100 µl -AT/HUL liquid media per well. In the next step 10 µl of this yeast suspension was used to inoculate deepwell plates containing 2 ml -AT/HUL medium per well. The baits were grown separately for 18-22 hours at 30 °C in a shaker to the early stationary phase ($OD_{600}$ of 1.5-3). At this time point bait-kinase combinations belonging to one biological replica of one pool were combined in one beaker. We combined 11-24 different bait clones in a manner that each biological replica contained all bait clone-kinase clone combinations for this bait clone. The pooled overnight culture was mixed and 35 µl were pipetted into each well of a 384well MTP. Using a pin tool prey strains freshly grown on selective agar were stirred into MTPs containing the bait pools. This bait and prey strain mixture was directly stamped onto YPD agar and incubated for 36-44 h at 30 °C. Grown yeast spots were resuspended in -ALT/HU

MTPs and transferred to -ALT/HU and -HAULT agar (solid-liquid-solid). The agar plates were incubated at 30 °C for 5 days to allow selective growth indicating successful mating (-ALT/HU agar) or a positive interaction between a specific prey and one of the baits in the pool (-HAULT agar).

#### *2.2.2.7 Retest*

After the primary screen, a retest was necessary to verify and deconvolute the results. Nonautoactive preys that grew in more than one biological replica of a pool were included in the retest and were picked from the prey matrix. The four biological replicas of interacting bait pools were combined in 384well MTPs. Prey and bait strains were solid-liquid-solid replicated three to four days before they were used in the retest mating experiment. One day before mating, prey strain yeast spots (0.5 cm in diameter) freshly grown on selective agar were stirred into 20-40 ml -L/HAUT liquid medium using an inoculation loop. After vortexing and incubation at 30 °C for 16-20 hours in a shaker (250 rpm) 40 µl liquid cultures were pipetted into each well of 384well MTPs. The freshly grown biological bait strain replicas were stirred from selective agar into MTPs containing the preys using a pin tool. This bait and prey strain mixture was directly stamped onto YPD agar and incubated for 36-44 h at 30 °C. Grown yeast colonies were resuspended in -ALT/HU MTPs and transferred to -ALT/HU and -HAULT agar (solid-liquid-solid). The plates were incubated at 30 °C for 5 days to allow selective growth indicating successful mating (-ALT/HU agar) or a positive interaction between a specific bait-prey pairing (-HAULT agar).

### 2.2.3 Work with mammalian cells

#### *2.2.3.1 Growth of mammalian cells*

HEK 293 were cultured in a humidified 5 % $CO_2$ atmosphere at 37 °C in Dulbecco's modified eagle medium (DMEM) supplemented with 4500 mg/L D-glucose, 110 mg/L sodium pyruvate and 10 % fetal bovine serum. Cells were maintained by growing to ~80 % confluency in 75 $cm^2$ flasks prior trypsinisation and splitting at a 1:10 dilution every 3-4 days as appropriate.

#### *2.2.3.2 Transfection of mammalian cells*

Cells were seeded in 96well MTPs to reach 60 % or 80 % confluency at the time of transfection for experiments requiring fixation (*i.e.* Venus PCA) or cell lysis (*i.e.* co-IP or western blot sample preparation), respectively. Cells were transiently transfected with 50 ng of plasmid DNA per well using Lipofectamine 2000 (Invitrogen) according to the manufacturer's instructions. Co-IP assays were performed as triplicate cotransfections with mixtures of 25 ng firefly- and 25 ng PA-plasmid DNA per well, whereas Venus PCA assays were performed as single cotransfections with mixtures of 25 ng Venus F1 and 25 ng Venus F2 plasmid DNA per well. We included one negative control (*i.e.* only water) and one positive control (*i.e.* a well-tried interaction pair combination) in each plate of all interaction assays. For single transfections 17.85 µl reduced serum medium (Opti-MEM I) were transferred into individual wells of 96well MTPs containing 50 ng plasmid DNA and mixed with the provided DNA. For each well to be transfected 23.5 µl Opti-MEM I were mixed with 0.25 µl Lipofectamine 2000 and the resulting 23.75 µl were directly added to the Opti-MEM I diluted plasmid DNA. The mixture was incubated for 30 minutes and 37.4 µl were added dropwise to wells containing seeded cells growing in 75 µl DMEM medium. The cells were incubated for 20-24 h or 44-48 h at 37 °C in a $CO_2$ incubator prior to fixation or lysis, respectively.

### 2.2.3.3 Preparation of cell lysates for western blots

HEK 293 cells were seeded in 96well MTPs and transfected as described above. Two days after transfection, the DMEM medium was removed and cells were lysed by addition of 20 µl 4x SDS gel loading buffer per well. Samples originating from three triplicate transfections were pooled in one tube and heated at 95 °C for 5 minutes prior to storage at -20 °C or analysis by SDS-PAGE.

### 2.2.3.4 Coating of plates for the 96well co-IP

Greiner high binding 96well MTPs were manually coated with antibodies for 96well co-IP assays (2.1.7.3). All incubation steps were performed at 4 °C. Sheep gamma globuline was diluted in 1x carbonate buffer at a ratio of 1:1000 and 100 µl of this coating solution were added to each well of the plates. After incubation for 3-24 h, the coating solution was removed and the plates were blocked for 1-24 h using carbonate buffer supplemented with 1 % BSA (300 µl per well). The solution was removed and the plates were washed three times with 300 µl TBST II. Rabbit anti-sheep-IgG was diluted in 1x carbonate buffer (1:750) and 100 µl of this capture solution were added to each well. After incubation for 3-24 h, the plates were washed three times with 300 µl TBST II. Plates can be stored at 4 °C wrapped in foil prior to usage in co-IP experiments.

### 2.2.3.5 96well co-IP

HEK 293 cells were seeded in greiner TPP 96well plates and cotransfected with 25 ng firefly- and 25 ng PA-plasmid DNA per well as described above. Two days after transfection, the DMEM medium was removed and cells were lysed in 100 µl Hepes buffer for 30 minutes at 4 °C. The lysate was cleared by centrifugation at 4000 rpm for 5 minutes. A part of the supernatant (5 µl) was transferred to greiner cellstar normal binding 96well plates containing 35 µl DPBS per well to determine the expression of the firefly fusion protein by measuring the firefly luciferase activity in the whole cell lysate. After addition of 40 µl self-made luciferase substrate solution, the firefly luciferase activity was determined by measuring the light that is produced during the luciferase catalyzed oxidation of luciferin to oxyluciferin in a luminescence plate reader (TECAN InfiniteM200). The residual supernatant (70 µl) was transferred to IgG-coated greiner high binding 96well plates and protein complexes were precipitated for 1 h at 4 °C. Unbound or unspecifically bound proteins were removed by washing with 100 µl ice-cold DPBS three times. As protein A (PA) binds specifically to the Fc region of IgG molecules protein A-tagged proteins get precipitated and interacting firefly-tagged proteins coimmunoprecipitated. The binding of the firefly fusion protein (co-IP) to the immunoprecipitated protein A fusion protein (IP) was determined through measuring the firefly luciferase activity. For this purpose 40 µl DPBS and 40 µl Bright-Glo luciferase substrate (Promega) were added to each well and the luciferase activity was measured in a luminescence plate reader (TECAN InfiniteM200). Each experiment was performed as triplicate transfection and the obtained relative luciferase intensity values were averaged and the standard deviation was determined. The fold change binding for a firefly fusion protein was calculated from average intensities measured in parallel with the protein of interest in comparison to a non-related protein PA fusion protein. Ratios larger than two were considered positive.

### 2.2.3.6 Construction of Venus PCA vectors

Venus PCA gateway destination vectors were generated by Eduard Stefan (University of Innsbruck). In principle, the gateway destination vectors were generated by amplifying the N-terminal fragment (1-158 aa; F1) and the C-terminal fragment (159-239 aa; F2) of Venus by polymerase chain reaction. These fragments were subcloned into a pcDNA 3.1 expression vector and a linker sequence (Gly-Gly-Gly-Gly-Ser) was inserted between the pcDNA 3.1 gatewayTM reading frame cassette and the Venus fragments. We obtained four gateway expression vectors (pVEN-F2N-DM, pVEN-F1N-DM, pVEN-F2C-DM, and pVEN-F1C-DM) from Eduard Stefan expressing a protein fused C- or N-terminally to the F1 or F2 Venus fragment, respectively. In order to generate gateway destination vectors from these expression vectors a BP-reaction with the donor vector pDONR221 was performed (see 2.2.4.8.1 Gateway BP-reaction). To obtain a destination vector with the backbone of the expression vector (ampicillin resistance gene) but the insert of the donor vector (ccdB suicide gene and chloramphenicol resistance gene) a ccdB-tolerant *E. coli* strain was transformed and colonies were grown on LB-agar supplemented with ampicillin and chloramphenicol.

### 2.2.3.7 Venus PCA assay

HEK 293 cells were seeded in greiner µclear 96well plates and cotransfected with 25 ng Venus F1 and 25 ng Venus F2 plasmid DNA per well as described above. One day after transfection, the DMEM medium was removed and cells were fixed using 2 % paraformaldehyde (PFA) in DPBS (2 % PFA). For this step 60 µl 2 % PFA were added to each well and plates were incubated for 15 minutes at room temperature in the dark. DAPI was diluted to a final concentration of 16 µg/ml in DPBS and 90 µl were added to each well after the 2 % PFA was removed. DAPI was removed after one minute, cells were washed once with 100 µl DPBS and wells were filled with 50 µl DPBS. Due to the low level of autofluorescence and high clarity of 96well µclear greiner plates they can be used in combination with a confocal microscope to screen for Venus positive cells. If two proteins interact and in which intracellular compartment the interaction takes place was determined using a fluorescence microscope (LSM 410-meta) at excitation wavelength 525 nm. If only fluorescent perinuclear structures without cytoplasmic fluorescence were observed the tested protein pair was regarded as non-interacting.

## 2.2.4 Molecular biology

### 2.2.4.1 Plasmid isolation from E. coli

#### 2.2.4.1.1 Custom 96well *E. coli* miniprep

This 96well miniprep protocol was used to produce DNA needed for LR-reactions, sequencing or yeast transformations. Deep well plates containing 2 ml LB-medium per well were inoculated with a single *E. coli* colony per well, sealed with a breathable sealing film and incubated in a shaker (Heydorf, 1000 rpm) at 37 °C. After 16-20 hours, glycerol stocks were created and cells were collected by centrifugation at 2500 rpm for 30 minutes at 4 °C. The supernatant was completely removed by tapping on a paper towel a couple of times before each pellet was resuspended in 300 µl cold Buffer P1 (including RNAse A) by vigorous vortexing for 2-3 minutes. Next, 300 µl Buffer P2 were added to each well and the resealed plates were mixed thoroughly by inverting the plates 3-4 times. After 5 minutes of incubation at room temperature, 300 µl Buffer P3 were added

to each well and the resealed plates were mixed thoroughly as described above. The lysate was cleared by centrifugation at 4000 rpm for one hour. The supernatant (750 µl) was transferred into the corresponding wells of a new deepwell plate. After 530 µl isopropanol were added, the new plate was sealed, mixed thoroughly and centrifuged for one hour at 4000 rpm at room temperature in order to precipitate the plasmid DNA. The supernatant was omitted and the plate was dried by tapping on a paper towel a couple of times before 1 ml 70 % ethanol were added to each well. The plate was sealed, mixed and centrifuged at 4000 rpm for 30 minutes at 4 °C. After removing the supernatant the pellets were air dried for 30-60 minutes and dissolved in 100 µl sterile water. The success of the miniprep was analyzed by BsrGI restriction analysis.

#### 2.2.4.1.2 Commercially available midiprep and miniprep kits

Commercially available miniprep kits (Qiagen) and midiprep kits (Promega) were preferred if only a small number of minipreps had to be done or if a large amount of plasmid DNA was needed, respectively. The volume of media used depended on the amount of DNA required; typically 3 ml were sufficient for a miniprep and 100 ml for a midiprep. DNA preps were undertaken according to the standard protocol in the manufactures guidelines.

### *2.2.4.2 Plasmid isolation from S. cerevisiae*

In order to validate the prey identities determined over the matrix position, prey plasmids were isolated from the diploid yeast spots grown on -HAULT 20 µM $Cu^{2+}$ agar. Yeast spots (0.5 cm in diameter) freshly grown on -HAULT 20 µM $Cu^{2+}$ agar were scraped off using an inoculation loop and stirred into 3 ml liquid -HAULT 20 µM $Cu^{2+}$ media. After vortexing, cells were grown for 16-20 hours in a shaker (250 rpm) at 30 °C. Yeast cultures were transferred into 2 ml microfuge tubes and cells were collected by centrifugation at 10.000 rpm for 5 minutes. The supernatant was completely removed by tapping on a paper towel a couple of times before each pellet was resuspended in 300 µl Buffer H1 (including Zymolase) by vigorous vortexing for 2-3 minutes. After incubation at 37 °C for 30 min, 300 µl Buffer P2 was added and mixed thoroughly. After 10 minutes of incubation at room temperature, 300 µl Buffer P3 was added and the mixed suspension was incubated on ice for 10 minutes. The lysate was cleared by centrifugation at 13.000 rpm for 10 minutes and was transferred into new microfuge tubes before 1 µl glycogen was added. After mixing 1 ml isopropanol was added and the samples were centrifuged for 45 minutes at 13.000 rpm at room temperature in order to precipitate the plasmid DNA. After the supernatant was omitted and the tubes were dried by tapping on a paper towel a couple of times, 500 µl 70 % ethanol were added. The tubes were mixed and centrifuged at 13.000 rpm for 30 minutes. After removing the supernatant the pellets were air dried for 30-60 minutes and dissolved in 5 µl sterile water. In order to gain a sufficient amount of plasmid DNA for BsrGI restriction analysis and sequencing, *E. coli* was transformed with the obtained plasmid DNA and a standard *E. coli* miniprep (2.2.4.1) was performed.

### *2.2.4.3 Restriction digest*

We used the restriction endonuclease Bsp1407I, a fast digest isoschizomer of BsrGI to control the success of minipreps and midipreps by restriction analysis. Typically 4 µl DNA sample were mixed with 16 µl restriction endonuclease mix (2 µl FastDigest Buffer, 0.1 µl FastDigest Bsp1407I, 13.9 µl $H_2O$) and incubated at 37 °C for 30 minutes prior to band size estimation by agarose gel electrophoresis.

### 2.2.4.4 Separation of DNA by agarose gel electrophoresis

Agarose gel electrophoresis was used for analytical purposes after restriction enzyme digestions. Agarose gels (1 %) were made by adding electrophoresis grade agarose to 0.5x TBE buffer. After the agarose was completely dissolved using a microwave, the solution was cooled down and agarose gels were poured. DNA samples of 250 ng were supplemented with Orange G sample buffer and loaded to agarose gels alongside with 5 µl of a 1 Kb Plus DNA ladder (Invitrogen) for band size estimation. After electrophoresis at 150 V for 45 minutes using 0.5x TBE as running buffer, the gels were stained for 15 minutes in a 1:20,000 dilution of SYBR Gold nucleic acid gel stain in 0.5x TBE. DNA bands were visualised using an ultraviolet light source.

### 2.2.4.5 Determination of DNA concentration

The concentration of DNA in aqueous solution was determined by measuring the absorbance at 260 nm in a spectrophotometer (NanoDrop ND-1000). Nuclease free water was used as standard and the absorbance of 1 µl DNA solution pipetted onto the NanoDrop pedestrial was measured.

### 2.2.4.6 DNA sequencing

Automated fluorescent DNA sequencing was performed by the in house sequencing service (MPI for Molecular Genetics) to verify ORF identity and reading frame of entry or destination vectors. The primers used for sequencing are listed in the material chapter (2.1.9.1).

### 2.2.4.7 Polymerase chain reaction (PCR)

#### 2.2.4.7.1 Site-directed mutagenesis

In order to introduce constitutively activating or inactivating point mutations into AKT1, site-directed mutagenesis was undertaken. The mutation of Ser473 and Thr308 to aspartate leads to phospho-mimicry and thus to constitutively active AKT1 (S473D T308D) whereas mutation of these residues to alanine leads to kinase dead AKT1 (S473A T308A) (Alessi, et al., 1996). Knowing that, primers with altered base pairs were designed to amplify the entire AKT containing vector (see 2.1.9.2). First, the Ser473 mutations were inserted by performing two separate PCR reactions with a wildtype AKT1 containing gateway entry vector (pDONR221). One PCR exchanged serine against alanine (Ser473A) and the other against aspartate (Ser473D). The introduction of these first mutations was validated by sequencing before a second PCR round was undertaken for introduction of the Thr308 mutations in the corresponding mutant AKT1 entry vectors. The PCRs were set up on ice and each 50 µl reaction contained 10 ng of AKT1 entry vector, 125 ng of each primer, 2.5 units of Pfu turbo DNA polymerase, 1 µl 2.5 mM dNTPs and 5 µl of 10x stratagene reaction buffer. Each reaction was adjusted to a final volume of 50 µl with sterile water and mixed before the reaction mixture was cycled in a PCR thermal cycler. The PCR was initialized by heating the reaction to a temperature of 95 °C for 30 seconds; before 18 cycles of denaturation (95 °C for 30 seconds), annealing (55 °C for 1 minute) and extension (68 °C for 4 minutes) were performed. We performed 18 cycles because this is the recommended number of cycles for introduction of a single amino acid change. For optimal yield, an extension time of 1 minute per kb is recommended and thus a 4 minute extension step was performed to amplify the AKT1 containing gateway entry vector (3787 bp). The reaction was stopped by cooling down to 4 °C and 1 µl of Dpn I restriction enzyme was added to each reaction prior to incubation at 37 °C for 1 hour. The Dpn I enzyme is specific to methylated DNA

and as most *E. coli* strains produce methylated DNA, the Dpn I enzyme digests only the parental DNA template but not the newly synthesized unmethylated mutant PCR product. The undigested mutant AKT1 containing gateway entry vectors were then used to transform competent cells (2.2.1.3). Clones showing the expected digestion pattern were sent for sequencing to verify the desired mutation.

#### 2.2.4.7.2 Two step PCR

In order to activate PKC isoforms catalytic domain fragments of PKCζ (592 aa) consisting of residues 238–592 and PKCα (672 aa) consisting of residues 330–672 were generated. These constructs are missing the inhibitory pseudosubstrate region and can be regarded as constitutively active (Crary, et al., 2006; Ranganathan, et al., 2007; Smith, et al., 2000). The C-terminal parts of the kinases were amplified and gateway recombination sites were added in two consecutive amplification steps. Gene-specific PCR primers were used to amplify the ORF in the first PCR round and to add minimal overhangs that contain part of the gateway attB-sequences. These overhangs were 5'AAAAAGCAGGCTTA[gene specific bases]3' for the forward primer and 5'AGAAAGCTGGGTC[gene specific bases]3' for the reverse primer (2.1.9.3). The second PCR round is carried out with two "universal gateway primers" that extend the attB-sequences and generate complete recombination sites (2.1.9.3). In the first amplification step, each 50 µl PCR reaction contained 150 ng of each gene-specific primer, 1 unit of phusion hot start DNA polymerase, 1 µl 10 mM dNTPs, 1.5 µl DMSO, 10 µl of 5x phusion reaction buffer and either 5 ng of PKCζ or PKCα entry vector. The reaction volume was adjusted to 50 µl with sterile water before the reaction mixture was cycled in a PCR thermal cycler. The PCR was initialized by heating the reaction to a temperature of 98 °C for 30 seconds; before 10 cycles of denaturation (98 °C for 8 seconds), annealing (62 °C for 23 seconds) and extension (72 °C for 45 seconds) were performed. After a final extension step for 8 minutes at 72 °C the reaction was cooled down to 4 °C. This first PCR product was used as template in a second PCR which was performed with the "universal gateway primers". For the second PCR reaction, 12.5 µl of the obtained PCR product were transferred into a new PCR tube and supplemented with the universal primers at 120 ng/reaction, 1 unit of phusion hot start DNA polymerase, 1 µl 10 mM dNTPs, 1.5 µl DMSO, 10 µl of 5x phusion reaction buffer. The PCR was initialized by heating the reaction to a temperature of 98 °C for 30 seconds, before 5 cycles of denaturation (98 °C for 8 seconds), annealing (45 °C for 30 seconds) and extension (72 °C for 45 seconds) were performed. After a further 20 cycles with increased annealing temperature (55 °C) and a final extension step (72 °C for 8 minutes) the reaction was cooled down to 4 °C. Before the PCR product was purified for the subsequent BP-reaction, its size and concentration was estimated using agarose gel electrophoresis.

#### 2.2.4.7.3 PCR Purification

PCR products were purified from agarose gels using a Qiagen QIAquick gel extraction kit according to the standard protocol in the manufactures guidelines. Briefly, the DNA band was excised from the gel using a clean scalpel and transferred to a clean microfuge tube. Furthermore, 300 µl buffer QG was added for every 100 µg agarose gel before the gel was dissolved at 50 °C for 10 minutes. In the next step, one gel volume of isopropanol was added and the mixture was applied to the QIAquick spin column through centrifugation for 1 minute. The bound DNA was washed with 750 µl buffer PE and residual ethanol was removed through centrifugation at top speed for 1 minute. The DNA was eluted in 30 µl endonuclease free water to avoid contamination.

### *2.2.4.8 Cloning with the gateway system*

#### 2.2.4.8.1 Gateway BP-reaction

Purified PCR products obtained from the two step PCR reaction were combined with the donor vector pDONR221 to generate an entry vector that can be used for shuttling the gene of interest between different expression vectors. BP-reactions were set up on ice. Each reaction was composed of 75 ng entry vector, 18 ng PCR product and 1 µl BP clonase enzyme mix II and was adjusted to a final volume of 5 µl with TE buffer. The reaction was mixed and incubated for 3-18 h at 25 °C before 0.5 µl of Proteinase K were added. The reaction was incubated for 10 minutes at 37 °C to inactivate the clonase enzyme prior to bacterial transformation or storage at -20 °C.

#### 2.2.4.8.2 Gateway LR-reaction

LR-reactions were performed to rapidly transfer the ORFs of interest into expression vectors for further studies. LR-reactions were set up on ice. Each reaction was composed of 75 ng destination vector, 200-300 ng entry vector, 1 µl LR clonase enzyme mix II and was adjusted to a final volume of 5 µl with TE buffer. The reaction was incubated at 25 °C for 3-18 hours to allow site specific recombination. After the addition of 0.5 µl Proteinase K solution to each reaction and incubation for 10 minutes at 37 °C, the reaction was directly used for bacterial cell transformation. Alternatively the reaction was stored at -20 °C.

## 2.2.5 Protein biochemistry

### *2.2.5.1 SDS-polyacrylamide gel electrophoresis (SDS-PAGE)*

In SDS-polyacrylamide gel electrophoresis (SDS-PAGE), proteins are separated largely on the basis of polypeptide length. In the Laemmli discontinuous gel system, two sequential gels are used. The top gel, called the stacking gel, is slightly acidic (pH 6.8) and has a low (5 %) acrylamide concentration to make a porous gel. The lower gel, called the separating or resolving gel, is more basic (pH 8.8) and has varying acrylamide concentrations depending on the expected size of the protein(s) to be analyzed. Gels were poured and assembled in a Mini-protean electrophoresis system (Bio-Rad). For a 20 ml resolving gel solution 5 ml 1.5 M Tris pH 8.8, 200 µl 10 % SDS, 150 µl 10 % APS and 15 µl TEMED were supplemented with 5 ml (10 %), 6 ml (12 %) or 7 ml (14 %) Rotiphorese Gel 40 (37.5:1) and adjusted to a final volume of 20 ml with water. 7 ml of this resolving gel solution were poured in between glass plates and isopropanol was placed above the gel to provide a smooth surface. After the gel was completely polymerized, the isopropanol was poured off. A standard 5 % acrylamide stacking gel (1.25 ml Rotiphorese Gel 40 (37.5:1), 1.25 ml 1 M Tris pH 6.8, 7.3 ml $H_2O$, 100 µl 10 % SDS, 100 µl 10 % APS and 20 µl TEMED) was added and the comb was placed into position at the top of the glass plates. Heat denatured protein samples in 4x SDS gel loading buffer (5-8 µl) were loaded alongside with 5 µl of a prestained protein ladder (PageRuler™ Plus, Fermentas) for band size estimation. Typically gels were run at 90 V for 15 minutes followed by 150 V for 40 minutes in 1x electrophoresis buffer. After gels were removed from the electrophoresis system, specific protein(s) were analyzed through western blotting whereas total protein content was determined through Coomassie blue or blue silver staining (see below).

### *2.2.5.2 Stain of protein gels*

#### 2.2.5.2.1 Coomassie blue stain

Gels were soaked in Coomassie blue stain on a rocker for 1 h at room temperature. Excess dye was eluted with destain solution. Stained gels were transferred to a light table and images were taken with a Canon EOS 400D camera.

#### 2.2.5.2.2 Blue silver stain

Gels were soaked in Blue silver stain until protein band were visible and excess dye was eluted with water. Stained gels were transferred to a light table and images were taken with a Canon EOS 400D camera.

### *2.2.5.3 Western blotting*

Proteins were transferred from the resolved gels to nitrocellulose or PVDF membranes using the Trans-blot SD semi-dry transfer cell (Bio-Rad) system. For that purpose six sheets Whatman 3 mm paper and one membrane at the size of the gel were soaked in transfer buffer and used for transfer stack assembly on the lower (positive) electrode plate of the blot cell. Three sheets of Whatman paper, the membrane, the gel and again three sheets of whatman paper were put on top of each other and air bubbles were removed by rolling over the transfer stack with a 10 ml pipette. The upper (negative) electrode plate was put on top of the stack and a constant current of 55 mA per gel was applied for one hour. The following incubation and washing steps were performed at room temperature under constant shaking unless otherwise stated. Membranes were washed once in TBS supplemented with 0.1 % (w/v) Tween 20 (TBST) before they were incubated for at least 1 hour in TBST supplemented with 5 % BSA (blocking buffer) to block unspecific binding. Subsequently, membranes were incubated for 1 hour at room temperature or overnight at 4 °C with a specific primary antibody diluted in blocking buffer. Afterwards, membranes were washed three times for 10 minutes in TBST prior to 1 h incubation with a secondary antibody diluted in blocking buffer. Again, membranes were washed three times for 10 minutes in TBST. Immunoreactive bands were visualized using a high resolution CCD camera (*i.e.* Fuji LAS 3000) according to the manufacturer's instructions. Depending on the secondary antibody 1 ml of the enhanced chemiluminescence (ECL) substrate western lightning plus-ECL (PerkinElmer) or 1 ml of the fluorimetric alkaline phosphatase substrate AttoPhos (Roche) were added. In contrast to the chemiluminescence detection method the chemifluorescence detection method requires illumination with blue LED light (460 nm) and a corresponding emission filter on the CCD camera (Y515-D). The dilutions used for each primary and secondary antibody are listed in chapter 2.1.7.

#### 2.2.5.3.1 Validation of firefly and PA fusion proteins

PA- and firefly-plasmid DNA corresponding to one clone were cotransfected in HEK 293 and expression of the two fusion proteins was assessed 24-36 hours later by immunoblotting. Protein A binds specifically to the Fc region of immunoglobulin (Ig) molecules of many mammalian species and shows strong affinity for rabbit IgGs. Consequently, PA fusion proteins were detected with a horseradish peroxidase coupled anti-goat-HRP antibody (derived from rabbit) in combination with an ECL substrate. HRP catalyzed the oxidation of the ECL substrate in the presence of chemical enhancers and caused the emission of light which was detected by a high resolution CCD camera (*i.e.* Fuji LAS 3000). Without any stripping or blocking steps in between the same

immunoblot was incubated with a second antibody suitable for the detection of firefly-V5 fusion proteins. The V5-tag was detected with alkaline phosphatase coupled anti-V5-APH antibody using AttoPhos (Roche) as fluorimetric substrate. Blots were illuminated with blue LED light (460 nm) and pictures were taken with a high resolution CCD camera (*i.e.* Fuji LAS 3000). With this procedure the PA- and the firefly-fusion of one protein can be controlled in one lane of the same immunoblot.

## 2.2.6 Construction and analysis of binary protein-protein interactions

### *2.2.6.1 Database curation*

When dealing with high-throughput data, it is crucial to minimize error through accurate and high quality data storage. All generated entry or destination vectors alongside with all tested Y2H interactions were stored in a relational database (SQL). To remove duplications or clarity issues, CloneIDs were used as unique identifier for each ORF. The CloneID was stored together with the clone position (bank, plate, row and column) and additional data (results of BsrGI restriction analysis and expression test, backbone vector). All tested Y2H interactions were recorded together with the corresponding screen-, agar- and plate-number including the plate-position as identifier and the final interaction result. This allows tested but negative results to be reported and simplifies the comparative and integrative analysis of the obtained data with reference datasets. We used the "global human physical protein interaction network" consisting of 80.922 physical interactions between 10.229 human proteins (Bossi and Lehner, 2009) and the interaction network identified by the Wanker laboratory (Max-Delbrück-Centrum for Molecular Medicine) as reference datasets. All unique identifiers were converted to EntrezGeneIDs and if two proteins interact on EntrezGeneID level in the reference and in the generated interaction dataset the interaction was counted as reported.

### *2.2.6.2 Cytoscape and yED Graph Editor*

Cytoscape version 2.6 was used for the visualization of the obtained PPI data in form of graphs. Graphs generated with Cytoscape were imported into the yED Graph editor for manual adjustments of the graphs. In the interaction networks generated here nodes represent proteins, while edges connecting these nodes represent biological interactions between these proteins.

# 3 Results

## 3.1 Identification of PPIs among associated disease proteins

### 3.1.1 Selection of proteins for PPI screening

Neurodegenerative diseases are characterized by progressive neuronal loss and synaptic abnormalities starting later in life which lead to decay of various mental and physical skills and premature death. Most NDs are marked by the abnormal accumulation of intra- or extracellular proteins (Hardy and Gwinn-Hardy, 1998) which are discussed to be the common reason for sporadic neurodegeneration (Soto, 2003). For instance, amyloid plaques and neurofibrillary tangles are the hallmarks of Alzheimer disease (Glenner and Wong, 1984), Lewy bodies accumulate in Parkinson's disease (Forno, et al., 1996; Spillantini, et al., 1997), nuclear aggregates appear in Huntington disease (DiFiglia, 1997) and superoxide dismutase accumulates in familial Amyotrophic Lateral Sclerosis (Bruijn, et al., 1998). In each of these cases, proteins that are found in the inclusions are known to cause familial forms of the disease if mutated. Although the familial forms explain only a very small fraction of ND cases, they are promoting the understanding of the molecular pathways involved in the common forms of ND and provide insights into the underlying molecular mechanisms. A further unifying feature of these protein aggregates is that they are Ub-positive, which probably results from incorporation of Ub-tagged proteins, if the degradative pathways are overwhelmed, which occurs during oxidative stress, endoplasmic reticulum stress and aging. Thus, aggregation and ubiquitination are central aspects of the biology of many neurodegenerative diseases, but their role and common mechanism have to be elucidated.

In order to analyze interactions of proteins related to neurological disorders in HTP-Y2H screens, we set out to clone 71 proteins reported to be associated with Alzheimer disease, Huntington disease, Parkinson's disease, Amyotrophic Lateral Sclerosis and Spinocerebellar Ataxia 1. Mutations in amyloid-β precursor protein (APP), huntingtin (HTT), the E3 ubiquitin protein ligase PARK2 (also known as parkin), α-synuclein (SNCA), soluble superoxide dismutase 1 (SOD1), presenilin 1 (PSEN1), the TAR DNA binding protein TARDBP, ataxin 1 (ATXN1) and ataxin 3 (ATXN3) are known to be related to these five diseases, respectively. These 9 proteins were represented by 25 clones in our study, including full length clones with or without disease-causing mutation and fragments. The residual 62 proteins were manually selected from the OMIM database because of their genetic relation to other neurological disorders. These 62 proteins were represented by 71 clones because nine proteins were represented by different full length clones, fragments or isoforms. Based on results of prior Y2H screens autoactivating bait clones were directly excluded. All cDNAs were obtained from Pablo Porras (Wanker laboratory, Max-Delbrück-Centrum for Molecular Medicine) as N-terminal LexA fusions in the gateway destination vector pBTM116-D9. All clones showed the expected digestion pattern. The ORF identity and reading frame was verified by 5' and 3' tag-sequencing. The selected disease-associated bait proteins were used in modified Y2H screens (3.1.4) in order to determine interaction partners.

### 3.1.2 Selection and constitutive activation of human kinases

Reversible posttranslational modifications modulate protein functionality and subsequently cellular responses. The covalent attachment of different functional groups (acetate, phosphate, lipids, and carbohydrates) occurs in consequence to changing conditions. Phosphorylation usually effects serine (Ser), threonine (Thr), and tyrosine (Tyr) residues in eukaryotic proteins and can turn a hydrophobic part of a protein over the addition of a

phosphate ($PO_4$) molecule into a polar and hydrophilic part. This can change the protein conformation, the interaction pattern and/or the enzymatic activity indicating that phosphorylation is an important regulatory mechanism (Olsen, et al., 2006). Kinases and following phosphorylation-dependent protein interactions are known to regulate the majority of cellular pathways, especially those involved in growth control. Interestingly, these are known to be deregulated in neurological disorders (Blume-Jensen and Hunter, 2001; Brunet, et al., 2001; Yuan and Yankner, 2000), for example, phosphorylation of ataxin 1 by AKT1 regulates binding to 14-3-3 and mediates neurodegeneration in Spinocerebellar Ataxia 1 (Chen, et al., 2003). Another example are PKC family members which are involved in induction and maintenance of long-term potentiation (LTP), which is the common physiological model of memory storage. Insufficient RTK signalling is also associated with the development of neurological diseases, such as multiple sclerosis and Alzheimer's disease (Bublil and Yarden, 2007).

In order to investigate Ser/Thr kinase-dependent protein interactions we decided to clone AKT1 and the two PKC isoforms PKCζ and PKCα. For Tyr kinase-dependent protein interactions four Tyr kinases from three different families were chosen: ABL2 (ABL-family member), TNK1 (ACK-family member), FYN and HCK (SRC-family members). Generally, kinases can get activated by the deletion of autoinhibitory domains or by the introduction of phosphorylation mimicking point mutations (Kemp and Pearson, 1991; Kurmangaliyev, et al., 2011; Nagata, et al., 2009; Soderling, 1993; Tarrant and Cole, 2009). Mutation of Ser473 and Thr308 to aspartate leads to phospho-mimicry and thus to constitutively active AKT1 (Akt DD, S473D T308D) whereas mutation of these residues to alanine leads to kinase dead AKT1 (Akt AA, S473A T308A) (Alessi, et al., 1996) (Figure 5).

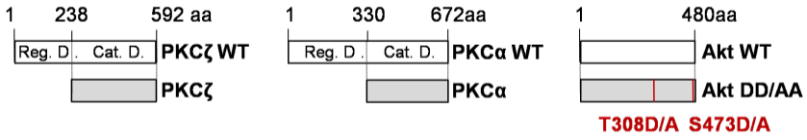


**Figure 5: Schematic diagram showing wildtype (white) and constitutively active (grey) kinases.**

The generated catalytic domain fragments of PKCζ WT (592 aa) and PKCα WT (672 aa) consists of residues 238–592 (PKCζ) and residues 330–672 (PKCα), respectively. AKT1 WT was activated by mutation of Ser473 and Thr308 to aspartate (AKT DD) or inactivated by mutation of these residues to alanine (AKT AA).

Quick change site-directed mutagenesis was employed to directly introduce these mutations. The mutations were inserted one after the other in a wildtype AKT1 containing gateway entry vector (pDONR221) in two separated, sequential PCR reactions. The introduction of the first mutation was validated by sequencing before the second PCR was undertaken to introduce the second mutation. Both, the inactive and active AKT1 double mutant (Akt AA and Akt DD) were successfully generated. In contrast to AKT1, PKC kinases were activated by the deletion of the autoinhibitory domain. All PKC isoforms share a pseudosubstrate region, which is bound to the substrate-binding cavity in the catalytic domain keeping the enzyme inactive. The second messenger requirements for the release of this autoinhibitory pseudosubstrate region differ between the PKC isoforms due to differences in the regulatory region (Newton, 1995). Both, naturally occurring (PKMζ (Crary, et al., 2006)) and artificially generated (Ranganathan, et al., 2007; Smith, et al., 2000) catalytic domain fragments of PKCζ are persistently active. In order to activate PKCζ and PKCα, we generated catalytic domain fragments of PKCζ (592 aa) consisting of residues 238–592 and PKCα (672 aa) consisting of residues 330–672 (Figure 5). The C-terminal parts of the kinases were amplified in a two step PCR and transferred to the entry vector (pDONR221) in a BP-reaction. Both PKCα and PKCζ catalytic domain fragments showed the expected digestion

pattern and 5' and 3' sequencing validated truncation and reading frame. The mutant AKT1, PKCα and PKCζ cDNAs were shuttled from gateway entry vectors to gateway destination vectors, *i.e.* $Cu^{2+}$-inducible yeast expression vectors without (pASZ-C) or with (pASZ-CN) N-terminal nuclear localisation sequence (NLS). Wildtype, full length clones of ABL2, FYN, HCK and TNK1 were obtained in these gateway destination vectors (Arndt Grossmann, Stelzl laboratory, MPI for Molecular Genetics). All clones showed the expected digestion pattern. The ORF identity and reading frame was verified by 5' and 3' tag-sequencing. The selected human kinase constructs were analyzed in order to determine if they are active in yeast (3.1.3) and suitable for the modified Y2H system.

### 3.1.3 Activation of human PKCα, PKCζ and AKT1 in yeast

To test the activation of the generated human kinase mutants (Figure 5) in yeast, the MATa yeast strains (L40c and L40ccU2) (Goehler, et al., 2004) were individually cotransformed with one of the kinase plasmids (PKCα+NLS, PKCζ+NLS, no kinase+NLS) and a bait plasmid (LexA-DBD fusion, pBTM116-D9) encoding CBL. After mating with a MATα strain (Goehler, et al., 2004) expressing the known CBL interactor CRK as prey (Gal4-AD fusion, pACT4-DM) L40c and L40ccU2 colonies grown on -HAULT medium supplemented with 20 µM $Cu^{2+}$ were pooled. The activity of the kinases was assessed by immunoblotting with anti-PKC-substrate antibody, which should recognize phosphorylated yeast proteins serving as substrate for the human PKC kinases (Figure 6). The catalytic domain fragments of PKCα (342 aa, 38 kDa) and PKCζ (354 aa, 39 kDa) are constitutively active. In contrast to an empty kinase vector, these kinases induce the phosphorylation of proteins at 25 kDa (arrow). Kinase activity in the absence of 20 µM $Cu^{2+}$ could be explained by promoter leakage, maybe caused by low $Cu^{2+}$ content in the nitrogen base used for media preparation. Induction with 20 µM $Cu^{2+}$ leads to enhanced kinase expression and stronger phosphorylation of yeast proteins at 25 kDa. The nuclear localization sequence has no influence on the activity of the PKCα and PKCζ catalytic domain fragments (data not shown), thus all generated PKCα and PKCζ kinase plasmids could be used in a modified Y2H system.

AKT1 activity was investigated by transforming yeast strain W303 with one of the AKT1 kinase plasmids (AKT1 DD+NLS, AKT1 AA+NLS, AKT1 WT+NLS, no kinase+NLS). The W303 yeast strain is known to yield relatively high protein expression (Markus Ralser, personal communication). Transformed W303 colonies grown on selective medium supplemented with 200 µM $Cu^{2+}$ were lysed and AKT1 activity was assessed by immunoblotting with anti-AKT-substrate antibody. The AKT1 mutants showed no differential activity under these conditions (Figure 6). This is in agreement with results from Rodriguez-Escudero *et al.* (Rodriguez-Escudero, et al., 2005), which also failed to identify differences between extracts of control yeast cells and yeast cells expressing AKT1 by immunoblotting with an anti-AKT-substrate antibody. They revealed that AKT1 is phosphorylated at Thr308 and Ser473 in yeast and conclude that endogenous yeast kinases phosphorylate and activate AKT1 but that efficient AKT1 substrates are absent in yeast (Rodriguez-Escudero, et al., 2005). However, the AKT1 specific signals could also be masked by the generally high Ser/Thr phosphorylation levels observed in the yeast background (Breitkreutz, et al., 2010; Mok, et al., 2010; Ptacek, et al., 2005). We observed that some Tyr kinases lead to kinase-dependent interactions in a modified Y2H without showing detectable tyrosine phosphorylation levels in yeast (Arndt Grossmann, personal communication) and consequently we did not exclude AKT1 from the modified Y2H screen. The selected human kinases were considered to be active in yeast and were used for the detection of kinase-dependent interactions in the modified Y2H system (3.1.4).

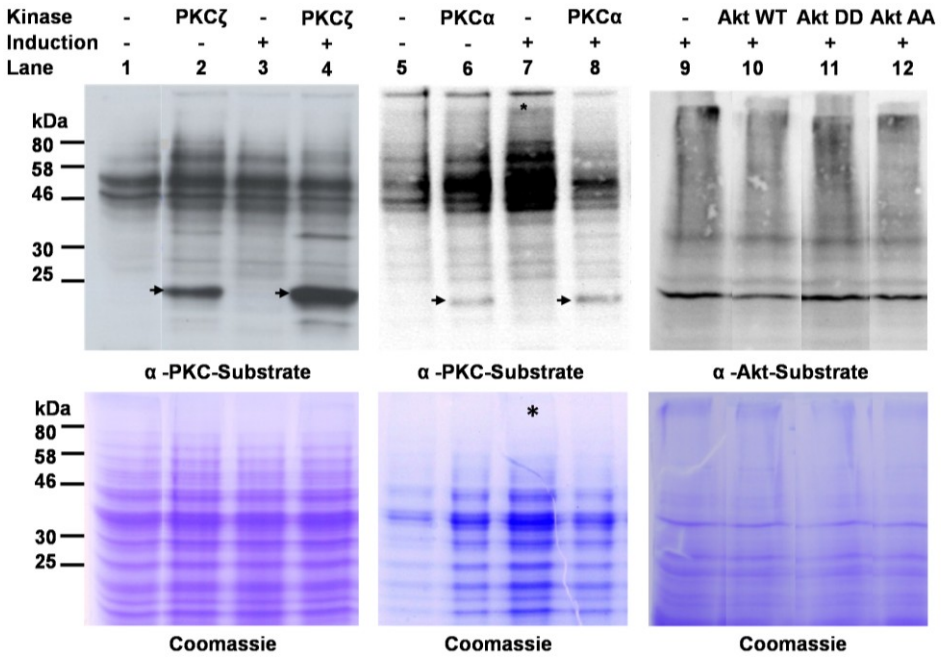


**Figure 6: Activity of human kinases expressed *S. cerevisiae*.**

Total cell lysate prepared from different yeast strains expressing NLS-tagged versions of human kinases were analyzed by immunoblotting using anti-PKC- or anti-AKT-substrate antibodies. The protein load was determined by performing coomassie gels in parallel.
**PKC blots,** diploid yeast colonies (representing the interacting bait-prey pair CBL-CRK) carrying a $Cu^{2+}$ inducible kinase vector (pASZ-CN) containing no kinase (lanes 1,3,5,7), a catalytic domain fragment of PKCζ (lanes 2,4) or catalytic domain fragment of PKCα (lanes 6,8) were grown on -HAULT agar supplemented with 20 µM $Cu^{2+}$ (kinase induction) or not (no induction). Diploid L40c and L40ccU2 colonies were pooled, lysed and the activity of PKC was assessed by immunoblotting with anti-PKC-substrate antibody (Cell signalling #2261, dilution 1:2500). Phosphorylation of yeast proteins at 25 kDa (arrow) was observed if PKCζ or PKCα were transformed and was enhanced by induction of kinase expression which suggests that both catalytic domain fragments are constitutively active. *Indicates higher protein load in the control yeast cell lysate than in the PKC expressing yeast cell lysate. Note that even under these conditions no phosphorylated yeast proteins at 25 kDa are visible in the control.
**AKT1 blots,** colonies of the yeast strain W303 carrying a $Cu^{2+}$ inducible kinase vector containing no kinase (lane 9), wildtype AKT1 (lane 10), constitutively active AKT1 (lane 11, AKT DD) or inactive AKT1 (lane 12, AKT AA) were grown on selective media supplemented with 200 µM $Cu^{2+}$ for kinase induction. Colonies were lysed and the activity of AKT1 was assessed by immunoblotting with anti-AKT-substrate antibody (Cell signalling #9611, dilution 1:2500). Differences in kinase activity between wildtype, inactive or constitutively active AKT1 were not detected under these conditions.

### 3.1.4 Development of the modified Y2H system and screening setup

Our aim was to identify kinase-dependent interactions of proteins associated with neurological disorders in a modified Y2H system. For that purpose combinations of disease-associated bait proteins (LexA fusions) and constitutively active human kinases were screened against a prey matrix. Tyrosine kinase-bait combinations were screened against 142 preys which contain known pTyr-binding modules, like SH2 or PTB domains (Schlessinger and Lemmon, 2003) and bait combinations with Ser/Thr kinases were screened against a prey matrix containing 13.910 prey proteins (Figure 7). This enables the identification of new pSer/pThr-binding domains because several families of pSer/pThr-binging motifs with remarkable differences in protein fold and phosphate group recognition mode have been identified so far (Yaffe, 2002). In order to proceed with the Y2H screen, the MATa yeast strains (L40c and L40ccU2) were individually cotransformed with one kinase (pASZ-C or pASZ-CN) and one bait (pBTM116-D9) plasmid using a high efficiency yeast transformation protocol as described in materials and methods. On clone level 768 combinations of 96 bait clones with 8 Ser/Thr kinase clones (AKT1_DD+/-NLS, PKCα+/-NLS, PKCζ+/-NLS, no kinase+/-NLS) or 8 Tyr kinase clones (ABL2+/-NLS, FYN+/-NLS, TNK1-NLS, HCK+NLS, no kinase+/-NLS) were generated. The use of two different MATa yeast strains (L40c and L40ccU2) doubled this amount to 3072 combinations on clone-strain level.

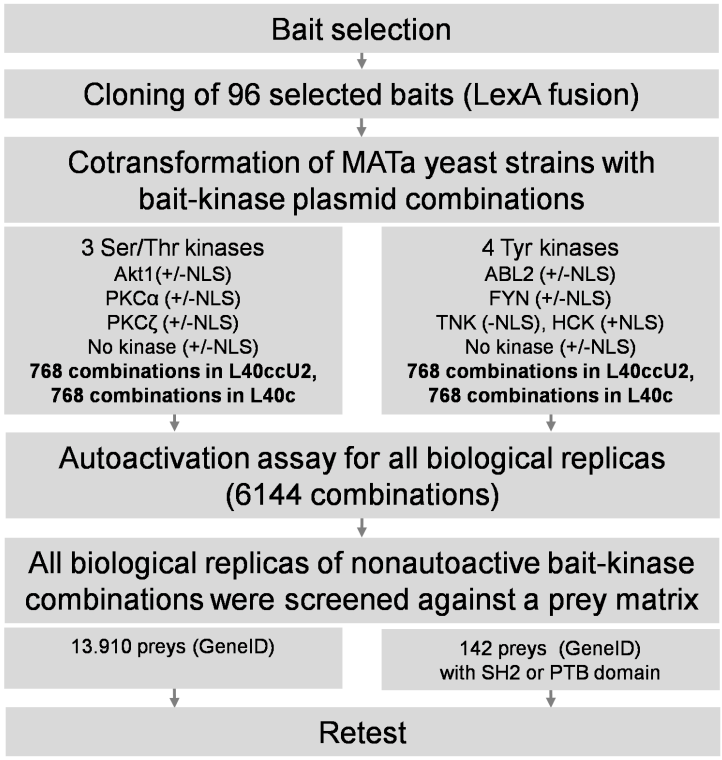


**Figure 7: Schematic depiction of the experimental flow.**

First, proteins involved in neurological disorders were selected and N-terminal LexA fusions (pBTM116-D9) were generated. In a second step, MATa strains were individually cotransformed with combinations of bait and kinase plasmids (pASZ-C or pASZ-CN) and tested for autoactivity. After removal of autoactive baits, baits were pooled and screened against a previously prepared prey matrix. Baits cotransformed with Ser/Thr kinases were screened against a matrix containing 13.910 prey proteins, whereas the same baits cotransformed with Tyr kinases were screened against a prey matrix containing 142 prey proteins with pTyr-binding domains. Preys that were positive in this primary screen were retested in an independent second experiment with fresh yeast in order to identify the interacting baits in the pool.

The use of two independently transformed yeast colonies of each strain leads to a final 6144 combinations on clone-strain-copy level. These four biological replicas are valuable controls because they were screened separately (see later in Figure 9) and consequently enhanced the quality of the Y2H signal. All 6144 yeast colonies were successfully generated (determined by the ability to grow on selective media) and were tested for autoactivation of reporter genes after mating with MATα strain carrying a prey plasmid (Gal4-AD fusion, pACT4-DM) without insert. Autoactivation is operationally defined as detectable bait-dependent reporter gene activation in the presence of any prey plasmid, even without insert (Walhout and Vidal, 1999). From the 96 bait clones only one (HTT e-HD506-Q23) showed autoactivation. Since 20 % of randomly selected full length bait ORFs tend to be autoactive (Nakayama, et al., 2002; Uetz, et al., 2000), this was a very low fraction and reflected the selection of nonautoactive bait clones in the first place. HTT e-HD506-Q23 was removed in all kinase, strain and copy combinations to avoid growth in the absence of true prey-dependent reporter gene activity in the Y2H screen. Nonautoactive bait-kinase combinations were screened against the prey matrix in order to obtain kinase-dependent interactions (3.1.5/3.1.6).

### 3.1.5 Identification of Ser/Thr kinase-dependent interactions

To find Ser/Thr kinase-dependent protein interactions with the selected disease-associated baits, yeast strains coexpressing kinase-bait combinations were screened against individually arrayed prey strains expressing one of 13.910 different prey proteins. This prey matrix was shared with the Wanker laboratory (Max-Delbrück-Centrum for Molecular Medicine). They extended an 5.632 prey clone containing Y2H matrix (Stelzl, et al., 2005) with prey clones generated from ORFs of the Invitrogen human ORF clone collection and the human MGC ORF collection (Rual, et al., 2004). The final collection of 16.857 prey clones (representing 13.910 proteins) included most of the currently available human full length cDNAs and covered over 65 % of the human protein coding genes, annotated with an EntrezGeneID (20.871). Over 1.5 million pairwise interaction tests would be needed to separately screen the 95 nonautoactive baits once against every strain in the prey matrix. Eight times more pairwise interaction tests need to be done if the 8 generated bait clone-kinase clone combinations per bait would be screened separately. To reduce screening effort and costs the 95 bait clones were divided in 4 pools consisting of 23-24 bait clones (representing 16 to 19 proteins). Every pool contained all generated bait clone-kinase clone combinations of a protein. Bait-kinase strains were grown separately and the strains which were tested together in one pool were combined directly before mating (Figure 8). Each prey was mated with each pool of baits and primary protein-protein interactions were identified after transfer to -HAULT medium supplemented with 20 µM $Cu^{2+}$. This pooling strategy required a retest to determine the prey-interacting bait in the pool and to decide if the obtained interaction is kinase-dependent.

The screen was repeated four times using four biological replicas (Figure 9). All together 16 screens (four biological replicas of 4 pools) were performed. In order to exclude autoactive/"sticky" preys from the retest, preys that showed up in more than 11 of these screens or with all 4 pools were excluded. Residual preys that show up in at least two of the four replicas of one pool were considered for the retest. These criteria were fulfilled by 56 prey clones (representing 56 proteins) which were consequently retested against the bait pool(s) they were interacting with. Of them, 50 prey proteins were retested against one bait pool and six prey proteins were retested against two different bait pools. For this purpose all bait-kinase combinations of one pool and of the same MATa yeast strain were individually arrayed in 384well plates (Figure 9). Two 384well plates (one for each MATa yeast strain) containing the 24 bait-kinase combinations of a pool in identical configuration were generated. Biological replicas were grown in diagonally positioned quadrants to avoid growth interference. This was crucial because the decision if the observed interaction is kinase-dependent or not, is based on negative growth signals. Biological replicas and growth interference control were important to rule out that missing growth reflects a false-negative signal and to confirm that missing growth is indeed caused by the lack of kinase coexpression.

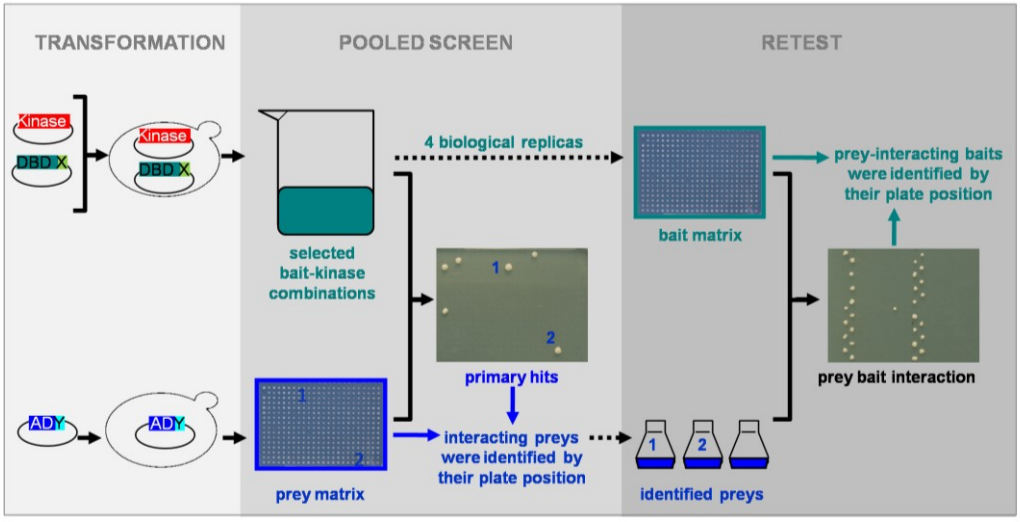


**Figure 8: Schematic workflow of the pooled Y2H screen.**

MATa strains individually cotransformed with bait-kinase plasmid combinations were grown separately and the bait-kinase combinations belonging to one pool were merged directly before mating. Each pool was individually mated with all preys of the 384well matrix and 5 days after transfer to -HAULT 20 µM $Cu^{2+}$ medium, the interacting preys were identified by their matrix position. For the retest, nonautoactive preys that show up with at least two of the four replicas of one pool were grown separately and retested against the arrayed baits of this pool. Five days after transfer to -HAULT 20 µM $Cu^{2+}$ medium, the interacting baits were identified by their position in the 384well plate.

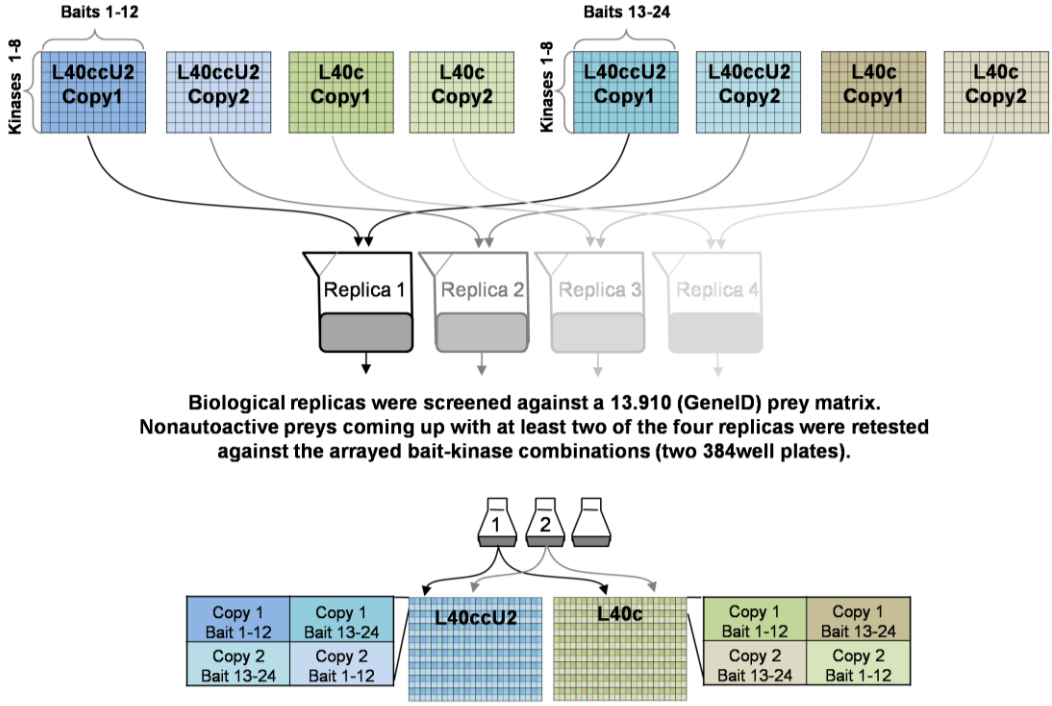


**Figure 9: Pooling strategy to screen for Ser/Thr kinase-dependent interactions.**

For each bait-kinase combination four replicas, represented by two independently transformed yeast colonies of two MATa strains (L40c and L40ccU), were generated using a high efficiency 96well yeast transformation protocol. Each bait was coexpressed with 8 kinases (one 96well plate column), thus the four replicas of 95 baits encompass 32 96well plates. In each plate columns correspond to one bait and rows to one kinase. The pooling strategy is exemplarily shown for one pool (8 plates). To screen for Ser/Thr kinase-dependent interactions 24 baits were tested together in one pool and were combined directly before mating. The four independent replicas of one pool were screened separately against the 13.910 (GeneID) prey matrix. Nonautoactive preys that show up with at least two of the four replicas of one pool were retested against the arrayed bait-kinase combinations of this pool in order to identify interacting baits and to determine kinase dependency. The retest was performed with fresh yeast in an independent second experiment. The baits 1-12 were arrayed into the first and fourth quadrant and baits 13-24 into the second and third quadrant. Prey strains were grown separately and mated with baits arrayed in 384well matrix format. Protein-protein interactions were identified after transfer to -HAULT medium supplemented with 20 µM $Cu^{2+}$.

Exemplarily the interaction between ASB3 and PARK7 is shown which occurs only in the presence of AktDD (Figure 10, C). In contrast to PARK7, the other baits NEFL (FL) and PRPH interact irrespective of whether a kinase is coexpressed or not. These interactions are represented by up to 16 independently grown colonies (Figure 10, B). Additionally, the original selective Y2H plates (three plates with 384 spots each) are shown (Figure 10, A). These plates give a detailed overview of the KRT19, NEFL (1-286 aa) and ASB3 interactions with the bait proteins NEFL (FL, 544 aa), PRPH and PARK7. Importantly only 10 %, 9 % and 5 % of the tested preys interact with NEFL (FL), PRPH or PARK7, respectively. Additionally, for each of these three bait proteins one unique interaction partner was identified as well, which demonstrates the specificity of the obtained Y2H results. All together 48.000 pairwise interaction tests were performed. Of the 56 retested preys, 43 preys were found to interact, 12 showed signs of autoactivity and one did not gave an interaction signal at all. For 27 of the 71 bait proteins (32 of the 95 bait clones) associated with neurological disorders an interaction partner was identified, the remaining 44 bait proteins did not result any interaction. In total this screen revealed 75 unique interactions among 70 proteins (see later in Figure 13).

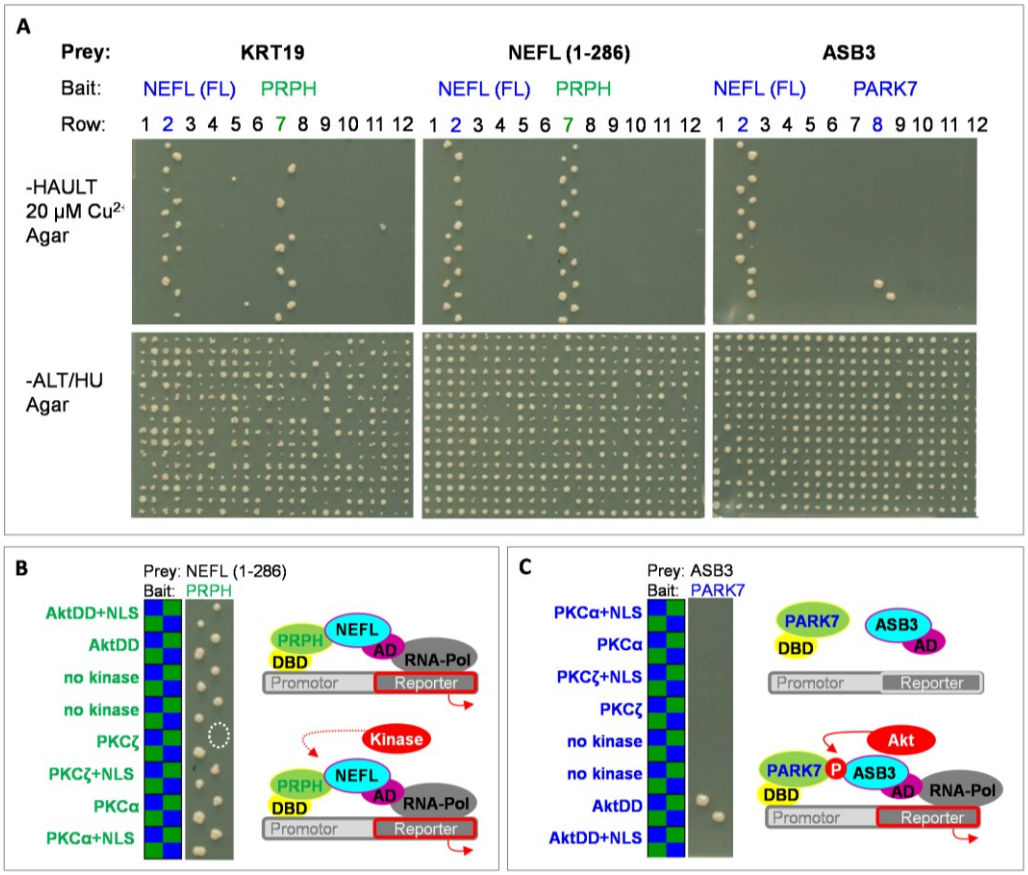


**Figure 10: Identification of modification-independent and kinase-dependent interactions.**

**A,** Three selective Y2H plates of a retest experiment are exemplarily shown. The preys KRT19, NEFL (1-286 aa) and ASB3 were mated with a 384well plate that contains 24 baits in two replicas. Colonies grown on -ALT/HU agar indicate diploid mated yeast and colonies on -HAULT 20 µM $Cu^{2+}$ agar an interacting bait-prey pair. All three preys interact with the NEFL (FL) expressing bait strain located in the second row (first/fourth quadrant) of the plate. Additionally, KRT19 and NEFL (1-286 aa) interact with the PRPH expressing bait strain located in the seventh row (second/third quadrant) whereas ASB3 interacts with the PARK7 expressing bait strain located in the eighth row (first/fourth quadrant). Full length NEFL (data not shown), PRPH and PARK7 only interact with selected preys which demonstrates the specificity of the used Y2H system. The row-kinase mapping differs between the first/fourth (baits depicted in blue) and the second/third (baits depicted in green) quadrant.
**B,** Independent interactions occur irrespective if a kinase is coexpressed or not. Exemplarily the interaction between PRPH and NEFL (1-286) is shown, which is represented by 15 of 16 independently mated and selected colonies in the second and third quadrant (green).
**C,** Kinase-dependent interactions occur if a specific kinase is coexpressed but not in the absence of kinase expression. Exemplarily, the kinase-dependent interaction between ASB3 and PARK7 is shown, which only occurs if constitutively active AKT (AKTDD, first/fourth quadrant-marked in blue) is coexpressed.

### 3.1.5.1 PARK7 interacts in a Ser/Thr kinase-dependent manner with ASB3, RNF31 and c11orf16

We detected three Ser/Thr kinase-dependent interactions with the Parkinson's disease-associated bait protein PARK7. Ring finger protein 31 (RNF31), ankyrin repeat and SOCS box containing 3 (ASB3) and chromosome 11 open reading frame 16 (c11orf16) interacted preferentially with PARK7 if PKCα+NLS or AKT1 DD were coexpressed (Figure 11).

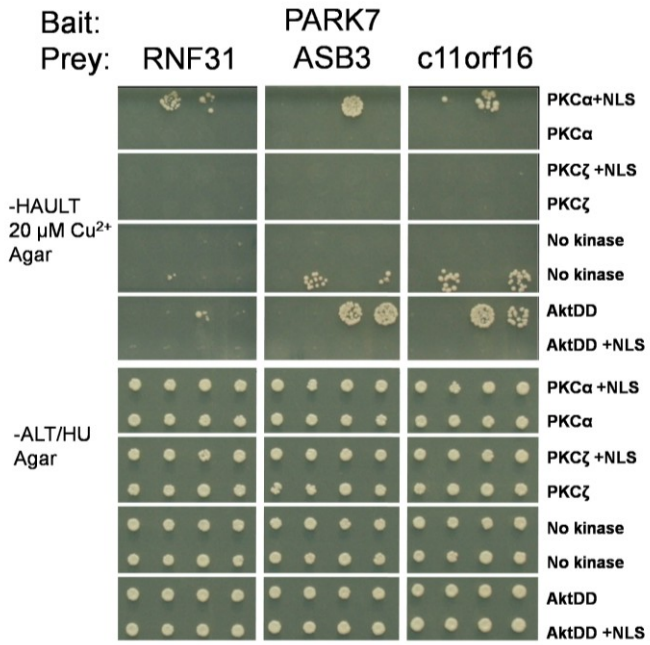


**Figure 11: PARK7 interacts in a kinase-dependent manner with ASB3, RNF31 and c11orf16.**

The preys RNF31, ASB3 and c11orf16 were positive in the primary screen and after retesting with the arrayed bait-kinase combinations in 384well format, PARK7 was identified as their interaction partner. In order to reproduce the characteristic growth patterns indicative for a kinase-dependent interaction, liquid cultures of the corresponding diploid yeast colonies were generated and 5 µl were dropped onto -ALT/HU and -HAULT 20 µM $Cu^{2+}$ agar in 96well format. The four rows shown for each prey correspond to four biological replicas of the PARK7 expressing bait strain. Colonies grown on -ALT/HU agar indicate diploid mated yeast and colonies grown on -HAULT 20 µM $Cu^{2+}$ agar an interacting bait-prey pair. Interactions with PARK7 were mediated by PKCα+NLS or constitutively active AKT (AKTDD). Weak growth without kinase expression was also observed in some cases.

The prey identities determined through the matrix position were validated. Therefore, prey plasmids were isolated from the obtained diploid yeast spots corresponding to the PARK7-RNF31, PARK7-ASB3 and PARK7-c11orf16 interactions able to grow on -HAULT 20 µM $Cu^{2+}$ medium. For ASB3 and c11orf16 the obtained plasmid DNA has been used successfully for transformation of *E. coli*, in the case of RNF31 repeatedly no *E. coli* colonies were obtained. As expected, sequencing verified that prey plasmids encoding c11orf16 and ASB3 were present in the diploid yeast. The identity of RNF31 was validated by direct sequencing of the prey plasmid used for MATα transformation. We concluded that RNF31, ASB3 and c11orf16 interact with PARK7 and searched for domains and Ser/Thr residues which could mediate the kinase-dependency (3.1.5.2).

### 3.1.5.2 Thr154 is a mapped PARK7 phosphorylation site and a predicted PKC site

In order to determine which Ser/Thr residues in ASB3, RNF31, c11orf16 or PARK7 could be responsible for the detected kinase-dependent interactions we used Phosphosite (Hornbeck, et al., 2004), Phosida (Gnad, et al., 2007) and PhosphoELM (Dinkel, et al., 2011) to search for known Ser/Thr phosphorylation sites. To determine which kinases would recognize the motifs surrounding the identified phosphorylation sites, we used NetworKIN (Linding, et al., 2007).

RNF31 (1072 aa) also known as HOIL1 interacting protein (HOIP) consists of three N-terminal zinc finger domains (ZnF_RBZ), one ubiquitin-associated domain (UBA), one RING domain, one in-between-RING domain (IBR) and either another IBR domain or due to overlapping domains another RING domain (see later in Figure 22). With this domain structure RNF31 was classified as RING-in-between-RING (RBR) protein family member (Marin, et al., 2004). Between the three ZnF_RBZ domains and the UBA domain one phosphorylation site (Ser466) was detected (Dephoure, et al., 2008) and ribosomal S6 kinases are predicted for mediating phosphorylation of this residue. The Ser/Thr kinase-dependent interaction with PARK7 occurred with a C-terminal RNF31 fragment (484-1072 aa) containing the UBA, the RING and the two IBR domains (named RNF31 UBA-IBR-IBR further on) but not the Ser466. The Ser/Thr kinase-dependent interaction between ASB3 and PARK7 occurred with a full length clone of ASB3 isoform 1 (518 aa) containing the N-terminal ankyrin repeats and the C-terminal SOCS box. For human ASB3 no phosphorylation sites are annotated but in mice Ser35 is found to be phosphorylated (Huttlin, et al., 2010). ASB3 Ser35 phosphorylation is predicted to be mediated by PKA-family members. The c11orf16 clone corresponds to the full length protein (404 aa) which does not contain any known domains or phosphorylation sites. All identified kinase-dependent interactions occur with full length PARK7 (189 aa) which has three annotated phosphorylation sites: Ser142 (Gnad, et al., 2007), Thr154 and Ser155 (Huang, et al., 2007). Whereas for PARK7 residues Ser142 and Ser155 no kinase family prediction was obtained, PARK7 Thr154 phosphorylation is predicted to be mediated by PKC-family members. This residue might mediate all three observed kinase-dependent interactions. However, this would imply that RNF31, ASB3 and c11orf16 contain three unknown and likely very different pSer/pThr-binding domains. Otherwise, PARK7 phosphorylation induced conformational changes which enabled PARK7 to interact with these three interaction partners.

## 3.1.6 Identification of Tyr kinase-dependent interactions

### 3.1.6.1 PIK3R3 interacts in a Tyr kinase-dependent manner with NF2 and PARK7

SH2 and PTB domains recognize proteins that have been phosphorylated on tyrosine residues in a sequence-specific fashion. To investigate Tyr kinase-dependent protein interactions, the selected disease-associated baits were coexpressed with Tyr kinases and screened against preys containing pTyr-binding domains. In this screen the prey matrix encompassed 142 prey proteins (represented by 297 clones) including 96 proteins with SH2 domain(s) (represented by 205 clones), 29 proteins with PTB domain(s) (represented by 59 clones) and 5 proteins (represented by 9 clones) with both of these domains. Ten proteins (represented by 18 clones) with pleckstrin homology (PH) or PH-like domains were included because PTB domains are structurally similar to PH domains and can be considered as part of the PH domain superfamily (Eck, et al., 1996; Zhou, et al., 1995). Additionally, two non-RTKs (represented by 6 clones) without known pTyr-binding domains were included. In the prey matrix every protein was represented two or more times by different clones or by independently

transformed prey strains expressing the same clone. To reduce screening effort, the 95 nonautoactive bait clones were divided in 8 pools of 11-12 bait clones (representing 8 to 11 proteins). Every pool contained all bait clone-kinase clone combinations of a bait protein. As described before (Figure 8) bait strains were grown separately, pooled, mated and primary protein-protein interactions were identified after transfer to -HAULT medium supplemented with 20 µM $Cu^{2+}$. All together 128 screens (8 pools in 16 replicas) were performed. For each pool the screen was repeated 16 times by mating of the four biological replicas with four technical copies of the 384well prey matrix. To convolute which baits in a pool are interacting with the prey and to determine if this interaction is kinase-dependent a retest was performed. Preys that showed up in more than 107 of these 128 screens were excluded from the retest. Residual preys that show up in at least two of the 16 replicas of one pool were considered for the retest. Thirteen prey clones (representing 6 SH2 domain proteins and 2 PTB domain proteins) fulfilled these criteria and were retested against the bait pool(s) they were interacting with. Four prey clones (representing 2 proteins) were retested against more than one bait pool. The retest identified 15 unique interactions among 10 bait proteins (represented by 12 clones) associated with neurological disorders and 8 SH2 or PTB containing prey proteins. Two of these interactions were kinase-dependent and occurred with PIK3R3 (also known as p55γ) which is a regulatory subunit of the phosphoinositide 3-kinase (PI3K). The interaction between the SH2 domain containing prey PIK3R3 and the Parkinson's disease-associated bait PARK7 or the neurofibromatosis type 2-associated bait NF2 were only detected if Tyr kinases were coexpressed (Figure 12). Both interactions were detected in the presence of ABL2+NLS or HCK+NLS; interactions with PARK7 also occurred if ABL2 without NLS or FYN+NLS were coexpressed. For validation of PIK3R3 identity, prey plasmids were isolated directly from the obtained diploid yeast spots growing on -HAULT 20 µM $Cu^{2+}$ medium and used for the transformation of *E. coli*.

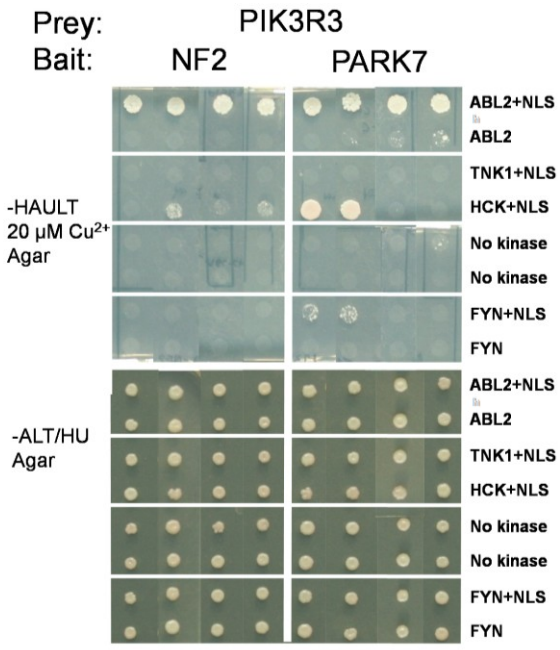


**Figure 12: PIK3R3 interacts in a kinase-dependent manner with PARK7 and NF2.**

Two independent prey clones encoding full length PIK3R3 were found to interact with PARK7 and NF2 in a kinase-dependent manner in the retest. To reproduce the characteristic growth patterns indicative for a kinase-dependent interaction, liquid cultures of the corresponding diploid yeast colonies were generated and 5 µl were dropped onto -ALT/HU and -HAULT 20 µM $Cu^{2+}$ agar in 96well format. Colonies grown on -ALT/HU agar indicate diploid mated yeast and colonies on -HAULT 20 µM $Cu^{2+}$ agar an interacting bait-prey pair. Interactions with PIK3R3 can be mediated by ABL2+NLS, HCK+NLS or in case of PARK7 by FYN+NLS.

Sequencing verified that prey plasmids encoding PIK3R3 were present in the diploid yeast colonies corresponding to the PARK7-PIK3R3 and NF2-PIK3R3 interactions. We conclude that PIK3R3 interacts with PARK7 and NF2 and propose that binding is mediated by one of the PIK3R3 SH2 domains and pTyr-residues in PARK7 and NF2 (3.1.6.2 ).

### *3.1.6.2 NF2 contains a predicted PIK3R3 SH2 binding site*

The SH2 domains of PIK3R3 probably recognize tyrosine phosphorylated NF2 and PARK7 residues. We searched for known tyrosine phosphorylation sites using Phosphosite, Phosida and PhosphoELM and for candidate kinases using NetworKIN. The PIK3R3 interacting NF2 clone encodes full length NF2 isoform 7 (507 aa) which consists of a conserved N-terminal FERM domain, followed by a coiled-coil domain and a charged C-terminal domain. So far no tyrosine phosphorylation sites for NF2 have been detected. NF2 shares significant sequence homology with proteins of the ERM family and thus we searched for known phosphorylation sites in the family members ezrin, radixin and moesin. With this method three tyrosine residues conserved in NF2 and phosphorylated in at least one ERM family member could be identified. Moesin Tyr116 (Mayya, et al., 2009), radixin Tyr134 (Kasyapa, et al., 2009) and ezrin Tyr191 (Srivastava, et al., 2005) are phosphorylated and correspond to Tyr49, Tyr67 and Tyr124 of NF2 isoform 7, respectively. Except for Tyr134, which is not conserved in ezrin all tyrosine residues are conserved in all four proteins.

PARK7 contains three tyrosine residues and Tyr67 and Tyr139 are known to be phosphorylated (Hornbeck, et al., 2004). NetworKIN did not reveal a kinase candidate for these NF2 or PARK7 phosphorylation sites. In a second approach we used NetPhorest (Miller, et al., 2008) to search for linear motifs predicted to be bound by SH2 domains. None of the three tyrosine residues in PARK7 lays in an SH2 binding site motif. In contrast NF2 isoform 7 contains two possible SH2 binding site motifs surrounding Tyr398 and Tyr445, where SH2 domains classified as “PIK3R3_1_PIK3R2_1_group” are predicted to bind with high probability. The regulatory subunit PIK3R3 (also known as p55γ, 461 aa) is highly similar to the C-terminal part of the regulatory subunit PIK3R2 (also known as p85β, 728 aa) and appears like a truncated PIK3R2 consisting of only the N- and C-terminal SH2 domains. This prediction identified Tyr398 of NF2 isoform 7 as SH2 domain binding site and thus a candidate site which gets probably specifically targeted by the N-terminal SH2 domain of PIK3R3.

## 3.1.7 Connection of disease-associated proteins

All interactions identified were combined in one large network consisting of 90 unique protein interactions among 79 proteins (Figure 13). For 29 of the 71 bait proteins associated with neurological disorders at least one interaction partner was identified. To search for reported interactions among the 90 discovered PPIs in this study, we used the “global human physical protein interaction network” consisting of 80,922 physical interactions among 10,229 human proteins (Bossi and Lehner, 2009) (Figure 13, blue lines). A comparison of our dataset with the reference dataset showed an overlap of two interactions, which were previously identified in an Y2H screen searching for proteins involved in inherited ataxias (Lim, et al., 2006). To analyze the sampling efficiency, (*i.e.* the fraction of previously obtained interactions in a similar Y2H screen) we compared our interactions with the interactions identified by the Wanker laboratory (Max-Delbrück-Centrum for Molecular Medicine). The Wanker laboratory screened all bait proteins that gave an interaction in our screens (29 proteins represented by 34 clones) against the same 16,857 prey matrix we used for the identification of Ser/Thr kinase-dependent interactions. The analysis revealed an overlap of 22 interactions for the whole PPI dataset (90 PPIs) and an

overlap of 21 interactions for the 75 PPIs obtained in the Ser/Thr kinase screen (Figure 13, grey lines). On average a sampling efficiency of 27 % was obtained which is comparable to other high-throughput screens (Venkatesan, et al., 2009). For 10 of 29 interacting bait proteins at least one interaction was recapitulated from the Wanker reference set.

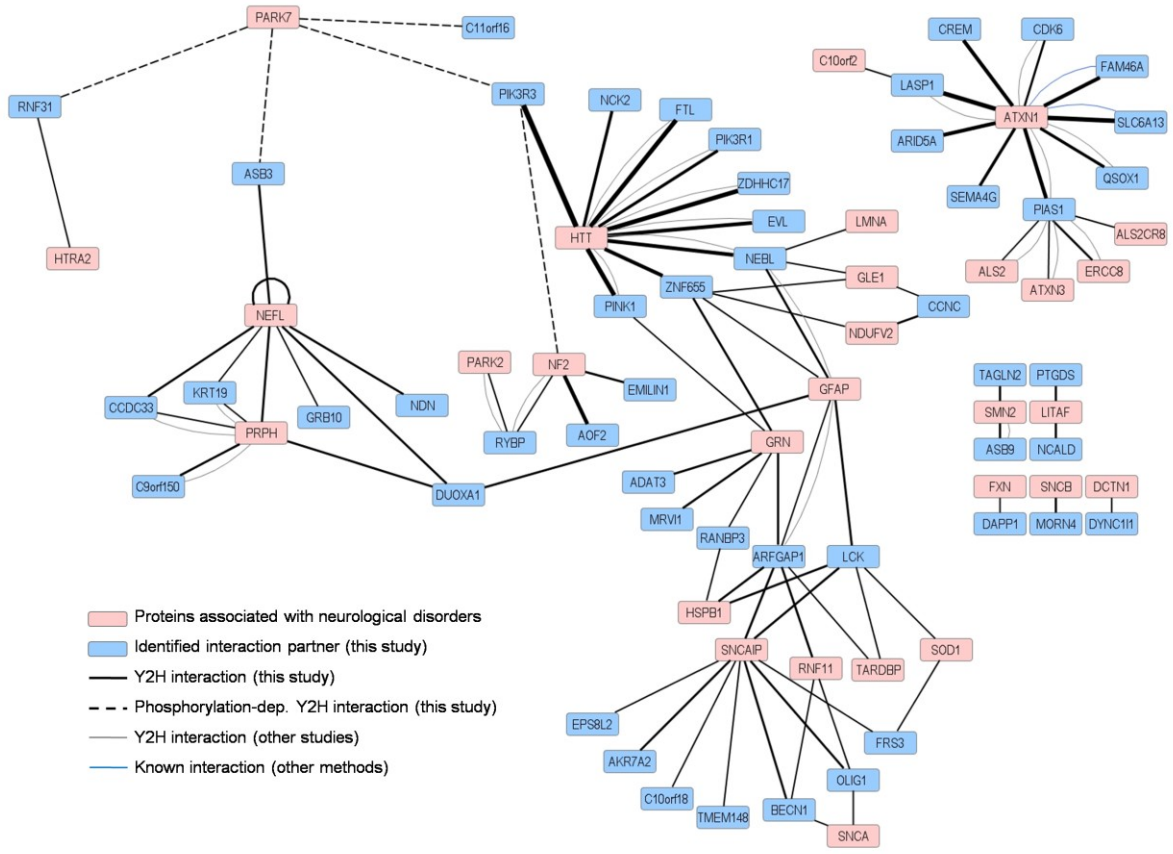


**Figure 13: An interaction network connecting disease-associated proteins.**

Nodes represent proteins and red nodes represent proteins associated with neurological disorders. Lines represent protein interactions and the line width indicates how often this interaction was found using different replicas or different clones for one protein. Protein interactions found in the Y2H screen are shown in black and are dashed if they were observed in a kinase-dependent manner. Additional lines shown in grey or blue represent known interactions detected by Y2H or other methods, respectively. Overall 90 unique protein interactions between 79 proteins were detected in this study. Nodes are labelled with the official NCBI Gene symbol. Additional information including the official full name and the EntrezGeneID can be found in the appendix (Figure 36).

### 3.1.8 Implication of PARK7 in ubiquitination processes

In order to learn more about PARK7 we analyzed the functions of the newly discovered interaction partners RNF31, ASB3, c11orf16 and PIK3R3. RNF31 and ASB3 are involved in ubiquitination processes: ASB3 is part of an E3 ubiquitin ligase complex mediating protein degradation (Chung, et al., 2005) and RNF31 is part of an ubiquitin ligase complex which assembles linear polyubiquitin chains (Kirisako, et al., 2006; Tokunaga, et al., 2009). Like PARK2, RNF31 belongs to the RING-in-between-RING (RBR) ubiquitin E3 ligases and interacts with PARK7 (Moore, et al., 2005; Olzmann, et al., 2007; Xiong, et al., 2009). As PARK2 and RNF31 share these two key properties and mutations of PARK2 and PARK7 are involved in forms of familial PD it's intriguing to ask which role ubiquitination processes play in this disease. A role for PARK7 in ubiquitination would be of biological interest and thus we wanted to substantiate this interesting finding and searched for further interaction

partners involved in ubiquitination. We focussed on kinase-dependent interactions connecting RNF31, ASB3, c11orf16, PARK7, PIK3R3, NF2 and independent interactions surrounding them and extended this subnetwork by adding interaction partners from five different sources (Figure 14). We used the "global human physical protein interaction network" generated by Bossi and Lehner (Bossi and Lehner, 2009), two interaction networks among ubiquitin-conjugating enzymes (E2) and ubiquitin protein E3 ligases (Markson, et al., 2009; van Wijk, et al., 2009) and Y2H interactions identified by the Wanker laboratory (Max-Delbrück-Centrum for Molecular Medicine) and Arndt Grossmann (Stelzl laboratory, MPI for Molecular Genetics). A second extension step was performed to add E2 or E3 ligases as interaction partners for the proteins identified in the first extension round (Markson, et al., 2009; van Wijk, et al., 2009). To determine which proteins are involved in ubiquitination processes PubMed entries were manually examined.

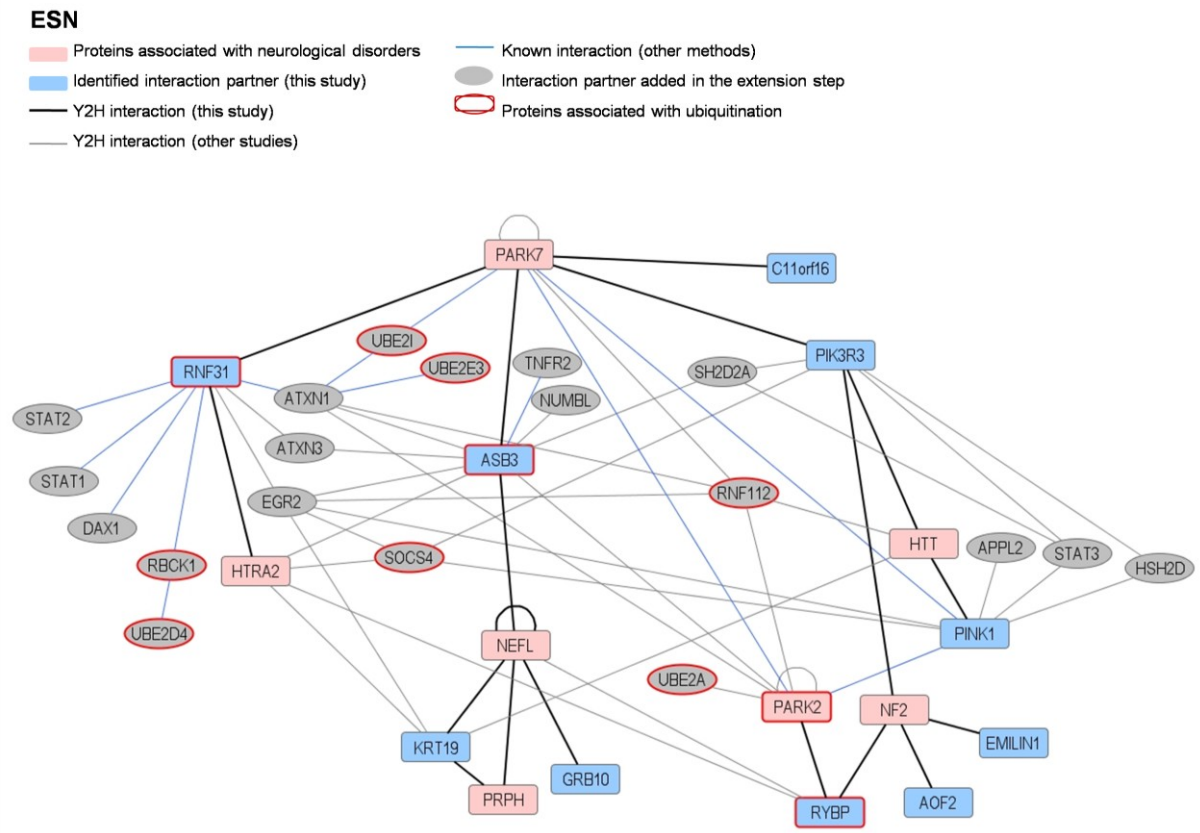


**Figure 14: The extended subnetwork (ESN) includes PARK7, NF2 and proteins involved in ubiquitination.**

The Y2H subnetwork (black lines, square–shaped nodes) was extended by the addition of known interactions detected by Y2H (grey lines) or other methods (blue lines). The newly added 19 interaction partners are represented by grey round-shaped nodes. Proteins involved in ubiquitination are represented by nodes with a red boarder colour. The extended subnetwork (ESN) contains 66 interactions among 36 proteins. Nodes are labelled with the official NCBI Gene symbol. Additional information including the official full name and the EntrezGeneID can be found in the appendix (see Figure 36 for proteins included in the original subnetwork (red/blue nodes) and Figure 37 for proteins added in the extension step which are represented as grey nodes here).

This approach leads to an extended subnetwork (ESN) consisting of 66 interactions among 36 proteins, 11 of these are involved in ubiquitination processes (Figure 14). We discovered that the two familial PD causing proteins PARK2 and PARK7 interact with the RING finger containing protein 112 (RNF112) and with ubiquitin-conjugating enzymes (UBE2A and UBE2I, respectively). Furthermore, PARK2 also interacts with the RING1 and YY1-binding protein (RYBP). RNF112, UBE2I, UBE2A and RYBP are involved in ubiquitination processes thus we concluded that familial Parkinson's disease is indeed tightly linked to ubiquitination and decided to validate these interactions in cell-based PPI assays.

## 3.2 Confirmation of extended subnetwork interactions with cell-based PPI assays

Different interaction assays are of complementary nature and can be used to detect distinct sets of protein interactions (Stelzl and Wanker, 2006). No method covers all possible interacting pairs, because different protein tags, *in vivo* or *in vitro* environments and mechanisms of interaction readout are used. Consequently, each assay has its own false-positive and false-negative rates. Thus we do not expect that all physiologically meaningful Y2H interactions can be detected in other cell-based assays such as coimmunoprecipitation assays or protein fragment complementation assays (PCAs) (Braun, et al., 2009). However, an interaction which is seen in different assays is less likely to be false-positive.

### 3.2.1 A luminescence-based IP method enables large-scale PPI validation in mammalian cells

Coimmunoprecipitation (co-IP) is a widely used *in vitro* method for verification of interactions detected with other systems such as the Y2H system. Co-IP complexes are captured by immunoglobulin (Ig)-binding proteins that are immobilized on a matrix in microfuge tubes and are visualized by immunoblotting after elution. This method involves laborious and time-consuming steps that limit throughput and reproducibility. To address these difficulties, gel-free luminescence-based IP methods in 96well format were developed (Barrios-Rodiles, et al., 2005) (Figure 15). The 96well format reduces the input cell number per experiment, allows simultaneous processing of multiple IP samples and enables much faster sample handling due to the use of liquid handling tools. Thus co-IP experiments can easily be done in replicates or repeated several times with consistent results. In the luminescence-based IP method developed by Barrios-Rodiles *et al.*, binding of the firefly fusion protein (co-IP) to the immunoprecipitated PA fusion protein (IP) is assed by measuring the firefly luciferase activity and the nature of the luminescence signals allows semiquantitative determination of affinities (Barrios-Rodiles, et al., 2005). We further refined this method.

Protein A and firefly fusion proteins were transiently expressed in HEK 293 cells in a pairwise manner and 24-36 hours after transfection cells were lysed in Hepes buffer. The cleared lysate was subjected to immunoprecipitation (IP) in IgG-coated plates and after three washes the binding of the firefly fusion protein to the immunoprecipitated PA fusion protein was determined through measuring the firefly luciferase activity. Each experiment was performed as triplicate transfection and the obtained relative luciferase intensity values were averaged and the standard deviation was determined. The fold change binding for a firefly fusion protein was calculated from averaged intensities measured in parallel with the protein of interest in comparison to a non-related PA fusion protein. Ratios larger than two were considered positive.

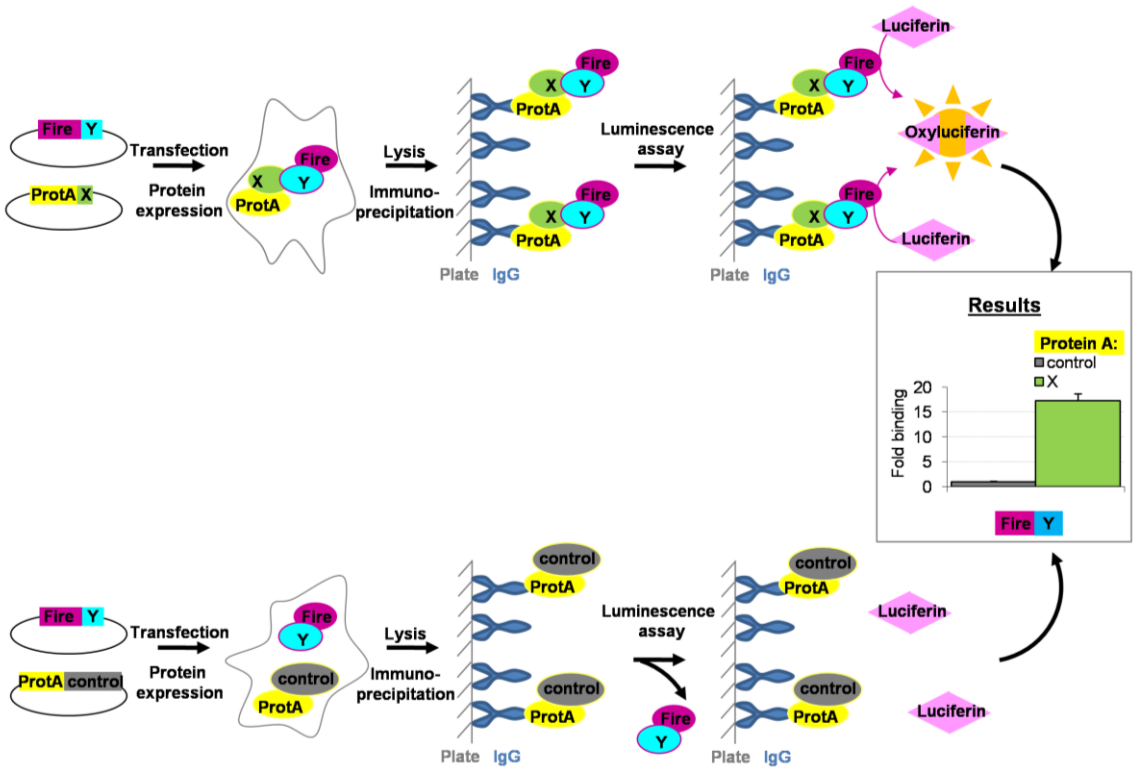


**Figure 15: Schematic overview of the gel-free luminescence-based 96well co-IP assay.**

In order to determine if two proteins interact, the firefly fusion protein of interest is separately coexpressed with two protein A (ProtA) fusion proteins (the putative interactor and a non-related protein) in HEK 293 cells for 24-36 hours. Cells are lysed and the cleared cell lysate is subjected to immunoprecipitation in IgG-coated plates. As protein A binds specifically to the Fc region of IgG molecules, protein A-tagged proteins are immobilized and interacting firefly-tagged proteins coimmunoprecipitated. Unbound or unspecifically bound proteins are removed by washing steps and the amount of firefly fusion protein (co-IP) bound specifically to the immunoprecipitated protein A fusion protein (IP) is assed by measuring the firefly luciferase activity. For that purpose the luciferase substrate luciferin is added and the light produced by the oxidation of luciferin to oxyluciferin is measured with a luminescence plate reader. The fold change binding for the protein pair of interest is calculated from the relative luciferase intensities measured with the putative interactor and the non-related PA fusion protein. Ratios larger than two are considered to indicate a positive interaction.

In order to validate Y2H interactions in co-IP assays, available cDNAs (representing 32 of the 36 proteins from the extended subnetwork) were transferred from gateway entry vectors into PA- and firefly-V5-tagged gateway destination vectors (Palidwor, et al., 2009). All clones showed the expected digestion pattern and the ORF identity and reading frame was verified by 5' and 3'-tag sequencing. PA- and firefly-plasmid DNA corresponding to one protein clone was cotransfected in HEK 293 and expression of the two fusion proteins was assessed 24-36 hours later by immunoblotting. The PA and the firefly fusion of one protein were controlled in one lane of the same immunoblot by testing first PA fusion protein expression with a horseradish peroxidase (HRP)-coupled antibody and then firefly-V5 fusion protein expression with an alkaline phosphatase (APH)-coupled antibody. Exemplarily, the expression of six proteins as PA and firefly-V5 fusions is shown (Figure 16). The PA-tag adds 15 kDa and the firefly-V5-tag 63 kDa to the molecular weight of the protein, consequently a shift of 43 kDa is observed between the PA and the firefly-V5 fusion protein. The absence of bands corresponding to PA fusion proteins in the anti-V5 immunoblots allows two conclusions: First, protein A is not able to bind to the anti-V5-APH antibody derived from mice and second the unstripped anti-goat-HRP antibody does not give a signal with the alkaline phosphatase substrate. We tested the expression of all generated fusion proteins and excluded five combinations (PA and firefly fusion) from the co-IP experiments because of their low expression levels. The remaining fusion proteins were used for the validation of interactions through co-IP (see 3.2.3).

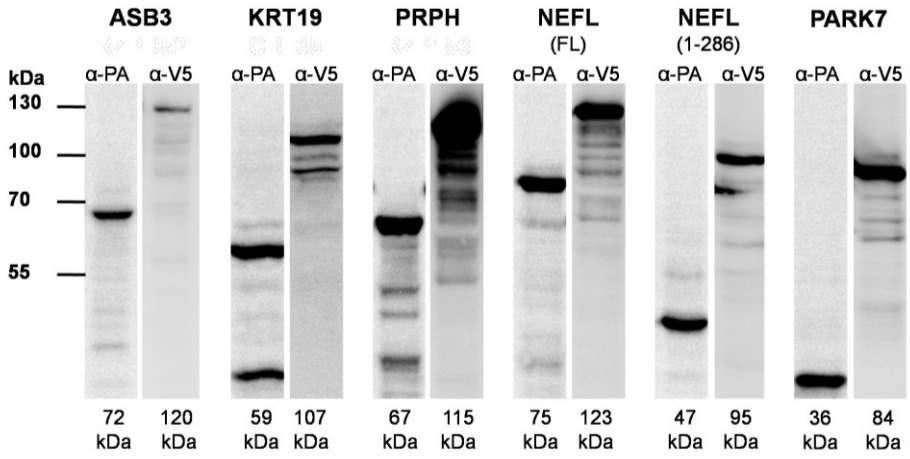


**Figure 16: Expression of PA- and firefly-V5-tagged human proteins in mammalian cells.**

Cell lysate prepared from HEK 293 cells coexpressing different combinations of PA- and firefly-V5-tagged proteins was analyzed by immunoblotting using anti-V5-APH or anti-goat-HRP antibodies. First, PA fusion protein expression was detected with an anti-goat-HRP antibody (Zymed # 61-1620, 1:3000) and a luminol reagent (*i.e.* enhanced chemiluminescence substrate). In a second step, without any stripping or blocking steps in between, the expression of firefly-V5-tagged proteins was detected with an anti-V5-APH antibody (Invitrogen # R962-25, 1:5000) and the fluorimetric alkaline phosphatase substrate AttoPhos (Roche). The expected molecular mass for each fusion protein is indicated at the bottom of the blot and is in agreement with the observed size.

### 3.2.2 A Venus-based PCA assay visualizes interaction localization in intact mammalian cells

Protein fragment complementation assays (PCAs) are suitable to detect transient and dynamic protein interactions in intact living cells with subcellular resolution (Remy, et al., 2004). In a PCA based on the yellow fluorescent protein (YFP) variant Venus (Nagai, et al., 2002), nonfluorescent F1 and F2 fragments of Venus are individually fused to the coding sequences of two separate proteins and expressed in mammalian cells. If the two fusion proteins interact, the fragments of Venus are brought into proximity, permitting folding and reconstitution of fluorescent Venus in vivo (Figure 17). No fluorescence is detected in the absence of an interaction because of the inability of the two separate Venus domains to fold by themselves (Magliery, et al., 2005). Furthermore, PCA based fluorescence only occurs if the fused proteins physically interact and is not caused by sole colocalisation (Lalonde, et al., 2008). This is a clear advantage over colocalisation studies performed with antibodies, where due to missing resolution two proteins could easily be contained within a colocalized volume even if they do not interact (Vogel, et al., 2006).

In order to validate interactions in a third system and to observe the localisation of protein interactions in intact cells, Venus PCA was performed. In a first step, cDNAs (representing 13 of the 36 proteins from the extended subnetwork) were transferred from gateway entry vectors into the Venus gateway destination vectors (pVEN-F2N-DM, pVEN-F1N-DM, pVEN-F2C-DM, and pVEN-F1C-DM) to tag proteins on their N- or C-terminus with the Venus fragments F1 or F2. ORFs without stop codon were transferred into all four vectors whereas ORFs with stop codon were only transferred into the two vectors which lead to N-terminal Venus fragment fusions. After the ORF identity and reading frame was verified by 5' and 3' tag-sequencing, the plasmid DNA was used for cotransfection of HEK 293 cells seeded in 96well µclear greiner plates, which show a low level of autofluorescence and high clarity. These plates can be used in combination with a confocal microscope (LSM 410-meta) to screen for Venus positive cells. Cells transiently coexpressing Venus F1 and Venus F2 fusion proteins for 24 hours were directly fixed in the plates and DAPI stain was used for visualization

of the cell nucleus. No fluorescence was seen if Venus fragment fusion proteins were expressed alone or with a non-related but complementary Venus fragment fusion protein. If fluorescent perinuclear structures without cytoplasmic fluorescence was observed the tested protein pair was regarded as non-interacting. The formation of these aggregates is probably unspecific and may result from coincidental reconstitution of the fluorescent Venus protein in the absence of true interaction between the fused proteins. This can be caused by high local protein concentration reached for example during protein degradation processes (Lalonde, et al., 2008) or endoplasmic reticulum-dependent folding.

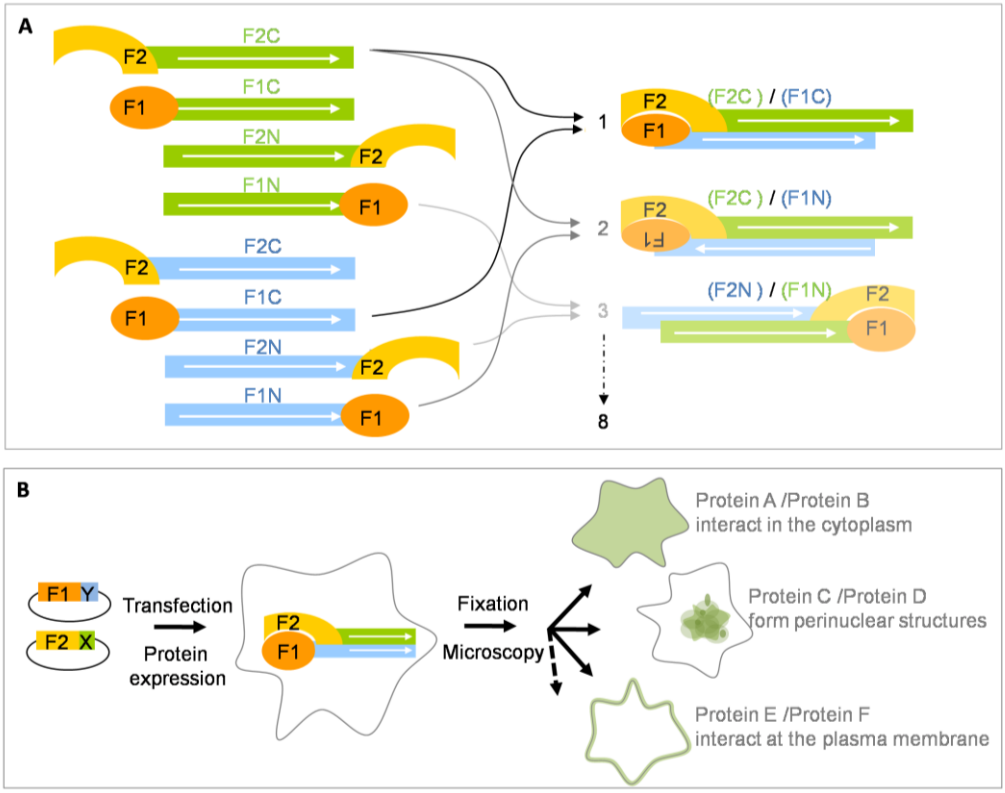


**Figure 17: Principle of the Venus PCA strategy capable to detect interactions in intact mammalian cells.**

**A**, Non-fluorescent N-terminal (1-158 aa; F1; yellow) and C-terminal (159-239 aa; F2; orange) Venus fragments are individually fused to the coding sequences of two separate proteins (marked green and blue). If the coding sequence does not contain a stop codon four fusion proteins per coding sequence can be generated, encompassing C- and N-terminal fusions of F1 and F2 Venus fragments. In order to determine if two proteins interact, Venus F1 and Venus F2 fragment fusion protein were combined. Up to 8 different combinations can be tested. **B**, In order to determine if two proteins interact, the corresponding Venus F1 and Venus F2 fragment fusion proteins are transiently coexpressed in HEK 293 cells. If the two fusion proteins interact with each other, the fragments of Venus are brought into close proximity and assemble to a fluorescent Venus protein in vivo. Protein interaction and interaction localisation can be determined by fluorescent microscopy.

### 3.2.3 Cell-based PPI assays further characterize interactions among disease-associated proteins

We tested a total of 38 interactions among 27 proteins from the ESN (Figure 14) in co-IP experiments. Nine proteins were excluded because matching cDNAs were not available or the generated fusion proteins did not express to detectable levels. 18 interactions could be confirmed in at least one orientation in the co-IP assay and 20 interactions were not detected under the conditions used (Figure 18). Seven co-IP experiments performed with the PARK7 firefly fusion were neglected because of the high background binding of the PARK7 firefly fusion to the IgG-coated plate. Interactions added in the extension steps were coprecipitated with a lower success

rate (6/20 were positive) compared to the Y2H interactions identified in this study (12/18 were positive). Performing co-IP experiments we found that NF2, KRT19, PRPH and PIK3R3 are able to build dimers and an interaction between NF2 and PARK7. These five additional interactions were not tested in the Y2H screens.

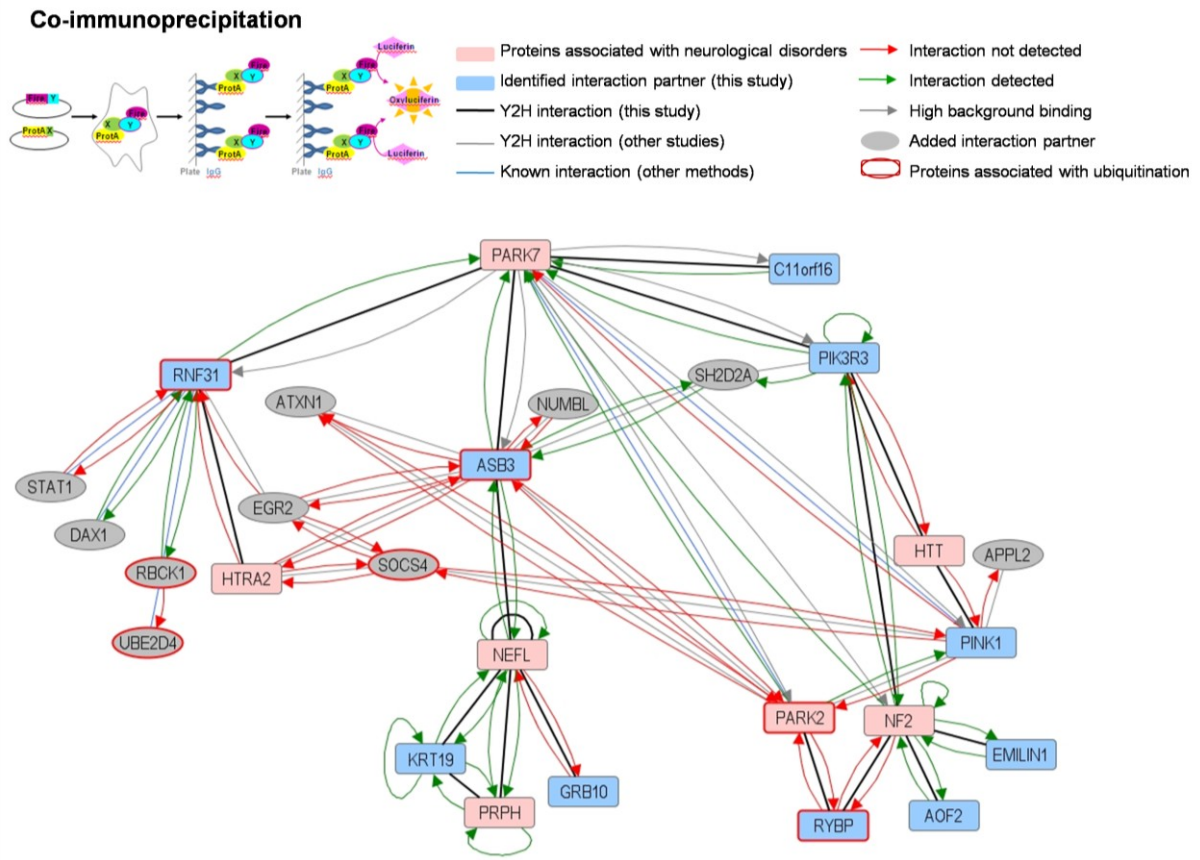


**Figure 18: Validation of ESN interactions using a gel-free luminescence-based co-IP strategy.**

Interactions of the ESN (see Figure 14) were tested in co-IP experiments. Arrows represent a performed co-IP experiment with the arrow direction indicating the co-IP orientation. The protein with the arrow starting point was used as firefly-tagged protein whereas the protein with the arrowhead was used as PA-tagged protein in this co-IP assay. Green arrows indicate a successfully validated interaction, whereas red arrows represent a negative co-IP signal. Grey arrows starting from PARK7 indicate that co-IP experiments performed with the PARK7 firefly fusion protein did not give useful results because the background binding to the IgG-coated plates was too high. 18 of 38 interactions among 27 proteins were confirmed in at least one orientation in the co-IP assays. Additional information about the genes (Figure 36, Figure 37), the signal strength and all control experiments (Figure 38, Figure 39) can be found in the appendix.

13 Y2H interactions confirmed by co-IP experiments and 3 interactions detected in co-IP experiments were tested with a Venus protein fragment complementation assay. With the PCA system 12 interactions were confirmed in at least one orientation and only the PIK3R3 dimer was not detected (Figure 19). Detailed results of the performed co-IP and Venus PCA experiments can be found in the appendix (Figure 38, Figure 39, and Figure 40). Recapitulation of known interactions showed that the used cell-based assays are feasible for the validation of protein interactions. Furthermore, we concluded that the generated fusion proteins are functional based on the investigation that well-known interactions were successfully recapitulated (*i.e.* RNF31 PPIs depicted as blue lines) and that the observed interaction localisation patterns were in agreement with the annotated protein localization (see 3.3.2 for RNF31 interactions and 3.5.2 for NF2 interactions).

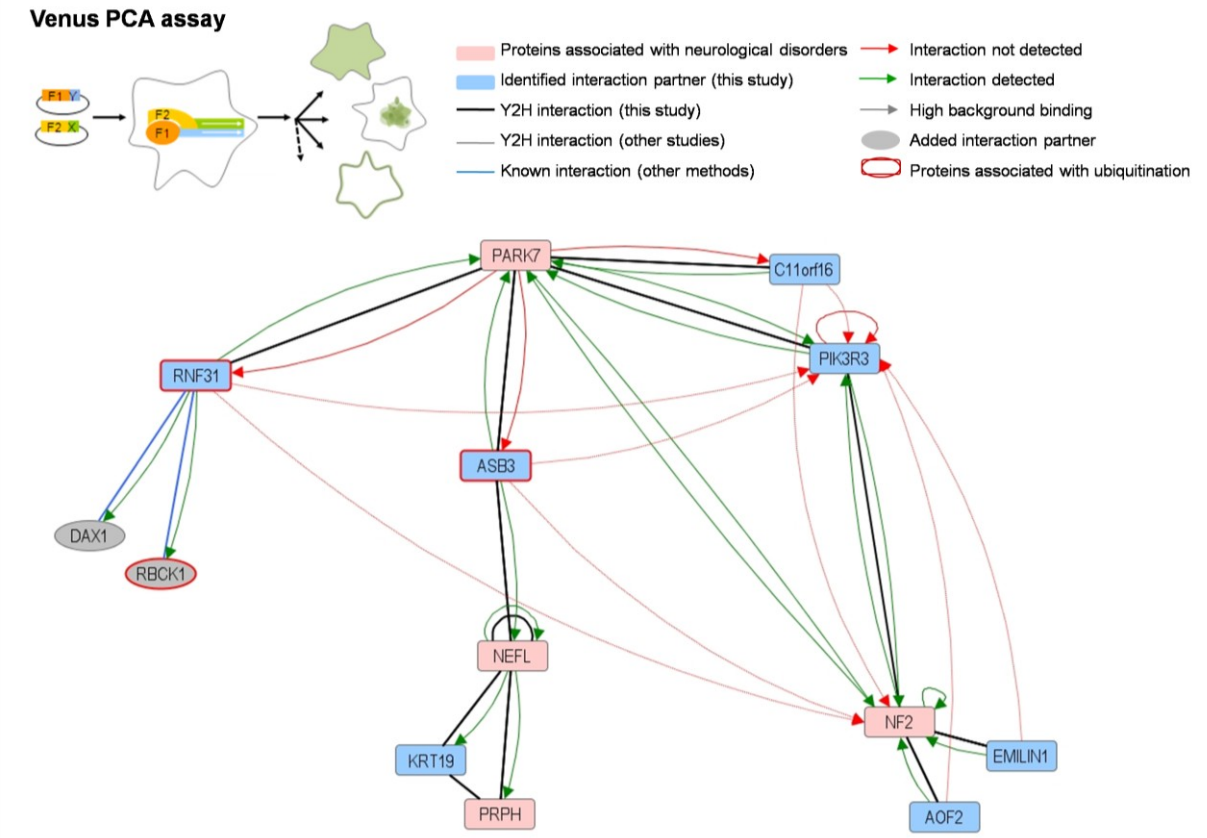


**Figure 19: Validation of ESN interactions using a fluorescent protein complementation assay.**

Interactions of the ESN (see Figure 14) were tested in Venus PCA experiments. Arrows represent a performed Venus PCA experiment. The protein with the arrow starting point was used as Venus F1 fragment fusion protein whereas the protein with the arrowhead was used as Venus F2 fragment fusion protein. Green arrows indicate a successfully validated interaction, whereas red arrows represent a negative Venus PCA signal. 12 of 16 interactions among 13 proteins were confirmed in at least one orientation with the Venus PCA assay. Additional information about the genes (Figure 36, Figure 37), the signal strength and subcellular localization of the observed fluorescence signals (Figure 40) can be found in the appendix.

## 3.2.4 Defining the interactions between intermediate filaments

### *3.2.4.1 Co-IP experiments confirm the intermediate filament interactions*

Intermediate filaments (IFs) are one of the three classes of cytoskeletal fibers in eukaryotic cells and IF genes are present in all metazoan animal genomes that have been analyzed so far (Erber, et al., 1998; Karabinos, et al., 2004; Zimek, et al., 2003). Intermediate filaments are dynamic polymers (10 nm in diameter) assembled from a large number of different IF proteins through several intermediate structures. Based on their sequence similarity, IF proteins are divided into five major types: acidic and basic keratins, type III IF proteins (*e.g.* peripherin, vimentin, desmin), type IV IF proteins (*e.g.* neurofilaments, syncoilin) and lamins (Herrmann and Aebi, 2004; Strelkov, et al., 2003). The organization of IFs into networks and bundles, mediated by various intermediate filament associated proteins (IFAPs), provides structural stability to cells. IFAPs also cross-link intermediate filaments to microtubules, microfilaments, plasma and nuclear membranes (Godsel, et al., 2008). Major degenerative diseases of skin, muscle, and neurons are caused by disruption of the IF cytoskeleton or its connections to other cell structures (Coulombe and Wong, 2004). Mutations in the type III IF protein peripherin (PRPH) found in neurons of the peripheral nervous system have been associated with susceptibility to Amyotrophic Lateral Sclerosis, whereas mutations in the light chain neurofilament protein NEFL lead to

neuropathies. Both IF proteins can be found within the same 10 nm-IF and mutant peripherin is known to disrupt neurofilament containing IFs (Beaulieu, et al., 1999; Parysek, et al., 1991).

Interestingly, we have found a direct link between these two proteins and an indirect one: both proteins interact with each other and with KRT19, the smallest known acidic keratin (Figure 20).

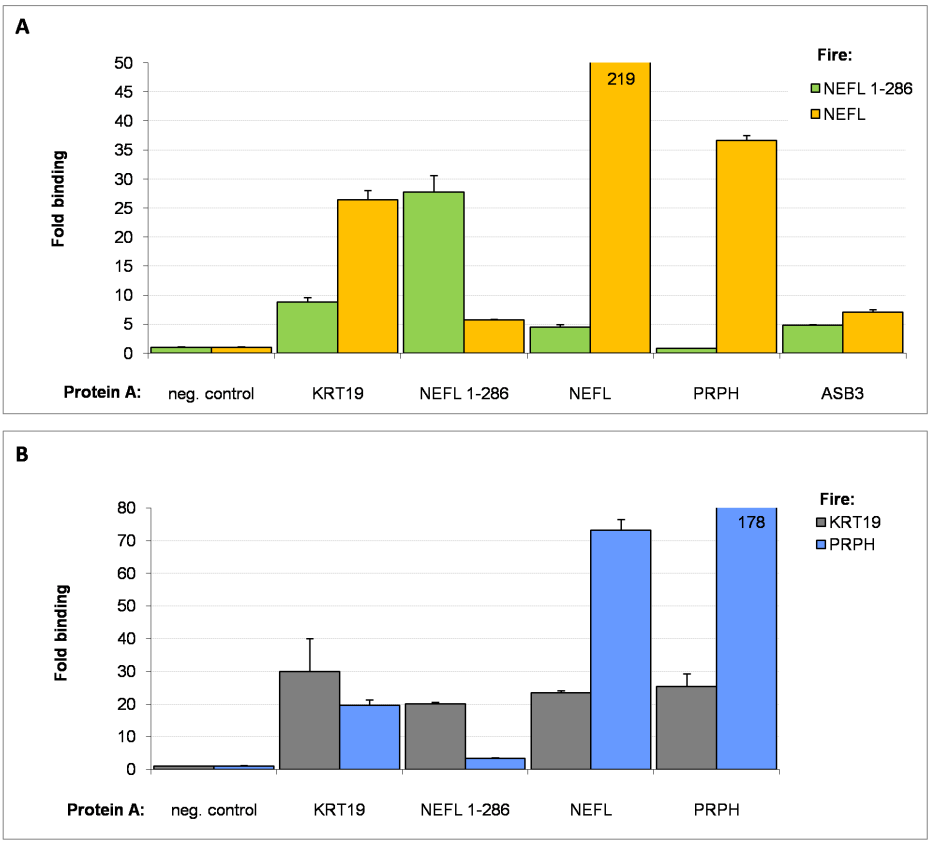


**Figure 20: Co-IP results confirm the intermediate filament interactions.**

**A**, Binding of full length NEFL and a N-terminal NEFL (1-286) fragment to KRT19, NEFL, PRPH, ASB3 and a non-related PA fusion protein. In order to compare the binding of NEFL firefly fusions the fold change binding was calculated from background binding intensities to the non-related PA fusion protein (neg. control).
**B**, Binding of KRT19 and PRPH firefly fusion proteins to KRT19, NEFL and PRPH PA fusion proteins.

Full length NEFL but not the N-terminal NEFL (1-286) fragment firefly fusion protein was coimmunoprecipitated using a PRPH protein A fusion protein (Figure 20, A). NEFL (1-286) was expressed in comparable levels to the full length construct, was able to build dimers (Goehler, et al., 2004) and to interact with KRT19 (Figure 20, A). This leads to the conclusion that the NEFL C-terminus is necessary for interaction with PRPH but not for interaction with KRT19 or dimerization. Performing the co-IP experiment in the other orientation led to the same results, compared to full length NEFL the N-terminal NEFL fragment showed an 20 times reduced binding to PRPH but no reduction in KRT19 firefly fusion protein binding (Figure 20, B). The co-IP assay failed to detect the PRPH-NEFL (1-286) interaction in one orientation and showed weak interaction signals for the other orientation whereas in the Y2H system strong interaction signals were reported (Figure 10, B). The interactions between PRPH, full length NEFL and KRT19 were confirmed in both orientations (Figure 20). In support of our results, interactions among type III IF proteins and keratins have been observed before including an interaction between the type III IF protein PRPH and KRT15, which is highly similar to KRT19 (Rual, et al., 2005). Additionally, the type IV IF protein NEFL is known to get incorporated into keratin

filaments (Carter, et al., 1997). The detected interaction between PRPH and KRT19 points into the direction that also type III IF proteins like PRPH can get incorporated into keratin filaments. Performing the co-IP experiments, we found that in addition to NEFL also KRT19 and PRPH were able to dimerize, which is not surprising, as homo- and heterodimerization of IF proteins is the first step in intermediate filament formation. NEFL and PRPH are known to form homodimers in contrast to acidic and basic keratins, which form heterodimers with each other. However, the two highly similar acidic keratins KRT19 and KRT15 have also been shown to interact with each other (Rual, et al., 2005). The interaction of NEFL with the non intermediate filament proteins GRB10 and ASB3 was also tested in coimmunoprecipitation experiments. Both, the full length NEFL protein and the N-terminal NEFL fragment failed to interact with GRB10 (data not shown) but showed comparable binding to ASB3 in all tested orientations. Thus four out of five identified NEFL interactions were successfully validated with coimmunoprecipitation experiments.

#### *3.2.4.2 Venus PCA experiments reveal the localization of intermediate filament interactions*

Interaction of C- or N-terminal Venus F2 fusions of full length NEFL or the N-terminal NEFL (1-286) fragment with ASB3-F1C (N-terminal Venus F1 fragment fusion) occurred in the cytoplasm (Figure 21, A, arrows and appendix Figure 40) whereas no interaction with ASB3-F1N (C-terminal Venus F1 fragment fusion) was detected (appendix Figure 40). Thus all four generated NEFL Venus F2 fusions are working and are not fluorescent if non-interacting. Using the same NEFL Venus F2 fusions we observed, that only full length NEFL was able to dimerize with C- or N-terminal NEFL (FL) Venus F1 fusions in cytoplasmic plaques (appendix Figure 40). This is in agreement with the coimmunoprecipitation results, where dimerization of two full length NEFL constructs was stronger than dimerization between full length NEFL and the N-terminal NEFL fragment (Figure 20, A). If NEFL (1-286) was able to dimerize as seen in co-IP experiments was not determined. Coexpression of C- or N-terminal NEFL (FL) Venus F1 fusions with C- or N-terminal KRT19 or PRPH Venus F2 fusions resulted in cytoplasmic plaque formation (Figure 21, B and appendix Figure 40) as seen for the NEFL dimer.

These cytoplasmic plaques do not fit to the expected more linear neurofilament distribution across the cell. However, NEFL Venus 2 fusion proteins are not generally prone to plaque formation because the NEFL-F2C/ASB3-F1C interaction is distributed homogenously in the cytoplasm (Figure 21, A, arrows). Additionally, the formation of intermediate filaments is not impaired in HEK 293 cells as they can be stained strongly and in a clearly filamentous pattern with antibodies against type IV IF proteins (NEFL, NEFM, NEFH, alpha-internexin), type III IF proteins (vimentin) and type I IF proteins (KRT18) (Ching and Liem, 1993; Shaw, et al., 2002). These observations prompted Graham *et. al* to perform a microarray analysis of HEK 293 cells using Affymetrix and Clontech arrays. This approach revealed that over 50 proteins which are predominantly expressed in neuronal lineage cells (including NEFL, NEFM, alpha-internexin, peripherin, vimentin and various keratins) are expressed in HEK 293 cells (Graham, et al., 1977; Shaw, et al., 2002)[1].

[1] Graham *et. al* hypothesize that a rare neuronal lineage cell type known to be present in the developing mammalian kidney was the target for adenoviral transformation during human embryonic kidney (HEK) cell lineage generation in 1977. They came to this conclusion because it has always been very difficult to generate lines from human embryonic kidney cultures and because adenoviruses tend to specifically transform neuronal lineage cells.

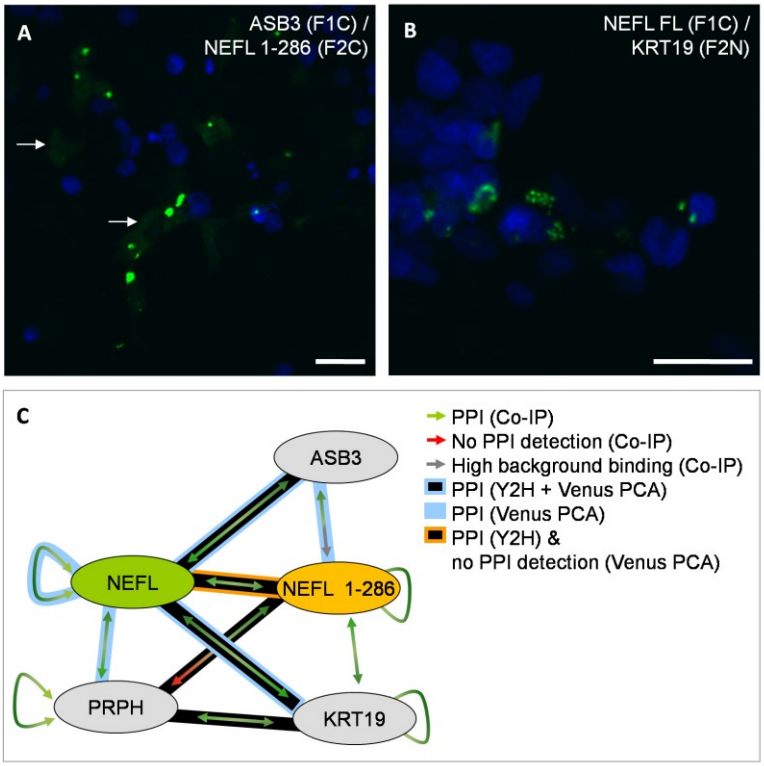


**Figure 21: The intermediate filament interaction subnetwork.**

**A**, NEFL (1-286)-F2C (N-terminal Venus F2 fusion) was transiently coexpressed with ASB3-F1C (N-terminal Venus F1 fusion) in HEK 293 cells for 24 hours. Fluorescent microscopy of fixed cells showed that NEFL and ASB3 interact in the cytoplasm (see arrows). Scale bar: 30 µm.
**B**, Coexpression of NEFL (FL)-F1C (N-terminal Venus F1 fusion) and C-terminal KRT19 Venus F2 fusion for 24 hours in HEK 293 cells resulted in cytoplasmic plaque formation probably reflecting the homo- and heterodimerization step prior to final intermediate filament formation. Scale bar: 30 µm.
**C,** Network illustration of the intermediate filament interactions. Lines represent protein interactions found by Y2H (black) or Venus PCA (blue) or both (blue line, black filling). Y2H interactions tested in Venus PCA without positive fluorescence signal are shown as orange lines with black filling. Arrows represent a performed co-IP experiment. The colour of the arrowhead pointing towards a protein node indicates if this interaction was detected (green) or not (red) if this protein was used as protein A fusion. Grey arrowheads indicate high background binding of the used firefly fusion protein in the co-IP assay.

We conclude that functional intermediate filaments can be formed in HEK 293 cells (Ching and Liem, 1993; Shaw, et al., 2002) and suggest that the observed non-filamentous staining pattern represent homo- and heterodimerization steps prior to final intermediate filament formation. The further steps are probably sterically inhibited by the C- and N-terminal Venus fragment fusions. In summary, four of the five identified NEFL interactions were successfully validated with co-IP and PCA experiments (Figure 21, C). As NEFL interacts with PRPH and KRT19 we conclude that there is a tight connection between different types of IFs which might influence their assembly and/or function probably in a cell type-dependent manner.

## 3.3 Implication of PD and the PD-associated gene product PARK7 in ubiquitination

### 3.3.1 Ubiquitination processes in PD

From thirteen genetic loci associated with Parkinson's disease (PD), defects in eight genes have been established to cause familial PD: α-synuclein (SNCA, PARK1, PARK4), parkin (PARK2), UCHL1 (PARK5), PINK1 (PARK6), DJ1 (PARK7), LRRK2 (PARK8), ATP13A2 (PARK9), and HTRA2 (PARK13) (Thomas and Beal, 2007). Four of these genes are implicated in ubiquitination and protein degradation pathways (Dawson and Dawson, 2003; Valente, et al., 2004) and changes in these pathways are considered to play a critical role in familial and sporadic PD pathogenesis (Giasson and Lee, 2003; McNaught, et al., 2001). In this study we identified two PARK7 interaction partners which are known members of ubiquitin ligase complexes: ASB3, which probably functions as a substrate-recognition subunit of a multi-protein E3 ubiquitin ligase complex that mediates the degradation of proteins (Chung, et al., 2005) and RNF31, which is part of an ubiquitin ligase complex that assembles linear polyubiquitin chains (Kirisako, et al., 2006; Tokunaga, et al., 2009). One of the several PARK7 functions described is its ability to modulate distinct ubiquitination processes (Clements, et al., 2006; Takahashi, et al., 2001; Xiong, et al., 2009) which challenged us to investigate the connection between PARK7 and these ubiquitin ligases.

### 3.3.2 Recapitulation and localisation of literature RNF31 interactions

RNF31 (also known as HOIL1 interacting protein, HOIP) and RBCK1 (also known as HOIL1) build together the linear ubiquitin chain assembly complex (LUBAC) (Kirisako, et al., 2006) which conjugates linear polyubiquitin chains to NEMO (also known as IKK-γ or IKBKG) and thus activates the NFκB pathway (Tokunaga, et al., 2009). RNF31 was shown to bind, ubiquitinylate and stabilize the mammalian orphan receptor DAX1 (Ehrlund, et al., 2009). These well established RNF31 interactions were used as positive controls for the generated RNF31 fusion proteins, containing the Ub-associated (UBA) domain and the C-terminal RBR domain (484-1072 aa, named RNF31 UBA-IBR-IBR further on) or only the UBA domain (484-637 aa, named RNF31 UBA further on) (Figure 22, A). For the co-IP experiments a RBCK1 isoform 1 construct missing the first 10 amino acids (NP_112506, 11-510 aa) and a splice variant lacking the C-terminal half (NP_112504.1, 231 aa, isoform 4 also known as RBCK2 or XAP3) was used (Figure 22, A). Amino acids 15 till 211 of RBCK1 isoform 4 match perfectly to amino acids 57 till 252 of RBCK1 isoform 1, thus both isoforms contain the Ub-like (UBL) domain and the Npl4 type zinc finger domain but only isoform 1 contains the RBR domain (Kirisako, et al., 2006). Both RBCK1 isoforms coimmunoprecipitate with RNF31 UBA-IBR-IBR firefly fusion equally well, but for RNF31 UBA a strong isoform-dependent difference was seen (Figure 22, B). As the UBL domain of RBCK1 was shown to be sufficient for interaction with the UBA domain of RNF31 in GST pulldown experiments (Kirisako, et al., 2006), it is surprising that we cannot detect an interaction between RNF31 UBA and the RBCK1 isoform 4. Our experiments point in the direction, that at least one interaction partner has to contain an RBR domain or in other words: RBCK1 isoform 1 can interact equally well with UBA and UBA-IBR-IBR, whereas the RBCK1 isoform 4 interaction depends on the RNF31 RBR domain in our assay. The functionality of both RNF31 constructs was further shown by relatively weak but reproducible binding to full length DAX1 (471 aa) protein A fusion (Figure 22, C).

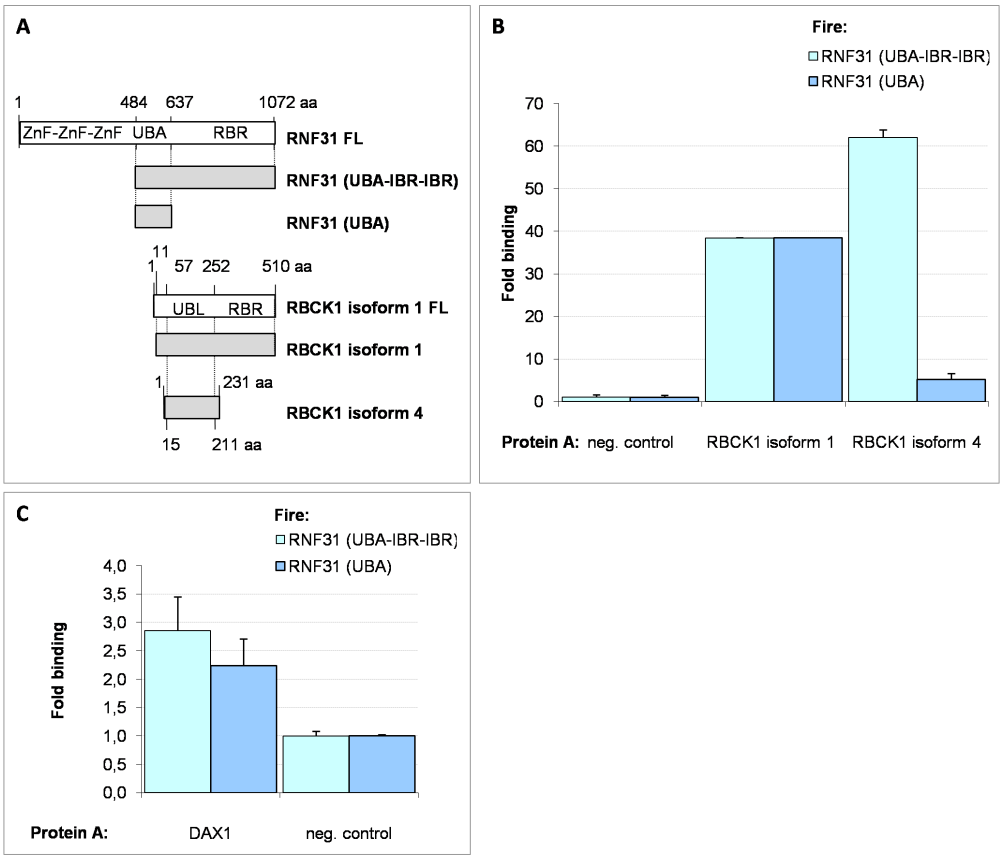


**Figure 22: RNF31 interacts with RBCK1 isoforms and DAX1 in co-IP experiments.**

**A**, Schematic overview showing the full length protein (white) and the used fragments (grey) of RBCK1 isoforms and RNF31. Domain and motif assignments are from HPRD, which chooses the most sensible prediction of the prediction program algorithms SMART and Pfam and includes experimental data on domains. SMART predicts that RNF31 (NP_060469.4/Q96EP0) contains three zinc finger domain also found in Ran-binding proteins (ZnF_RBZ, 301-436 aa), one RING domain (698-748 aa), one IBR domain (778-842 aa) and either another IBR domain (852-931 aa, R-IBR-IBR) or due to overlapping domains another RING domain (870-917 aa, R-IBR-R). Additionally, Pfam predicts with low significance an ubiquitin-associated domain (UBA, 579-609 aa). Additionally, a nuclear export signal (NES) was identified starting at residue L151 (Ehrlund, et al., 2009). RBCK1 isoform 1 (NP_112506/Q9BYM8.1) contains following SMART prediction one ZnF_RBZ domain (194-220 aa) and one RING domain (281-327 aa). Additionally, Pfam predicts two IBR domains located between residues 362-476 with high significance and an ubiquitin-like domain (UBL, 70-120 aa) with low significance. Amino acids 15 till 211 of RBCK1 isoform 4 (NP_112504.1/Q9BYM8-4) match perfectly to amino acids 57 till 252 of RBCK1 isoform 1 consequently isoform 4 contains only the UBL and the ZnF_RBZ domain. The predicted domains for RNF31 and RBCK1 are in agreement with experimental domain mapping (Kirisako, et al., 2006) and the conclusion that these proteins belongs to the RING-in-between-RING (RBR) protein family (Marin, et al., 2004).
**B**, Co-IP experiments were performed and analyzed as described in material and methods. Binding of RNF31 UBA-IBR-IBR and RNF31 UBA firefly fusions to RBCK1 isoforms was investigated. Binding to RBCK1 isoform 4 is severely reduced if the RBR domain of RNF31 is missing.
**C**, Co-IP experiments were performed and analyzed as described in material and methods. Binding of RNF31 UBA-IBR-IBR and RNF31 UBA firefly fusions to DAX1 was investigated. Binding to DAX1 is independent of the RBR domain of RNF31.

The RNF31 UBA domain was sufficient for DAX1 binding and as expected binding was not enhanced in presence of the RBR domain (Ehrlund, et al., 2009). The interactions between RNF31-DAX1 and RNF31-RBCK1 were reproduced by performing co-IP experiments in the other orientation using RNF31 UBA-IBR-IBR protein A fusion (appendix Figure 38).

Venus PCA assays were performed to test the functionality of the generated RNF31 Venus fragment fusion proteins and to determine where the interactions in the cell occur. Endogenous RNF31 is found in both nuclear and cytoplasmic compartments and shuttling between these compartments is regulated by a nuclear export signal present in the N-terminus (Ehrlund, et al., 2009), which is not present in either of the two RNF31 constructs used in this study (Figure 22, A). DAX1 is also found in these two compartments and colocalisation of RNF31 and DAX1 is observed predominantly in the cytoplasm (Ehrlund, et al., 2009). C- or N-terminal

Venus F1 fusions of RNF31 UBA-IBR-IBR were tested with DAX1 fused C- or N-terminal to Venus F2. One of the four different fusion protein combinations tested was positive and showed the expected cytoplasmic localisation pattern (RNF31-F1C/DAX1-F2C) (Figure 23, A). The same RNF31 UBA-IBR-IBR Venus F1 fusions were able to interact with both RBCK1 isoforms fused C- or N-terminal to Venus F2 (appendix Figure 38). For RBCK1 isoform 1 two out of four different combinations were tested positive and for RBCK1 isoform 4 all four tested combinations were positive (appendix Figure 38 and Figure 23, B and C).

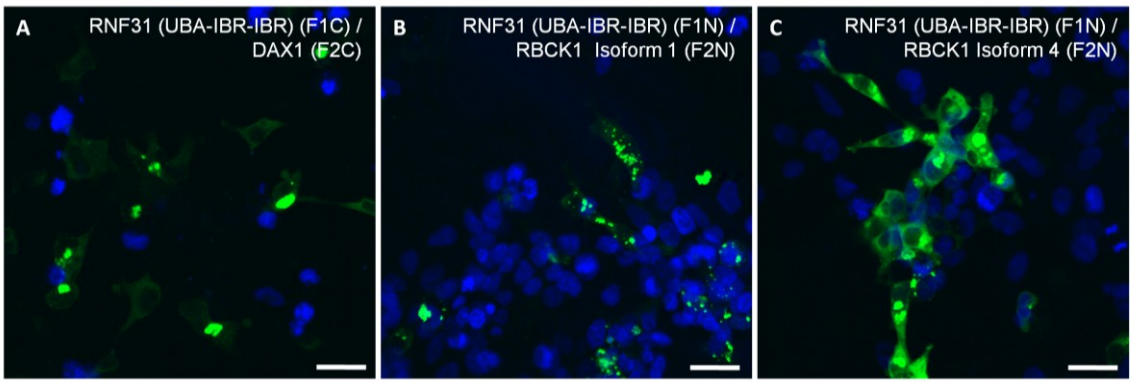


**Figure 23: RNF31 interacts with RBCK1 isoforms and DAX1 in intact mammalian cells.**

**A**, Coexpression of RNF31 UBA-IBR-IBR-F1C (N-terminal Venus F1 fusion) with DAX1-F2C (N-terminal Venus F2 fusion) for 24 h in HEK 293 cells resulted in cytoplasmic fluorescence. Scale bar: 30 µm.
**B** and **C**, Coexpression of RNF31 UBA-IBR-IBR-F1N (C-terminal Venus F1 fusion) with C-terminal RBCK1 Venus F2 fusions resulted in cytoplasmic fluorescence irrespective which RBCK1 isoform is coexpressed. RBCK1 isoform 4 generally gave a stronger cytoplasmic stain (C). Scale bar: 30 µm.

RBCK1 isoform 1 contains nuclear export and localization signals and has been shown to shuttle between the cytoplasm and the nucleus whereas its splice variant RBCK1 isoform 4 contains only the nuclear export signal and is usually present in the cytoplasm (Yoshimoto, et al., 2005). This explains why RBCK1 isoform 4 generally gave a stronger cytoplasmic stain. Furthermore, the observed punctae like structures might represent nuclear bodies, because RBCK1 isoform 1 is known to accumulate in nuclear bodies and to interact with nuclear body proteins (Tatematsu, et al., 2005). We conclude that the generated RNF31 fusion proteins are functional because they were able to bind to known interaction partners in two cell-based assays. Furthermore, the observed interaction localization was in agreement with the annotated protein localization.

### 3.3.3 Validation and localisation of PARK7 interactions

In order to validate PARK7 interactions, a PARK7 protein A fusion was used to coimmunoprecipitate firefly-tagged interaction partners. Interactions with ASB3, c11orf16 and RNF31 were successfully confirmed in this orientation of the co-IP assay (Figure 24, D). Experiments performed with PARK7 firefly did not give useful results because background binding to the IgG-coated plates was too high. The initial Y2H interaction between PARK7 and the ubiquitin ligase RNF31 (1072 aa) has been found with a C-terminal RNF31 fragment (484-1072 aa) containing the UBA and the RBR domain (RNF31 UBA-IBR-IBR) (Figure 24, E). Because a second ubiquitin ligase, namely PARK2, is known to interact with PARK7 via its N-terminal RBR domain (Xiong, et al., 2009) we tested if a RNF31 firefly fusion containing only the UBA domain (RNF31 UBA) was still able to bind to PARK7. Although RNF31 UBA was expressed at higher levels than RNF31 UBA-IBR-IBR and was able to interact with RBCK1 isoform 1 (Figure 22, B) it failed to bind to PARK7 (Figure 24, D).

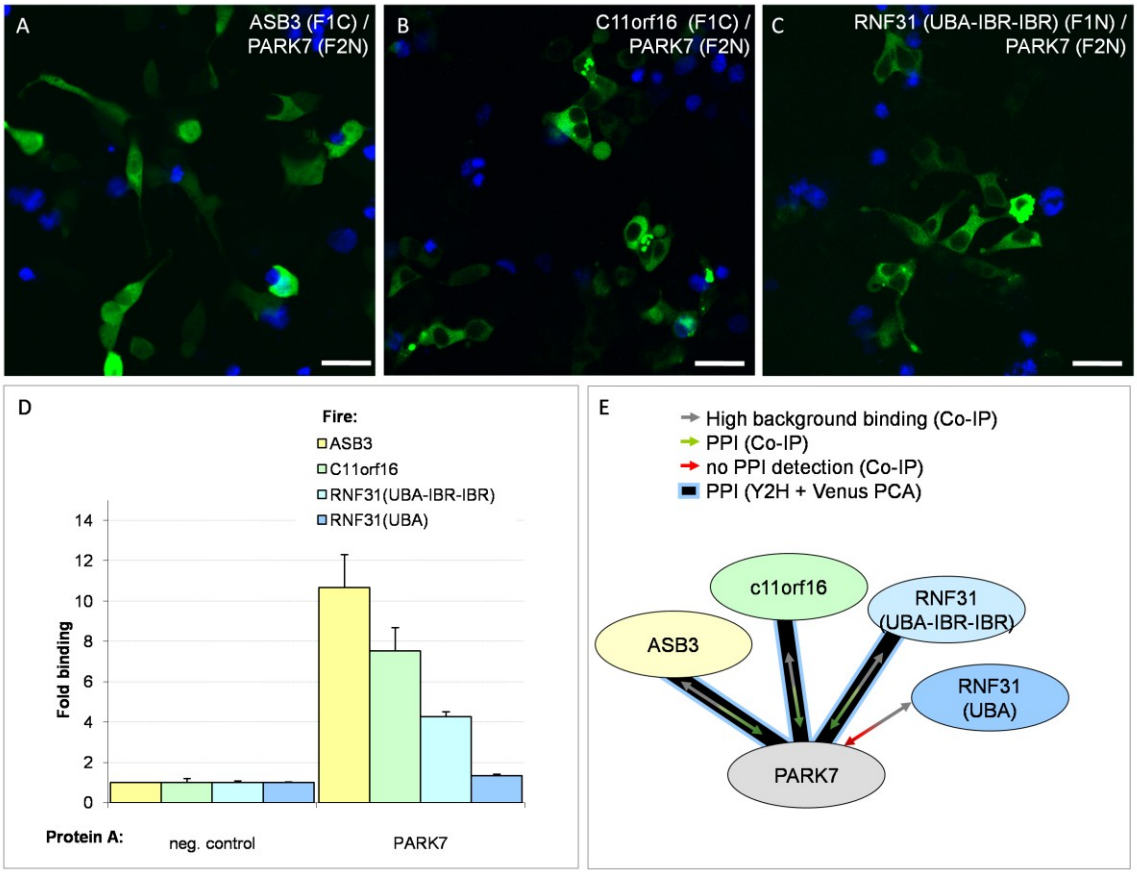


**Figure 24: ASB3, c11orf16 and RNF31 interact with PARK7 in different cell-based assays.**

**A**, **B** and **C**; Coexpression of PARK7 F2N (C-terminal Venus F2 fusion) with ASB3-F1C (A), c11orf16-F1C (B) or RNF31-F1N (C) for 24 h in HEK 293 cells resulted in cytoplasmic fluorescence. Scale bar: 30 µm.
**D,** Co-IP experiments were performed and analyzed as described in material and methods. Binding of ASB3, c11orf16, RNF31 UBA and RNF31 UBA-IBR-IBR firefly fusions to PARK7 was investigated. Additional co-IP experiments with a RNF31 fragment (RNF31 UBA) showed that the interaction between PARK7 and RNF31 depends on the RBR domain of RNF31.
**E**, Network illustration of the PARK7 interactions.

We conclude that similar to the PARK2-PARK7 interaction, which depends on the RBR domain of PARK2, also the RNF31-PARK7 interaction depends on the RNF31 RBR domain (Figure 22, A).

To determine where these interactions occur in intact cells we performed Venus PCA assays. PARK7 C- or N-terminal Venus F2 fusions were found to interact with ASB3, RNF31 and c11orf16 Venus F1 fusions and the fluorescence was distributed homogenously in the cytoplasm (Figure 24, A, B and C). Performing the experiment in the other orientation with PARK7 Venus F1 fusions did not work except for the interaction between PARK7-F1C and c11orf16-F2C which occurred in the cytoplasm. For each PARK7 interaction four out of eight different Venus fusion protein combinations were tested positive. All PARK7 interactions occurred in the cytoplasm. As these newly discovered interactions (*e.g.* PARK7-RNF31) reproduce the observed cytoplasmic interaction localisation pattern of the well-studied RBCK1-RNF31 and the DAX1-RNF31 interaction, we conclude that the observed interactions and interaction localisations are physiogical meaningful. The PARK7 interactions were observed in three different interaction assays and link PARK7 to two proteins involved in ubiquitination processes. However, although several experimental approaches were undertaken (see discussion 4.1.2) we failed to reproduce the kinase-dependency observed in the modified Y2H system.

## 3.4 Contribution of PIK3R3 SH2 domains to PARK7 binding

The PD-associated gene product PARK7 was also identified as PIK3R3 interactor in the performed Y2H screens. PIK3R3 is one of five regulatory PI3K subunits known to form heterodimers with p110 catalytic subunits that have lipid and Ser/Thr kinase activity (Fruman, et al., 1998; Vanhaesebroeck and Waterfield, 1999). Each of the regulatory subunits can interact with each of the three p110 catalytic subunit isoforms, which suggests that different heterodimers may mediate signalling in different PI3K pathways such as cell growth, proliferation, apoptosis, motility, differentiation, survival, and intracellular trafficking (Foster, et al., 2003). In order to validate the kinase-dependent interaction between the SH2 domain containing PI3K subunit (PIK3R3) and PARK7, we performed co-IP and Venus PCA experiments with PIK3R3 SH2 domain mutants. SH2 domains consists of 2 α-helices and 7 β-strands and point mutations in the highly conserved FLVRES motif of the second β-strand (βB) are known to reduce their binding to the phosphotyrosine and tyrosine-phosphorylated cellular proteins (Mayer, et al., 1992). Thus we exchanged the argenine (R) residue in this motif with leucine (L) or lysine (K) in both of the two PIK3R3 SH2 domains (named PIK3R3 LL or KK further on) and tested the binding of mutant and wildtype PIK3R3 to PARK7.

In co-IP experiments the PIK3R3 LL firefly fusion protein was expressed to higher levels than the wildtype protein but was not able to bind PARK7 (Figure 25, D). Mutant PIK3R3 binding to PARK7 did not differ significantly from background binding to a non-related PA fusion protein. Additionally, wildtype PIK3R3 binding was 5 times stronger than mutant PIK3R3 LL binding.

We performed Venus PCA assays to determine where these interactions occur in intact cells and if the fluorescence signal is diminished with the PIK3R3 mutants. First, PIK3R3 Venus F1 fusions were coexpressed with PARK7 Venus F2 fusions. Twelve different combinations were possible because C- and N-terminal fusions of PARK7, PIK3R3, PIK3R3 LL and PIK3R3 KK were used. Wildtype PIK3R3-F1N gave a strong fluorescence signal, while the PIK3R3 mutants with PARK7-F2C resulted in a much lower signal (Figure 25, B). No mutant effect was seen if the same PIK3R3-F1N fusion proteins were coexpressed with PARK7-F2N. If PIK3R3-F1C fusion proteins were used, wildtype PIK3R3 gave again a substantially stronger fluorescence signal than mutant PIK3R3 with PARK7-F2N (Figure 25, A) while for PARK7-F2C no mutant effect was seen (appendix Figure 41). In a second step six additional experiments in the other orientation were performed. PARK7-F1C resulted again in stronger fluorescence signals for wildtype than mutant PIK3R3 Venus F2 fusions, irrespective if N- or C-terminal PIK3R3 fusions were used (data shown in the appendix Figure 41). Experiments with PARK7-F1N were not performed because PARK7-F1N was incapable to bind to wildtype PIK3R3 in the first place.

To summarize, we were able to validate the interaction between PARK7 and PIK3R3, showed that it occurred in the cytoplasm and that PIK3R3 SH2 domain mutants showed substantially reduced binding to PARK7 in three different experimental setups (Figure 25, C).

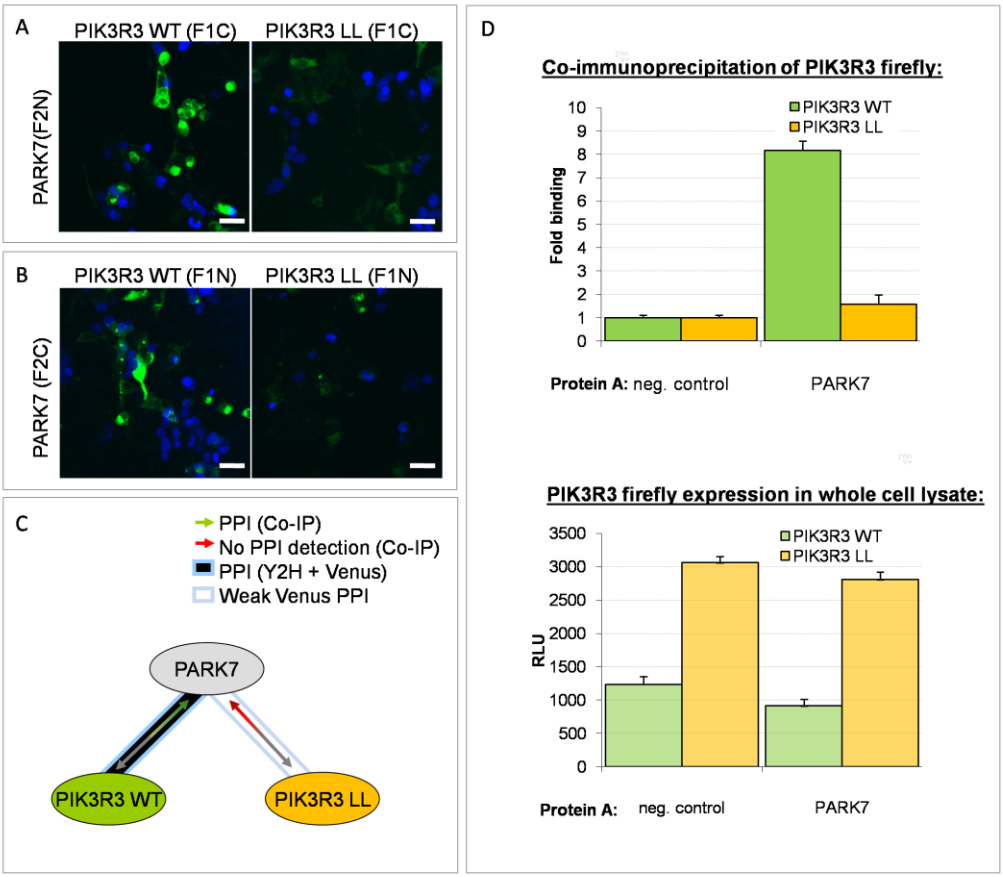


**Figure 25: Contribution of PIK3R3 SH2 domains to PARK7 binding.**

**A** and **B,** Coexpression of PARK7-F2N/PIK3R3-F1C (A) or PARK7-F2C/PIK3R3-F1N (B) for 24 h in HEK 293 cells resulted in PCA induced cytoplasmic fluorescence. This fluorescence signal was substantially diminished if SH2 domain mutants like PIK3R3 LL-F1C (A) or PIK3R3 LL-F1N (B) were used. Scale bar: 30 µm.
**C**, The Y2H interaction between wildtype PIK3R3 and PARK7 was successfully validated in Venus PCA experiments (blue line with black filling) and co-IP experiments (green arrowhead pointing towards PARK7). We could not detect an interaction between PIK3R3 LL and PARK7 in co-IP experiments and compared to wildtype PIK3R3 the obtained fluorescence signal was substantially reduced in Venus PCA experiments.
**D**, Co-IP experiments were performed and analyzed as described in material and methods. Wildtype (PIK3R3) and mutant (PIK3R3 LL) PIK3R3 firefly fusions were coexpressed with PARK7. In order to compare wildtype and mutant PIK3R3 firefly fusion coimmunoprecipitation levels with each other, the fold change binding was calculated from luciferase intensities measured with the non-related PA fusion protein (neg. control). Even though relative luciferase units (RLU) measured for mutant PIK3R3 LL firefly fusion were higher (bottom graph), which corresponds to higher firefly fusion expression levels, no binding to PARK7 was detected (upper graph).

## 3.5 Unravelling the cellular function of NF2 and its isoforms

### 3.5.1 Dimerization differences between NF2 isoforms

Inactivation of NF2 (also known as merlin and neurofibromin 2) causes Neurofibromatosis type 2 and other sporadic cancers (Hanemann, 2008). Neurofibromatosis type 2 is an autosomal dominant disorder which is characterized by the development of bilateral vestibular schwannomas. NF2 inactivation underlies various sporadic tumours of the nervous system, heterozygous NF2 mutant mice ($NF2^{+/-}$) develop human-like schwannomas (McClatchey and Giovannini, 2005; Okada, et al., 2007) and NF2 induces growth suppression in tumourigenic cell lines (Gutmann, et al., 1998). These studies suggest that NF2 is a tumour suppressor. The NF2 gene is composed of 17 exons and is subject to alternative splicing. Two predominant isoforms (isoform 1 and 2) and a number of minor isoforms are produced which differ in subcellular localization and function (Sherman, et al., 1997). Isoform 1 (NP_000259.1/P35240), lacking only exon 16, encodes for a 595 amino acid protein with a

predicted molecular mass of 66 kDa (Rouleau, et al., 1993; Trofatter, et al., 1993) (Figure 26, A). Isoform 2 (590 aa, NP_057502.2/P35240-3) contains the frameshift causing exon 16, which results in premature stop and consequently a shortened protein with different C-terminus (PQAQGRRPICI instead of LTLQSAKSRVAFFEEL) (Bianchi, et al., 1994; Hara, et al., 1994). Isoform 7 (507 aa, 56 kDa, NP_861968.1/P35240-4) lacks exons 2 and 3 but contains the frameshift causing exon 16. The resulting protein lacks the first subdomain of the globular FERM domain (representing amino acids 39-121 of isoform 1 and 2) and has the same C-terminus as isoform 2 (Figure 26, A).

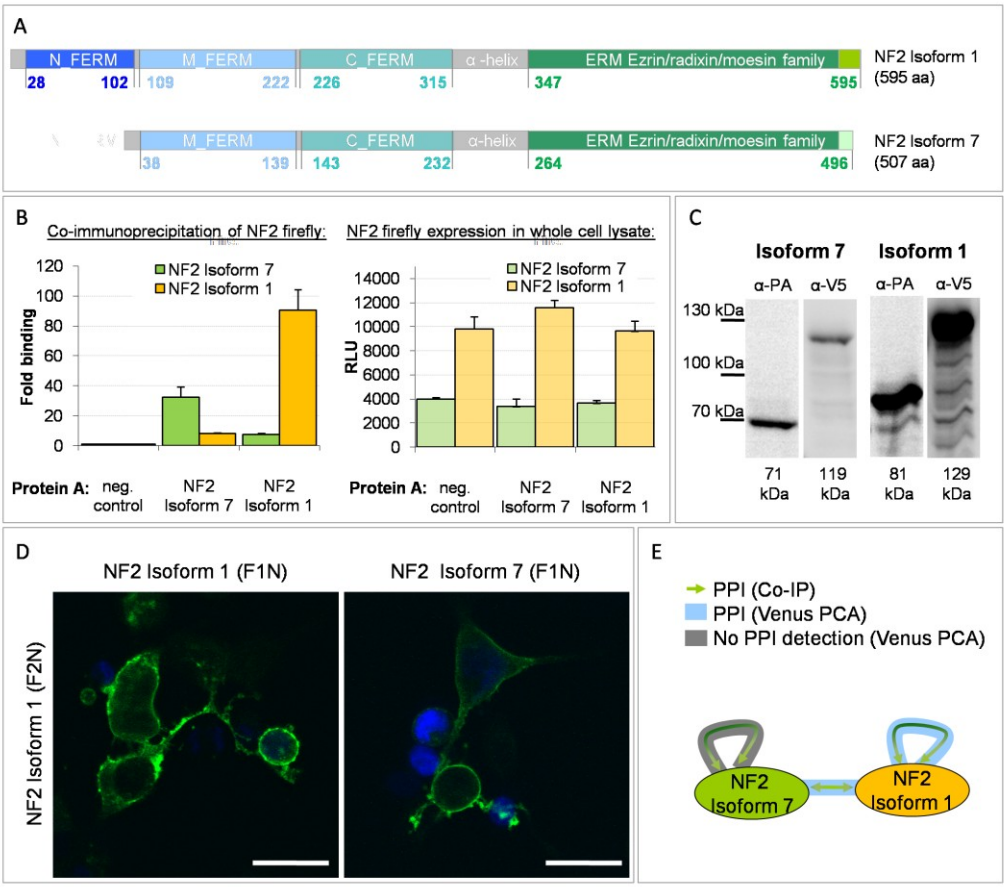


**Figure 26: NF2 isoforms show different dimerization abilities.**

**A**, Schematic diagram showing the domain structure of NF2 isoform 1 (595 aa, NP_000259.1/P35240) and NF2 isoform 7 (507 aa, NP_861968.1/P35240-4). Pfam predicts that NF2 isoform 1 contains an N-terminal (28-102 aa), central (109-222 aa) and C-terminal (226-315 aa) FERM domain and an ERM domain (347-595 aa) whereas NF2 isoform 7 only contains the central (38-139 aa) and C-terminal (143-233 aa) FERM domain and the ERM domain (264-496 aa). Both isoforms are derived from the same gene by alternative splicing. Isoform 7 lacks exons 2 and 3 (representing amino acids 39-121 of isoform 1) but contains the frameshift and premature stop causing exon 16. Sequence alignments showed that amino acids 1-38 and 39-497 of NF2 isoform 7 match perfectly to amino acids 1-38 and 122-579 of isoform 1, respectively, which means that the complete N-terminal FERM and a few residues of the central FERM domain are not present in isoform 7. The frameshift and premature stop causing exon 16 in isoform 7 leads to a completely different C-terminal tail (PQAQGRRPICI) compared to isoform 1 (LTLQSAKSRVAFFEEL).
**B**, Co-IP experiments were performed and analyzed as described in material and methods. Dimerization of NF2 isoforms was investigated. Both isoforms were able to build hetero- and homodimers but showed a strong preference for homodimerization (left graph). Relative luciferase units (RLU) measured for NF2 isoform 1 were higher (right graph).
**C**, Cell lysate prepared from HEK 293 cells coexpressing NF2 PA- and NF2 firefly-V5 fusion proteins was analyzed by immunoblotting using anti-V5-APH or anti-goat-HRP antibodies. Both isoforms were expressed and the observed size was in agreement with the predicted molecular mass of the fusion proteins indicated at the bottom of the blot. Note that the PA-tag adds 15 kDa and the firefly-tag 63 kDa to the original molecular weight of the protein.
**D**, Coexpression of NF2 isoform 1-F2N with NF2 isoform 1-F1N or NF2 isoform 7-F1N resulted in fluorescence at the plasma membrane. In the Venus PCA system no preference for homodimerization was observed. NF2 isoform 1/isoform 7 heterodimers and NF2 isoform 1 homodimers showed comparable fluorescence intensities and cellular localisation. Scale bar: 30 µm.
**E**, Homodimerization and heterodimerization of both NF2 isoforms was observed in co-IP experiments (green arrows). In the Venus PCA assay homodimerization of NF2 isoform 1 and heterodimerization between isoform 1 and 7 was visualized (blue line), whereas NF2 isoform 7 homodimerization was not detected (grey line) in this system.

Interestingly, full length NF2 isoform 2 and truncated NF2 isoform 1 lacking the C-terminal tail fail to induce growth suppression (Sherman, et al., 1997). The NF2 tumour suppressive function is believed to be regulated by self-association between the FERM and the C-terminal domain (head-to-tail interaction). The observation that formation of the head-to-tail interaction requires residues 585-595 (KSRVAFFEEL) (Gronholm, et al., 1999), which are lacking in isoform 2 and 7, points to the direction that NF2 proteins in an open conformation can not act as tumour suppressor (Sherman, et al., 1997). The NF2 isoform 1 head-to-tail interaction between residues 302-308 in the FERM domain and residues 580-595 in the C-terminal domain depends on proper folding of the FERM domain which requires self-association of residues 8-121 and 200-302 (Gutmann, et al., 1999). These intramolecular interactions modulate the molecular function and the subcellular localization of the NF2 isoforms. Proper folding of the N-terminal FERM domain of isoform 1 is required for localization beneath the plasma membrane, in membrane ruffles and filopodia (Brault, et al., 2001; Gonzalez-Agosti, et al., 1996; Sainio, et al., 1997) whereas deletion of exon 2 and 3 (residues 39-121) results in improper FERM domain folding and impaired membrane localization of these isoforms (Brault, et al., 2001; Deguen, et al., 1998; den Bakker, et al., 2000; Koga, et al., 1998; Kressel and Schmucker, 2002). Furthermore, NF2 residues 50-70 (encoded by exon 2) are bound by the molecular adaptor paxillin (Fernandez-Valle, et al., 2002) which is one of the cytoskeletal proteins like βII spectrin (Scoles, et al., 1998) and other ERM proteins (Gronholm, et al., 1999; Meng, et al., 2000) that indirectly link NF2 to the actin cytoskeleton. Additionally, membrane localization is achieved by direct interaction with transmembrane and scaffolding proteins like CD44 (Sainio, et al., 1997), CD43 (Yonemura, et al., 1998), layilin (Bono, et al., 2005), paranodin (Denisenko-Nehrbass, et al., 2003), β-integrin (Obremski, et al., 1998), NHERF (Murthy, et al., 1998) and syntenin (Jannatipour, et al., 2001).

Isoforms 1 and 7 were the only isoforms included in the initial Y2H screen and cDNAs for the other isoforms were not available, therefore we focused our analysis on these isoforms and their PPI pattern. The generated NF2 protein A and firefly fusion proteins were expressed and showed the expected size (Figure 26, C). The 10 kDa larger isoform 1 was generally expressed to higher levels than isoform 7. The stronger bands seen on the immunoblot for isoform 1 firefly fusions are in agreement with the higher relative luciferase intensities measured (Figure 26, B, right graph).

In order to test the functionality of the generated fusion proteins we tested their ability to form dimers in co-IP and Venus PCA experiments. It has been discussed that the domains responsible for the intramolecular head-to-tail interaction could also mediate intermolecular head-to-tail interactions of ERM proteins (Gary and Bretscher, 1995; Henry, et al., 1995; Martin, et al., 1995). Both the intra- and/or the intermolecular interaction model could explain the differential activity of NF2 because the head-to-tail closed monomers but also the dimers could represent the active (*i.e.* tumour suppressive) form of the protein. Furthermore, it is known that the full length isoform 1 is able to form homodimers and heterodimers with isoform 2 (Gronholm, et al., 1999; Sherman, et al., 1997). Performing the co-IP experiments, we found that both isoforms showed a strong preference for homo-dimerization (Figure 26, B, left graph). Interactions with the other isoform were also detected but at much lower level. The ability of NF2 to self-associate requires residues 585-595 (KSRVAFFEEL) (Gronholm, et al., 1999; Sherman, et al., 1997) and thus it is surprising that we detected homodimerization of NF2 isoform 7 which lacks these residues. However, homodimerization of NF2 isoform 2 which is also lacking these residues was detected before (Meng, et al., 2000; Scoles, et al., 2002). Heterodimerization between isoform 1 and isoform 2 was reported to be weaker (Gronholm, et al., 1999), stronger (Meng, et al., 2000) or equal (Scoles, et al., 2002) compared to homodimerization of isoform 1. In contrast, in Venus PCA experiments

performed in this study only isoform 1 was able to build homodimers. We tested four fusion protein combinations per isoform, and observed two interacting pairs for isoform 1 (isoform 1-F1N/isoform 1-F2N and isoform 1-F1C/isoform 1-F2C) (Figure 26, D) and none for isoform 7. Additionally, heterodimerization between the isoforms was detected in two out of eight fusion protein combinations tested (isoform 1-F1N/isoform 7-F2N and isoform 7-F1N/isoform 1-F2N) (Figure 26, D). NF2 isoform 1 homodimers are located beneath the cell membrane which is in agreement with reports that the cytoskeleton-associated membrane-organizing protein NF2 is localized at the plasma membrane, in membrane ruffles and filopodia (Gonzalez-Agosti, et al., 1996; Sainio, et al., 1997). Interestingly, the heterodimer between NF2 isoform 7 and isoform 1 is localized to the membrane which is probably a result of the properly folded FERM domain in isoform 1. We conclude that the generated NF2 fusion proteins are functional because they showed the expected localization and dimerization behaviour.

### 3.5.2 Localisation differences between NF2 isoforms

In the Y2H screen we identified RYBP, AOF2, EMILIN1 and PIK3R3 as interaction partners for NF2 isoform 7 and AOF2 and EMILIN1 as interaction partners for NF2 isoform 1. The interaction between EMILIN1 and NF2 isoform 7 was obtained in all four biological replicas (29 from 32 spots) whereas the interaction with isoform 1 was only partially observed in one replica (3 from 32 spots). To further elucidate the differential interaction pattern of the isoforms, we performed co-IP experiments.

NF2 firefly fusions were tested against a panel of PA-tagged proteins (Figure 27, B). In agreement with the Y2H results AOF2, EMILIN1 and PIK3R3 showed a preference for isoform 7. Binding to isoform 1 was also detected but was on average 2 times weaker. Performing these co-IP experiments we found an interaction between NF2 and PARK7, which was included as control because both proteins were interacting with PIK3R3 in Y2H experiments. In contrast to the other PA-tagged proteins, PARK7 showed a stronger binding to NF2 isoform 1, thus the observed preferences can be regarded as isoform specific. Performing co-IP experiments in the other orientation resulted in even stronger isoform-specific signals (Figure 27, A). AOF2, EMILIN1 and PIK3R3 firefly fusions strongly bound to isoform 7 whereas binding to isoform 1 was not detected. As the non-interacting NF2 isoform 1 protein A fusion was functional in prior dimerization experiments (Figure 26, B), the observed differences may reflect isoform-specific binding preferences. In NF2 isoform 1, the C-terminal tail adopts an extended conformation, interacts with the FERM domain and might mask binding sites for other proteins (Pearson, et al., 2000). In contrast, NF2 isoforms lacking the C-terminal tail (585-595 aa, KSRVAFFEEL) are unable to form a head-to-tail closed molecule and may thus constitutively expose different interaction surfaces for other proteins (Pearson, et al., 2000). As this head-to-tail interaction is modulated by phosphorylation we expect that a small fraction of the cellular NF2 isoform 1 protein pool is in the open conformation and is thus able to interact. This model is consistent with our observation that AOF2, EMILIN1 and PIK3R3 preferred binding to NF2 isoform 7 in the Y2H and the co-IP experiments. The interaction between NF2 and RYBP was tested with both NF2 isoforms in both orientations with negative outcome and was thus not validated.

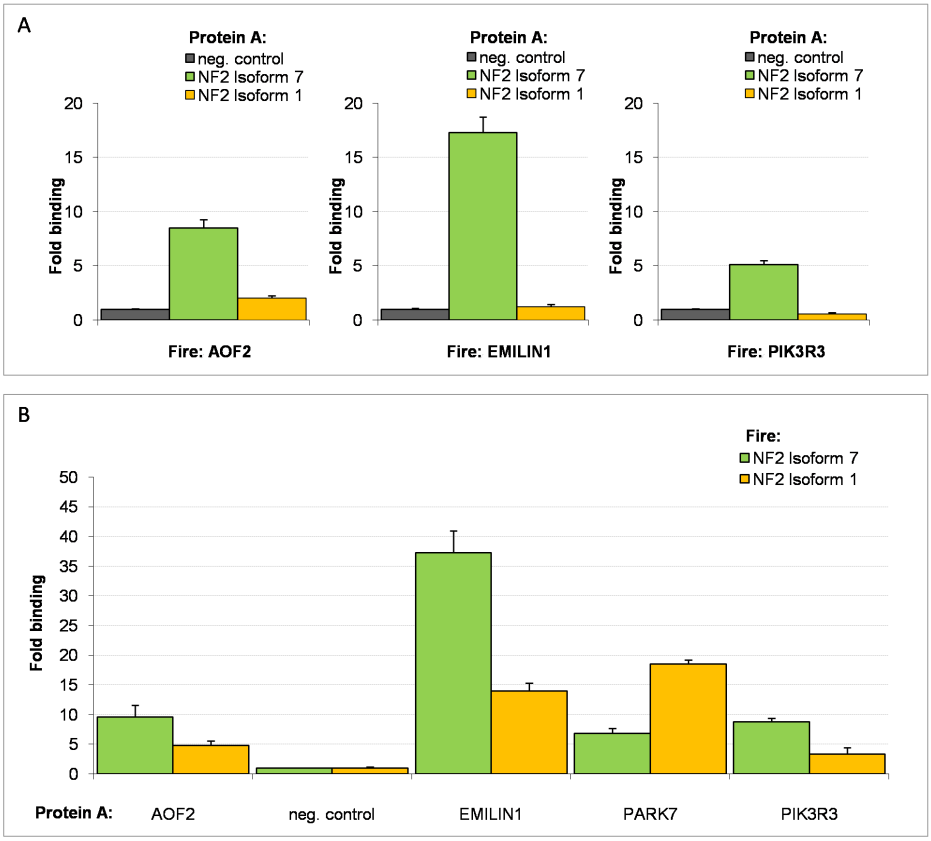


**Figure 27: NF2 isoforms differ in interaction pattern.**

Co-IP experiments were performed and analyzed as described in material and methods.
**A**, Binding of AOF2, EMILIN1, PIK3R3 firefly fusions to NF2 isoforms was investigated. In contrast to NF2 isoform 1, NF2 isoform 7 was able to interact with AOF2, EMILIN1 and PIK3R3.
**B**, Binding of NF2 firefly fusions to AOF2, EMILIN1, PIK3R3, and PARK7 was investigated. AOF2, EMILIN1, PIK3R3, and PARK7 protein A fusion proteins were able to interact with both isoforms. AOF2, EMILIN1 and PIK3R3 showed a strong preference for isoform 7, whereas PARK7 showed stronger binding to NF2 isoform 1.

In contrast to the co-IP experiments, in the Venus PCA assay NF2 isoform 1 was able to interact with AOF2, EMILIN1 and PIK3R3. Both isoforms fused C- or N-terminal to Venus F2 bound to PARK7, AOF2, EMILIN1 and PIK3R3 Venus F1 fusions (Figure 28 A). However, the interactions occurred at a distinct subcellular localization compared to isoform 7. Interactions with isoform 1 were located to the membrane whereas the corresponding interactions with isoform 7 occurred in the cytoplasm. The observed subcellular localizations coincide with the literature knowledge (Deguen, et al., 1998; den Bakker, et al., 2000; Gonzalez-Agosti, et al., 1996; Sainio, et al., 1997). Additionally, the membrane localization of NF2 isoform 1 interactions is in agreement with the results of the dimerization experiments preformed in this study. Interestingly, isoform 7 interacted with PARK7, AOF2, EMILIN1 and PIK3R3 in the cytoplasm but with NF2 isoform 1 beneath the cell membrane where all isoform 1 interactions occurred. This shows that isoform 7 is located in the cytoplasm and/or at the cell membrane because interactions with isoform 7 can occur at either subcellular compartment. Probably the interaction localisation depends on the localization of the interaction partner. The different subcellular interaction localization patterns probably reflect the different cellular functions of the NF2 isoforms. NF2 isoform-specific binding to SCHIP1, HGS isoforms and βII-spectrin has been detected before in different interaction assays (Goutebroze, et al., 2000; Scoles, et al., 1998). For example, NF2 isoform 2 and the FERM domain of NF2 isoform 1 (1-314 aa) differed in SCHIP1 binding compared to full length isoform 1 (Goutebroze, et al., 2000). Furthermore, full length NF2 isoform 1 was able to heterodimerize with ezrin in co-IP

experiments but failed to interact in Y2H experiments. The heterotypic interaction between NF2 and ezrin was only obtained in Y2H experiments if NF2 isoform 1 was expressed as truncated protein (Gronholm, et al., 1999). However, we performed three different interaction assays with two isoforms in parallel and observed that both NF2 isoforms were capable to bind to AOF2, PIK3R3, PARK7 and EMILIN1 in at least two distinct interaction assays (Figure 28 B). In agreement with the literature knowledge about NF2 isoform localization, these novel interactions were localized in the cytoplasm or beneath the cell membrane for isoform 7 or isoform 1, respectively. This suggests that the naturally occurring splice variant lacking exons 2 and 3 (*i.e.* isoform 7) has a different cellular function than the full length protein.

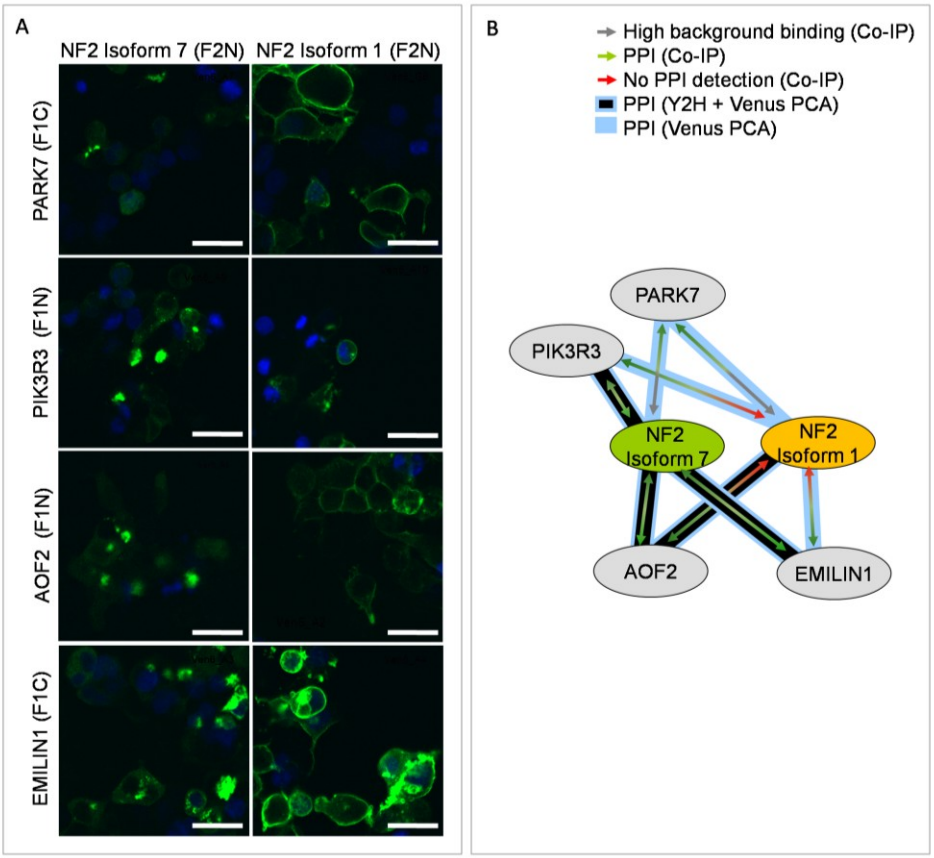


**Figure 28: NF2 isoforms differ in interaction localization.**

**A**, Coexpression of PARK7, PIK3R3, AOF2 and EMILIN1 Venus F1 fusions with NF2 isoform 7-F2N resulted in cytoplasmic fluorescence whereas coexpression with NF2 isoform 1-F2N resulted in fluorescence at the plasma membrane. The only difference between these experiments was the employment of different NF2 isoforms. Scale bar: 30 µm.
**B**, Network illustration of the NF2 interactions. Both NF2 isoforms were shown to interact with PIK3R3, PARK7, AOF2 and EMILIN1 in at least two different interaction assays. In Venus PCA and co-IP assays NF2 isoform 1 was shown to interact with EMILIN1 and PIK3R3, which were identified as NF2 isoform 7 interaction partners in the Y2H screen. Interactions with NF2 isoform 1 were generally weaker in co-IP experiments (with exception of PARK7) and showed cytoplasmic localization in Venus PCA experiments.

### 3.5.3 Contribution of PIK3R3 SH2 domains to NF2 binding

In order to validate the kinase-dependent interactions between the SH2 domain containing PI3K regulating subunit (PIK3R3) and NF2, we performed co-IP and Venus PCA experiments with PIK3R3 SH2 domain mutants with reduced pTyr-binding capability. While performing co-IP experiments with PARK7 PA fusions we observed that mutant and wild type PIK3R3 firefly fusion proteins were expressed to different levels. The firefly expression was measured and adjusted to higher mutant expression, consequently co-IP experiments can be well controlled in this orientation (Figure 25, C and Figure 29, B). Although PIK3R3 LL firefly expression was three

times higher than PIK3R3 WT firefly expression, the binding to NF2 isoform 7 was reproducibly and substantially reduced (Figure 29, B). However, we wished to perform the assay also in the other orientation and thus we had to control wild type and mutant PIK3R3 PA fusion protein expression. Consequently, we transfected the normal (150 ng) and the doubled (300 ng) amount of PIK3R3 protein A plasmid DNA to enhance expression, immunoprecipitation (IP) and if it would be an expression-dependent effect also coimmunoprecipitation (Figure 29, A).

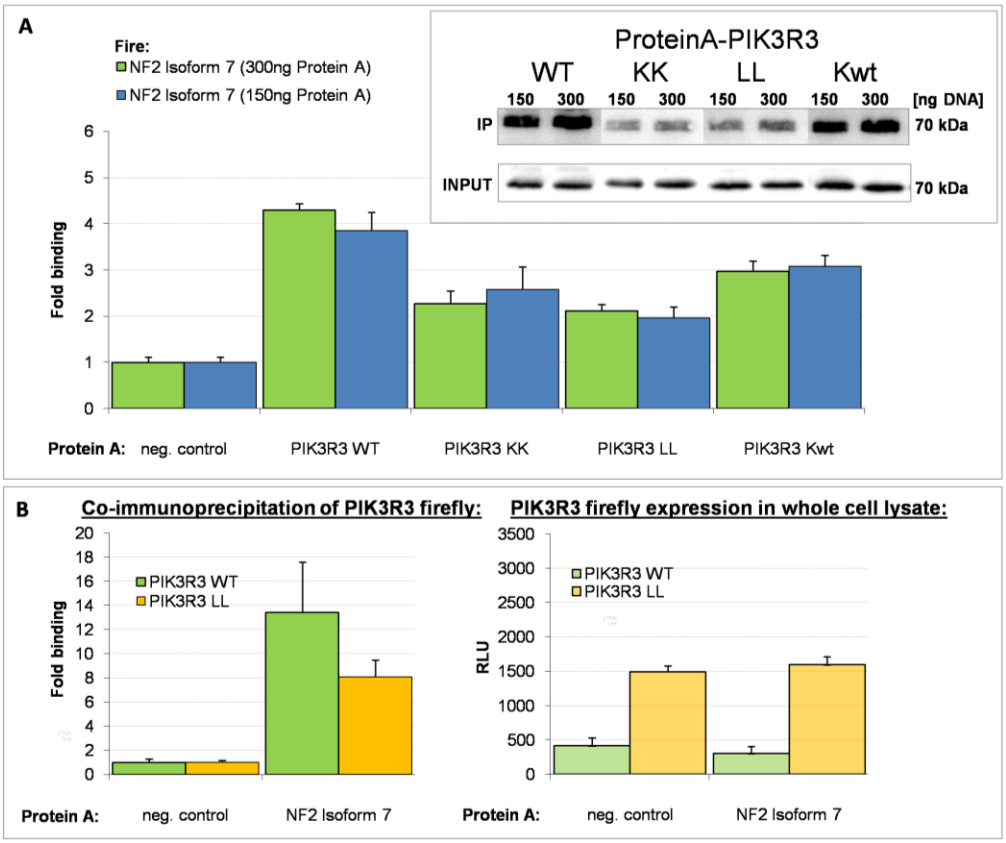


**Figure 29: NF2 firefly fusion protein binding does not correlate with the amount of transfected mutant or wild type PIK3R3 PA fusion protein.**

Co-IP experiments were performed and analyzed as described in material and methods.
**A**, In this co-IP experiment 150 ng (blue panel) or 300 ng (green panel) of PIK3R3 protein A plasmid DNA were cotransfected with a constant amount of NF2 firefly plasmid DNA (150 ng). After 36 hours, binding of NF2 isoform 7 to wildtype (WT) and mutant (KK, LL, Kwt) PIK3R3 was investigated. The increase in transfected PIK3R3 protein A plasmid DNA (300 ng) led to enhanced PIK3R3 expression and immunoprecipitation but not to enhanced NF2 firefly fusion protein coimmunoprecipitation.
**Insert**: The cell lysate used for co-IP experiments (Input) and the amount of immunoprecipitated Protein A fusion protein (IP) was analyzed by immunoblotting using anti-goat-HRP (Zymed # 61-1620, 1:3000) antibodies to control for PIK3R3 protein A expression and immunoprecipitation, respectively. The PA-tag adds 15 kDa to the original molecular weight of 54.5 kDa and the observed size matches to the calculated molecular mass of 70 kDa.
**B**, Wildtype (PIK3R3) and mutant (PIK3R3 LL) PIK3R3 firefly fusions were coexpressed with NF2 or a non-related PA fusion protein. Although mutant PIK3R3 LL firefly fusion expression was higher than wild type PIK3R3 firefly expression in the whole cell lysate (right graph, RLU: relative luciferase units) the binding to NF2 was reproducibly reduced (left graph).

To control for equal expression of PA fusions a part of the cell lysate used for co-IP experiments was analyzed by immunoblotting which shows that the expression of the PIK3R3 protein A fusion proteins was comparable (Figure 29, A, Insert). After the binding of the firefly fusion protein (co-IP) to the PA fusion protein (IP) was assessed by measuring the firefly luciferase activity, the amount of immunoprecipitated PA fusion protein was analyzed by immunoblotting. The PIK3R3 protein A fusions can be divided in two groups with PIK3R3 WT and Kwt being strongly and PIK3R3 LL and KK being moderately immunoprecipitated. NF2 isoform 7 was able to bind to PIK3R3 WT and Kwt but not to PIK3R3 KK or LL. The coimmunoprecipitation pattern of NF2 reflects

the immunoprecipitation pattern of PIK3R3 and thus the observed reduced binding can result from the low immunoprecipitation of the PIK3R3 mutants or the introduced SH2 domain mutations. However, NF2 isoform 7 coimmunoprecipitation could not be enhanced by transfection of the doubled amount of PIK3R3 protein A plasmid DNA (Figure 29, A). Therefore we conclude that the seen reduction in binding is due to SH2 domain mutation. Mutation of the N-terminal SH2 domain (PIK3R3 Kwt) does not influence the binding but if additionally the C-terminal SH2 domain is mutated (PIK3R3 KK or LL) the binding is abolished. That the C-terminal SH2 is responsible for NF2 binding is in agreement with the report that the C-terminal SH2 of PIK3R1 is responsible for binding to ezrin, a highly similar ERM-family member (Gautreau, et al., 1999). However, the responsible residue Tyr353 is not conserved between ezrin and NF2. This residue lies in the C-terminal ERM domain which is less conserved (approximately 25 % homology) between ERM family members than the N-terminal FERM domain (approximately 63 % homology). Performing this experiment with adjusted PIK3R3 protein A expression levels showed that binding to PIK3R3 KK and LL was reduced by half in comparison to the wildtype PIK3R3 (Figure 30, A).

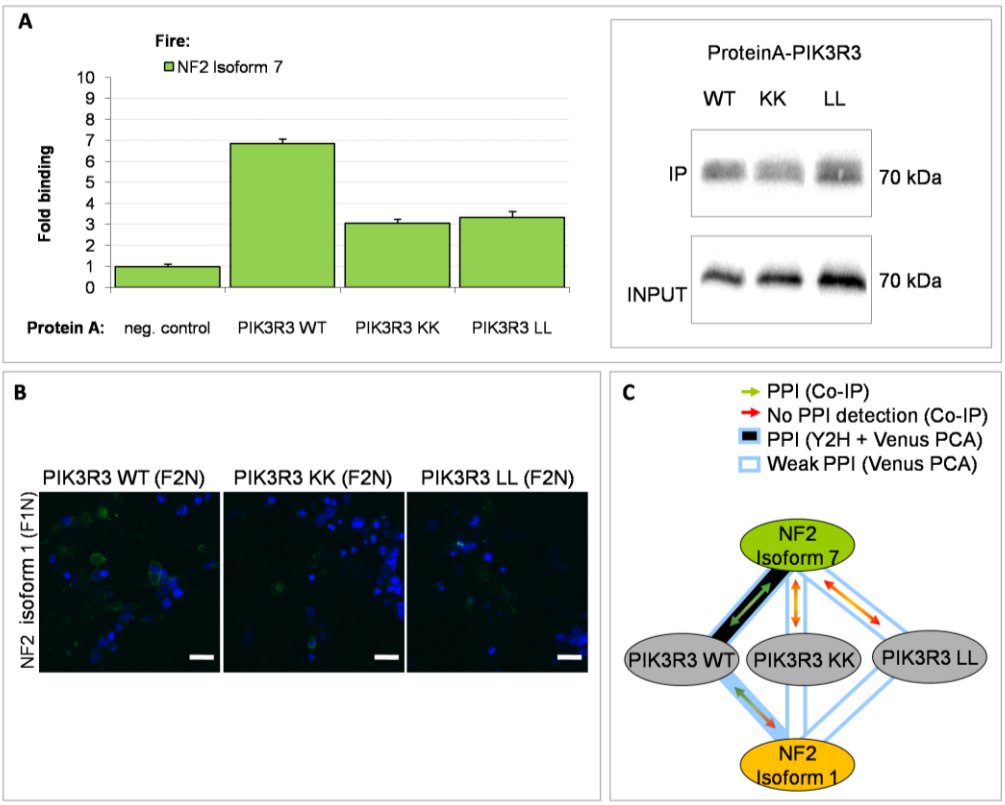


**Figure 30: PIK3R3 SH2 domains contribute to stable NF2 binding.**

**A**, Co-IP experiments were performed and analyzed as described in material and methods. Binding of NF2 isoform 7 to wildtype (WT) and mutant (KK, LL) PIK3R3 was investigated. Only wildtype PIK3R3 was able to interact with NF2 and the results with the mutant PIK3R3 fusions indicate that SH2 domains are required for this process.
**Insert:** The cell lysate used for co-IP experiments (Input) and the amount of immunoprecipitated protein A fusion protein (IP) was analyzed by immunoblotting using an anti-goat-HRP (Zymed # 61-1620, 1:3000) antibody to control for PIK3R3 protein A expression and immunoprecipitation, respectively. All PIK3R3 protein A fusions were expressed and immunoprecipitated to the same extend.
**B**, Coexpression of NF2 isoform 1-F1N with PIK3R3 WT-F2N for 24 h in HEK 293 cells results in cytoplasmic fluorescence. This fluorescence signal is substantially diminished if SH2 domain mutants like PIK3R3 LL-F2N or PIK3R3 KK-F2N were used. Scale bar: 30 µm.
**C**, The Y2H interaction between wildtype PIK3R3 and NF2 isoform 7 was successfully validated in Venus PCA experiments (blue line with black filling) and co-IP experiments (green arrow). NF2 isoform 1 was found to interact with PIK3R3 in Venus PCA experiments (blue line) and in one orientation in co-IP experiments (green and red arrow). The interaction between PIK3R3 LL or PIK3R3 KK and NF2 was severely reduced compared to wildtype PIK3R3 in co-IP and Venus PCA experiments.

Analysis of the cell lysate and the immunoprecipitated PA fusion proteins by immunoblotting confirmed comparable expression levels and immunoprecipitation rates. This experiment clearly showed that the pTyr-binding ability of SH2 domains contributed substantially to NF2 binding. In order to validate this SH2 domain-dependent binding in a different system we performed Venus PCA experiments with PIK3R3 SH2 domain mutants. In the Venus PCA system both NF2 isoforms were able to interact with PIK3R3. Several combinations were tested and we repeatedly observed a stronger fluorescence signal with wildtype PIK3R3 than with mutant PIK3R3 (PIK3R3 KK or LL) for both NF2 isoforms (all results are shown in the appendix Figure 41). Exemplarily one experiment with NF2 isoform 1-F1N and wildtype or mutant PIK3R3 Venus F2N fusions is shown (Figure 30, B).

We conclude that the PIK3R3 SH2 domains contribute to stable NF2 binding, irrespective of the NF2 isoform. PIK3R3 was weakly bound to NF2 isoform 1 in co-IP experiments but was shown to interact in a SH2 domain-dependent manner in the Venus PCA system. NF2 isoform 7 showed in both cell-based assays a clear preference for wildtype PIK3R3. In addition, this newly identified phosphorylation-dependent interaction between PIK3R3 and NF2 was located to different cellular compartments depending on the NF2 isoform. Similar to other NF2 interactions identified in this study, the interaction with PIK3R3 was localized in the cytoplasm or beneath the cell membrane for NF2 isoform 7 and 1, respectively. The results obtained in Y2H, co-IP and Venus PCA experiments suggest a conditional isoform-specific mode of interaction, localisation and probably function.

# 4 Discussion

## 4.1 Detection of kinase-dependent interactions

### 4.1.1 Relevance of kinase-dependent interactions

Signalling networks control many different aspects of cellular behaviour and are required for the dynamic response to extracellular signals. The dynamic and rapid transfer of signals in these networks is mediated by post-translational protein modifications (PTMs) which alter the properties of a protein by adding chemical groups or by covalent attachment of Ub-like proteins. PTMs function as switches in interaction networks as they enable proteins to interact with new interaction partners. PTMs induce interactions by changing the protein conformation and by triggering the exposure of priory inaccessible interaction surfaces or by serving as interaction motif for proteins containing PTM-recognition domains. The extensive array of highly dynamic and reversible PTMs provides flexibility and diversity, so that a limited set of signalling proteins can offer distinct biological functions in different cellular contexts. An ubiquitous regulatory mechanism in signalling networks across all species is phosphorylation. The importance of this PTM is underlined by the fact that genes encoding kinases and phosphatases account for 1.5–2 % of the protein-coding genome in eukaryotes (Manning, et al., 2002). The addition of phosphate groups to serine or threonine residues regulates amongst other processes cell cycle progression, the DNA-damage response and cellular growth (Nurse, 2000) whereas tyrosine phosphorylation is predominantly involved in transmembrane receptor signalling pathways regulating cellular proliferation and differentiation (Ullrich and Schlessinger, 1990). Some examples how phosphorylation and phosphorylation-dependent interactions regulate these processes will be highlighted in the following section.

Tyrosine phosphorylation is predominantly used in signalling through transmembrane receptors: ligand-mediated dimerization, activation and autophosphorylation of RTKs recruit different sets of pTyr-binding proteins depending on the sequence context of the autophosphorylation site, the ligand and the receptor (Bradshaw and Waksman, 2002; Sun, et al., 1991; Uhlik, et al., 2005). Domains involved in pTyr-recognition are structurally well-defined and include SH2, PTB and C2 (conserved region-2 of protein kinase C) domains (Benes, et al., 2005; Kavanaugh, et al., 1995). PTB domain containing proteins like IRS1 or SHC typically function as docking proteins which bind pTyr-residues on activated RTKs. Quite often PTB domain containing proteins get phosphorylated themselves and get bound by SH2 domain containing proteins which finally activate distinct signalling pathways (Sun, et al., 1991; Uhlik, et al., 2005). SH2 proteins cover a wide range of biological functions. They have been shown to regulate GTPase signalling (by guanine nucleotide exchange factors and GTPase-activating proteins), ubiquitination mediated by Cbl E3 protein-ubiquitin ligases (Liu, et al., 2006), gene expression by STAT transcription factors, cytoskeletal organization by tensin proteins, tyrosine phosphorylation (through cytoplasmic Tyr kinases and tyrosine phosphatases), and phospholipid metabolism (by PI3K, PLCγ and inositol phosphatases). SH2-mediated binding of the regulatory PI3K subunit to Tyr-phosphorylated RTKs or RTKs-associated proteins, for example, recruits the PI3K heterodimer to the membrane and activates its lipid kinase activity (Cully, et al., 2006).

Probably pSer/pThr-dependent interactions are even more common since 83 % of the human kinome are Ser/Thr kinases and phosphorylation events occur to over 98 % on Ser/Thr-residues (Nita-Lazar, 2010). Thirteen different pSer/pThr-binding domains have already been reported (Seet, et al., 2006) and very likely there are more of them, which need to be discovered. The structurally unrelated domains belonging to the FHA, MH2,

WD40, BRCT, Polo-Box, FF, WW and 14-3-3 family regulate cellular functions ranging from cell cycle to gene expression and metabolism (Seet, et al., 2006). 14-3-3 proteins, for example, promote the cellular stress response, cell division and survival by regulating the conformation, the interaction pattern and the localization of their phosphorylated interaction partners (Mackintosh, 2004). WD40 domains of F-box proteins serve as phosphorylation-dependent substrate recognition sites of multi-protein E3 ubiquitin ligase complexes and mediate phosphorylation-dependent substrate ubiquitination and degradation (Seet, et al., 2006). FHA domains are pThr-binding modules found in DNA-damage-activated protein kinases, cell cycle checkpoint proteins phosphatases, transcriptional control proteins and regulators of small GTPases (Yaffe and Elia, 2001).

Phosphorylation represents a common mechanism through which signalling systems are controlled and the dynamic behaviour of the cell is regulated. To determine the organization of these signalling pathways is the crucial fundament to understand cellular behaviour in health and disease states. Many human disorders result from perturbations in signal transduction and especially neurodegeneration has been linked to phosphorylation-dependent signalling processes. Analysis of protein interaction networks in neurodegenerative diseases revealed that 14–3–3 proteins, PTB and WW domain containing proteins are overrepresented (Kanehisa, et al., 2010; Limviphuvadh, et al., 2007). The 14-3-3 proteins represent 1 % of the soluble brain proteins and are known to be relevant in the pathogenesis of neurodegenerative diseases, including Alzheimer's disease, Parkinson’s disease, polyglutamine diseases, Amyotrophic Lateral Sclerosis (Steinacker, et al., 2011) and Spinocerebellar Ataxia 1 (Chen, et al., 2003). Furthermore domains found in PKC (*i.e.* pfam: C1_1, C1_3, Pkinase_C) and tyrosine phosphatases (*i.e.* pfam: Y_phosphatase) were also enriched in these networks (Limviphuvadh, et al., 2007). These studies strongly implicate phosphorylation recognition in signalling pathways involved in NDs and caused us to analyze phosphorylation-dependent interactions involving proteins associated with neurological disorders. The identified interactions especially the modification-dependent ones could offer new points of actions for drugs against NDs (Fry and Vassilev, 2005; Ozbabacan, et al., 2011; Rudolph, 2007).

### 4.1.2 A modified Y2H system capable to detect modification-dependent PPIs

Currently available protein interaction datasets are mainly collections of constitutive PPIs. Datasets which additionally collect information about the cellular circumstances under which an interaction occurs or specifically which upstream enzyme triggers the interaction would dramatically change our understanding of signal transduction pathways. However, most of the currently available datasets do not include this information and high-throughput methods for the detection of modification-dependent interactions and simultaneous detection of candidate enzymes are missing. So far only strategies suited for small-scale identification of modification-dependent interactions plus the causative enzyme have been reported (Guo, et al., 2004; Osborne, et al., 1995; Shaywitz, et al., 2000; Yamada, et al., 2001). As Y2H systems are most widely used to identify PPIs in a high-throughput format and as phosphorylation represents the most abundant type of post-translational modification we designed a modified Y2H system capable to detect phosphorylation-dependent interactions.

Modified Y2H systems designed to detect phosphorylation-dependent interactions and a candidate human kinase in one step, however, might have to cope with the endogenous yeast kinase activity. Against all odds a modified yeast-based, cytoplasmic two-hybrid system was able to identify several JNK1-dependent interactions between human proteins in yeast (Da Costa, et al., 2010; Nateri, et al., 2004; Nateri, et al., 2005). This was

possible although several MAPK signalling cascades are conserved from yeast to humans (Widmann, et al., 1999) including a JNK1 yeast homologue (Brewster, et al., 1993; Galcheva-Gargova, et al., 1994; Han, et al., 1994; Levin-Salomon, et al., 2009). Additionally, pSer/pThr-dependent interactions between yeast proteins could be detected in a Y2H system if bait proteins were fused to their corresponding yeast kinase (Guo, et al., 2004). This system has the disadvantage that substrate and kinase have to be tethered. However, for Tyr kinases an approach with a third plasmid containing the kinase was shown to be successful (Cao, et al., 2002; Osborne, et al., 1995; Sylvester, et al., 2010; Yamada, et al., 2001).

In our modified Y2H system modification of the bait or prey protein is evoked by exogenous expression of human kinases from a third vector. The overexpression of a heterologous kinase which is normally lacking in yeast may cause cellular growth arrest (Hardwick, et al., 1996; Kornbluth, et al., 1987; Yamada, et al., 2001). To avoid this we used $Cu^{2+}$-inducible yeast expression vectors to fine-tune the kinase expression to levels that are tolerated by the two-hybrid host. One limitation of the classical Y2H approach is that bait and prey proteins must be able to enter the nucleus to activate transcription (Fields and Song, 1989). In respect to this we expressed kinases with or without N-terminal nuclear localization signal (NLS) to allow phosphorylation of the bait and prey proteins in the cytoplasm before they shuttle to the nucleus or after shuttling (*i.e.* in the nucleus). In our Y2H system the bait proteins are fused to the DNA binding domain of LexA and the prey proteins to the activation domain of Gal4 such that an interaction between any bait and prey pair reconstitutes a functional transcription factor that drives reporter gene expression. If kinase-mediated phosphorylation is responsible for bait-prey interaction than a functional transcription factor is only reconstituted if the corresponding kinase is coexpressed, which leads to conditional growth signals on selective media. This is achieved by selection for diploid yeast colonies expressing two reporter genes and simultaneously carrying all three Y2H vectors (bait, prey and kinase vector which either contains a kinase or not). Generally speaking phosphorylation-dependent interactions only promote growth on selective media if the causative kinase is coexpressed but never in its absence (empty kinase vector) whereas independent interactions do not require kinase coexpression for growth promotion.

The experimental setup was the following: First, several replicas of bait-kinase coexpressing MATa strains were screened in a poolwise manner against an array of prey protein expressing MATα strains. In a second step nonautoactive preys that occurred with more than one replica of one pool were retested against a matrix which includes all bait-kinase combinations and all replicas of this pool. This retest identified the interacting bait-prey pairs and determined the kinase dependency.

Screening yeast strains cotransformed with Tyr kinase-bait combinations revealed that Tyr kinase-dependent interactions show a clear kinase-dependent Y2H signal because bait strains lacking kinase coexpression consistently failed to grow (3.1.6). In case of Ser/Thr kinase-dependent interactions we observed sometimes that strains lacking exogenous kinase coexpression gained the ability to grow. This might be caused by the ability of endogenous yeast kinases to phosphorylate the bait or prey protein to levels that can sustain reporter activation (3.1.5).

The screen of 71 bait proteins involved in neurological disorders against two different prey matrixes (see 3.1.5 for detailed information) identified two Tyr kinase- and three Ser/Thr kinase-dependent interactions, which resembled 13 % or 4 % of all identified interactions in these screens, respectively (3.1.7). That the fraction of identified Tyr kinase-dependent PPIs was larger is not astonishing since this experimental setup only provided prey proteins with pTyr-binding domains for bait interaction. For 40 % of all tested bait proteins an interaction

partner was identified and a sampling efficiency of 24 % was reached, which is comparable with other high-throughput screens (Venkatesan, et al., 2009). We conclude that both screens were technically well done (3.1.7). Furthermore, a fraction of the detected Y2H interactions was tested in co-IP experiments with a success rate of 66 %. All interactions validated in co-IP experiments were also positive in Venus PCA experiments (3.2.3). To demonstrate the applicability of the modified Y2H system to detect phosphorylation-dependent interactions we further analyzed these interactions in cell-based assays. We clearly showed that the Tyr kinase-dependent interactions detected with the modified Y2H system were triggered by tyrosine phosphorylation in mammalian cells because SH2 domain mutants with reduced pTyr-binding capability failed to interact in co-IP experiments and showed reduced fluorescence signals in Venus PCA experiments (3.4, 3.5.3). However, we were not able to consistently disrupt the detected Ser/Thr kinase-dependent interactions in cell culture experiments. Treatment of starved or non-starved cells with different concentrations of the kinase inhibitor Gö6983 or the kinase activator PMA did not reproducibly modulate co-IP signals. Furthermore phosphatase treatments during cell lysis or after immunoprecipitation failed to reduce co-IP signals. We suggest that the activity of endogenous kinases in mammalian cells is responsible for these observations and further experiments including peptide arrays with mutated phosphorylation sites will be performed to analyze the nature of these interactions. We conclude that the developed modified yeast system is more suitable to discover pSer/pThr-dependent interactions than approaches in mammalian cell culture although both systems have to cope with endogenous kinase activity (discussed below). Better validation tools are required to demonstrate the applicability of the modified Y2H system to detect pSer/pThr-dependent interactions.

### 4.1.3 Conservation of phosphorylation-recognition pathways between yeast and human

Phosphorylation-dependent signalling pathways are build from three molecular components: kinases that add the modification, phosphatases that remove these modifications and proteins with phosphorylation-recognition domains that read these modifications and transfer the signal to downstream signalling proteins (Lim and Pawson, 2010). Tyrosine kinase signalling is based on tyrosine phosphorylation and subsequent recognition of these residues by pTyr-binding domains like SH2 or PTB domains. Components of the tyrosine phosphorylation signalling pathways, including tyrosine kinases and pTyr-recognition domains, emerged coordinated during eukaryotic evolution (Pincus, et al., 2008). Sequencing of the budding yeast genome revealed that it does not encode Tyr kinases but 129 Ser/Thr kinases (Breitkreutz, et al., 2010). Furthermore the yeast genome encodes only one SH2 protein but 20 proteins implicated in pSer/pThr-binding including FHA and WW domain containing proteins and 14-3-3 family members (Hunter and Plowman, 1997). In contrast, the human genome encodes for 110 SH2 proteins (Liu, et al., 2006) and 518 kinases including 58 RTKs and 32 non-RTKs (Manning, et al., 2002). Comparison of the human kinome with those of yeast revealed that of 187 human kinase subfamilies 55 are present in the yeast kinome including AKT-, PKC-, MAPK-, PDK-, PI3K-family members (Manning, et al., 2002). In light of this it is not astonishing that several pSer/pThr-dependent interactions between human proteins have been detected with Y2H systems (Chen, et al., 2003; Chiba, et al., 2009; Garcia-Guzman, et al., 1999; Godde, et al., 2006; Izaki, et al., 2005; Robertson, et al., 1997). However, in all of these interactions 14-3-3 proteins were responsible for pSer/pThr-recognition and to our knowledge no pSer/pThr-dependent interaction between other human proteins has been detected with Y2H systems so far. Residues which participate in 14-3-3 phosphospecific binding are highly conserved from yeast to human and

recognize the sequence R(S/Ar)XpSXP and RX(Ar/S)XpSXP in which pS denotes pSer/pThr and Ar denotes aromatic residues (Muslin, et al., 1996; Yaffe, et al., 1997). Basic residues like argenine (R) in positions -3 to -5 relative to the phosphorylated site are found in almost all 14-3-3 binding sites. Conserved basophilic kinases of the AGC (protein kinase A/protein kinase G/protein kinase C) and CaMK ($Ca^{2+}$/calmodulin-dependent protein kinase) subfamilies are implicated in recognition and phosphorylation of these sites (Linding, et al., 2008; Manning, et al., 2002; Martin, et al., 2009). These kinase subfamilies are conserved in yeast and include family members that are homologues to AKT, PKC and PKA (Hunter and Plowman, 1997). In yeast activation of the target of rapamycin (TOR) kinase signalling pathway triggers phosphospecific 14-3-3 binding (Beck and Hall, 1999). DNA-damage-activated protein kinase (Chk1)-mediated binding of 14-3-3 to Cdc25 is conserved from yeast to human (Peng, et al., 1997; Sanchez, et al., 1997). These studies imply that major protein components, the kinase-motif recognition, the mode of pSer/pThr-recognition and the binding by 14-3-3 are conserved. Collectively, the above mentioned studies explain why the detection of pSer/pThr-dependent interactions mediated by 14-3-3 proteins is possible in Y2H screens and suggest that endogenous yeast kinases might be able to phosphorylate human Y2H fusion proteins and thus enable the detection of those pSer/pThr-dependent interactions in Y2H. However, standard Y2H systems do not differentiate between phosphorylation-dependent and independent interactions. Further experimental steps to recognize the nature of the identified interactions are required.

We focused our analysis on bait proteins involved in neurological disorders and chose Ser/Thr kinases implicated in neurodegenerative processes (*i.e.* AKT1, PKCα and PKCζ) even though AKT1 (Casamayor, et al., 1999; Rodriguez-Escudero, et al., 2005) and PKC (Levin and Bartlett-Heubusch, 1992; Levin, et al., 1990; Watanabe, et al., 1994) have functional homologues in yeast. In agreement with the studies mentioned above we detected phosphorylation-dependent 14-3-3 PPIs without exogenous kinase coexpression in our system, including the interaction between CBL and 14-3-3 which is mediated by PKC phosphorylation (Melander, et al., 2004). This suggests that endogenous yeast kinases indeed masked some phosphorylation-dependent interactions in our modified Y2H system. In order to investigate if endogenous yeast kinases are responsible for the observed background growth we performed approaches with cercosporamide, which selectively inhibits the yeast PKC1 but not the human PKC versions (Sussman, et al., 2004). However, the phosphorylation-dependent interaction between CBL and 14-3-3 was not disturbed if cercosporamide was added to the selective media used for interaction selection of the corresponding diploid yeast colonies. Furthermore the growth was not influenced irrespective if the diploid yeast colonies (representing a bait-prey interaction) coexpressed a human PKC or not.

These results allow two conclusions: First, other yeast kinases than PKC1 might promote this interaction. Second, the residual PKC1 kinase activity under cercosporamide treatment might be sufficient to promote phosphorylation-dependent interactions to levels that sustain reporter gene activation due to the ability of the Y2H method to trap interactions. To address these hypotheses, we performed more general experiments using several phosphatase inhibitors in order to enhance the differential signal between diploid yeast strains coexpressing human kinases or not. Supplementation of the selective media with Calyculin A, Cantharidin, Sodium fluoride and Okadaic acid did not influence the growth of diploid yeast colonies expressing CBL and 14-3-3 irrespective if a human kinase was coexpressed or not. We conclude that the detection of pSer/pThr-dependent interactions in modified Y2H systems is challenging due to endogenous kinase activity and suggest that further studies might be undertaken with human specific kinase subfamilies. However, using the described system we were able to identify three pSer/pThr-dependent interactions and two pTyr-dependent interactions.

## 4.2 Functional modules revealed by the generated disease network

The investigation of proteins involved in neurological disorders with the modified Y2H system developed in this study revealed an interaction map consisting of 90 partially modification-dependent interactions between 79 proteins. We tested a fraction of these Y2H interactions in co-IP and Venus PCA experiments and obtained a validation rate of over 66 %. High-quality binary protein interaction maps like the one described here, can be used to gain insight into the signal transduction machinery in health and disease states (Goehler, et al., 2004; Lim, et al., 2006). This study connected 21 proteins involved in neurological disorders with mostly novel interaction partners. Among them are the PD-associated gene product PARK7 (DJ1, Parkinson protein 7) and the Neurofibromatosis type 2-associated tumour suppressor NF2 (merlin, neurofibromin 2). Interestingly, both proteins interact with the regulatory PI3K subunit PIK3R3 and functional PIK3R3 pTyr-recognition modules (SH2 domains) are required for this interaction. These findings implicate the PI3K/AKT survival pathway in both of these very distinct neurological disorders, being associated with the formation of nervous system tumours or neuronal apoptosis in the SNpc, respectively (4.3). Additional NF2 binding partners identified include the demethylase AOF2 (KDM1A, LSD1), which is discussed to mediate the downregulation of the phosphatase MYPT1 necessary for dephosphorylation and activation of NF2 itself (4.4.1) and EMILIN1, a known inhibitor of proliferative TGF-β signalling (4.4.2). The simultaneous investigation of two NF2 isoforms (1 and 7) allowed insight on isoform level in dimerization (4.4.3) and interaction (4.4.4) behaviour. Furthermore, the network revealed that PARK7 is connected with two components of E3 ligase complexes: ASB3 and RNF31. Deregulated ubiquitination pathways are discussed to be responsible for the degeneration of dopaminergic SNpc neurons in sporadic and familial PD and the phosphorylation-dependent PARK7 interactions identified here might reveal dynamic regulatory mechanisms connecting PD pathogenesis with ASB3- and RNF31-mediated ubiquitination processes (4.5). The possible roles of the above mentioned interaction modules will be discussed in detail in the following chapters.

## 4.3 PI3K pathway (de)regulation in Parkinson's disease and Neurofibromatosis type 2

Multiple tumour types harbor mutations in components of the PI3K-PTEN signalling pathway leading to increased AKT signalling, cell survival and proliferation (Cully, et al., 2006; Vivanco and Sawyers, 2002). We found that the regulatory subunit 3 of PI3K (PIK3R3, also known as p55γ) interacts with the tumour suppressor NF2 and the Parkinson protein 7 (PARK7).

*The PI3K/AKT pathway.* PIK3R3 is one of five regulatory PI3K subunits that form heterodimers with one of three p110 catalytic subunits. PI3K heterodimers consisting of a p110 catalytic subunit belong to the class 1A PI3Ks which phosphorylate and convert the lipid second messenger $PIP_2$ into phosphatidylinositol 3,4,5-trisphosphate ($PIP_3$). $PIP_3$ recruits and activates PDK1, which in turn phosphorylates and activates AKT. Activation of the AKT1 pathway promotes cell proliferation and survival (Cully, et al., 2006). In contrast, PTEN functions as a tumour suppressor by dephosphorylating $PIP_3$ and generating $PIP_2$ (Stambolic, et al., 1998).

*PARK7 regulates the PI3K/AKT pathway.* Several mechanisms have been proposed to explain why AKT1 is hyperactivated in 25–75 % of human breast and lung tumours although these cells rarely have PTEN mutations (David, et al., 2004; Kim, et al., 2005). Several reports link PARK7 to PI3K/AKT activation and thus to cell proliferation and tumourigenesis. For example, elevated PARK7 expression levels correlate with enhanced AKT1 phosphorylation levels in tumours, suggesting that PARK7 might inhibit PTEN or provide another type of AKT1-activating signal (Kim, et al., 2005). We identified a direct interaction between PARK7 and a regulatory PI3K subunit, thus it is likely that we have found a missing AKT1-activating signal. Interestingly, PARK7 is required for membrane translocation of AKT1 (Aleyasin, et al., 2009) which further points into the direction that PARK7 stimulates PI3K and $PIP_3$ production. PH domain-mediated binding of $PIP_3$ leads to plasma membrane recruitment of AKT, which is the necessary prior event before its phosphorylation and activation can occur (Franke, et al., 1997). Consistent with this, expression of a membrane-targeted form of AKT bypasses the need for PARK7-mediated AKT activation in PARK7 deficient cells and rescues from cell death induced by oxidative stress (Aleyasin, et al., 2009).

*The PI3K/AKT pathway is deregulated in PD.* As loss-of-function PARK7 mutations are one known cause of familial PD (Bonifati, et al., 2003; Moore, et al., 2003) this raises the question if PI3K/AKT signalling is impaired in PD. Indeed, AKT seems to be linked to PD because a specific AKT haplotype is significantly associated with reduced disease risk suggesting that AKT protects from PD (Xiromerisiou, et al., 2008). Furthermore, several compounds that activate the PI3K/AKT pathway such as caffeine, the herbal medicine Yi-Gan San and the insulin-like growth factor 1 (IGF-1) have been shown to protect against apoptotic cell death in human dopaminergic neuroblastoma cells which serve as PD model (Doo, et al., 2010; Nakaso, et al., 2008; Wang, et al., 2010). PI3K/AKT signalling and stress response are also impaired in a drosophila model of PD (Yang, et al., 2005). These results implicate impairment of PI3K/AKT signalling and oxidative stress response in PARK7-associated disease pathogenesis and thus link the PI3K/AKT pathway to PD.

Collectively these studies suggest that PARK7 promotes proliferation in cancer cells and that the same pathways are involved in protection from oxidative stress of SNpc dopaminergic neurons. Specifically, loss-of-function PARK7 mutations might lead to downregulation of the PI3K/AKT survival pathway which might contribute to the PD characteristic progressive and massive loss of SNpc neurons. On the other hand PARK7 (over)activation might lead to enhanced AKT signalling and tumourigenesis.

Interestingly, we discovered that PIK3R3 interacts with another protein involved in tumourigenesis, the tumour suppressor NF2. Mutational inactivation of the NF2 gene results in NF2-associated tumours (Neurofibromatosis type 2). Additionally, loss of NF2 expression and NF2 mutations have been reported in several other types of cancers (Bianchi, et al., 1994; Lau, et al., 2008; McClatchey and Giovannini, 2005; Okada, et al., 2007; Sekido, et al., 1995).

*PI3K signalling is deregulated in Neurofibromatosis type 2 and disease models*. PI3K is linked to Neurofibromatosis type 2 because the PI3K signalling pathway is activated in human schwannoma (Ammoun, et al., 2008; Hilton, et al., 2009; Jacob, et al., 2008), in human malignant gliomas (Lassman, 2004) where NF2 expression was shown to be reduced (Lau, et al., 2008) and in malignant mesotheliomas from $NF2^{+/-}$ mice (Altomare, et al., 2005). Schwannomas are brain tumours that arise from Schwann cells due to reduced NF2 protein expression or functionality. Normal Schwann cell survival depends on the PI3K/AKT pathway (Li, et al., 2001) and thus it is possible that overactivation of this pathway induced by NF2 loss promotes tumourigenesis. Indeed, a compound targeting the AKT pathway was investigated as a chemotherapeutic in preclinical studies for

vestibular schwannomas (Lee, et al., 2009).

*NF2 is connected with the PI3K/AKT pathway.* In non-disease state, NF2 might promote its tumour suppressive function by inhibiting PI3K signalling pathways through growth factor receptor degradation (Fraenzer, et al., 2003). Alternatively, NF2 could inhibit PI3K activity through disrupting PI3K binding to the long form of PI3K-enhancer (PIKE-L), which is a brain-specific GTPase that stimulates PI3K activity (Rong, et al., 2004). In line with this AKT was shown to feed back and phosphorylate NF2 on residues Thr230 and Ser315, which disrupts its binding to PIKE-L (Okada, et al., 2009; Tang, et al., 2007). Furthermore, AKT-mediated phosphorylation of NF2 on residues Thr230, Ser315 (Okada, et al., 2009) and Ser10 (Laulajainen, et al., 2011) was shown to disrupt the tumour suppressing closed conformation of NF2 and to promote proteasome-mediated degradation of the tumour suppressor.

We might have identified another NF2-mediated PI3K inhibitory mechanism because we identified a direct interaction between NF2 and one regulatory subunit of PI3K. This raises the possibility that NF2 inhibits PI3K by modulating the activity or stability of the PI3K heterodimer which obligatory consists of a regulatory and a catalytic subunit. Collectively these studies suggest that NF2 inactivation in Neurofibromatosis type 2 relieves PI3K from NF2-mediated inhibition which evokes enhanced cell proliferation.

In summary, several studies discussed here link deregulated PI3K signalling to Neurofibromatosis type 2, tumourigenesis and PD and identify NF2 and PARK7 as possible regulators (Figure 31). We have identified NF2 and PARK7 as PIK3R3 interactors in this study and have shown that PIK3R3 binds to these proteins in a Tyr kinase-dependent manner in a modified Y2H system (3.1.6). In mammalian cells PIK3R3 SH2 domain mutants with reduced pTyr-binding capability fail to interact (3.4, 3.5.3). This argues for a model where activation of Tyr kinases and phosphorylation of PARK7 and NF2 are required prior to SH2 domain-dependent binding of PIK3R3.

*The role of PARK7 in tyrosine phosphorylation signalling.* PARK7 has that far not been linked to tyrosine kinase signalling even though it contains two tyrosine residues (Tyr67 and Tyr139) that are known to be phosphorylated (Hornbeck, et al., 2004) (3.1.6.2). Although PARK7 does not contain a known or predicted SH2 domain binding site, we could clearly show that binding of PIK3R3 depends on PIK3R3 SH2 domains (3.4). The interaction of PARK7 and PIK3R3 was located to the cytoplasm in Venus PCA experiments and not as expected beneath the membrane which might be caused by incomplete or lacking stimulation of the appropriate signalling pathways. We conclude that activation of RTKs promotes tyrosine phosphorylation of PARK7, PIK3R3 binding and PI3K activation.

*The role of NF2 in tyrosine phosphorylation signalling.* Interestingly, NF2 is known to negatively regulate the activity and availability of several RTKs like EGFR (Curto, et al., 2007), PDGFR (Fraenzer, et al., 2003) and ERBB2 (Lallemand, et al., 2009) and was shown to directly interact with ERBB2 (Fernandez-Valle, et al., 2002) and GRB2 (Lim, et al., 2006). So far no tyrosine phosphorylation sites for NF2 have been detected but three tyrosine residues known to be phosphorylated in other members of the ERM protein-family are conserved in NF2 and additionally two PIK3R3 SH2 binding site motifs have been predicted (3.1.6.2). We propose that NF2 bound to RTKs or RTKs-associated proteins gets phosphorylated on tyrosine residues in SH2 binding site motifs which provokes PIK3R3 binding and inhibits PI3K lipid kinase activity. Alternatively NF2 might disrupt the activating binding of PIK3R3 to RTKs by successfully competing for binding sites. In agreement with this we found that the tumour suppressive NF2 isoform 1 interacts with PIK3R3 at the cell membrane (3.5.3).

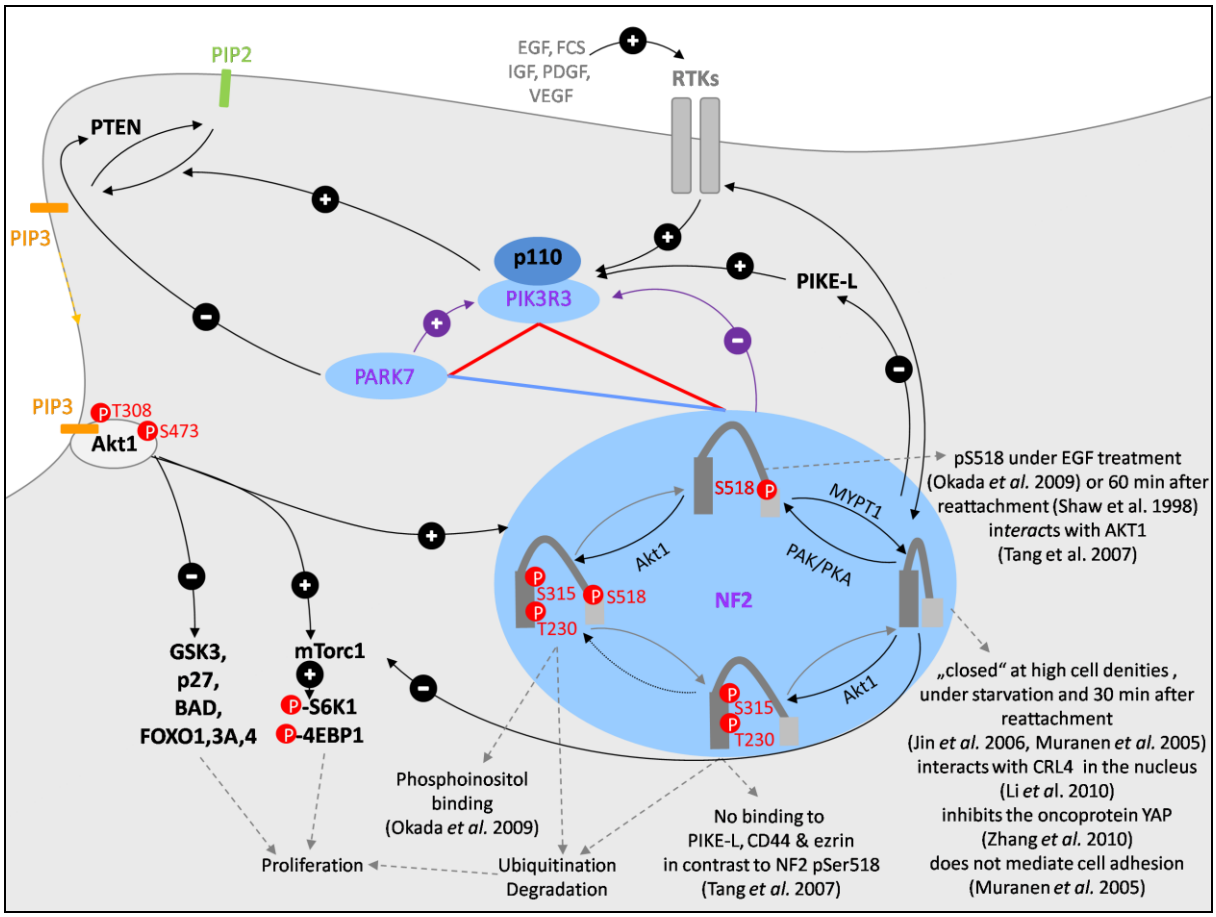


**Figure 31: PARK7 and NF2 in RTKs/PI3K signalling.**

We observed that PIK3R3 binding to PARK7 and NF2 depends on functional PIK3R3 SH2 domains and tyrosine phosphorylation of PARK2 and NF2 (red lines). Furthermore we detected a direct interaction between NF2 and PARK7 (blue line). We suggest that receptor tyrosine kinase (RTK) signalling activates PARK7s stimulatory effect on the lipidkinase activity of the PI3K heterodimer consisting of a regulatory (PIK3R3) and a catalytic (p110) subunit whereas tyrosine phosphorylation of the tumour suppressor NF2 negatively regulates PI3K activity (violet arrows). NF2 and PARK7 are implicated in the regulation of the proliferative PI3K/AKT1 pathway and NF2 is a recognized AKT1 phosphorylation substrate (black arrows). The Ser/Thr phosphorylation status of NF2 is known to regulate NF2 conformation, interaction pattern, localisation, degradation and is tightly controlled by several kinases (including AKT1, PAK and PKA) and the phosphatase MYPT1. This study implicates for the first time tyrosine phosphorylation in interaction regulation of NF2 and PARK7 and suggests that pTyr-triggered interaction with the regulatory PI3K subunit influence PI3K lipidkinase activity and following pro-survival pathway activation.

*The PI3K modulators PARK7 and NF2 interact with each other*. As discussed above PARK7 and NF2 have been discussed to activate and inhibit the PI3K pathway, respectively. Interestingly, we could show a direct interaction between NF2 and PARK7 in co-IP and Venus PCA assays (3.5.2). This further enlarges the scope how these three proteins influence each other's functionality in disease and non-disease states. NF2 has a negative effect on PI3K activity and PARK7 a positive effect on PI3K activity consequently it seems most likely that NF2 inhibits PARK7s property to activate PI3K and thus protects from tumourigenesis in non-disease state. This effect could hypothetically be mediated by competitive binding of NF2 and PARK7 to PIK3R3. However, the question remains how NF2 and PARK7 mechanistically trigger and regulate PI3K activity.

In conclusion, our results suggest that activation of PI3K might be enhanced as a consequence of PARK7 binding and reduced as a consequence of NF2 binding and that changes in protein levels cause over- or underactivation of the PI3K pathway in brain tumour formation or PD, respectively (Figure 31). Furthermore this study links PARK7 and NF2 for the first time to Tyr kinase signalling because it was shown that their tyrosine phosphorylation status directly influenced their interaction abilities. NF2 was thus far only considered to be

regulated by phosphorylation on Ser/Thr residues although it is from an evolutionary point of view plausible that FERM domain proteins like NF2 are involved in Tyr kinase signalling. Evolutionarily, the FERM domain arose during the transition to multicellularity and genome sequencing of one of the closest eukaryotic unicellular relatives of metazoans revealed that FERM domains and even a putative NF2 orthologue (King, et al., 2008) coevolved with Tyr kinase receptors, SH2 domains and intercellular junctions (Abedin and King, 2008; King and Carroll, 2001).

## 4.4 Modulation of cellular processes by NF2

### 4.4.1 The MYPT1-PP1δ demethylase AOF2 is implicated in NF2 regulation

*AOF2 is an enzyme capable to demethylate histones and non-histone proteins.* The discovery of the first lysine-specific demethylase AOF2 (also known as lysine-specific demethylase 1, LSD1 or KDM1) revealed that methylation is reversible like other modifications, such as acetylation and phosphorylation (Shi, et al., 2004). Several studies suggest that post-translational modification by methylation regulates protein activity. For a long time, only the histone-demethylase activity of AOF2 has been described (Shi, et al., 2004). AOF2 has been shown to repress gene expression by removing active methylation marks in association with different corepressor complexes including CoREST (Lee, et al., 2005; Shi, et al., 2005), CtBP (Wang, et al., 2007), a subset of HDAC complexes (You, et al., 2001) and the NuRD complex (Wang, et al., 2009) but AOF2 also activates gene expression in association with the androgen receptor (AR) (Metzger, et al., 2005). Later on it was demonstrated that AOF2 can also demethylate methylated non-histone proteins like the murine DNA methyltransferase 1 (Wang, et al., 2009), the tumour protein p53 (Huang, et al., 2007) and the myosin phosphatase 1 (Cho, et al., 2011).

*AOF2 is implicated in tumourigenesis and interacts with the tumour suppressor NF2.* We found an interaction between AOF2 and the tumour suppressor NF2. AOF2 contains a C-terminal amine oxidase domain and a central protein-protein interaction motif, the SWIRM domain, which is found in multiple chromatin-associated proteins. Recent studies have implicated AOF2 in several growth-promoting pathways and have linked AOF2 to certain high-risk tumours (Cho, et al., 2011; Hayami, et al., 2011; Huang, et al., 2007; Kahl, et al., 2006; Metzger, et al., 2005; Shi, 2007; Wang, et al., 2007; Wang, et al., 2009). AOF2 expression is significantly elevated in several carcinomas (Hayami, et al., 2011; Kahl, et al., 2006), AOF2 knock down suppresses proliferation (Hayami, et al., 2011; Metzger, et al., 2005) and introduction of exogenous AOF2 promotes cell cycle progression (Hayami, et al., 2011). Expression profile analysis showed that AOF2 affects the expression of genes involved in various chromatin-modifying pathways which might explain its role in carcinogenesis (Hayami, et al., 2011). AOF2 has been shown to stimulate AR-dependent transcription which leads to cell proliferation (Kahl, et al., 2006; Metzger, et al., 2005). However, AOF2 was also found to be downregulated in breast carcinomas and in this cellular context AOF2 inhibits invasion and suppresses breast cancer metastatic potential by repressing TGF-β expression in association with the NuRD complex (Wang, et al., 2009). These studies imply that AOF2 histone demethylation has diverse functions in carcinogenesis. But also demethylation of non-histone substrates has been shown to affect growth-promoting pathways, for example, AOF2 interacts and demethylates p53 which leads to repression of p53-mediated transcriptional activation and inhibition of p53-mediated apoptosis (Huang, et al., 2007). Furthermore, silencing of AOF2 leads to enhanced protein levels of the myosin phosphatase targeting subunit MYPT1, which is directed to ubiquitin-proteasomal

degradation after AOF2-mediated demethylation (Cho, et al., 2011). MYPT1 is a phosphatase-targeting subunit which prefers PP1δ as catalytic subunit (Ito, et al., 2004). Interestingly, recent studies have shown that NF2 is a direct substrate of this AOF2-regulated phosphatase (Jin, et al., 2006) which points into the direction that AOF2 regulates proliferation by influencing the phosphorylation status and thus the tumour suppressor function of NF2. Dephosphorylation of NF2 (Ser518) by MYPT1 in association with its catalytic subunit PP1δ (MYPT1-PP1δ) activates the tumour suppressor function of NF2 by enabling self-association between the FERM and the C-terminal domain of NF2 (Jin, et al., 2006; Sherman, et al., 1997). Collectively, these results suggest a model where AOF2-mediated demethylation and destabilization of MYPT1 will decrease the steady state level of phosphorylated, tumour suppressive NF2. The direct interaction between AOF2 and NF2 which we discovered might display a possible feedback loop.

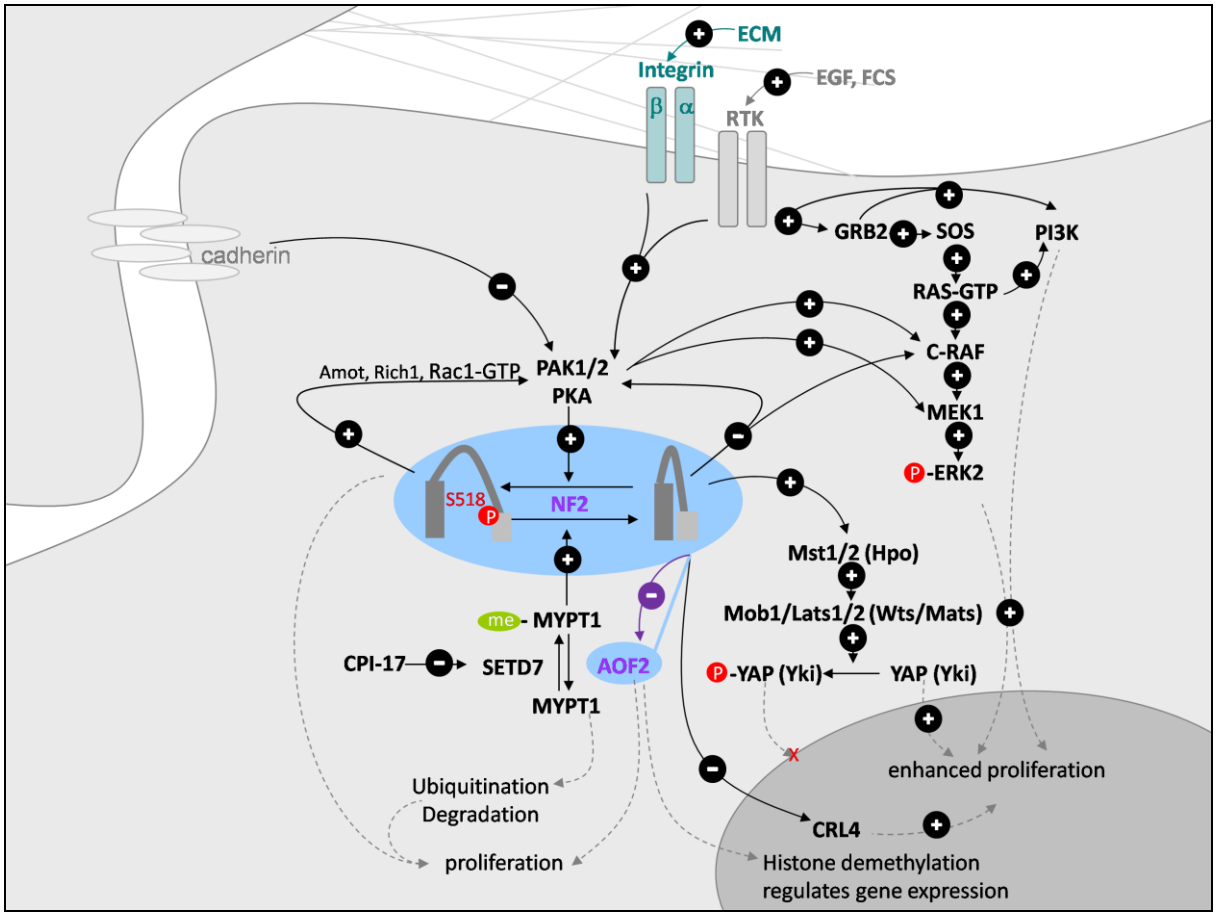


**Figure 32: Feedback loop from NF2 to the NF2-coformation regulating demethylase AOF2.**

AOF2 is known to modulate the tumour suppressor activity of NF2 by regulating the degradation and thus the availability of the phosphatase-targeting subunit MYPT1. MYPT1 dephosphorylates NF2 (Ser518) in association with its catalytic subunit PP1δ (MYPT1-PP1δ) and activates the tumour suppressor function of NF2 by enabling the head-to-tail interaction between the FERM and the C-terminal domain. On the other hand integrin, cadherin, RTKs signalling and NF2 itself regulate the activity of kinases which abrogate the head-to-tail interaction and thus have the potential to end the tumour suppressive NF2 effects mediated by CRL4 inhibition, enhanced YAP phosphorylation and decreased ERK phosphorylation. We detected a direct interaction between NF2 and AOF2 (blue line) and suggest that this interaction might negatively regulate the pro-proliferative AOF2 effects (violet arrow).

*Two NF2 isoforms differing in conformation, localisation and function interact with AOF2.* We suggest that only the dephosphorylated closed form of NF2 is able to bind to AOF2 and to inhibit AOF2-mediated pro-proliferative functions including the ones which lead to reduction in pSer518 NF2 levels. This model would be in agreement with the generally believed view that only dephosphorylated, closed NF2 can acts as a tumour suppressor. However, we observed that also a constitutively open isoform of NF2 (*i.e.* isoform 7) is able to

interact with AOF2. In contrast to isoform 1 which can switch between a closed and an open conformation this isoform lacks the C-terminal domain (residues 585-595, KSRVAFFEEL) and parts of the FERM domain which are required for phosphorylation regulated self-association (Gronholm, et al., 1999; Gutmann, et al., 1999). Furthermore, most studies conclude that the closed formation and membrane association are necessary for the growth-suppressive function of NF2 (Brault, et al., 2001; Gonzalez-Agosti, et al., 1996; Sainio, et al., 1997). This is interesting because we found that AOF2 interacts with the switchable isoform 1 beneath the membrane whereas it interacts with the constitutively open isoform 7 in the cytoplasm. Deletions in the FERM domain are known to disrupt proper FERM domain folding which is required for the head-to-tail interaction (Gutmann, et al., 1999) and membrane localization (Brault, et al., 2001). This explains why the localization and the interaction pattern of the isoforms differ and suggests that not only interaction but also interaction localization is important for NF2 tumour suppressor function.

### 4.4.2 The interaction partners NF2 and EMILIN1 are involved in common signalling pathways

*Extracellular EMILIN1 is associated with elastic fibers.* An extracellular network of elastic fibers is essential to allow lung, aorta and skin tissues to stretch and recoil without damage. This network consists of polymerized tropoelastin monomers surrounded by a mantle of microfibrils (Wagenseil and Mecham, 2007). Elastin microfibril interface-located protein 1 (EMILIN1) is one of several elastic fiber-associated proteins identified (Kielty, et al., 2002) and is found at the interface between the elastin core and surrounding microfibrils (Bressan, et al., 1993; Zanetti, et al., 2004). EMILIN1 consists of an N-terminal cysteine-rich elastin microfibril interface (EMI) domain, a long coiled-coil domain, a short collagenous domain, and a region homologous to the globular domain of C1q (gC1q) at the C-terminus (Zacchigna, et al., 2006). The gC1q globular domain is important for oligomerization (Mongiat, et al., 2000) and the interaction of homotrimers with β-integrin, which couples EMILIN1 to cell adhesion and migration (Spessotto, et al., 2003; Verdone, et al., 2008), trophoblast invasion (Spessotto, et al., 2006) and cell proliferation (Danussi, et al., 2011). EMILIN1 knockout mice present dermal and epidermal hyperproliferation which results from upregulated phospho-Erk1/2 levels and inhibited cytostatic Smad signalling caused by absence of the β-integrin-EMILIN1 interaction (Danussi, et al., 2011).

*EMILIN1 is linked to hypertension causing TGF-β signalling.* The EMI domain of EMILIN1 interacts with pro-transforming growth factor-β (proTGF-β) and prevents its maturation by protein convertases (Zacchigna, et al., 2006). The systemic blood pressure is significantly increased in EMILIN1 knockout mice due to increased TGF-β signalling and blood pressure can be reduced by inactivation of a single TGF-β allele in these mice which links EMILIN1 to TGF-β signalling and to arterial hypertension (Zacchigna, et al., 2006). TGF-β signalling and hypertension have been linked before because TGF-β signalling increases vasoactive molecules and remodels blood vessel architecture (Ghosh, et al., 2005). TGF-β is synthesized as homodimeric inactive pro-protein (proTGF-β) which gets cleaved in the trans-Golgi by furin convertases but remains noncovalently associated until the complex is secreted and thrombospondin-1, integrins or other proteins induce the release of TGF-β (Annes, et al., 2003). Interestingly, Zacchigna *et al.* found that EMILIN1 interacts exclusively with proTGF-β (Zacchigna, et al., 2006). This could either be explained by proTGF-β secretion prior to cleavage or by interaction with intracellular EMILIN1 monomers.

*What is the role of intracellular EMILIN1?* It is known that EMILIN1 exists as monomer within cells and that after secretion, in the extracellular space disulfide bonds between the monomers are formed (Colombatti, et

al., 2000). Furthermore in pulmonary and aortic heart valves EMILIN1 is found intra- and extracellularly (Angel, et al., 2011). Additionally, EMILIN1 was found to interact with the N-myc interactor (NMI) and the myotubularin related protein 9 (MTMR9) which are both cytoplasmic proteins (Rual, et al., 2005). In the light of this knowledge it is not surprising that we found that EMILIN1 is able to interact with another intracellular protein, namely NF2 (3.5.2).

*Hypertension causing TGF-β signalling regulates NF2 and NF2 deficiency causes hypertension.* Recently it has been shown that patients with Neurofibromatosis type 2 have a significant higher blood pressure than control patients (Cordeiro, et al., 2006; Hornigold, et al., 2011). Indeed, hypertension causing TGF-β signalling (Zacchigna, et al., 2006) has also been linked to NF2 because it induces PAK2-mediated inhibition of NF2 tumour suppressor function and thus proliferation (Wilkes, et al., 2009). This means that reduction in protein levels of both interaction partners (EMILIN1 and NF2) cause hypertension (Cordeiro, et al., 2006; Zacchigna, et al., 2006) and hyperproliferation (Danussi, et al., 2011; McClatchey and Giovannini, 2005) and that both of these processes are linked to elevated TGF-β signalling (Figure 33).

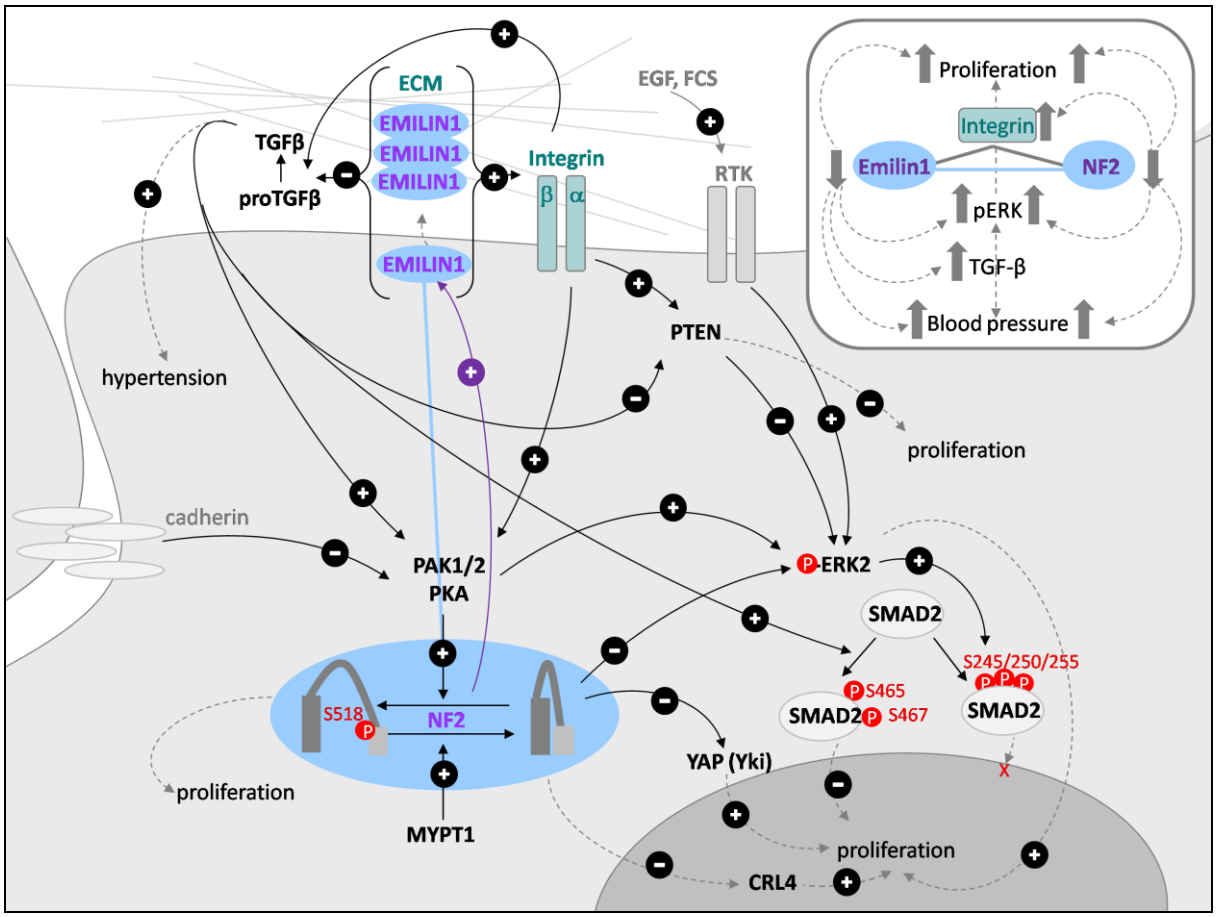


**Figure 33: EMILIN1 and NF2 in TGF-β and integrin signalling.**

We observed a direct interaction between NF2 and EMILIN1 (blue line). EMILIN1 negatively regulates the maturation of TGF-β and thus inhibits TGF-β-mediated hypertension causing signalling. TGF-β is known to induce PAK2-mediated inhibition of NF2 tumour suppressor function, inhibit PTEN-mediated suppression of the pro-proliferative PI3K/AKT1 pathway but also to stimulate anti-proliferative Smad signalling. If the anti-proliferative Smad signalling is bypassed by prior ERK-mediated Smad phosphorylation on inhibitory sites, only the pro-proliferative TGF-β signals maintain. Possibly EMILIN1 protects from this bypassing because the EMILIN1-integrin interaction (grey line) is known to reduce ERK activation by inhibiting PTEN. We suggest that the observed interaction between EMILIN1 and NF2 enhances the described EMILIN1 functions which might be mechanisms of NF2 to suppress tumourigenesis. NF2 is known to interact with β-integrin (grey line) and to inhibit ERK activation, thus both interaction partners are tightly linked to β-integrin and TGF-β signalling. **Insert:** Functional connection between β-integrin signalling, TGF-β signalling, proliferation, and blood pressure homeostasis under decreased EMILIN1 and NF2 protein levels.

*EMILIN1 might inhibit the proliferative site of TGF-β signalling.* It has long been recognized that TGF-β signalling can promote proliferation if its growth-inhibitory mechanisms are bypassed (Wilkes, et al., 2009). TGF-β activates antiproliferative signalling pathways mainly through Smad2 (Ser465/467) phosphorylation but simultaneously induces Smad-independent reduction of PTEN expression (Chow, et al., 2008; Ebert, et al., 2002). If Smad phosphorylation on Ser465/467 is disturbed by Erk activation only the proliferative PI3K/AKT signals maintain which lead to TGF-β-mediated proliferation (Kretzschmar, et al., 1999). EMILIN1 probably inhibits the TGF-β bypassing mechanism by reducing Erk activation over its interaction with β-integrin which is in line with results from EMILIN1 deficient cells where Erk activation is increased and the antiproliferative TGF-β signalling is bypassed (Danussi, et al., 2011).

*The tumour suppressor NF2 and its interaction partner EMILIN1 are implicated in various, partially overlapping cell proliferation processes.* We could show a direct interaction between NF2 and EMILIN1, consequently it is tempting to ask if and how the tumour suppressor NF2 and EMILIN1 influence each other. EMILIN1-mediated inhibition of proliferative TGF-β signalling and EMILIN1-mediated integrin signalling might be mechanisms of NF2 to suppress tumourigenesis. Interestingly, also NF2 is known to interact with β-integrin (Obremski, et al., 1998) and NF2 deficient cells also show increased Erk activation which involves the integrin/focal adhesion kinase/Src/Ras signalling cascade (Ammoun, et al., 2008). Furthermore, TGF-β induced epithelial to mesenchymal transition is a hallmark of cancer metastasis (Oft, et al., 1998) and is achieved by downregulation of cell-cell adhesion molecules (Birchmeier, et al., 1996) and upregulation of extracellular matrix associated proteins (Stewart, et al., 2004). NF2 deficient cells like schwannomas and meningiomas also display reduced β-catenin and E-cadherin (Brunner, et al., 2006) but elevated integrin levels which leads to enhanced proliferation (Ammoun, et al., 2011; Lopez-Lago, et al., 2009). Furthermore, studies have shown that NF2 and EMILIN1 influence cell spreading and motility (Bretscher, et al., 2002; Gutmann, et al., 1998; Koga, et al., 1998; Lallemand, et al., 2003; Okada, et al., 2005), suggesting that both proteins are involved in signalling pathways that regulate cell proliferation, migration, adhesion and spreading.

We summarize, that the interaction partners NF2 and intracellular EMILIN1 are both tightly linked to β-integrin signalling, TGF-β signalling, proliferation, and blood pressure homeostasis and that these processes are within themselves very connected because β-integrins regulate proliferation and TGF-β maturation, and TGF-β signalling influences blood pressure and proliferation.

### 4.4.3 The NF2 heterodimerization results challenge existing dimerization models

*NF2 dimerization models.* With the discovery of complementary association domains in NF2 more than one model that describes NF2 dimerization can be proposed. If the domains responsible for the intramolecular head-to-tail interaction also mediate the intermolecular head-to-tail interaction of ERM proteins (Gary and Bretscher, 1995; Henry, et al., 1995; Martin, et al., 1995) the intramolecular interactions in the monomer have to be disturbed in order to unmask the interaction domains required for dimerization. One alternative to this hypothesis would be that NF2 contains one or more additional association domains which mediate an intermolecular interaction between two head-to-tail closed NF2 proteins. That additional association domains are present would be supported by the findings of this study, Meng *et al*. and Scoles *et al*. which show that NF2 isoforms lacking the C-terminal tail required for self-association are able to dimerize (Meng, et al., 2000; Scoles, et al., 2002).

*What is the function of NF2 dimerization?* It is interesting to speculate about how tertiary and quartiary structure influence the functionality of NF2 and under which of these conditions NF2 acts as tumour suppressor. However, dimerization is not a unique feature of the tumour suppressing isoform 1 but could well be a general mechanism to regulate the availability of the physiological active state. Possibly the monomer:dimer ratio influences cellular functions as observed for ezrin (Berryman, et al., 1995; Gautreau, et al., 2000). Studies which modulate intra- or intermolecular associations or use constitutively open isoforms (like isoform 2 or 7) or unmasked protein domains have shown that dimerization and self-association influence the interaction ability of NF2. For example, NF2 isoform 1 binds weaker to NHERF than isoform 2 but isoform 1 binding can be enhanced by phospholipid treatment which decreases intra- or intermolecular interactions and unmasks the NHERF binding site (Gonzalez-Agosti, et al., 1999). Unmasking is also required for SCHIP1 interaction: an N-terminal NF2 isoform 1 fragment (1-314 aa) and NF2 isoform 2 were able to interact but not the full length isoform 1 (Goutebroze, et al., 2000). Furthermore, β-spectrin interacts with NF2 isoform 2 but fails to interact with isoform 1 under the same conditions (Scoles, et al., 1998). Similarly, isoform 1 binds ezrin only under conditions that activate, or unmask, either or both proteins, whereas the interaction between isoform 2 and ezrin does not depend on activation (Meng, et al., 2000). As full-length NF2 isoform 1 is able to bind N- and C-terminal NF2 fragments but not N- and C-terminal ezrin fragments unless NF2 is truncated, it was suggested that homodimerization sites on NF2 are exposed while the binding sites for ezrin on NF2 isoform 1 are masked (Gronholm, et al., 1999). Indeed heterodimerization between NF2 isoforms 1 and 2 was shown to inhibit the interaction of either NF2 isoform with ezrin (Meng, et al., 2000). The hetero- and homodimerization of NF2 has probably a broad significance and further interactions are likely to be regulated by NF2 dimerization.

*In need of new dimerization models.* This study revealed that in addition to isoform 1 and 2 also isoform 7 is able to homodimerize (Gronholm, et al., 1999; Meng, et al., 2000; Scoles, et al., 1998; Sherman, et al., 1997). This is astonishing because isoform 7 is lacking a properly folded FERM domain and the C-terminal tail which are both required for the head-to-tail inter- or intramolecular interaction (Gronholm, et al., 1999; Gutmann, et al., 1999). We could further show that isoform 1 is able to heterodimerize with isoform 7 which questions the head-to-tail dimerization model proposed for isoform 1-isoform 2 (Gonzalez-Agosti, et al., 1999; Meng, et al., 2000; Sherman, et al., 1997) because neither the properly folded FERM domain nor the C-terminal tail of isoform 1 find a matching intact interaction domain in isoform 7. The homodimerization of isoform 7 and its heterodimerization with isoform 1 could probably be mediated by a tail-to-tail interaction, because the C-terminal half of isoform 1 (296–595 aa) and the C-terminal half of isoform 2 (296–590 aa, with residues 580-590 differing from those in isoform 1) were shown to interact with each other but not with themselves (Meng, et al., 2000). This tail-to-tail interaction might occur between the central α-helical domains present in these constructs because the αC and αB-helices have been shown to form a coiled-coil (Hennigan, et al., 2010).

Collectively, these results point into the direction that NF2 contains additional association domains which could mediate the observed intermolecular interactions. Furthermore, NF2 regulation might be more complex than previously envisioned which means that it seems likely that not only the well described switch between open and closed monomer conformation are involved in this process. Also the improved model which is derived from the capability of ERM proteins to form homo- and heterotypic associations between family members and acknowledges that the domains required for intramolecular self-association could also mediate an intermolecular head-to-tail dimerization (Gary and Bretscher, 1995) is probably not sufficient. Instead we propose that

monomers of constitutively open isoforms and probably also self-associated closed isoforms are able to dimerize via unidentified associating domains. Dimerization might regulate the availability of the physiological active state, affect interaction with other proteins and as shown here for NF2 isoform 7 might occur at a distinct intracellular localization than other interactions. We observed that heterodimerization of isoform 7 with the membrane located tumour suppressing NF2 isoform 1 is the only isoform 7 PPI that occurs beneath the membrane (3.5.2) whereas all other interactions with EMILIN1, PIK3R3 and AOF2 occurred in the cytoplasm. Dimerization and interaction localisation might thus modify the functionality of either isoform.

### 4.4.4 The differential NF2 isoform interaction patterns suggest functional differences

We observed that isoform 1 and isoform 7 show overlapping but distinct interaction patterns. AOF2, EMILIN1 and PIK3R3 prefer binding to NF2 isoform 7 in the Y2H and the co-IP experiments but were able to interact with both isoforms in the Venus PCA assay. Interestingly, these interactions and NF2 dimers were located to the membrane whenever NF2 isoform 1 was included as interaction partner. NF2 isoform 1 fusion proteins used in Y2H and co-IP experiments were functional so we concluded that these isoforms show differential interaction and localization patterns depending on the experimental setup. Furthermore, some interactions that showed a membranous localization in Venus PCA experiments were detected in Y2H or co-IP experiments which excludes the possibility that the localization pattern influences the interaction detection in these systems. In Y2H and co-IP experiments only N-terminal fusion proteins were tested whereas in the Venus PCA system N- and C-terminal fusion proteins were tested. C-terminal fusion of NF2 isoform 1 results in interaction detection and N-terminal fusions resulted in decreased or abrogated fluorescence signals (except for isoform 1 dimerization). However, fluorescence signals with N-terminal NF2 isoform 7 fusions were also decreased so we were uncertain if we fail to detect isoform 1 interactions in Y2H and co-IP experiments because of N-terminal fusion. Nevertheless it should be considered that the observed effects mirror false negative results caused by steric hindrance or conformational changes because the nature of the complementation fragments and the length and flexibility of the linker differs in all these assays. It is for example possible that the C-terminal fusion disturbs the head-to-tail conformation of NF2 isoform 1 which leads to exposure of interaction domains that are normally hidden in the protein structure unless a context-dependent protein modification (like Ser518 phosphorylation) occurs.

*Can these differential interaction patterns be modulated?* It remained elusive if the observed effects are mediated through modifications, conformational changes or are just site effects of different interaction assays thus we tried to modulate co-IP and Venus PCA interaction signals. The conformation and localisation of NF2 depends on the phosphorylation status and phosphatidylinositol binding, processes which are known to be regulated by cadherin and integrin signalling. Consequently, we decided to treat starved and non-starved cells with various kinase inhibitors (Staurosporine, Wortmannin, IPA-3), kinase activators (EGF, FBS), $PIP_3$, the phosphatase inhibitor $H_2O_2$, the nuclear export inhibitor Leptomycin B and hyaluronan which activates integrin receptor signalling. However, all these treatments did not reproducibly modulate co-IP and Venus PCA signals. This might partially be explained by the irreversible fluorescent protein folding in fluorescence complementation assays (Kerppola, 2008; Kerppola, 2009) like the Venus PCA system. Alternatively C-terminal fusion of the Venus fragments might arrest NF2 isoform 1 in a constitutively open conformation due to steric hindrance, which might prohibit modulation of the fluorescence signal.

*Different interaction localization–different output?* Still, although we were not able to determine why the NF2 isoforms show differential interaction ability in different experimental setups and although we failed to identify the molecular switches that lead to different interaction localisation in Venus PCA experiments, we suggest that the interaction localisation influences the outcome of the determined NF2 interactions and probably tumour suppressor function. The observed differences in localisation pattern are in agreement with the observation that mutants and isoforms which cannot form an intramolecular head-to-tail interaction cannot localize to the membrane and cannot inhibit cell proliferation (Gronholm, et al., 1999; Sherman, et al., 1997).

Collectively, these results point into the direction that interaction localization and dimerization might affect the functionality of the different NF2 isoforms. We showed that an isoform which is generally believed to be unable to perform inter- or intramolecular self-association is able to homo- and heterodimerize, furthermore, we showed that this isoform has an overlapping interaction pattern with the tumour suppressive isoform 1. We suggest that the open conformation of isoform 1 is required to reproduce the interaction of the constitutively open isoform 7, which might be achieved by C-terminal fusions in Venus PCA experiments but not in Y2H or co-IP experiments. NF2 membrane localisation requires proper FERM domain folding and consequently only interactions with isoform 1 occur beneath the membrane whereas isoform 7 interactions are located to the cytoplasm. These results point to the direction that the observed functional differences between the NF2 isoforms and the different conformational states might be mediated by interaction localisation. Furthermore in addition to the self-association switch which requires proper FERM domain folding and the C-terminal tail, the availability of interaction domains to binding partners might be controlled by dimerization in NF2 isoforms missing these self-association domains.

## 4.5 Connection of cellular survival pathways by PARK7

*PARK7 is implicated in various cellular processes.* Defects in the PARK7 gene (also known as DJ1) cause autosomal recessive early-onset Parkinson's disease (Bonifati, et al., 2003). Some disease causing mutations impair PARK7 dimerization which leads to protein destabilization and effective knockout (Moore, et al., 2003). This suggests a loss-of-function disease phenotype. However, the function of PARK7 remains elusive because it is reported to affect ras-dependent transformation (Nagakubo, et al., 1997), control fertility (Wagenfeld, et al., 1998), modulate AR-signalling (Niki, et al., 2003; Takahashi, et al., 2001; Tillman, et al., 2007), act as a protein chaperone (Shendelman, et al., 2004), act as a protease (Koide-Yoshida, et al., 2007; Olzmann, et al., 2004), affect transcription (Clements, et al., 2006; Taira, et al., 2004), bind mRNA (Blackinton, et al., 2009), alter dopamine receptor signalling (Goldberg, et al., 2005), suppress apoptosis (Kim, et al., 2005), alter p53 signalling (Bretaud, et al., 2007; Fan, et al., 2008; Shinbo, et al., 2005), alter AKT1 function (Aleyasin, et al., 2009; Yang, et al., 2005) and to protect against oxidative stress (Guzman, et al., 2011). Probably PARK7 has an unsolved activity capable of mediating all these different effects.

*PARK7 belongs to the ThiJ/PfpI-family which members encompass a conserved cysteine residue.* The NCBI search for conserved domains in PARK7 revealed that PARK7 contains a ThiJ/PfpI domain which is a member of the glutamine amidotransferase (GAT)-like domains (Marchler-Bauer, et al., 2011). The majority of domains in this group have a reactive cysteine residue found in a sharp turn between a β-strand and an α-helix termed the nucleophile elbow and in some of these domains the cysteine residue forms a Cys-His-Asp/Glu catalytic triad in the active site. Catalytic triads are responsible for the catalytic activity of family members including chaperones (Quigley, et al., 2003), proteases (Du, et al., 2000) and several GAT domain containing

biosynthetic enzymes (Horvath and Grishin, 2001). Interestingly, PARK7 contains such a triad with the cysteine residue being located between a β-strand and an α-helix but if this triad consisting of Cys106, His126 and Glu18 (in human PARK7) forms a functional active site remains to be determined (Tao and Tong, 2003). The cysteine residue is absolutely conserved, reacts with reactive oxygen species and is required for the ability of PARK7 to protect against oxidative stress (Canet-Aviles, et al., 2004; Meulener, et al., 2006; Taira, et al., 2004).

*Conserved cysteine residues are found in enzymes implicated in ubiquitination processes.* Proteins with a papain-like protease fold with a Cys-His-Asp/Asn/Glu/Gln catalytic triad were shown to act as deamidase that specifically deamidate Gln40 in ubiquitin. This Gln40 deamidated ubiquitin is defective in being transferred from E2 to the acceptor ubiquitin during E3-catalyzed chain synthesis (Cui, et al., 2010). Furthermore, cysteine residues are the known active sites in E1, E2 and E3 enzymes of the ubiquitination cascade. E1 enzymes activate ubiquitin in an ATP-dependent manner and conjugate it to their own active-site cysteine residue (Schulman and Harper, 2009), before it is transferred to the next sulfhydryl group of the active-site cysteine on the E2 conjugating enzyme (Wenzel, et al., 2011). The final step of the ubiquitination cascade is performed by different types of E3 ligases differing in domain content and the ubiquitin transfer mechanism. The RING domain containing E3 ligases directly transfer the ubiquitin from the E2 ligase to the substrate whereas the HECT domain (Huibregtse, et al., 1995) or RBR domain (Wenzel, et al., 2011) containing E3 ligases require a cysteine residue for the formation of a covalent E3-ubiquitin intermediate before the ubiquitin is finally transferred to the substrate protein. The conserved cysteine residue of PARK7 lies between a β-strand and an α-helix which makes it accessible, like the conserved cysteine residues in E2 ligases (Burroughs, et al., 2008).

*PARK7 interacts with proteins implicated in ubiquitination processes.* There are several studies that speculate about PARK7s role in ubiquitinylation processes: PARK7 inhibits the ubiquitination and degradation of NFE2L2, a transcription factor in oxidative stress response (Clements, et al., 2006) and abolishes the inhibitory effect of the E3 sumo ligase PIAS2 on the androgen receptor transcriptional activity (Takahashi, et al., 2001). But PARK7 was also shown to have positive effects on ubiquitination processes since a complex consisting of PARK7, the ubiquitin E3 ligase PARK2 (also known as Parkin) and the PTEN-induced putative kinase 1 (PINK1) was shown to promote protein ubiquitination and degradation (Xiong, et al., 2009). In this study we identified two further PARK7 interaction partners involved in ubiquitination: ASB3 and RNF31. ASB3 probably functions as a substrate-recognition subunit of a multi-protein E3 ubiquitin ligase complex that mediates the degradation of proteins (Chung, et al., 2005) and RNF31 is part of an ubiquitin ligase complex which assembles linear polyubiquitin chains (Kirisako, et al., 2006; Tokunaga, et al., 2009).

*The PARK7 interacting E3 ligases RNF31 and PARK2 share significant functional homology.* RNF31 belongs to the RBR E3 ligase subfamily (Li, et al., 2008) like the known PARK7 interactor PARK2 (Moore, et al., 2005; Olzmann, et al., 2007; Xiong, et al., 2009). Very recently the RBR-family member ARIH1 was shown to function like a HECT-type E3 enzyme, because the ubiquitin transfer required an trans-thiolation step with a Cys357 in the second RING of the RBR domain (Wenzel, et al., 2011). This residue corresponds to Cys431 in PARK2 (Wenzel, et al., 2011) and point mutations of this residue are related to familial PD (http://www.uniprot.org/uniprot/O60260) and have been shown to affect E3 ligase activity (Chen, et al., 2010; Chung, et al., 2001; Satoh and Kuroda, 1999; Shin, et al., 2011). Interestingly, sequence alignments performed by us revealed conservation in RNF31 (Cys885) which suggests that the RNF31-PARK7 interaction might be functionally similar to the PARK2-PARK7 interaction (Figure 34). A complex consisting of PARK7, the Ser/Thr kinase PINK1 and the ubiquitin E3 ligase PARK2 was shown to promote ubiquitination and degradation

of un- and misfolded proteins (Xiong, et al., 2009), which suggest that PD-pathogenic mutations impair E3 ligase activity of the complex. This will be related to protein accumulation and aggregation which is one known mechanism underlying PD pathogenesis (Forno, et al., 1996; Spillantini, et al., 1997). Although the molecular causes of PD disease are still unclear it is well-known that the UPS and defects in protein degradation play a critical role in PD pathogenesis (Giasson and Lee, 2003; McNaught, et al., 2001).

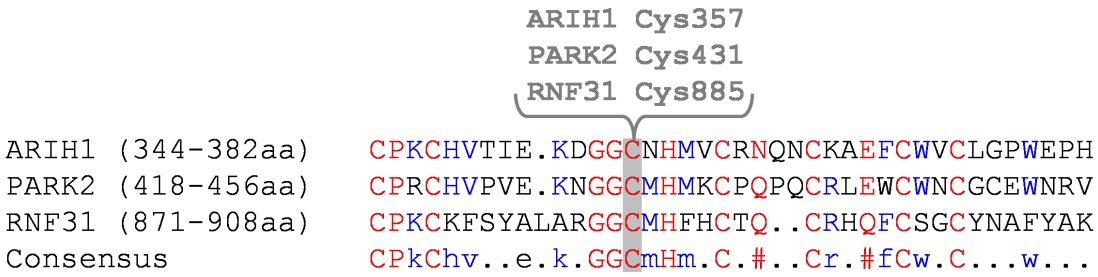


**Figure 34: Sequence alignment of RING2 domains from human RBR ligases.**

The RING-in-between-RING (RBR) family of E3s includes among others PARK2 (also known as parkin), the human homologue of ARIH1 (HHARI; also known as ariadne) and RNF31. RBR E3 ligases function like HECT-type E3 ligases: they bind E2s via a RING domain, but transfer Ub through a trans-thiolation step requiring a conserved cysteine residue (grey box) in the RING2 domain. The alignment was performed using MultAlin at INRA. Sequence names (NCBI Gene symbols) appear at the beginning of each row and the portion of aligned amino acids (aa) is indicated in the brackets. High consensus portions are shown in red, blue regions are conserved in at least 2 out of 3 sequences and the neutral portions are shown in black.

*The assembly of RNF31 and PARK2 E3 ligase complexes might be regulated by phosphorylation*. We have shown that PARK7 binds to RNF31 and ASB3 in a Ser/Thr kinase-dependent manner in a modified Y2H system (3.1.5.1) which suggests that Ser/Thr kinases like PINK1, AKT or PKC might regulate ubiquitin E3 ligase complex formation. Indeed, PARK2 phosphorylation by PINK1 was shown to activate its E3 ligase function and enhance polyubiquitination of NEMO (also known as IKK-γ or IKBKG) in dopaminergic cells (Sha, et al., 2010). However, the signalling pathway(s) responsible for PINK1 activation and subsequent NEMO ubiquitination remain to be determined.

*The RNF31 and PARK2 E3 ligase complexes are implicated in NFκB signalling*. The functional properties of RNF31 have only been partially characterized but it is known that the RNF31 containing LUBAC complex conjugates linear polyubiquitin chains to NEMO, which activates the NFκB pathway (Tokunaga, et al., 2009) and inhibits apoptosis (Ikeda, et al., 2011). This directly links two PARK7 interacting E3 ligases with NEMO ubiquitination and NFκB pathway activation which suggests that deregulated NFκB neuroprotective signalling is involved in the pathogenesis of PD. This hypothesis is further supported by the finding that inhibitors of IKK-β or NEMO have been found to influence neurodegeneration of dopaminergic neurons in murine and primate models of PD (Flood, et al., 2011). Additionally, PARK7 was shown to interact with and to inhibit the deubiquitinase Cezanne which results in enhanced NFκB nuclear translocation and cell survival (McNally, et al., 2011). NFκB signalling has been implicated among others in processes affected in PD: synaptic plasticity, learning and memory (Albensi and Mattson, 2000; Kaltschmidt, et al., 2006; Meffert, et al., 2003).

O*xidative stress activates NFκB signalling and is implicated in PD.* NFκB signalling is activated by increased levels of reactive oxygen species caused by environmental stress like hypoxia (Chandel, et al., 2000; Oliver, et al., 2009) and ultraviolet light exposure (Basu, et al., 1998). Interestingly, oxidative stress, caused by cell damage due to increased ROS levels is widely viewed as being responsible for the PD characteristic progressive and massive loss of SNpc neurons (Schapira, 2008). Oxidative stress evoked by pacemaking in dopaminergic SNpc neurons is attenuated by PARK7 (Guzman, et al., 2011), PARK7 deficient mice are

hypersensitive to oxidative stress (Kim, et al., 2005) and the association between PARK7 and PARK2 is enhanced under oxidative stress (Moore, et al., 2005). These studies suggest that the protective NFκB pathway activation during the oxidative stress response might depend on ubiquitination processes mediated by PARK7 in concert with different E3 ligases or E3 ligase complexes. Notably, oxidative stress activates the Ser/Thr kinases AKT (Wang, et al., 2000) and PKC (Gopalakrishna and Jaken, 2000) which promote the kinase-dependent PARK7 interactions in our modified Y2H system (3.1.5.1). Alternative to oxidative stress, PARK7 itself might stimulate AKT kinase activity required for subsequent phosphorylation-dependent PARK7 interactions. As discussed before (4.2), we identified the regulatory PI3K subunit PIK3R3 as PARK7 interaction partner and proposed that PARK7 might have a positive effect on PI3K lipid kinase activity. Elevated $PIP_3$ levels promote membrane recruitment and activation of AKT (Franke, et al., 1997) required to induce PARK7 interactions described here (Figure 35). This would represent a feedback loop.

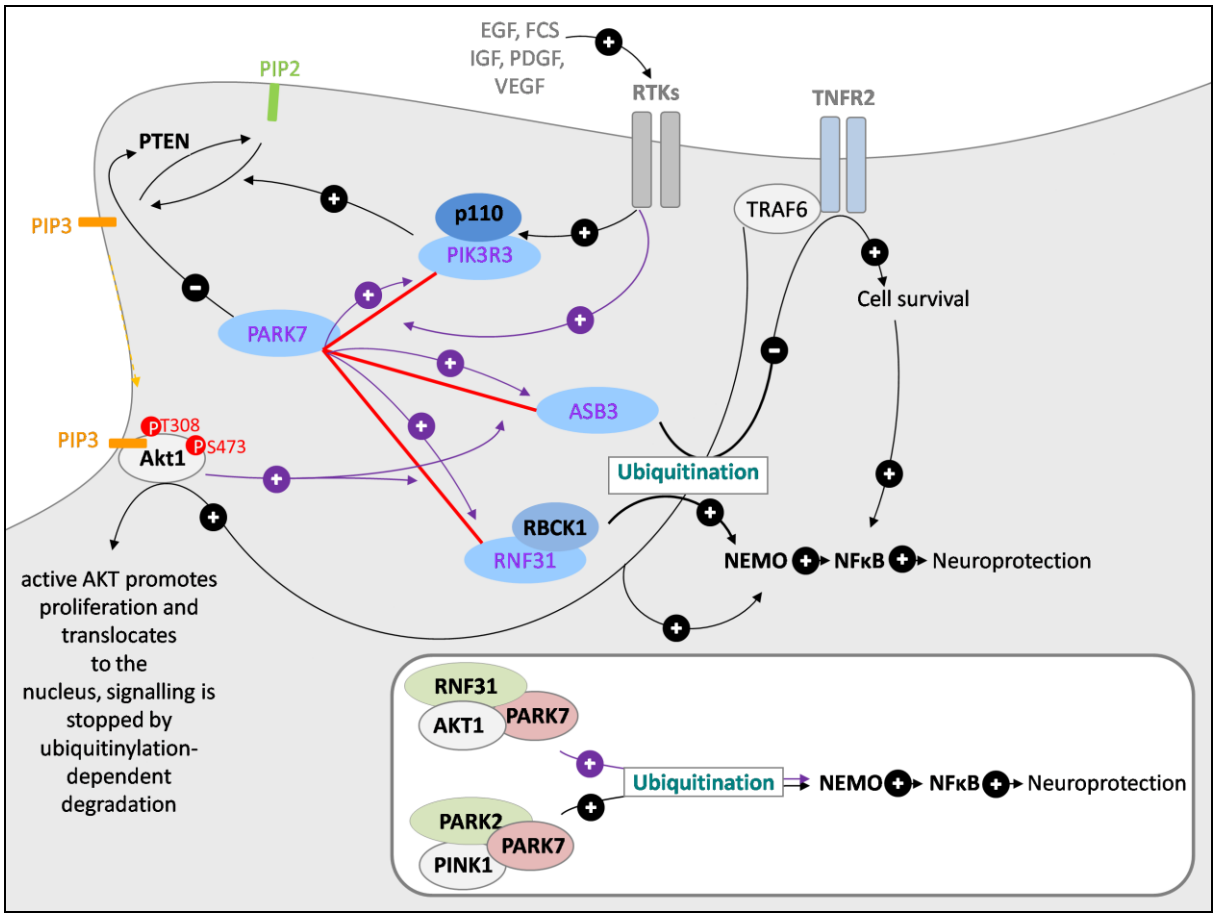


**Figure 35: Connection of cellular survival pathways by PARK7.**

We observed that PARK7 interacts with the regulatory PI3K subunit PIK3R3 after RTKs activation (red line) and suggest that this interaction has a positive effect on PI3K lipid kinase activity (violet arrow) because PARK7 has been implicated in PI3K/AKT1 pathway upregulation before (black arrow). Furthermore we observed that constitutively active AKT1 mediates the interaction between PARK7 and subunits of distinct E3 ligase complexes (red line). We suggest a feedback loop in which PARK7 stimulates the kinase required for subsequent pSer/pThr-dependent interactions. We further propose that interaction of PARK7 enhances the ability of RNF31 to activate the NFκB pathway and suggest that PARK7 modulates ASB3-mediated TNFR2 ubiquitination processes in a manner that enhance cell survival. TNF receptor associated factor 6 (TRAF6) is known to mediate signal transduction from members of the TNF receptor superfamily (Ha, et al., 2009) and to function as signal transducer in the NFκB pathway (Gautheron, et al., 2010). TRAF6 mediates Lys63 chain ubiquitination of AKT which promotes AKT membrane localization and phosphorylation (Yang, et al., 2009; Yang, et al., 2010).
**Insert:** the observed AKT1-mediated interaction between the RBR E3 ligase RNF31 and PARK7 shows structural and functional similarity to a complex which consists of the RBR E3 ligase PARK2, PARK7 and the Ser/Thr kinase PINK1 which has been implicated in NEMO ubiquitinylation like RNF31 (in association with RBCK1).

It has been speculated that PARK7 has more than one function and switches between them in response to the oxidative stress level (Bonifati, et al., 2004). In analogy, an *E. coli* stress-inducible chaperone belonging to the same superfamily as PARK7 (ThiJ/PfpI superfamily) is known to switch between chaperone and protease function depending on the temperature (Quigley, et al., 2003). We suggest that mild oxidative stress induces the phosphorylation-dependent interaction between PARK7 and RNF31 which might result in NFκB activation and cell survival as observed for complexes containing either of these proteins. These studies directly link PARK7-mediated oxidative stress protection to ubiquitination processes and NFκB activation although the exact mechanisms how PARK7 modulates E3 ligase activity remain unclear.

*PARK7 interacts with the ASB3 subunit of a multi-protein E3 ubiquitin ligase complex involved in tumour necrosis factor (TNF)-signalling*. Another link between PARK7 and the ubiquitination system was revealed with the discovery of the interaction between PARK7 and ASB3. The substrate-recognition subunit ASB3 is part of a multi-protein E3 ubiquitin ligase complex which is known to mediate TNF receptor 2 (TNFR2) ubiquitination and to promote subsequent TNFR2 proteolysis via the proteasome pathway resulting in reduced apoptosis caused by missing JNK activation (Chung, et al., 2005). Elevated levels of TNF are evident in a large number of neurological disorders including Parkinson's disease (Boka, et al., 1994) and evidence from histopathologic, epidemiologic, and pharmacologic studies support a role for TNF in triggering dopaminergic neuron loss (McCoy and Tansey, 2008). However, it has to be mentioned that TNF induces a complex signalling network that includes besides the pro-apoptotic acting JNK and caspase cascade also pro-survival gene transcription by NFκB (Aggarwal, 2003). We observed in the modified Y2H system that the interaction between PARK7 and ASB3 depends on the presence of constitutively active AKT1 or PKCα. Interestingly, TNF induced signalling pathways activate AKT1 (Ozes, et al., 1999) and PKCα in various cell types (Park, et al., 2000; Prasanna, et al., 1998; Wang, et al., 2010) and could thus promote phosphorylation-dependent interactions including the one between PARK7 and ASB3. PARK7 is widely viewed as being neuroprotective, consequently we suggest that the PARK7 interaction has a positive effect on ASB3 functionality which would enhance TNFR2 degradation and promote cell survival.

*What is the role of PARK7 in these ubiquitination processes?* Collectively these results strongly argue for a function of PARK7 in the ubiquitination cascade. However, if PARK7 works as ubiquitin ligase or regulatory component of a multi-protein E3 ubiquitin ligase complex remains to be determined. That PARK7 is just an ubiquitin E3 ligases substrate is possible but unlikely since PARK2 does not ubiquitinylate wildtype PARK7 (Moore, et al., 2005; Olzmann, et al., 2007) and ubiquitination and subsequent degradation has only been reported for misfolded mutant PARK7 (Miller, et al., 2003; Olzmann, et al., 2004; Olzmann, et al., 2007; Zucchelli, et al., 2010).

In agreement with several studies (Dawson and Dawson, 2003; Liu, et al., 2002; Valente, et al., 2004; Xiong, et al., 2009), we conclude that impairment of ubiquitination pathways may be a unifying mechanism responsible for the degeneration of dopaminergic SNpc neurons in sporadic and familial PD. This study identified ASB3 and RNF31, two components of E3 ligase complexes as novel PARK7 interaction partners. We suggest models in which these newly identified phosphorylation-dependent interactions modulate distinct survival pathways and account for the neuroprotective function of PARK7.

## 4.6 Summary and future directions

This study presents a modified Y2H system capable to detect phosphorylation-dependent, isoform-specific interactions on a proteome-wide scale and illustrates the ability of this system to generate interaction networks encompassing conditional and static interactions. In a proteome-wide screen we identified novel PPIs for 21 proteins associated with neurological disorders including three Ser/Thr kinase-dependent PPIs and two Tyr kinase-dependent PPIs involving the PD-associated gene product PARK7 (DJ1, Parkinson protein 7) and isoforms of the Neurofibromatosis type 2-associated tumour suppressor NF2 (merlin, neurofibromin 2). The generated network connects 79 proteins through 90 PPIs and was further extended by addition of interaction partners involved in ubiquitination. In total 38 interactions between 27 proteins were tested in co-IP and Venus PCA experiments. Interactions added in the extension step were validated with a lower success rate (*i.e.* 6 of 20 PPIs) compared to the Y2H PPIs identified in this study (*i.e.* 12 from 18 PPIs). For the tested Y2H interactions this corresponds to a validation rate of over 66 %, which underscores the stringency of the method and the precision of the obtained Y2H data (Worseck, et al., 2012). This represents another step taken towards generating conditional interaction information and towards building a more complete interaction map for neurological disorders.

High-quality binary protein interaction maps created for specific ND diseases, like HD (Goehler, et al., 2004; Kaltenbach, et al., 2007), AD (Soler-Lopez, et al., 2011) or SCAs (Lim, et al., 2006) reveal high connectedness and novel target proteins. The interaction network generated in this study substantiates the established connection between PD and ubiquitination-mediated proteasome functions (Cook and Petrucelli, 2009; Giasson and Lee, 2003; Malkus, et al., 2009). Two novel PPIs of the PD-associated gene product PARK7 with the E3 ligase components ASB3 and RNF31 (HOIP) were identified. Interestingly, these PARK7 interactions were triggered by AKT-mediated Ser/Thr phosphorylation in our system. This implicates phosphorylation in the regulation of RNF31- and ASB3-mediated ubiquitination processes known to control cell survival via NFκB- and TNF-signalling, respectively. Thus the approach uncovered dynamic regulatory mechanisms connecting PARK7-related PD pathogenesis and ubiquitination processes.

Furthermore, with the network-based approach described here, we successfully identified proteins that are associated with more than one disorder. For example, PARK7 and NF2 isoforms interact with the regulatory PI3K subunit PIK3R3. Both interactions require functional PIK3R3 pTyr-recognition modules (SH2 domains) and are thus Tyr phosphorylation-dependent interactions. We propose that the PARK7 interaction has a positive effect on PI3K and thus on AKT activity and the coupled survival pathways. This might represent a feedback loop as PARK7 interactions with E3 ligase components are mediated by AKT (see above). NF2 has been implicated in PI3K/AKT survival pathway inhibition before and we suggest a causative role for the direct PIK3R3/NF2 interaction discovered here. NF2 deficiency or malfunction in Neurofibromatosis type 2 might relieve PI3K from NF2-mediated inhibition which could promote the disease-specific tumour formation. Ser/Thr phosphorylation is known to regulate intra- and intermolecular NF2 interactions, whereas to our knowledge, this is the first study showing that Tyr phosphorylation is also implicated in NF2 interaction regulation.

Additional NF2 interaction partners identified in this study encompass the demethylase AOF2 (KDM1A, LSD1) and EMILIN1. AOF2 mediates the downregulation of the phosphatase MYPT1 which is necessary to dephosphorylate NF2 and to activate NF2 tumour suppressor function. EMILIN1 is a known inhibitor of proliferative TGF-β signalling and further literature studies revealed that NF2 and EMILIN1 are both tightly

linked to processes which are within themselves very connected: TGF-β signalling, β-integrin signalling, proliferation, and blood pressure homeostasis.

PIK3R3, AOF2 and EMILIN1 have been shown to interact with two distinct NF2 isoforms, the tumour suppressing isoform 1 and the poorly characterized isoform 7. In contrast to isoform 1, isoform 7 is lacking a properly folded FERM domain and the C-terminal tail which are required for the head-to-tail interaction (Gronholm, et al., 1999; Gutmann, et al., 1999). These differences in domain structure result in different conformation, subcellular localization and probably function. The interactions with isoform 1 occurred at the membrane (including a heterodimeric interaction with isoform 7) whereas the interactions with isoform 7 occurred in the cytoplasm. We suggest that the interaction localisation influences the output of these interactions. In contrast to current models, we observed that NF2 isoform 7 is able to homodimerize and to heterodimerize with NF2 isoform 1 which points into the direction that distinct dimerization surfaces must exist. This study enables insight into NF2 function on isoform level. Further investigations are necessary to unravel the complete set of NF2 regulatory mechanisms which probably include a complex interplay between inter- and intramolecular interactions, homo- and heterodimerization and in addition to Ser/Thr phosphorylation also Tyr phosphorylation.

This study provides a partially validated interaction map which allows insight into several human neurological disorders. The presented interaction network and the generated models provide strong hypotheses for the molecular function of NF2 and PARK7 that build the basis for directed future investigations. The development of experimental techniques capable to detect isoform-specific and modification-dependent interactions including the improvement of secondary interaction assays will refine our picture of cellular signaling pathways. Knowledge about modification-dependent alterations in the interactome and isoform-specificity will aid our understanding of a broad range of biological processes in health and disease.

# References


Abedin, M. and King, N. (2008): The premetazoan ancestry of cadherins, Science 319 [5865], pp. 946-8.

Aggarwal, B. B. (2003): Signalling pathways of the TNF superfamily: a double-edged sword, Nat Rev Immunol 3 [9], pp. 745-56.

Albensi, B. C. and Mattson, M. P. (2000): Evidence for the involvement of TNF and NF-kappaB in hippocampal synaptic plasticity, Synapse 35 [2], pp. 151-9.

Alessi, D. R.; Andjelkovic, M.; Caudwell, B.; Cron, P.; Morrice, N.; Cohen, P. and Hemmings, B. A. (1996): Mechanism of activation of protein kinase B by insulin and IGF-1, EMBO J 15 [23], pp. 6541-51.

Aleyasin, H.; Rousseaux, M. W.; Marcogliese, P. C.; Hewitt, S. J.; Irrcher, I.; Joselin, A. P.; Parsanejad, M.; Kim, R. H.; Rizzu, P.; Callaghan, S. M.; Slack, R. S.; Mak, T. W. and Park, D. S. (2009): DJ-1 protects the nigrostriatal axis from the neurotoxin MPTP by modulation of the AKT pathway, Proc Natl Acad Sci U S A 107 [7], pp. 3186-91.

Alfthan, K.; Heiska, L.; Gronholm, M.; Renkema, G. H. and Carpen, O. (2004): Cyclic AMP-dependent protein kinase phosphorylates merlin at serine 518 independently of p21-activated kinase and promotes merlin-ezrin heterodimerization, J Biol Chem 279 [18], pp. 18559-66.

Altomare, D. A.; Vaslet, C. A.; Skele, K. L.; De Rienzo, A.; Devarajan, K.; Jhanwar, S. C.; McClatchey, A. I.; Kane, A. B. and Testa, J. R. (2005): A mouse model recapitulating molecular features of human mesothelioma, Cancer Res 65 [18], pp. 8090-5.

Ammoun, S.; Flaiz, C.; Ristic, N.; Schuldt, J. and Hanemann, C. O. (2008): Dissecting and targeting the growth factor-dependent and growth factor-independent extracellular signal-regulated kinase pathway in human schwannoma, Cancer Res 68 [13], pp. 5236-45.

Ammoun, S.; Schmid, M. C.; Zhou, L.; Ristic, N.; Ercolano, E.; Hilton, D. A.; Perks, C. M. and Hanemann, C. O. (2011): Insulin-like growth factor-binding protein-1 (IGFBP-1) regulates human schwannoma proliferation, adhesion and survival, Oncogene.

Angel, P. M.; Nusinow, D.; Brown, C. B.; Violette, K.; Barnett, J. V.; Zhang, B.; Baldwin, H. S. and Caprioli, R. M. (2011): Networked-based characterization of extracellular matrix proteins from adult mouse pulmonary and aortic valves, J Proteome Res 10 [2], pp. 812-23.

Annes, J. P.; Munger, J. S. and Rifkin, D. B. (2003): Making sense of latent TGFbeta activation, J Cell Sci 116 [Pt 2], pp. 217-24.

Bandyopadhyay, S.; Chiang, C. Y.; Srivastava, J.; Gersten, M.; White, S.; Bell, R.; Kurschner, C.; Martin, C. H.; Smoot, M.; Sahasrabudhe, S.; Barber, D. L.; Chanda, S. K. and Ideker, T. (2010): A human MAP kinase interactome, Nat Methods 7 [10], pp. 801-5.

Bandyopadhyay, S. and Cookson, M. R. (2004): Evolutionary and functional relationships within the DJ1 superfamily, BMC Evol Biol 4, p. 6.

Barret, C.; Roy, C.; Montcourrier, P.; Mangeat, P. and Niggli, V. (2000): Mutagenesis of the phosphatidylinositol 4,5-bisphosphate (PIP(2)) binding site in the NH(2)-terminal domain of ezrin correlates with its altered cellular distribution, J Cell Biol 151 [5], pp. 1067-80.

Barrios-Rodiles, M.; Brown, K. R.; Ozdamar, B.; Bose, R.; Liu, Z.; Donovan, R. S.; Shinjo, F.; Liu, Y.; Dembowy, J.; Taylor, I. W.; Luga, V.; Przulj, N.; Robinson, M.; Suzuki, H.; Hayashizaki, Y.; Jurisica, I. and Wrana, J. L. (2005): High-throughput mapping of a dynamic signaling network in mammalian cells, Science 307 [5715], pp. 1621-5.

Bashour, A. M.; Meng, J. J.; Ip, W.; MacCollin, M. and Ratner, N. (2002): The neurofibromatosis type 2 gene product, merlin, reverses the F-actin cytoskeletal defects in primary human Schwannoma cells, Mol Cell Biol 22 [4], pp. 1150-7.

Basu, S.; Rosenzweig, K. R.; Youmell, M. and Price, B. D. (1998): The DNA-dependent protein kinase participates in the activation of NF kappa B following DNA damage, Biochem Biophys Res Commun 247 [1], pp. 79-83.

Beaulieu, J. M.; Robertson, J. and Julien, J. P. (1999): Interactions between peripherin and neurofilaments in cultured cells: disruption of peripherin assembly by the NF-M and NF-H subunits, Biochem Cell Biol 77 [1], pp. 41-5.

Beck, T. and Hall, M. N. (1999): The TOR signalling pathway controls nuclear localization of nutrient-regulated transcription factors, Nature 402 [6762], pp. 689-92.

Beeser, A.; Jaffer, Z. M.; Hofmann, C. and Chernoff, J. (2005): Role of group A p21-activated kinases in activation of extracellular-regulated kinase by growth factors, J Biol Chem 280 [44], pp. 36609-15.

Benes, C. H.; Wu, N.; Elia, A. E.; Dharia, T.; Cantley, L. C. and Soltoff, S. P. (2005): The C2 domain of

PKCdelta is a phosphotyrosine binding domain, Cell 121 [2], pp. 271-80.

Berryman, M.; Gary, R. and Bretscher, A. (1995): Ezrin oligomers are major cytoskeletal components of placental microvilli: a proposal for their involvement in cortical morphogenesis, J Cell Biol 131 [5], pp. 1231-42.

Betarbet, R.; Sherer, T. B. and Greenamyre, J. T. (2005): Ubiquitin-proteasome system and Parkinson's diseases, Exp Neurol 191 Suppl 1, pp. S17-27.

Bianchi, A. B.; Hara, T.; Ramesh, V.; Gao, J.; Klein-Szanto, A. J.; Morin, F.; Menon, A. G.; Trofatter, J. A.; Gusella, J. F.; Seizinger, B. R. and et al. (1994): Mutations in transcript isoforms of the neurofibromatosis 2 gene in multiple human tumour types, Nat Genet 6 [2], pp. 185-92.

Birchmeier, C.; Birchmeier, W. and Brand-Saberi, B. (1996): Epithelial-mesenchymal transitions in cancer progression, Acta Anat (Basel) 156 [3], pp. 217-26.

Blackinton, J.; Ahmad, R.; Miller, D. W.; van der Brug, M. P.; Canet-Aviles, R. M.; Hague, S. M.; Kaleem, M. and Cookson, M. R. (2005): Effects of DJ-1 mutations and polymorphisms on protein stability and subcellular localization, Brain Res Mol Brain Res 134 [1], pp. 76-83.

Blackinton, J.; Kumaran, R.; van der Brug, M. P.; Ahmad, R.; Olson, L.; Galter, D.; Lees, A.; Bandopadhyay, R. and Cookson, M. R. (2009): Post-transcriptional regulation of mRNA associated with DJ-1 in sporadic Parkinson disease, Neurosci Lett 452 [1], pp. 8-11.

Blume-Jensen, P. and Hunter, T. (2001): Oncogenic kinase signalling, Nature 411 [6835], pp. 355-65.

Boka, G.; Anglade, P.; Wallach, D.; Javoy-Agid, F.; Agid, Y. and Hirsch, E. C. (1994): Immunocytochemical analysis of tumor necrosis factor and its receptors in Parkinson's disease, Neurosci Lett 172 [1-2], pp. 151-4.

Bonifati, V.; Oostra, B. A. and Heutink, P. (2004): Linking DJ-1 to neurodegeneration offers novel insights for understanding the pathogenesis of Parkinson's disease, J Mol Med (Berl) 82 [3], pp. 163-74.

Bonifati, V.; Rizzu, P.; van Baren, M. J.; Schaap, O.; Breedveld, G. J.; Krieger, E.; Dekker, M. C.; Squitieri, F.; Ibanez, P.; Joosse, M.; van Dongen, J. W.; Vanacore, N.; van Swieten, J. C.; Brice, A.; Meco, G.; van Duijn, C. M.; Oostra, B. A. and Heutink, P. (2003): Mutations in the DJ-1 gene associated with autosomal recessive early-onset parkinsonism, Science 299 [5604], pp. 256-9.

Bono, P.; Cordero, E.; Johnson, K.; Borowsky, M.; Ramesh, V.; Jacks, T. and Hynes, R. O. (2005): Layilin, a cell surface hyaluronan receptor, interacts with merlin and radixin, Exp Cell Res 308 [1], pp. 177-87.

Bossi, A. and Lehner, B. (2009): Tissue specificity and the human protein interaction network, Mol Syst Biol 5, p. 260.

Bradshaw, J. M. and Waksman, G. (2002): Molecular recognition by SH2 domains, Adv Protein Chem 61, pp. 161-210.

Brault, E.; Gautreau, A.; Lamarine, M.; Callebaut, I.; Thomas, G. and Goutebroze, L. (2001): Normal membrane localization and actin association of the NF2 tumor suppressor protein are dependent on folding of its N-terminal domain, J Cell Sci 114 [Pt 10], pp. 1901-12.

Braun, P.; Tasan, M.; Dreze, M.; Barrios-Rodiles, M.; Lemmens, I.; Yu, H.; Sahalie, J. M.; Murray, R. R.; Roncari, L.; de Smet, A. S.; Venkatesan, K.; Rual, J. F.; Vandenhaute, J.; Cusick, M. E.; Pawson, T.; Hill, D. E.; Tavernier, J.; Wrana, J. L.; Roth, F. P. and Vidal, M. (2009): An experimentally derived confidence score for binary protein-protein interactions, Nat Methods 6 [1], pp. 91-7.

Breitkreutz, A.; Choi, H.; Sharom, J. R.; Boucher, L.; Neduva, V.; Larsen, B.; Lin, Z. Y.; Breitkreutz, B. J.; Stark, C.; Liu, G.; Ahn, J.; Dewar-Darch, D.; Reguly, T.; Tang, X.; Almeida, R.; Qin, Z. S.; Pawson, T.; Gingras, A. C.; Nesvizhskii, A. I. and Tyers, M. (2010): A global protein kinase and phosphatase interaction network in yeast, Science 328 [5981], pp. 1043-6.

Bressan, G. M.; Daga-Gordini, D.; Colombatti, A.; Castellani, I.; Marigo, V. and Volpin, D. (1993): Emilin, a component of elastic fibers preferentially located at the elastin-microfibrils interface, J Cell Biol 121 [1], pp. 201-12.

Bretaud, S.; Allen, C.; Ingham, P. W. and Bandmann, O. (2007): p53-dependent neuronal cell death in a DJ-1-deficient zebrafish model of Parkinson's disease, J Neurochem 100 [6], pp. 1626-35.

Bretscher, A.; Edwards, K. and Fehon, R. G. (2002): ERM proteins and merlin: integrators at the cell cortex, Nat Rev Mol Cell Biol 3 [8], pp. 586-99.

Brewster, J. L.; de Valoir, T.; Dwyer, N. D.; Winter, E. and Gustin, M. C. (1993): An osmosensing signal transduction pathway in yeast, Science 259 [5102], pp. 1760-3.

Bruijn, L. I.; Houseweart, M. K.; Kato, S.; Anderson, K. L.; Anderson, S. D.; Ohama, E.; Reaume, A. G.; Scott, R. W. and Cleveland, D. W. (1998): Aggregation and motor neuron toxicity of an ALS-linked SOD1 mutant independent from wild-type SOD1, Science 281 [5384], pp. 1851-4.

Brunet, A.; Datta, S. R. and Greenberg, M. E. (2001): Transcription-dependent and -independent control of neuronal survival by the PI3K-Akt signaling pathway, Curr Opin Neurobiol 11 [3], pp. 297-305.

Brunner, E. C.; Romeike, B. F.; Jung, M.; Comtesse, N. and Meese, E. (2006): Altered expression of beta-catenin/E-cadherin in meningiomas, Histopathology 49 [2], pp. 178-87.

Bublil, E. M. and Yarden, Y. (2007): The EGF receptor family: spearheading a merger of signaling and therapeutics, Curr Opin Cell Biol 19 [2], pp. 124-34.

Burroughs, A. M.; Jaffee, M.; Iyer, L. M. and Aravind, L. (2008): Anatomy of the E2 ligase fold: implications for enzymology and evolution of ubiquitin/Ub-like protein conjugation, J Struct Biol 162 [2], pp. 205-18.

Bushell, K. M.; Sollner, C.; Schuster-Boeckler, B.; Bateman, A. and Wright, G. J. (2008): Large-scale screening for novel low-affinity extracellular protein interactions, Genome Res 18 [4], pp. 622-30.

Canet-Aviles, R. M.; Wilson, M. A.; Miller, D. W.; Ahmad, R.; McLendon, C.; Bandyopadhyay, S.; Baptista, M. J.; Ringe, D.; Petsko, G. A. and Cookson, M. R. (2004): The Parkinson's disease protein DJ-1 is neuroprotective due to cysteine-sulfinic acid-driven mitochondrial localization, Proc Natl Acad Sci U S A 101 [24], pp. 9103-8.

Cao, H.; Courchesne, W. E. and Mastick, C. C. (2002): A phosphotyrosine-dependent protein interaction screen reveals a role for phosphorylation of caveolin-1 on tyrosine 14: recruitment of C-terminal Src kinase, J Biol Chem 277 [11], pp. 8771-4.

Carter, J. E.; Robertson, J.; Anderton, B. H. and Gallo, J. M. (1997): Incorporation of NF-L into keratin filaments in transfected epithelial cells, Neuroreport 8 [9-10], pp. 2225-8.

Casamayor, A.; Torrance, P. D.; Kobayashi, T.; Thorner, J. and Alessi, D. R. (1999): Functional counterparts of mammalian protein kinases PDK1 and SGK in budding yeast, Curr Biol 9 [4], pp. 186-97.

Chandel, N. S.; Trzyna, W. C.; McClintock, D. S. and Schumacker, P. T. (2000): Role of oxidants in NF-kappa B activation and TNF-alpha gene transcription induced by hypoxia and endotoxin, J Immunol 165 [2], pp. 1013-21.

Chen, D.; Gao, F.; Li, B.; Wang, H.; Xu, Y.; Zhu, C. and Wang, G. (2010): Parkin mono-ubiquitinates Bcl-2 and regulates autophagy, J Biol Chem 285 [49], pp. 38214-23.

Chen, H. K.; Fernandez-Funez, P.; Acevedo, S. F.; Lam, Y. C.; Kaytor, M. D.; Fernandez, M. H.; Aitken, A.; Skoulakis, E. M.; Orr, H. T.; Botas, J. and Zoghbi, H. Y. (2003): Interaction of Akt-phosphorylated ataxin-1 with 14-3-3 mediates neurodegeneration in spinocerebellar ataxia type 1, Cell 113 [4], pp. 457-68.

Chen, Y. C.; Rajagopala, S. V.; Stellberger, T. and Uetz, P. (2010): Exhaustive benchmarking of the yeast two-hybrid system, Nat Methods 7 [9], pp. 667-8; author reply 668.

Chiba, S.; Tokuhara, M.; Morita, E. H. and Abe, S. (2009): TTP at Ser245 phosphorylation by AKT is required for binding to 14-3-3, J Biochem 145 [3], pp. 403-9.

Ching, G. Y. and Liem, R. K. (1993): Assembly of type IV neuronal intermediate filaments in nonneuronal cells in the absence of preexisting cytoplasmic intermediate filaments, J Cell Biol 122 [6], pp. 1323-35.

Cho, H. S.; Suzuki, T.; Dohmae, N.; Hayami, S.; Unoki, M.; Yoshimatsu, M.; Toyokawa, G.; Takawa, M.; Chen, T.; Kurash, J. K.; Field, H. I.; Ponder, B. A.; Nakamura, Y. and Hamamoto, R. (2011): Demethylation of RB regulator MYPT1 by histone demethylase LSD1 promotes cell cycle progression in cancer cells, Cancer Res 71 [3], pp. 655-60.

Choudhary, C. and Mann, M. (2010): Decoding signalling networks by mass spectrometry-based proteomics, Nat Rev Mol Cell Biol 11 [6], pp. 427-39.

Chow, J. Y.; Cabral, J. A.; Chang, J. and Carethers, J. M. (2008): TGFbeta modulates PTEN expression independently of SMAD signaling for growth proliferation in colon cancer cells, Cancer Biol Ther 7 [10], pp. 1694-9.

Christine, C. W. and Aminoff, M. J. (2004): Clinical differentiation of parkinsonian syndromes: prognostic and therapeutic relevance, Am J Med 117 [6], pp. 412-9.

Chung, A. S.; Guan, Y. J.; Yuan, Z. L.; Albina, J. E. and Chin, Y. E. (2005): Ankyrin repeat and SOCS box 3 (ASB3) mediates ubiquitination and degradation of tumor necrosis factor receptor II, Mol Cell Biol 25 [11], pp. 4716-26.

Chung, K. K.; Zhang, Y.; Lim, K. L.; Tanaka, Y.; Huang, H.; Gao, J.; Ross, C. A.; Dawson, V. L. and Dawson, T. M. (2001): Parkin ubiquitinates the alpha-synuclein-interacting protein, synphilin-1: implications for Lewy-body formation in Parkinson disease, Nat Med 7 [10], pp. 1144-50.

Ciechanover, A. (1998): The ubiquitin-proteasome pathway: on protein death and cell life, EMBO J 17 [24], pp. 7151-60.

Clements, C. M.; McNally, R. S.; Conti, B. J.; Mak, T. W. and Ting, J. P. (2006): DJ-1, a cancer- and Parkinson's

disease-associated protein, stabilizes the antioxidant transcriptional master regulator Nrf2, Proc Natl Acad Sci U S A 103 [41], pp. 15091-6.

Colombatti, A.; Doliana, R.; Bot, S.; Canton, A.; Mongiat, M.; Mungiguerra, G.; Paron-Cilli, S. and Spessotto, P. (2000): The EMILIN protein family, Matrix Biol 19 [4], pp. 289-301.

Conway, K. A.; Harper, J. D. and Lansbury, P. T. (1998): Accelerated in vitro fibril formation by a mutant alpha-synuclein linked to early-onset Parkinson disease, Nat Med 4 [11], pp. 1318-20.

Cook, C. and Petrucelli, L. (2009): A critical evaluation of the ubiquitin-proteasome system in Parkinson's disease, Biochim Biophys Acta 1792 [7], pp. 664-75.

Cookson, M. R. (2010): DJ-1, PINK1, and their effects on mitochondrial pathways, Mov Disord 25 Suppl 1, pp. S44-8.

Cordeiro, N. J.; Gardner, K. R.; Huson, S. M.; Stewart, H.; Elston, J. S.; Howard, E. L.; Tullus, K. O. and Pike, M. G. (2006): Renal vascular disease in neurofibromatosis type 2: association or coincidence?, Dev Med Child Neurol 48 [1], pp. 58-9.

Coulombe, P. A. and Wong, P. (2004): Cytoplasmic intermediate filaments revealed as dynamic and multipurpose scaffolds, Nat Cell Biol 6 [8], pp. 699-706.

Crary, J. F.; Shao, C. Y.; Mirra, S. S.; Hernandez, A. I. and Sacktor, T. C. (2006): Atypical protein kinase C in neurodegenerative disease I: PKMzeta aggregates with limbic neurofibrillary tangles and AMPA receptors in Alzheimer disease, J Neuropathol Exp Neurol 65 [4], pp. 319-26.

Cui, J.; Yao, Q.; Li, S.; Ding, X.; Lu, Q.; Mao, H.; Liu, L.; Zheng, N.; Chen, S. and Shao, F. (2010): Glutamine deamidation and dysfunction of ubiquitin/NEDD8 induced by a bacterial effector family, Science 329 [5996], pp. 1215-8.

Cully, M.; You, H.; Levine, A. J. and Mak, T. W. (2006): Beyond PTEN mutations: the PI3K pathway as an integrator of multiple inputs during tumorigenesis, Nat Rev Cancer 6 [3], pp. 184-92.

Curto, M.; Cole, B. K.; Lallemand, D.; Liu, C. H. and McClatchey, A. I. (2007): Contact-dependent inhibition of EGFR signaling by Nf2/Merlin, J Cell Biol 177 [5], pp. 893-903.

Da Costa, C. R.; Villadiego, J.; Sancho, R.; Fontana, X.; Packham, G.; Nateri, A. S. and Behrens, A. (2010): Bag1-L is a phosphorylation-dependent coactivator of c-Jun during neuronal apoptosis, Mol Cell Biol 30 [15], pp. 3842-52.

Danussi, C.; Petrucco, A.; Wassermann, B.; Pivetta, E.; Modica, T. M.; Belluz, L. D.; Colombatti, A. and Spessotto, P. (2011): EMILIN1-{alpha}4/{alpha}9 integrin interaction inhibits dermal fibroblast and keratinocyte proliferation, J Cell Biol.

David, O.; Jett, J.; LeBeau, H.; Dy, G.; Hughes, J.; Friedman, M. and Brody, A. R. (2004): Phospho-Akt overexpression in non-small cell lung cancer confers significant stage-independent survival disadvantage, Clin Cancer Res 10 [20], pp. 6865-71.

Dawson, T. M. and Dawson, V. L. (2003): Molecular pathways of neurodegeneration in Parkinson's disease, Science 302 [5646], pp. 819-22.

de Rijk, M. C.; Launer, L. J.; Berger, K.; Breteler, M. M.; Dartigues, J. F.; Baldereschi, M.; Fratiglioni, L.; Lobo, A.; Martinez-Lage, J.; Trenkwalder, C. and Hofman, A. (2000): Prevalence of Parkinson's disease in Europe: A collaborative study of population-based cohorts. Neurologic Diseases in the Elderly Research Group, Neurology 54 [11 Suppl 5], pp. S21-3.

Deguen, B.; Merel, P.; Goutebroze, L.; Giovannini, M.; Reggio, H.; Arpin, M. and Thomas, G. (1998): Impaired interaction of naturally occurring mutant NF2 protein with actin-based cytoskeleton and membrane, Hum Mol Genet 7 [2], pp. 217-26.

den Bakker, M. A.; Riegman, P. H.; Suurmeijer, A. P.; Vissers, C. J.; Sainio, M.; Carpen, O. and Zwarthoff, E. C. (2000): Evidence for a cytoskeleton attachment domain at the N-terminus of the NF2 protein, J Neurosci Res 62 [6], pp. 764-71.

Denisenko-Nehrbass, N.; Goutebroze, L.; Galvez, T.; Bonnon, C.; Stankoff, B.; Ezan, P.; Giovannini, M.; Faivre-Sarrailh, C. and Girault, J. A. (2003): Association of Caspr/paranodin with tumour suppressor schwannomin/merlin and beta1 integrin in the central nervous system, J Neurochem 84 [2], pp. 209-21.

Dephoure, N.; Zhou, C.; Villen, J.; Beausoleil, S. A.; Bakalarski, C. E.; Elledge, S. J. and Gygi, S. P. (2008): A quantitative atlas of mitotic phosphorylation, Proc Natl Acad Sci U S A 105 [31], pp. 10762-7.

DiFiglia, M. (1997): Clinical Genetics, II. Huntington's disease: from the gene to pathophysiology, Am J Psychiatry 154 [8], p. 1046.

Dinkel, H.; Chica, C.; Via, A.; Gould, C. M.; Jensen, L. J.; Gibson, T. J. and Diella, F. (2011): Phospho.ELM: a database of phosphorylation sites--update 2011, Nucleic Acids Res 39 [Database issue], pp. D261-7.

Doo, A. R.; Kim, S. N.; Park, J. Y.; Cho, K. H.; Hong, J.; Eun-Kyung, K.; Moon, S. K.; Jung, W. S.; Lee, H.;

Jung, J. H. and Park, H. J. (2010): Neuroprotective effects of an herbal medicine, Yi-Gan San on MPP+/MPTP-induced cytotoxicity in vitro and in vivo, J Ethnopharmacol 131 [2], pp. 433-42.

Du, X.; Choi, I. G.; Kim, R.; Wang, W.; Jancarik, J.; Yokota, H. and Kim, S. H. (2000): Crystal structure of an intracellular protease from Pyrococcus horikoshii at 2-A resolution, Proc Natl Acad Sci U S A 97 [26], pp. 14079-84.

Ebert, M. P.; Fei, G.; Schandl, L.; Mawrin, C.; Dietzmann, K.; Herrera, P.; Friess, H.; Gress, T. M. and Malfertheiner, P. (2002): Reduced PTEN expression in the pancreas overexpressing transforming growth factor-beta 1, Br J Cancer 86 [2], pp. 257-62.

Eck, M. J.; Dhe-Paganon, S.; Trub, T.; Nolte, R. T. and Shoelson, S. E. (1996): Structure of the IRS-1 PTB domain bound to the juxtamembrane region of the insulin receptor, Cell 85 [5], pp. 695-705.

Ehrlund, A.; Anthonisen, E. H.; Gustafsson, N.; Venteclef, N.; Robertson Remen, K.; Damdimopoulos, A. E.; Galeeva, A.; Pelto-Huikko, M.; Lalli, E.; Steffensen, K. R.; Gustafsson, J. A. and Treuter, E. (2009): E3 ubiquitin ligase RNF31 cooperates with DAX-1 in transcriptional repression of steroidogenesis, Mol Cell Biol 29 [8], pp. 2230-42.

Erber, A.; Riemer, D.; Bovenschulte, M. and Weber, K. (1998): Molecular phylogeny of metazoan intermediate filament proteins, J Mol Evol 47 [6], pp. 751-62.

Evans, D. G. (2009): Neurofibromatosis type 2 (NF2): a clinical and molecular review, Orphanet J Rare Dis 4, p. 16.

Eyckerman, S.; Verhee, A.; der Heyden, J. V.; Lemmens, I.; Ostade, X. V.; Vandekerckhove, J. and Tavernier, J. (2001): Design and application of a cytokine-receptor-based interaction trap, Nat Cell Biol 3 [12], pp. 1114-9.

Fan, J.; Ren, H.; Jia, N.; Fei, E.; Zhou, T.; Jiang, P.; Wu, M. and Wang, G. (2008): DJ-1 decreases Bax expression through repressing p53 transcriptional activity, J Biol Chem 283 [7], pp. 4022-30.

Fernandez-Valle, C.; Tang, Y.; Ricard, J.; Rodenas-Ruano, A.; Taylor, A.; Hackler, E.; Biggerstaff, J. and Iacovelli, J. (2002): Paxillin binds schwannomin and regulates its density-dependent localization and effect on cell morphology, Nat Genet 31 [4], pp. 354-62.

Fields, S. and Song, O. (1989): A novel genetic system to detect protein-protein interactions, Nature 340 [6230], pp. 245-6.

Flood, P. M.; Qian, L.; Peterson, L. J.; Zhang, F.; Shi, J. S.; Gao, H. M. and Hong, J. S. (2011): Transcriptional Factor NF-kappaB as a Target for Therapy in Parkinson's Disease, Parkinsons Dis 2011, p. 216298.

Forno, L. S.; DeLanney, L. E.; Irwin, I. and Langston, J. W. (1996): Electron microscopy of Lewy bodies in the amygdala-parahippocampal region. Comparison with inclusion bodies in the MPTP-treated squirrel monkey, Adv Neurol 69, pp. 217-28.

Foster, F. M.; Traer, C. J.; Abraham, S. M. and Fry, M. J. (2003): The phosphoinositide (PI) 3-kinase family, J Cell Sci 116 [Pt 15], pp. 3037-40.

Fraenzer, J. T.; Pan, H.; Minimo, L., Jr.; Smith, G. M.; Knauer, D. and Hung, G. (2003): Overexpression of the NF2 gene inhibits schwannoma cell proliferation through promoting PDGFR degradation, Int J Oncol 23 [6], pp. 1493-500.

Franke, T. F.; Kaplan, D. R.; Cantley, L. C. and Toker, A. (1997): Direct regulation of the Akt proto-oncogene product by phosphatidylinositol-3,4-bisphosphate, Science 275 [5300], pp. 665-8.

Fruman, D. A.; Meyers, R. E. and Cantley, L. C. (1998): Phosphoinositide kinases, Annu Rev Biochem 67, pp. 481-507.

Fry, D. C. and Vassilev, L. T. (2005): Targeting protein-protein interactions for cancer therapy, J Mol Med (Berl) 83 [12], pp. 955-63.

Galcheva-Gargova, Z.; Derijard, B.; Wu, I. H. and Davis, R. J. (1994): An osmosensing signal transduction pathway in mammalian cells, Science 265 [5173], pp. 806-8.

Garcia-Guzman, M.; Dolfi, F.; Russello, M. and Vuori, K. (1999): Cell adhesion regulates the interaction between the docking protein p130(Cas) and the 14-3-3 proteins, J Biol Chem 274 [9], pp. 5762-8.

Gary, R. and Bretscher, A. (1995): Ezrin self-association involves binding of an N-terminal domain to a normally masked C-terminal domain that includes the F-actin binding site, Mol Biol Cell 6 [8], pp. 1061-75.

Gautheron, J.; Pescatore, A.; Fusco, F.; Esposito, E.; Yamaoka, S.; Agou, F.; Ursini, M. V. and Courtois, G. (2010): Identification of a new NEMO/TRAF6 interface affected in incontinentia pigmenti pathology, Hum Mol Genet 19 [16], pp. 3138-49.

Gautreau, A.; Louvard, D. and Arpin, M. (2000): Morphogenic effects of ezrin require a phosphorylation-induced transition from oligomers to monomers at the plasma membrane, J Cell Biol 150 [1], pp. 193-203.

Gautreau, A.; Poullet, P.; Louvard, D. and Arpin, M. (1999): Ezrin, a plasma membrane-microfilament linker, signals cell survival through the phosphatidylinositol 3-kinase/Akt pathway, Proc Natl Acad Sci U S A 96 [13], pp. 7300-5.

Ghosh, J.; Murphy, M. O.; Turner, N.; Khwaja, N.; Halka, A.; Kielty, C. M. and Walker, M. G. (2005): The role of transforming growth factor beta1 in the vascular system, Cardiovasc Pathol 14 [1], pp. 28-36.

Giasson, B. I. and Lee, V. M. (2003): Are ubiquitination pathways central to Parkinson's disease?, Cell 114 [1], pp. 1-8.

Giot, L.; Bader, J. S.; Brouwer, C.; Chaudhuri, A.; Kuang, B.; Li, Y.; Hao, Y. L.; Ooi, C. E.; Godwin, B.; Vitols, E.; Vijayadamodar, G.; Pochart, P.; Machineni, H.; Welsh, M.; Kong, Y.; Zerhusen, B.; Malcolm, R.; Varrone, Z.; Collis, A.; Minto, M.; Burgess, S.; McDaniel, L.; Stimpson, E.; Spriggs, F.; Williams, J.; Neurath, K.; Ioime, N.; Agee, M.; Voss, E.; Furtak, K.; Renzulli, R.; Aanensen, N.; Carrolla, S.; Bickelhaupt, E.; Lazovatsky, Y.; DaSilva, A.; Zhong, J.; Stanyon, C. A.; Finley, R. L., Jr.; White, K. P.; Braverman, M.; Jarvie, T.; Gold, S.; Leach, M.; Knight, J.; Shimkets, R. A.; McKenna, M. P.; Chant, J. and Rothberg, J. M. (2003): A protein interaction map of Drosophila melanogaster, Science 302 [5651], pp. 1727-36.

Glenner, G. G. and Wong, C. W. (1984): Alzheimer's disease: initial report of the purification and characterization of a novel cerebrovascular amyloid protein, Biochem Biophys Res Commun 120 [3], pp. 885-90.

Gnad, F.; Ren, S.; Cox, J.; Olsen, J. V.; Macek, B.; Oroshi, M. and Mann, M. (2007): PHOSIDA (phosphorylation site database): management, structural and evolutionary investigation, and prediction of phosphosites, Genome Biol 8 [11], p. R250.

Godde, N. J.; D'Abaco, G. M.; Paradiso, L. and Novak, U. (2006): Efficient ADAM22 surface expression is mediated by phosphorylation-dependent interaction with 14-3-3 protein family members, J Cell Sci 119 [Pt 16], pp. 3296-305.

Godsel, L. M.; Hobbs, R. P. and Green, K. J. (2008): Intermediate filament assembly: dynamics to disease, Trends Cell Biol 18 [1], pp. 28-37.

Goehler, H.; Lalowski, M.; Stelzl, U.; Waelter, S.; Stroedicke, M.; Worm, U.; Droege, A.; Lindenberg, K. S.; Knoblich, M.; Haenig, C.; Herbst, M.; Suopanki, J.; Scherzinger, E.; Abraham, C.; Bauer, B.; Hasenbank, R.; Fritzsche, A.; Ludewig, A. H.; Bussow, K.; Coleman, S. H.; Gutekunst, C. A.; Landwehrmeyer, B. G.; Lehrach, H. and Wanker, E. E. (2004): A protein interaction network links GIT1, an enhancer of huntingtin aggregation, to Huntington's disease, Mol Cell 15 [6], pp. 853-65.

Goh, K. I.; Cusick, M. E.; Valle, D.; Childs, B.; Vidal, M. and Barabasi, A. L. (2007): The human disease network, Proc Natl Acad Sci U S A 104 [21], pp. 8685-90.

Goldberg, M. S. and Lansbury, P. T., Jr. (2000): Is there a cause-and-effect relationship between alpha-synuclein fibrillization and Parkinson's disease?, Nat Cell Biol 2 [7], pp. E115-9.

Goldberg, M. S.; Pisani, A.; Haburcak, M.; Vortherms, T. A.; Kitada, T.; Costa, C.; Tong, Y.; Martella, G.; Tscherter, A.; Martins, A.; Bernardi, G.; Roth, B. L.; Pothos, E. N.; Calabresi, P. and Shen, J. (2005): Nigrostriatal dopaminergic deficits and hypokinesia caused by inactivation of the familial Parkinsonism-linked gene DJ-1, Neuron 45 [4], pp. 489-96.

Gonzalez-Agosti, C.; Wiederhold, T.; Herndon, M. E.; Gusella, J. and Ramesh, V. (1999): Interdomain interaction of merlin isoforms and its influence on intermolecular binding to NHE-RF, J Biol Chem 274 [48], pp. 34438-42.

Gonzalez-Agosti, C.; Xu, L.; Pinney, D.; Beauchamp, R.; Hobbs, W.; Gusella, J. and Ramesh, V. (1996): The merlin tumor suppressor localizes preferentially in membrane ruffles, Oncogene 13 [6], pp. 1239-47.

Gopalakrishna, R. and Jaken, S. (2000): Protein kinase C signaling and oxidative stress, Free Radic Biol Med 28 [9], pp. 1349-61.

Goutebroze, L.; Brault, E.; Muchardt, C.; Camonis, J. and Thomas, G. (2000): Cloning and characterization of SCHIP-1, a novel protein interacting specifically with spliced isoforms and naturally occurring mutant NF2 proteins, Mol Cell Biol 20 [5], pp. 1699-712.

Graham, F. L.; Smiley, J.; Russell, W. C. and Nairn, R. (1977): Characteristics of a human cell line transformed by DNA from human adenovirus type 5, J Gen Virol 36 [1], pp. 59-74.

Gronholm, M.; Sainio, M.; Zhao, F.; Heiska, L.; Vaheri, A. and Carpen, O. (1999): Homotypic and heterotypic interaction of the neurofibromatosis 2 tumor suppressor protein merlin and the ERM protein ezrin, J Cell Sci 112 ( Pt 6), pp. 895-904.

Grundke-Iqbal, I.; Iqbal, K.; Quinlan, M.; Tung, Y. C.; Zaidi, M. S. and Wisniewski, H. M. (1986): Microtubule-associated protein tau. A component of Alzheimer paired helical filaments, J Biol Chem 261 [13], pp. 6084-9.

Guo, D.; Hazbun, T. R.; Xu, X. J.; Ng, S. L.; Fields, S. and Kuo, M. H. (2004): A tethered catalysis, two-hybrid

system to identify protein-protein interactions requiring post-translational modifications, Nat Biotechnol 22 [7], pp. 888-92.

Gutmann, D. H.; Geist, R. T.; Xu, H.; Kim, J. S. and Saporito-Irwin, S. (1998): Defects in neurofibromatosis 2 protein function can arise at multiple levels, Hum Mol Genet 7 [3], pp. 335-45.

Gutmann, D. H.; Haipek, C. A. and Hoang Lu, K. (1999): Neurofibromatosis 2 tumor suppressor protein, merlin, forms two functionally important intramolecular associations, J Neurosci Res 58 [5], pp. 706-16.

Guzman, J. N.; Sanchez-Padilla, J.; Wokosin, D.; Kondapalli, J.; Ilijic, E.; Schumacker, P. T. and Surmeier, D. J. (2011): Oxidant stress evoked by pacemaking in dopaminergic neurons is attenuated by DJ-1, Nature 468 [7324], pp. 696-700.

Ha, H.; Han, D. and Choi, Y. (2009): TRAF-mediated TNFR-family signaling, Curr Protoc Immunol Chapter 11, p. Unit11 9D.

Han, J.; Lee, J. D.; Bibbs, L. and Ulevitch, R. J. (1994): A MAP kinase targeted by endotoxin and hyperosmolarity in mammalian cells, Science 265 [5173], pp. 808-11.

Hanemann, C. O. (2008): Magic but treatable? Tumours due to loss of merlin, Brain 131 [Pt 3], pp. 606-15.

Hara, T.; Bianchi, A. B.; Seizinger, B. R. and Kley, N. (1994): Molecular cloning and characterization of alternatively spliced transcripts of the mouse neurofibromatosis 2 gene, Cancer Res 54 [2], pp. 330-5.

Hardwick, K. G.; Weiss, E.; Luca, F. C.; Winey, M. and Murray, A. W. (1996): Activation of the budding yeast spindle assembly checkpoint without mitotic spindle disruption, Science 273 [5277], pp. 953-6.

Hardy, J. and Gwinn-Hardy, K. (1998): Genetic classification of primary neurodegenerative disease, Science 282 [5391], pp. 1075-9.

Hayami, S.; Kelly, J. D.; Cho, H. S.; Yoshimatsu, M.; Unoki, M.; Tsunoda, T.; Field, H. I.; Neal, D. E.; Yamaue, H.; Ponder, B. A.; Nakamura, Y. and Hamamoto, R. (2011): Overexpression of LSD1 contributes to human carcinogenesis through chromatin regulation in various cancers, Int J Cancer 128 [3], pp. 574-86.

Hennigan, R. F.; Foster, L. A.; Chaiken, M. F.; Mani, T.; Gomes, M. M.; Herr, A. B. and Ip, W. (2010): Fluorescence resonance energy transfer analysis of merlin conformational changes, Mol Cell Biol 30 [1], pp. 54-67.

Henry, M. D.; Gonzalez Agosti, C. and Solomon, F. (1995): Molecular dissection of radixin: distinct and interdependent functions of the amino- and carboxy-terminal domains, J Cell Biol 129 [4], pp. 1007-22.

Herrmann, H. and Aebi, U. (2004): Intermediate filaments: molecular structure, assembly mechanism, and integration into functionally distinct intracellular Scaffolds, Annu Rev Biochem 73, pp. 749-89.

Hershko, A. and Ciechanover, A. (1998): The ubiquitin system, Annu Rev Biochem 67, pp. 425-79.

Hilton, D. A.; Ristic, N. and Hanemann, C. O. (2009): Activation of ERK, AKT and JNK signalling pathways in human schwannomas in situ, Histopathology 55 [6], pp. 744-9.

Hornbeck, P. V.; Chabra, I.; Kornhauser, J. M.; Skrzypek, E. and Zhang, B. (2004): PhosphoSite: A bioinformatics resource dedicated to physiological protein phosphorylation, Proteomics 4 [6], pp. 1551-61.

Hornigold, R. E.; Golding, J. F. and Ferner, R. E. (2011): Neurofibromatosis 2: a novel risk factor for hypertension?, Am J Med Genet A 155A [7], pp. 1721-2.

Horvath, M. M. and Grishin, N. V. (2001): The C-terminal domain of HPII catalase is a member of the type I glutamine amidotransferase superfamily, Proteins 42 [2], pp. 230-6.

Huang, J.; Sengupta, R.; Espejo, A. B.; Lee, M. G.; Dorsey, J. A.; Richter, M.; Opravil, S.; Shiekhattar, R.; Bedford, M. T.; Jenuwein, T. and Berger, S. L. (2007): p53 is regulated by the lysine demethylase LSD1, Nature 449 [7158], pp. 105-8.

Huang, L.; Ichimaru, E.; Pestonjamasp, K.; Cui, X.; Nakamura, H.; Lo, G. Y.; Lin, F. I.; Luna, E. J. and Furthmayr, H. (1998): Merlin differs from moesin in binding to F-actin and in its intra- and intermolecular interactions, Biochem Biophys Res Commun 248 [3], pp. 548-53.

Huang, S. Y.; Tsai, M. L.; Chen, G. Y.; Wu, C. J. and Chen, S. H. (2007): A systematic MS-based approach for identifying in vitro substrates of PKA and PKG in rat uteri, J Proteome Res 6 [7], pp. 2674-84.

Huibregtse, J. M.; Scheffner, M.; Beaudenon, S. and Howley, P. M. (1995): A family of proteins structurally and functionally related to the E6-AP ubiquitin-protein ligase, Proc Natl Acad Sci U S A 92 [7], pp. 2563-7.

Hunter, T. (2007): The age of crosstalk: phosphorylation, ubiquitination, and beyond, Mol Cell 28 [5], pp. 730-8.

Hunter, T. and Plowman, G. D. (1997): The protein kinases of budding yeast: six score and more, Trends Biochem Sci 22 [1], pp. 18-22.

Huttlin, E. L.; Jedrychowski, M. P.; Elias, J. E.; Goswami, T.; Rad, R.; Beausoleil, S. A.; Villen, J.; Haas, W.;

Sowa, M. E. and Gygi, S. P. (2010): A tissue-specific atlas of mouse protein phosphorylation and expression, Cell 143 [7], pp. 1174-89.

Ikeda, F.; Deribe, Y. L.; Skanland, S. S.; Stieglitz, B.; Grabbe, C.; Franz-Wachtel, M.; van Wijk, S. J.; Goswami, P.; Nagy, V.; Terzic, J.; Tokunaga, F.; Androulidaki, A.; Nakagawa, T.; Pasparakis, M.; Iwai, K.; Sundberg, J. P.; Schaefer, L.; Rittinger, K.; Macek, B. and Dikic, I. (2011): SHARPIN forms a linear ubiquitin ligase complex regulating NF-kappaB activity and apoptosis, Nature 471 [7340], pp. 637-41.

Ito, M.; Nakano, T.; Erdodi, F. and Hartshorne, D. J. (2004): Myosin phosphatase: structure, regulation and function, Mol Cell Biochem 259 [1-2], pp. 197-209.

Ito, T.; Chiba, T.; Ozawa, R.; Yoshida, M.; Hattori, M. and Sakaki, Y. (2001): A comprehensive two-hybrid analysis to explore the yeast protein interactome, Proc Natl Acad Sci U S A 98 [8], pp. 4569-74.

Izaki, T.; Kamakura, S.; Kohjima, M. and Sumimoto, H. (2005): Phosphorylation-dependent binding of 14-3-3 to Par3beta, a human Par3-related cell polarity protein, Biochem Biophys Res Commun 329 [1], pp. 211-8.

Jacob, A.; Lee, T. X.; Neff, B. A.; Miller, S.; Welling, B. and Chang, L. S. (2008): Phosphatidylinositol 3-kinase/AKT pathway activation in human vestibular schwannoma, Otol Neurotol 29 [1], pp. 58-68.

James, M. F.; Han, S.; Polizzano, C.; Plotkin, S. R.; Manning, B. D.; Stemmer-Rachamimov, A. O.; Gusella, J. F. and Ramesh, V. (2009): NF2/merlin is a novel negative regulator of mTOR complex 1, and activation of mTORC1 is associated with meningioma and schwannoma growth, Mol Cell Biol 29 [15], pp. 4250-61.

James, M. F.; Manchanda, N.; Gonzalez-Agosti, C.; Hartwig, J. H. and Ramesh, V. (2001): The neurofibromatosis 2 protein product merlin selectively binds F-actin but not G-actin, and stabilizes the filaments through a lateral association, Biochem J 356 [Pt 2], pp. 377-86.

Jankovic, J. (2008): Parkinson's disease: clinical features and diagnosis, J Neurol Neurosurg Psychiatry 79 [4], pp. 368-76.

Jannatipour, M.; Dion, P.; Khan, S.; Jindal, H.; Fan, X.; Laganiere, J.; Chishti, A. H. and Rouleau, G. A. (2001): Schwannomin isoform-1 interacts with syntenin via PDZ domains, J Biol Chem 276 [35], pp. 33093-100.

Jin, H.; Sperka, T.; Herrlich, P. and Morrison, H. (2006): Tumorigenic transformation by CPI-17 through inhibition of a merlin phosphatase, Nature 442 [7102], pp. 576-9.

Kahl, P.; Gullotti, L.; Heukamp, L. C.; Wolf, S.; Friedrichs, N.; Vorreuther, R.; Solleder, G.; Bastian, P. J.; Ellinger, J.; Metzger, E.; Schule, R. and Buettner, R. (2006): Androgen receptor coactivators lysine-specific histone demethylase 1 and four and a half LIM domain protein 2 predict risk of prostate cancer recurrence, Cancer Res 66 [23], pp. 11341-7.

Kaltenbach, L. S.; Romero, E.; Becklin, R. R.; Chettier, R.; Bell, R.; Phansalkar, A.; Strand, A.; Torcassi, C.; Savage, J.; Hurlburt, A.; Cha, G. H.; Ukani, L.; Chepanoske, C. L.; Zhen, Y.; Sahasrabudhe, S.; Olson, J.; Kurschner, C.; Ellerby, L. M.; Peltier, J. M.; Botas, J. and Hughes, R. E. (2007): Huntingtin interacting proteins are genetic modifiers of neurodegeneration, PLoS Genet 3 [5], p. e82.

Kaltschmidt, B.; Ndiaye, D.; Korte, M.; Pothion, S.; Arbibe, L.; Prullage, M.; Pfeiffer, J.; Lindecke, A.; Staiger, V.; Israel, A.; Kaltschmidt, C. and Memet, S. (2006): NF-kappaB regulates spatial memory formation and synaptic plasticity through protein kinase A/CREB signaling, Mol Cell Biol 26 [8], pp. 2936-46.

Kanehisa, M.; Limviphuvadh, V. and Tanabe, M. (2010): Knowledge-Based Analysis of Protein Interaction Networks in Neurodegenerative Diseases.

Karabinos, A.; Schunemann, J. and Weber, K. (2004): Most genes encoding cytoplasmic intermediate filament (IF) proteins of the nematode Caenorhabditis elegans are required in late embryogenesis, Eur J Cell Biol 83 [9], pp. 457-68.

Kasyapa, C.; Gu, T. L.; Nagarajan, L.; Polakiewicz, R. and Cowell, J. K. (2009): Phosphorylation of the SSBP2 and ABL proteins by the ZNF198-FGFR1 fusion kinase seen in atypical myeloproliferative disorders as revealed by phosphopeptide-specific MS, Proteomics 9 [16], pp. 3979-88.

Kavanaugh, W. M.; Turck, C. W. and Williams, L. T. (1995): PTB domain binding to signaling proteins through a sequence motif containing phosphotyrosine, Science 268 [5214], pp. 1177-9.

Kawahara, K.; Hashimoto, M.; Bar-On, P.; Ho, G. J.; Crews, L.; Mizuno, H.; Rockenstein, E.; Imam, S. Z. and Masliah, E. (2008): alpha-Synuclein aggregates interfere with Parkin solubility and distribution: role in the pathogenesis of Parkinson disease, J Biol Chem 283 [11], pp. 6979-87.

Kemp, B. E. and Pearson, R. B. (1991): Intrasteric regulation of protein kinases and phosphatases, Biochim Biophys Acta 1094 [1], pp. 67-76.

Kerppola, T. K. (2008): Bimolecular fluorescence complementation: visualization of molecular interactions in living cells, Methods Cell Biol 85, pp. 431-70.

Kerppola, T. K. (2009): Visualization of molecular interactions using bimolecular fluorescence complementation analysis: characteristics of protein fragment complementation, Chem Soc Rev 38 [10], pp. 2876-86.

Kiachopoulos, S.; Heske, J.; Tatzelt, J. and Winklhofer, K. F. (2004): Misfolding of the prion protein at the plasma membrane induces endocytosis, intracellular retention and degradation, Traffic 5 [6], pp. 426-36.

Kielty, C. M.; Sherratt, M. J. and Shuttleworth, C. A. (2002): Elastic fibres, J Cell Sci 115 [Pt 14], pp. 2817-28.

Kim, R. H.; Peters, M.; Jang, Y.; Shi, W.; Pintilie, M.; Fletcher, G. C.; DeLuca, C.; Liepa, J.; Zhou, L.; Snow, B.; Binari, R. C.; Manoukian, A. S.; Bray, M. R.; Liu, F. F.; Tsao, M. S. and Mak, T. W. (2005): DJ-1, a novel regulator of the tumor suppressor PTEN, Cancer Cell 7 [3], pp. 263-73.

Kim, R. H.; Smith, P. D.; Aleyasin, H.; Hayley, S.; Mount, M. P.; Pownall, S.; Wakeham, A.; You-Ten, A. J.; Kalia, S. K.; Horne, P.; Westaway, D.; Lozano, A. M.; Anisman, H.; Park, D. S. and Mak, T. W. (2005): Hypersensitivity of DJ-1-deficient mice to 1-methyl-4-phenyl-1,2,3,6-tetrahydropyrindine (MPTP) and oxidative stress, Proc Natl Acad Sci U S A 102 [14], pp. 5215-20.

King, N. and Carroll, S. B. (2001): A receptor tyrosine kinase from choanoflagellates: molecular insights into early animal evolution, Proc Natl Acad Sci U S A 98 [26], pp. 15032-7.

King, N.; Westbrook, M. J.; Young, S. L.; Kuo, A.; Abedin, M.; Chapman, J.; Fairclough, S.; Hellsten, U.; Isogai, Y.; Letunic, I.; Marr, M.; Pincus, D.; Putnam, N.; Rokas, A.; Wright, K. J.; Zuzow, R.; Dirks, W.; Good, M.; Goodstein, D.; Lemons, D.; Li, W.; Lyons, J. B.; Morris, A.; Nichols, S.; Richter, D. J.; Salamov, A.; Sequencing, J. G.; Bork, P.; Lim, W. A.; Manning, G.; Miller, W. T.; McGinnis, W.; Shapiro, H.; Tjian, R.; Grigoriev, I. V. and Rokhsar, D. (2008): The genome of the choanoflagellate Monosiga brevicollis and the origin of metazoans, Nature 451 [7180], pp. 783-8.

Kinumi, T.; Kimata, J.; Taira, T.; Ariga, H. and Niki, E. (2004): Cysteine-106 of DJ-1 is the most sensitive cysteine residue to hydrogen peroxide-mediated oxidation in vivo in human umbilical vein endothelial cells, Biochem Biophys Res Commun 317 [3], pp. 722-8.

Kirisako, T.; Kamei, K.; Murata, S.; Kato, M.; Fukumoto, H.; Kanie, M.; Sano, S.; Tokunaga, F.; Tanaka, K. and Iwai, K. (2006): A ubiquitin ligase complex assembles linear polyubiquitin chains, EMBO J 25 [20], pp. 4877-87.

Kissil, J. L.; Johnson, K. C.; Eckman, M. S. and Jacks, T. (2002): Merlin phosphorylation by p21-activated kinase 2 and effects of phosphorylation on merlin localization, J Biol Chem 277 [12], pp. 10394-9.

Kitada, T.; Asakawa, S.; Hattori, N.; Matsumine, H.; Yamamura, Y.; Minoshima, S.; Yokochi, M.; Mizuno, Y. and Shimizu, N. (1998): Mutations in the parkin gene cause autosomal recessive juvenile parkinsonism, Nature 392 [6676], pp. 605-8.

Koga, H.; Araki, N.; Takeshima, H.; Nishi, T.; Hirota, T.; Kimura, Y.; Nakao, M. and Saya, H. (1998): Impairment of cell adhesion by expression of the mutant neurofibromatosis type 2 (NF2) genes which lack exons in the ERM-homology domain, Oncogene 17 [7], pp. 801-10.

Koide-Yoshida, S.; Niki, T.; Ueda, M.; Himeno, S.; Taira, T.; Iguchi-Ariga, S. M.; Ando, Y. and Ariga, H. (2007): DJ-1 degrades transthyretin and an inactive form of DJ-1 is secreted in familial amyloidotic polyneuropathy, Int J Mol Med 19 [6], pp. 885-93.

Kornbluth, S.; Jove, R. and Hanafusa, H. (1987): Characterization of avian and viral p60src proteins expressed in yeast, Proc Natl Acad Sci U S A 84 [13], pp. 4455-9.

Kressel, M. and Schmucker, B. (2002): Nucleocytoplasmic transfer of the NF2 tumor suppressor protein merlin is regulated by exon 2 and a CRM1-dependent nuclear export signal in exon 15, Hum Mol Genet 11 [19], pp. 2269-78.

Kretzschmar, M.; Doody, J.; Timokhina, I. and Massague, J. (1999): A mechanism of repression of TGFbeta/ Smad signaling by oncogenic Ras, Genes Dev 13 [7], pp. 804-16.

Kurmangaliyev, Y. Z.; Goland, A. and Gelfand, M. S. (2011): Evolutionary patterns of phosphorylated serines, Biol Direct 6, p. 8.

Lallemand, D.; Curto, M.; Saotome, I.; Giovannini, M. and McClatchey, A. I. (2003): NF2 deficiency promotes tumorigenesis and metastasis by destabilizing adherens junctions, Genes Dev 17 [9], pp. 1090-100.

Lallemand, D.; Manent, J.; Couvelard, A.; Watilliaux, A.; Siena, M.; Chareyre, F.; Lampin, A.; Niwa-Kawakita, M.; Kalamarides, M. and Giovannini, M. (2009): Merlin regulates transmembrane receptor accumulation and signaling at the plasma membrane in primary mouse Schwann cells and in human schwannomas, Oncogene 28 [6], pp. 854-65.

Lallemand, D.; Saint-Amaux, A. L. and Giovannini, M. (2009): Tumor-suppression functions of merlin are independent of its role as an organizer of the actin cytoskeleton in Schwann cells, J Cell Sci 122 [Pt 22], pp. 4141-9.

Lalonde, S.; Ehrhardt, D. W.; Loque, D.; Chen, J.; Rhee, S. Y. and Frommer, W. B. (2008): Molecular and

cellular approaches for the detection of protein-protein interactions: latest techniques and current limitations, Plant J 53 [4], pp. 610-35.

Lassman, A. B. (2004): Molecular biology of gliomas, Curr Neurol Neurosci Rep 4 [3], pp. 228-33.

Lau, Y. K.; Murray, L. B.; Houshmandi, S. S.; Xu, Y.; Gutmann, D. H. and Yu, Q. (2008): Merlin is a potent inhibitor of glioma growth, Cancer Res 68 [14], pp. 5733-42.

Laulajainen, M.; Muranen, T.; Carpen, O. and Gronholm, M. (2008): Protein kinase A-mediated phosphorylation of the NF2 tumor suppressor protein merlin at serine 10 affects the actin cytoskeleton, Oncogene 27 [23], pp. 3233-43.

Laulajainen, M.; Muranen, T.; Nyman, T. A.; Carpen, O. and Gronholm, M. (2011): Multistep phosphorylation by oncogenic kinases enhances the degradation of the NF2 tumor suppressor merlin, Neoplasia 13 [7], pp. 643-52.

Lee, M. G.; Wynder, C.; Cooch, N. and Shiekhattar, R. (2005): An essential role for CoREST in nucleosomal histone 3 lysine 4 demethylation, Nature 437 [7057], pp. 432-5.

Lee, S. J.; Kim, S. J.; Kim, I. K.; Ko, J.; Jeong, C. S.; Kim, G. H.; Park, C.; Kang, S. O.; Suh, P. G.; Lee, H. S. and Cha, S. S. (2003): Crystal structures of human DJ-1 and Escherichia coli Hsp31, which share an evolutionarily conserved domain, J Biol Chem 278 [45], pp. 44552-9.

Lee, T. X.; Packer, M. D.; Huang, J.; Akhmametyeva, E. M.; Kulp, S. K.; Chen, C. S.; Giovannini, M.; Jacob, A.; Welling, D. B. and Chang, L. S. (2009): Growth inhibitory and anti-tumour activities of OSU-03012, a novel PDK-1 inhibitor, on vestibular schwannoma and malignant schwannoma cells, Eur J Cancer 45 [9], pp. 1709-20.

Lemeer, S. and Heck, A. J. (2009): The phosphoproteomics data explosion, Curr Opin Chem Biol 13 [4], pp. 414-20.

Lemmens, I.; Eyckerman, S.; Zabeau, L.; Catteeuw, D.; Vertenten, E.; Verschueren, K.; Huylebroeck, D.; Vandekerckhove, J. and Tavernier, J. (2003): Heteromeric MAPPIT: a novel strategy to study modification-dependent protein-protein interactions in mammalian cells, Nucleic Acids Res 31 [14], p. e75.

Lesage, S. and Brice, A. (2009): Parkinson's disease: from monogenic forms to genetic susceptibility factors, Hum Mol Genet 18 [R1], pp. R48-59.

Levin-Salomon, V.; Maayan, I.; Avrahami-Moyal, L.; Marbach, I.; Livnah, O. and Engelberg, D. (2009): When expressed in yeast, mammalian mitogen-activated protein kinases lose proper regulation and become spontaneously phosphorylated, Biochem J 417 [1], pp. 331-40.

Levin, D. E. and Bartlett-Heubusch, E. (1992): Mutants in the S. cerevisiae PKC1 gene display a cell cycle-specific osmotic stability defect, J Cell Biol 116 [5], pp. 1221-9.

Levin, D. E.; Fields, F. O.; Kunisawa, R.; Bishop, J. M. and Thorner, J. (1990): A candidate protein kinase C gene, PKC1, is required for the S. cerevisiae cell cycle, Cell 62 [2], pp. 213-24.

Li, S.; Armstrong, C. M.; Bertin, N.; Ge, H.; Milstein, S.; Boxem, M.; Vidalain, P. O.; Han, J. D.; Chesneau, A.; Hao, T.; Goldberg, D. S.; Li, N.; Martinez, M.; Rual, J. F.; Lamesch, P.; Xu, L.; Tewari, M.; Wong, S. L.; Zhang, L. V.; Berriz, G. F.; Jacotot, L.; Vaglio, P.; Reboul, J.; Hirozane-Kishikawa, T.; Li, Q.; Gabel, H. W.; Elewa, A.; Baumgartner, B.; Rose, D. J.; Yu, H.; Bosak, S.; Sequerra, R.; Fraser, A.; Mango, S. E.; Saxton, W. M.; Strome, S.; Van Den Heuvel, S.; Piano, F.; Vandenhaute, J.; Sardet, C.; Gerstein, M.; Doucette-Stamm, L.; Gunsalus, K. C.; Harper, J. W.; Cusick, M. E.; Roth, F. P.; Hill, D. E. and Vidal, M. (2004): A map of the interactome network of the metazoan C. elegans, Science 303 [5657], pp. 540-3.

Li, W.; Bengtson, M. H.; Ulbrich, A.; Matsuda, A.; Reddy, V. A.; Orth, A.; Chanda, S. K.; Batalov, S. and Joazeiro, C. A. (2008): Genome-wide and functional annotation of human E3 ubiquitin ligases identifies MULAN, a mitochondrial E3 that regulates the organelle's dynamics and signaling, PLoS One 3 [1], p. e1487.

Li, W.; You, L.; Cooper, J.; Schiavon, G.; Pepe-Caprio, A.; Zhou, L.; Ishii, R.; Giovannini, M.; Hanemann, C. O.; Long, S. B.; Erdjument-Bromage, H.; Zhou, P.; Tempst, P. and Giancotti, F. G. (2010): Merlin/NF2 suppresses tumorigenesis by inhibiting the E3 ubiquitin ligase CRL4(DCAF1) in the nucleus, Cell 140 [4], pp. 477-90.

Li, Y.; Tennekoon, G. I.; Birnbaum, M.; Marchionni, M. A. and Rutkowski, J. L. (2001): Neuregulin signaling through a PI3K/Akt/Bad pathway in Schwann cell survival, Mol Cell Neurosci 17 [4], pp. 761-7.

Lim, J.; Hao, T.; Shaw, C.; Patel, A. J.; Szabo, G.; Rual, J. F.; Fisk, C. J.; Li, N.; Smolyar, A.; Hill, D. E.; Barabasi, A. L.; Vidal, M. and Zoghbi, H. Y. (2006): A protein-protein interaction network for human inherited ataxias and disorders of Purkinje cell degeneration, Cell 125 [4], pp. 801-14.

Lim, J. Y.; Kim, H.; Jeun, S. S.; Kang, S. G. and Lee, K. J. (2006): Merlin inhibits growth hormone-regulated

Raf-ERKs pathways by binding to Grb2 protein, Biochem Biophys Res Commun 340 [4], pp. 1151-7.

Lim, K. L.; Chew, K. C.; Tan, J. M.; Wang, C.; Chung, K. K.; Zhang, Y.; Tanaka, Y.; Smith, W.; Engelender, S.; Ross, C. A.; Dawson, V. L. and Dawson, T. M. (2005): Parkin mediates nonclassical, proteasomal-independent ubiquitination of synphilin-1: implications for Lewy body formation, J Neurosci 25 [8], pp. 2002-9.

Lim, W. A. and Pawson, T. (2010): Phosphotyrosine signaling: evolving a new cellular communication system, Cell 142 [5], pp. 661-7.

Limviphuvadh, V.; Tanaka, S.; Goto, S.; Ueda, K. and Kanehisa, M. (2007): The commonality of protein interaction networks determined in neurodegenerative disorders (NDDs), Bioinformatics 23 [16], pp. 2129-38.

Linding, R.; Jensen, L. J.; Ostheimer, G. J.; van Vugt, M. A.; Jorgensen, C.; Miron, I. M.; Diella, F.; Colwill, K.; Taylor, L.; Elder, K.; Metalnikov, P.; Nguyen, V.; Pasculescu, A.; Jin, J.; Park, J. G.; Samson, L. D.; Woodgett, J. R.; Russell, R. B.; Bork, P.; Yaffe, M. B. and Pawson, T. (2007): Systematic discovery of in vivo phosphorylation networks, Cell 129 [7], pp. 1415-26.

Linding, R.; Jensen, L. J.; Pasculescu, A.; Olhovsky, M.; Colwill, K.; Bork, P.; Yaffe, M. B. and Pawson, T. (2008): NetworKIN: a resource for exploring cellular phosphorylation networks, Nucleic Acids Res 36 [Database issue], pp. D695-9.

Liu, B. A.; Jablonowski, K.; Raina, M.; Arce, M.; Pawson, T. and Nash, P. D. (2006): The human and mouse complement of SH2 domain proteins-establishing the boundaries of phosphotyrosine signaling, Mol Cell 22 [6], pp. 851-68.

Liu, Y.; Fallon, L.; Lashuel, H. A.; Liu, Z. and Lansbury, P. T., Jr. (2002): The UCH-L1 gene encodes two opposing enzymatic activities that affect alpha-synuclein degradation and Parkinson's disease susceptibility, Cell 111 [2], pp. 209-18.

Lopez-Lago, M. A.; Okada, T.; Murillo, M. M.; Socci, N. and Giancotti, F. G. (2009): Loss of the tumor suppressor gene NF2, encoding merlin, constitutively activates integrin-dependent mTORC1 signaling, Mol Cell Biol 29 [15], pp. 4235-49.

Lucking, C. B.; Durr, A.; Bonifati, V.; Vaughan, J.; De Michele, G.; Gasser, T.; Harhangi, B. S.; Meco, G.; Denefle, P.; Wood, N. W.; Agid, Y. and Brice, A. (2000): Association between early-onset Parkinson's disease and mutations in the parkin gene, N Engl J Med 342 [21], pp. 1560-7.

Mackintosh, C. (2004): Dynamic interactions between 14-3-3 proteins and phosphoproteins regulate diverse cellular processes, Biochem J 381 [Pt 2], pp. 329-42.

Magliery, T. J.; Wilson, C. G.; Pan, W.; Mishler, D.; Ghosh, I.; Hamilton, A. D. and Regan, L. (2005): Detecting protein-protein interactions with a green fluorescent protein fragment reassembly trap: scope and mechanism, J Am Chem Soc 127 [1], pp. 146-57.

Malkus, K. A.; Tsika, E. and Ischiropoulos, H. (2009): Oxidative modifications, mitochondrial dysfunction, and impaired protein degradation in Parkinson's disease: how neurons are lost in the Bermuda triangle, Mol Neurodegener 4, p. 24.

Malovannaya, A.; Lanz, R. B.; Jung, S. Y.; Bulynko, Y.; Le, N. T.; Chan, D. W.; Ding, C.; Shi, Y.; Yucer, N.; Krenciute, G.; Kim, B. J.; Li, C.; Chen, R.; Li, W.; Wang, Y.; O'Malley, B. W. and Qin, J. (2011): Analysis of the human endogenous coregulator complexome, Cell 145 [5], pp. 787-99.

Malovannaya, A.; Li, Y.; Bulynko, Y.; Jung, S. Y.; Wang, Y.; Lanz, R. B.; O'Malley, B. W. and Qin, J. (2009): Streamlined analysis schema for high-throughput identification of endogenous protein complexes, Proc Natl Acad Sci U S A 107 [6], pp. 2431-6.

Mann, M. and Jensen, O. N. (2003): Proteomic analysis of post-translational modifications, Nat Biotechnol 21 [3], pp. 255-61.

Manning, G.; Plowman, G. D.; Hunter, T. and Sudarsanam, S. (2002): Evolution of protein kinase signaling from yeast to man, Trends Biochem Sci 27 [10], pp. 514-20.

Manning, G.; Whyte, D. B.; Martinez, R.; Hunter, T. and Sudarsanam, S. (2002): The protein kinase complement of the human genome, Science 298 [5600], pp. 1912-34.

Marchler-Bauer, A.; Lu, S.; Anderson, J. B.; Chitsaz, F.; Derbyshire, M. K.; DeWeese-Scott, C.; Fong, J. H.; Geer, L. Y.; Geer, R. C.; Gonzales, N. R.; Gwadz, M.; Hurwitz, D. I.; Jackson, J. D.; Ke, Z.; Lanczycki, C. J.; Lu, F.; Marchler, G. H.; Mullokandov, M.; Omelchenko, M. V.; Robertson, C. L.; Song, J. S.; Thanki, N.; Yamashita, R. A.; Zhang, D.; Zhang, N.; Zheng, C. and Bryant, S. H. (2011): CDD: a Conserved Domain Database for the functional annotation of proteins, Nucleic Acids Res 39 [Database issue], pp. D225-9.

Marin, I.; Lucas, J. I.; Gradilla, A. C. and Ferrus, A. (2004): Parkin and relatives: the RBR family of ubiquitin ligases, Physiol Genomics 17 [3], pp. 253-63.

Markson, G.; Kiel, C.; Hyde, R.; Brown, S.; Charalabous, P.; Bremm, A.; Semple, J.; Woodsmith, J.; Duley, S.; Salehi-Ashtiani, K.; Vidal, M.; Komander, D.; Serrano, L.; Lehner, P. and Sanderson, C. M. (2009): Analysis of the human E2 ubiquitin conjugating enzyme protein interaction network, Genome Res 19 [10], pp. 1905-11.

Martin, D. M.; Miranda-Saavedra, D. and Barton, G. J. (2009): Kinomer v. 1.0: a database of systematically classified eukaryotic protein kinases, Nucleic Acids Res 37 [Database issue], pp. D244-50.

Martin, M.; Andreoli, C.; Sahuquet, A.; Montcourrier, P.; Algrain, M. and Mangeat, P. (1995): Ezrin NH2-terminal domain inhibits the cell extension activity of the COOH-terminal domain, J Cell Biol 128 [6], pp. 1081-93.

Matsumoto, A.; Comatas, K. E.; Liu, L. and Stamler, J. S. (2003): Screening for nitric oxide-dependent protein-protein interactions, Science 301 [5633], pp. 657-61.

Mattson, M. P. and Sherman, M. (2003): Perturbed signal transduction in neurodegenerative disorders involving aberrant protein aggregation, Neuromolecular Med 4 [1-2], pp. 109-32.

Mayer, B. J.; Jackson, P. K.; Van Etten, R. A. and Baltimore, D. (1992): Point mutations in the abl SH2 domain coordinately impair phosphotyrosine binding in vitro and transforming activity in vivo, Mol Cell Biol 12 [2], pp. 609-18.

Mayya, V.; Lundgren, D. H.; Hwang, S. I.; Rezaul, K.; Wu, L.; Eng, J. K.; Rodionov, V. and Han, D. K. (2009): Quantitative phosphoproteomic analysis of T cell receptor signaling reveals system-wide modulation of protein-protein interactions, Sci Signal 2 [84], p. ra46.

McClatchey, A. I. and Fehon, R. G. (2009): Merlin and the ERM proteins--regulators of receptor distribution and signaling at the cell cortex, Trends Cell Biol 19 [5], pp. 198-206.

McClatchey, A. I. and Giovannini, M. (2005): Membrane organization and tumorigenesis--the NF2 tumor suppressor, Merlin, Genes Dev 19 [19], pp. 2265-77.

McCoy, M. K. and Tansey, M. G. (2008): TNF signaling inhibition in the CNS: implications for normal brain function and neurodegenerative disease, J Neuroinflammation 5, p. 45.

McNally, R. S.; Davis, B. K.; Clements, C. M.; Accavitti-Loper, M. A.; Mak, T. W. and Ting, J. P. (2011): DJ-1 enhances cell survival through the binding of Cezanne, a negative regulator of NF-kappaB, J Biol Chem 286 [6], pp. 4098-106.

McNaught, K. S.; Belizaire, R.; Isacson, O.; Jenner, P. and Olanow, C. W. (2003): Altered proteasomal function in sporadic Parkinson's disease, Exp Neurol 179 [1], pp. 38-46.

McNaught, K. S.; Olanow, C. W.; Halliwell, B.; Isacson, O. and Jenner, P. (2001): Failure of the ubiquitin-proteasome system in Parkinson's disease, Nat Rev Neurosci 2 [8], pp. 589-94.

Meffert, M. K.; Chang, J. M.; Wiltgen, B. J.; Fanselow, M. S. and Baltimore, D. (2003): NF-kappa B functions in synaptic signaling and behavior, Nat Neurosci 6 [10], pp. 1072-8.

Melander, F.; Andersson, T. and Dib, K. (2004): Engagement of beta2 integrins recruits 14-3-3 proteins to c-Cbl in human neutrophils, Biochem Biophys Res Commun 317 [4], pp. 1000-5.

Meng, J. J.; Lowrie, D. J.; Sun, H.; Dorsey, E.; Pelton, P. D.; Bashour, A. M.; Groden, J.; Ratner, N. and Ip, W. (2000): Interaction between two isoforms of the NF2 tumor suppressor protein, merlin, and between merlin and ezrin, suggests modulation of ERM proteins by merlin, J Neurosci Res 62 [4], pp. 491-502.

Meredith, S. C. (2005): Protein denaturation and aggregation: Cellular responses to denatured and aggregated proteins, Ann N Y Acad Sci 1066, pp. 181-221.

Metzger, E.; Wissmann, M.; Yin, N.; Muller, J. M.; Schneider, R.; Peters, A. H.; Gunther, T.; Buettner, R. and Schule, R. (2005): LSD1 demethylates repressive histone marks to promote androgen-receptor-dependent transcription, Nature 437 [7057], pp. 436-9.

Meulener, M. C.; Xu, K.; Thomson, L.; Ischiropoulos, H. and Bonini, N. M. (2006): Mutational analysis of DJ-1 in Drosophila implicates functional inactivation by oxidative damage and aging, Proc Natl Acad Sci U S A 103 [33], pp. 12517-22.

Michnick, S. W.; Ear, P. H.; Manderson, E. N.; Remy, I. and Stefan, E. (2007): Universal strategies in research and drug discovery based on protein-fragment complementation assays, Nat Rev Drug Discov 6 [7], pp. 569-82.

Miller, D. W.; Ahmad, R.; Hague, S.; Baptista, M. J.; Canet-Aviles, R.; McLendon, C.; Carter, D. M.; Zhu, P. P.; Stadler, J.; Chandran, J.; Klinefelter, G. R.; Blackstone, C. and Cookson, M. R. (2003): L166P mutant DJ-1, causative for recessive Parkinson's disease, is degraded through the ubiquitin-proteasome system, J Biol Chem 278 [38], pp. 36588-95.

Miller, M. L.; Jensen, L. J.; Diella, F.; Jorgensen, C.; Tinti, M.; Li, L.; Hsiung, M.; Parker, S. A.; Bordeaux, J.; Sicheritz-Ponten, T.; Olhovsky, M.; Pasculescu, A.; Alexander, J.; Knapp, S.; Blom, N.; Bork, P.; Li, S.;

Cesareni, G.; Pawson, T.; Turk, B. E.; Yaffe, M. B.; Brunak, S. and Linding, R. (2008): Linear motif atlas for phosphorylation-dependent signaling, Sci Signal 1 [35], p. ra2.

Mitsumoto, A. and Nakagawa, Y. (2001): DJ-1 is an indicator for endogenous reactive oxygen species elicited by endotoxin, Free Radic Res 35 [6], pp. 885-93.

Mitsumoto, A.; Nakagawa, Y.; Takeuchi, A.; Okawa, K.; Iwamatsu, A. and Takanezawa, Y. (2001): Oxidized forms of peroxiredoxins and DJ-1 on two-dimensional gels increased in response to sublethal levels of paraquat, Free Radic Res 35 [3], pp. 301-10.

Mok, J.; Kim, P. M.; Lam, H. Y.; Piccirillo, S.; Zhou, X.; Jeschke, G. R.; Sheridan, D. L.; Parker, S. A.; Desai, V.; Jwa, M.; Cameroni, E.; Niu, H.; Good, M.; Remenyi, A.; Ma, J. L.; Sheu, Y. J.; Sassi, H. E.; Sopko, R.; Chan, C. S.; De Virgilio, C.; Hollingsworth, N. M.; Lim, W. A.; Stern, D. F.; Stillman, B.; Andrews, B. J.; Gerstein, M. B.; Snyder, M. and Turk, B. E. (2010): Deciphering protein kinase specificity through large-scale analysis of yeast phosphorylation site motifs, Sci Signal 3 [109], p. ra12.

Mongiat, M.; Taylor, K.; Otto, J.; Aho, S.; Uitto, J.; Whitelock, J. M. and Iozzo, R. V. (2000): The protein core of the proteoglycan perlecan binds specifically to fibroblast growth factor-7, J Biol Chem 275 [10], pp. 7095-100.

Montastruc, J. L.; Llau, M. E.; Rascol, O. and Senard, J. M. (1994): Drug-induced parkinsonism: a review, Fundam Clin Pharmacol 8 [4], pp. 293-306.

Moore, D. J.; Zhang, L.; Dawson, T. M. and Dawson, V. L. (2003): A missense mutation (L166P) in DJ-1, linked to familial Parkinson's disease, confers reduced protein stability and impairs homo-oligomerization, J Neurochem 87 [6], pp. 1558-67.

Moore, D. J.; Zhang, L.; Troncoso, J.; Lee, M. K.; Hattori, N.; Mizuno, Y.; Dawson, T. M. and Dawson, V. L. (2005): Association of DJ-1 and parkin mediated by pathogenic DJ-1 mutations and oxidative stress, Hum Mol Genet 14 [1], pp. 71-84.

Mrak, R. E.; Griffin, S. T. and Graham, D. I. (1997): Aging-associated changes in human brain, J Neuropathol Exp Neurol 56 [12], pp. 1269-75.

Muranen, T.; Gronholm, M.; Renkema, G. H. and Carpen, O. (2005): Cell cycle-dependent nucleocytoplasmic shuttling of the neurofibromatosis 2 tumour suppressor merlin, Oncogene 24 [7], pp. 1150-8.

Murthy, A.; Gonzalez-Agosti, C.; Cordero, E.; Pinney, D.; Candia, C.; Solomon, F.; Gusella, J. and Ramesh, V. (1998): NHE-RF, a regulatory cofactor for Na(+)-H+ exchange, is a common interactor for merlin and ERM (MERM) proteins, J Biol Chem 273 [3], pp. 1273-6.

Muslin, A. J.; Tanner, J. W.; Allen, P. M. and Shaw, A. S. (1996): Interaction of 14-3-3 with signaling proteins is mediated by the recognition of phosphoserine, Cell 84 [6], pp. 889-97.

Nagai, T.; Ibata, K.; Park, E. S.; Kubota, M.; Mikoshiba, K. and Miyawaki, A. (2002): A variant of yellow fluorescent protein with fast and efficient maturation for cell-biological applications, Nat Biotechnol 20 [1], pp. 87-90.

Nagakubo, D.; Taira, T.; Kitaura, H.; Ikeda, M.; Tamai, K.; Iguchi-Ariga, S. M. and Ariga, H. (1997): DJ-1, a novel oncogene which transforms mouse NIH3T3 cells in cooperation with ras, Biochem Biophys Res Commun 231 [2], pp. 509-13.

Nagata, D.; Kiyosue, A.; Takahashi, M.; Satonaka, H.; Tanaka, K.; Sata, M.; Nagano, T.; Nagai, R. and Hirata, Y. (2009): A new constitutively active mutant of AMP-activated protein kinase inhibits anoxia-induced apoptosis of vascular endothelial cell, Hypertens Res 32 [2], pp. 133-9.

Nakaso, K.; Ito, S. and Nakashima, K. (2008): Caffeine activates the PI3K/Akt pathway and prevents apoptotic cell death in a Parkinson's disease model of SH-SY5Y cells, Neurosci Lett 432 [2], pp. 146-50.

Nakayama, M.; Kikuno, R. and Ohara, O. (2002): Protein-protein interactions between large proteins: two-hybrid screening using a functionally classified library composed of long cDNAs, Genome Res 12 [11], pp. 1773-84.

Nateri, A. S.; Riera-Sans, L.; Da Costa, C. and Behrens, A. (2004): The ubiquitin ligase SCFFbw7 antagonizes apoptotic JNK signaling, Science 303 [5662], pp. 1374-8.

Nateri, A. S.; Spencer-Dene, B. and Behrens, A. (2005): Interaction of phosphorylated c-Jun with TCF4 regulates intestinal cancer development, Nature 437 [7056], pp. 281-5.

Newton, A. C. (1995): Protein kinase C: structure, function, and regulation, J Biol Chem 270 [48], pp. 28495-8.

Niki, T.; Takahashi-Niki, K.; Taira, T.; Iguchi-Ariga, S. M. and Ariga, H. (2003): DJBP: a novel DJ-1-binding protein, negatively regulates the androgen receptor by recruiting histone deacetylase complex, and DJ-1 antagonizes this inhibition by abrogation of this complex, Mol Cancer Res 1 [4], pp. 247-61.

Nita-Lazar, A. (2010): Quantitative analysis of phosphorylation-based protein signaling networks in the immune system by mass spectrometry, Wiley Interdiscip Rev Syst Biol Med 3 [3], pp. 368-76.

Nurse, P. (2000): A long twentieth century of the cell cycle and beyond, Cell 100 [1], pp. 71-8.

Obremski, V. J.; Hall, A. M. and Fernandez-Valle, C. (1998): Merlin, the neurofibromatosis type 2 gene product, and beta1 integrin associate in isolated and differentiating Schwann cells, J Neurobiol 37 [4], pp. 487-501.

Oft, M.; Heider, K. H. and Beug, H. (1998): TGFbeta signaling is necessary for carcinoma cell invasiveness and metastasis, Curr Biol 8 [23], pp. 1243-52.

Okada, M.; Wang, Y.; Jang, S. W.; Tang, X.; Neri, L. M. and Ye, K. (2009): Akt phosphorylation of merlin enhances its binding to phosphatidylinositols and inhibits the tumor-suppressive activities of merlin, Cancer Res 69 [9], pp. 4043-51.

Okada, T.; Lopez-Lago, M. and Giancotti, F. G. (2005): Merlin/NF-2 mediates contact inhibition of growth by suppressing recruitment of Rac to the plasma membrane, J Cell Biol 171 [2], pp. 361-71.

Okada, T.; You, L. and Giancotti, F. G. (2007): Shedding light on Merlin's wizardry, Trends Cell Biol 17 [5], pp. 222-9.

Oliver, K. M.; Taylor, C. T. and Cummins, E. P. (2009): Hypoxia. Regulation of NFkappaB signalling during inflammation: the role of hydroxylases, Arthritis Res Ther 11 [1], p. 215.

Olsen, J. V.; Blagoev, B.; Gnad, F.; Macek, B.; Kumar, C.; Mortensen, P. and Mann, M. (2006): Global, in vivo, and site-specific phosphorylation dynamics in signaling networks, Cell 127 [3], pp. 635-48.

Olzmann, J. A.; Brown, K.; Wilkinson, K. D.; Rees, H. D.; Huai, Q.; Ke, H.; Levey, A. I.; Li, L. and Chin, L. S. (2004): Familial Parkinson's disease-associated L166P mutation disrupts DJ-1 protein folding and function, J Biol Chem 279 [9], pp. 8506-15.

Olzmann, J. A.; Li, L.; Chudaev, M. V.; Chen, J.; Perez, F. A.; Palmiter, R. D. and Chin, L. S. (2007): Parkin-mediated K63-linked polyubiquitination targets misfolded DJ-1 to aggresomes via binding to HDAC6, J Cell Biol 178 [6], pp. 1025-38.

Osborne, M. A.; Dalton, S. and Kochan, J. P. (1995): The yeast tribrid system--genetic detection of trans-phosphorylated ITAM-SH2-interactions, Biotechnology (N Y) 13 [13], pp. 1474-8.

Ozbabacan, S. E.; Engin, H. B.; Gursoy, A. and Keskin, O. (2011): Transient protein-protein interactions, Protein Eng Des Sel 24 [9], pp. 635-48.

Ozes, O. N.; Mayo, L. D.; Gustin, J. A.; Pfeffer, S. R.; Pfeffer, L. M. and Donner, D. B. (1999): NF-kappaB activation by tumour necrosis factor requires the Akt serine-threonine kinase, Nature 401 [6748], pp. 82-5.

Palidwor, G. A.; Shcherbinin, S.; Huska, M. R.; Rasko, T.; Stelzl, U.; Arumughan, A.; Foulle, R.; Porras, P.; Sanchez-Pulido, L.; Wanker, E. E. and Andrade-Navarro, M. A. (2009): Detection of alpha-rod protein repeats using a neural network and application to huntingtin, PLoS Comput Biol 5 [3], p. e1000304.

Papapetropoulos, S.; Adi, N.; Ellul, J.; Argyriou, A. A. and Chroni, E. (2007): A prospective study of familial versus sporadic Parkinson's disease, Neurodegener Dis 4 [6], pp. 424-7.

Park, C. W.; Kim, J. H.; Lee, J. H.; Kim, Y. S.; Ahn, H. J.; Shin, Y. S.; Kim, S. Y.; Choi, E. J.; Chang, Y. S. and Bang, B. K. (2000): High glucose-induced intercellular adhesion molecule-1 (ICAM-1) expression through an osmotic effect in rat mesangial cells is PKC-NF-kappa B-dependent, Diabetologia 43 [12], pp. 1544-53.

Parysek, L. M.; McReynolds, M. A.; Goldman, R. D. and Ley, C. A. (1991): Some neural intermediate filaments contain both peripherin and the neurofilament proteins, J Neurosci Res 30 [1], pp. 80-91.

Pearson, M. A.; Reczek, D.; Bretscher, A. and Karplus, P. A. (2000): Structure of the ERM protein moesin reveals the FERM domain fold masked by an extended actin binding tail domain, Cell 101 [3], pp. 259-70.

Peng, C. Y.; Graves, P. R.; Thoma, R. S.; Wu, Z.; Shaw, A. S. and Piwnica-Worms, H. (1997): Mitotic and G2 checkpoint control: regulation of 14-3-3 protein binding by phosphorylation of Cdc25C on serine-216, Science 277 [5331], pp. 1501-5.

Petrucelli, L.; O'Farrell, C.; Lockhart, P. J.; Baptista, M.; Kehoe, K.; Vink, L.; Choi, P.; Wolozin, B.; Farrer, M.; Hardy, J. and Cookson, M. R. (2002): Parkin protects against the toxicity associated with mutant alpha-synuclein: proteasome dysfunction selectively affects catecholaminergic neurons, Neuron 36 [6], pp. 1007-19.

Pickart, C. M. and Eddins, M. J. (2004): Ubiquitin: structures, functions, mechanisms, Biochim Biophys Acta 1695 [1-3], pp. 55-72.

Pincus, D.; Letunic, I.; Bork, P. and Lim, W. A. (2008): Evolution of the phospho-tyrosine signaling machinery in premetazoan lineages, Proc Natl Acad Sci U S A 105 [28], pp. 9680-4.

Poetz, O.; Hoeppe, S.; Templin, M. F.; Stoll, D. and Joos, T. O. (2009): Proteome wide screening using peptide

affinity capture, Proteomics 9 [6], pp. 1518-23.

Poser, I.; Sarov, M.; Hutchins, J. R.; Heriche, J. K.; Toyoda, Y.; Pozniakovsky, A.; Weigl, D.; Nitzsche, A.; Hegemann, B.; Bird, A. W.; Pelletier, L.; Kittler, R.; Hua, S.; Naumann, R.; Augsburg, M.; Sykora, M. M.; Hofemeister, H.; Zhang, Y.; Nasmyth, K.; White, K. P.; Dietzel, S.; Mechtler, K.; Durbin, R.; Stewart, A. F.; Peters, J. M.; Buchholz, F. and Hyman, A. A. (2008): BAC TransgeneOmics: a high-throughput method for exploration of protein function in mammals, Nat Methods 5 [5], pp. 409-15.

Prasanna, G.; Dibas, A.; Brown, K. and Yorio, T. (1998): Activation of protein kinase C by tumor necrosis factor-alpha in human non-pigmented ciliary epithelium, J Ocul Pharmacol Ther 14 [5], pp. 401-12.

Ptacek, J.; Devgan, G.; Michaud, G.; Zhu, H.; Zhu, X.; Fasolo, J.; Guo, H.; Jona, G.; Breitkreutz, A.; Sopko, R.; McCartney, R. R.; Schmidt, M. C.; Rachidi, N.; Lee, S. J.; Mah, A. S.; Meng, L.; Stark, M. J.; Stern, D. F.; De Virgilio, C.; Tyers, M.; Andrews, B.; Gerstein, M.; Schweitzer, B.; Predki, P. F. and Snyder, M. (2005): Global analysis of protein phosphorylation in yeast, Nature 438 [7068], pp. 679-84.

Quigley, P. M.; Korotkov, K.; Baneyx, F. and Hol, W. G. (2003): The 1.6-A crystal structure of the class of chaperones represented by Escherichia coli Hsp31 reveals a putative catalytic triad, Proc Natl Acad Sci U S A 100 [6], pp. 3137-42.

Rajagopala, S. V.; Hughes, K. T. and Uetz, P. (2009): Benchmarking yeast two-hybrid systems using the interactions of bacterial motility proteins, Proteomics 9 [23], pp. 5296-302.

Ramachandran, N.; Hainsworth, E.; Bhullar, B.; Eisenstein, S.; Rosen, B.; Lau, A. Y.; Walter, J. C. and LaBaer, J. (2004): Self-assembling protein microarrays, Science 305 [5680], pp. 86-90.

Ranganathan, S.; Wang, Y.; Kern, F. G.; Qu, Z. and Li, R. (2007): Activation loop phosphorylation-independent kinase activity of human protein kinase C zeta, Proteins 67 [3], pp. 709-19.

Remy, I.; Ghaddar, G. and Michnick, S. W. (2007): Using the beta-lactamase protein-fragment complementation assay to probe dynamic protein-protein interactions, Nat Protoc 2 [9], pp. 2302-6.

Remy, I. and Michnick, S. W. (2006): A highly sensitive protein-protein interaction assay based on Gaussia luciferase, Nat Methods 3 [12], pp. 977-9.

Remy, I.; Montmarquette, A. and Michnick, S. W. (2004): PKB/Akt modulates TGF-beta signalling through a direct interaction with Smad3, Nat Cell Biol 6 [4], pp. 358-65.

Robertson, H.; Langdon, W. Y.; Thien, C. B. and Bowtell, D. D. (1997): A c-Cbl yeast two hybrid screen reveals interactions with 14-3-3 isoforms and cytoskeletal components, Biochem Biophys Res Commun 240 [1], pp. 46-50.

Rodriguez-Escudero, I.; Roelants, F. M.; Thorner, J.; Nombela, C.; Molina, M. and Cid, V. J. (2005): Reconstitution of the mammalian PI3K/PTEN/Akt pathway in yeast, Biochem J 390 [Pt 2], pp. 613-23.

Rong, R.; Tang, X.; Gutmann, D. H. and Ye, K. (2004): Neurofibromatosis 2 (NF2) tumor suppressor merlin inhibits phosphatidylinositol 3-kinase through binding to PIKE-L, Proc Natl Acad Sci U S A 101 [52], pp. 18200-5.

Rouleau, G. A.; Merel, P.; Lutchman, M.; Sanson, M.; Zucman, J.; Marineau, C.; Hoang-Xuan, K.; Demczuk, S.; Desmaze, C.; Plougastel, B. and et al. (1993): Alteration in a new gene encoding a putative membrane-organizing protein causes neuro-fibromatosis type 2, Nature 363 [6429], pp. 515-21.

Rual, J. F.; Hirozane-Kishikawa, T.; Hao, T.; Bertin, N.; Li, S.; Dricot, A.; Li, N.; Rosenberg, J.; Lamesch, P.; Vidalain, P. O.; Clingingsmith, T. R.; Hartley, J. L.; Esposito, D.; Cheo, D.; Moore, T.; Simmons, B.; Sequerra, R.; Bosak, S.; Doucette-Stamm, L.; Le Peuch, C.; Vandenhaute, J.; Cusick, M. E.; Albala, J. S.; Hill, D. E. and Vidal, M. (2004): Human ORFeome version 1.1: a platform for reverse proteomics, Genome Res 14 [10B], pp. 2128-35.

Rual, J. F.; Venkatesan, K.; Hao, T.; Hirozane-Kishikawa, T.; Dricot, A.; Li, N.; Berriz, G. F.; Gibbons, F. D.; Dreze, M.; Ayivi-Guedehoussou, N.; Klitgord, N.; Simon, C.; Boxem, M.; Milstein, S.; Rosenberg, J.; Goldberg, D. S.; Zhang, L. V.; Wong, S. L.; Franklin, G.; Li, S.; Albala, J. S.; Lim, J.; Fraughton, C.; Llamosas, E.; Cevik, S.; Bex, C.; Lamesch, P.; Sikorski, R. S.; Vandenhaute, J.; Zoghbi, H. Y.; Smolyar, A.; Bosak, S.; Sequerra, R.; Doucette-Stamm, L.; Cusick, M. E.; Hill, D. E.; Roth, F. P. and Vidal, M. (2005): Towards a proteome-scale map of the human protein-protein interaction network, Nature 437 [7062], pp. 1173-8.

Rudolph, J. (2007): Inhibiting transient protein-protein interactions: lessons from the Cdc25 protein tyrosine phosphatases, Nat Rev Cancer 7 [3], pp. 202-11.

Safaei, J.; Manuch, J.; Gupta, A.; Stacho, L. and Pelech, S. (2011): Prediction of 492 human protein kinase substrate specificities, Proteome Sci 9 Suppl 1, p. S6.

Sainio, M.; Zhao, F.; Heiska, L.; Turunen, O.; den Bakker, M.; Zwarthoff, E.; Lutchman, M.; Rouleau, G. A.; Jaaskelainen, J.; Vaheri, A. and Carpen, O. (1997): Neurofibromatosis 2 tumor suppressor protein colocalizes with ezrin and CD44 and associates with actin-containing cytoskeleton, J Cell Sci 110 ( Pt

18), pp. 2249-60.

Samii, A.; Nutt, J. G. and Ransom, B. R. (2004): Parkinson's disease, Lancet 363 [9423], pp. 1783-93.

Sanchez, Y.; Wong, C.; Thoma, R. S.; Richman, R.; Wu, Z.; Piwnica-Worms, H. and Elledge, S. J. (1997): Conservation of the Chk1 checkpoint pathway in mammals: linkage of DNA damage to Cdk regulation through Cdc25, Science 277 [5331], pp. 1497-501.

Satoh, J. and Kuroda, Y. (1999): Association of codon 167 Ser/Asn heterozygosity in the parkin gene with sporadic Parkinson's disease, Neuroreport 10 [13], pp. 2735-9.

Schapira, A. H. (2008): Mitochondria in the aetiology and pathogenesis of Parkinson's disease, Lancet Neurol 7 [1], pp. 97-109.

Schlessinger, J. and Lemmon, M. A. (2003): SH2 and PTB domains in tyrosine kinase signaling, Sci STKE 2003 [191], p. RE12.

Schlossmacher, M. G.; Frosch, M. P.; Gai, W. P.; Medina, M.; Sharma, N.; Forno, L.; Ochiishi, T.; Shimura, H.; Sharon, R.; Hattori, N.; Langston, J. W.; Mizuno, Y.; Hyman, B. T.; Selkoe, D. J. and Kosik, K. S. (2002): Parkin localizes to the Lewy bodies of Parkinson disease and dementia with Lewy bodies, Am J Pathol 160 [5], pp. 1655-67.

Schulman, B. A. and Harper, J. W. (2009): Ubiquitin-like protein activation by E1 enzymes: the apex for downstream signalling pathways, Nat Rev Mol Cell Biol 10 [5], pp. 319-31.

Schwartz, A. S.; Yu, J.; Gardenour, K. R.; Finley, R. L., Jr. and Ideker, T. (2009): Cost-effective strategies for completing the interactome, Nat Methods 6 [1], pp. 55-61.

Scoles, D. R.; Chen, M. and Pulst, S. M. (2002): Effects of Nf2 missense mutations on schwannomin interactions, Biochem Biophys Res Commun 290 [1], pp. 366-74.

Scoles, D. R.; Huynh, D. P.; Morcos, P. A.; Coulsell, E. R.; Robinson, N. G.; Tamanoi, F. and Pulst, S. M. (1998): Neurofibromatosis 2 tumour suppressor schwannomin interacts with betaII-spectrin, Nat Genet 18 [4], pp. 354-9.

Seet, B. T.; Dikic, I.; Zhou, M. M. and Pawson, T. (2006): Reading protein modifications with interaction domains, Nat Rev Mol Cell Biol 7 [7], pp. 473-83.

Sekido, Y.; Pass, H. I.; Bader, S.; Mew, D. J.; Christman, M. F.; Gazdar, A. F. and Minna, J. D. (1995): Neurofibromatosis type 2 (NF2) gene is somatically mutated in mesothelioma but not in lung cancer, Cancer Res 55 [6], pp. 1227-31.

Selkoe, D. J. (2004): Cell biology of protein misfolding: the examples of Alzheimer's and Parkinson's diseases, Nat Cell Biol 6 [11], pp. 1054-61.

Serpell, L. C.; Blake, C. C. and Fraser, P. E. (2000): Molecular structure of a fibrillar Alzheimer's A beta fragment, Biochemistry 39 [43], pp. 13269-75.

Sha, D.; Chin, L. S. and Li, L. (2010): Phosphorylation of parkin by Parkinson disease-linked kinase PINK1 activates parkin E3 ligase function and NF-kappaB signaling, Hum Mol Genet 19 [2], pp. 352-63.

Shaw, G.; Morse, S.; Ararat, M. and Graham, F. L. (2002): Preferential transformation of human neuronal cells by human adenoviruses and the origin of HEK 293 cells, FASEB J 16 [8], pp. 869-71.

Shaw, R. J.; Paez, J. G.; Curto, M.; Yaktine, A.; Pruitt, W. M.; Saotome, I.; O'Bryan, J. P.; Gupta, V.; Ratner, N.; Der, C. J.; Jacks, T. and McClatchey, A. I. (2001): The Nf2 tumor suppressor, merlin, functions in Rac-dependent signaling, Dev Cell 1 [1], pp. 63-72.

Shaywitz, A. J.; Dove, S. L.; Kornhauser, J. M.; Hochschild, A. and Greenberg, M. E. (2000): Magnitude of the CREB-dependent transcriptional response is determined by the strength of the interaction between the kinase-inducible domain of CREB and the KIX domain of CREB-binding protein, Mol Cell Biol 20 [24], pp. 9409-22.

Shendelman, S.; Jonason, A.; Martinat, C.; Leete, T. and Abeliovich, A. (2004): DJ-1 is a redox-dependent molecular chaperone that inhibits alpha-synuclein aggregate formation, PLoS Biol 2 [11], p. e362.

Sherman, L.; Xu, H. M.; Geist, R. T.; Saporito-Irwin, S.; Howells, N.; Ponta, H.; Herrlich, P. and Gutmann, D. H. (1997): Interdomain binding mediates tumor growth suppression by the NF2 gene product, Oncogene 15 [20], pp. 2505-9.

Shi, Y. (2007): Histone lysine demethylases: emerging roles in development, physiology and disease, Nat Rev Genet 8 [11], pp. 829-33.

Shi, Y. J.; Matson, C.; Lan, F.; Iwase, S.; Baba, T. and Shi, Y. (2005): Regulation of LSD1 histone demethylase activity by its associated factors, Mol Cell 19 [6], pp. 857-64.

Shi, Y.; Lan, F.; Matson, C.; Mulligan, P.; Whetstine, J. R.; Cole, P. A. and Casero, R. A. (2004): Histone demethylation mediated by the nuclear amine oxidase homolog LSD1, Cell 119 [7], pp. 941-53.

Shimizu, T.; Seto, A.; Maita, N.; Hamada, K.; Tsukita, S. and Hakoshima, T. (2002): Structural basis for

neurofibromatosis type 2. Crystal structure of the merlin FERM domain, J Biol Chem 277 [12], pp. 10332-6.

Shimura, H.; Schlossmacher, M. G.; Hattori, N.; Frosch, M. P.; Trockenbacher, A.; Schneider, R.; Mizuno, Y.; Kosik, K. S. and Selkoe, D. J. (2001): Ubiquitination of a new form of alpha-synuclein by parkin from human brain: implications for Parkinson's disease, Science 293 [5528], pp. 263-9.

Shin, J. H.; Ko, H. S.; Kang, H.; Lee, Y.; Lee, Y. I.; Pletinkova, O.; Troconso, J. C.; Dawson, V. L. and Dawson, T. M. (2011): PARIS (ZNF746) repression of PGC-1alpha contributes to neurodegeneration in Parkinson's disease, Cell 144 [5], pp. 689-702.

Shinbo, Y.; Taira, T.; Niki, T.; Iguchi-Ariga, S. M. and Ariga, H. (2005): DJ-1 restores p53 transcription activity inhibited by Topors/p53BP3, Int J Oncol 26 [3], pp. 641-8.

Smith, L.; Chen, L.; Reyland, M. E.; DeVries, T. A.; Talanian, R. V.; Omura, S. and Smith, J. B. (2000): Activation of atypical protein kinase C zeta by caspase processing and degradation by the ubiquitin-proteasome system, J Biol Chem 275 [51], pp. 40620-7.

Soderling, T. R. (1993): Protein kinases and phosphatases: regulation by autoinhibitory domains, Biotechnol Appl Biochem 18 ( Pt 2), pp. 185-200.

Soler-Lopez, M.; Zanzoni, A.; Lluis, R.; Stelzl, U. and Aloy, P. (2011): Interactome mapping suggests new mechanistic details underlying Alzheimer's disease, Genome Res 21 [3], pp. 364-76.

Soto, C. (2001): Protein misfolding and disease; protein refolding and therapy, FEBS Lett 498 [2-3], pp. 204-7.

Soto, C. (2003): Unfolding the role of protein misfolding in neurodegenerative diseases, Nat Rev Neurosci 4 [1], pp. 49-60.

Spessotto, P.; Bulla, R.; Danussi, C.; Radillo, O.; Cervi, M.; Monami, G.; Bossi, F.; Tedesco, F.; Doliana, R. and Colombatti, A. (2006): EMILIN1 represents a major stromal element determining human trophoblast invasion of the uterine wall, J Cell Sci 119 [Pt 21], pp. 4574-84.

Spessotto, P.; Cervi, M.; Mucignat, M. T.; Mungiguerra, G.; Sartoretto, I.; Doliana, R. and Colombatti, A. (2003): beta 1 Integrin-dependent cell adhesion to EMILIN-1 is mediated by the gC1q domain, J Biol Chem 278 [8], pp. 6160-7.

Spillantini, M. G.; Schmidt, M. L.; Lee, V. M.; Trojanowski, J. Q.; Jakes, R. and Goedert, M. (1997): Alpha-synuclein in Lewy bodies, Nature 388 [6645], pp. 839-40.

Spotts, J. M.; Dolmetsch, R. E. and Greenberg, M. E. (2002): Time-lapse imaging of a dynamic phosphorylation-dependent protein-protein interaction in mammalian cells, Proc Natl Acad Sci U S A 99 [23], pp. 15142-7.

Srivastava, J.; Elliott, B. E.; Louvard, D. and Arpin, M. (2005): Src-dependent ezrin phosphorylation in adhesion-mediated signaling, Mol Biol Cell 16 [3], pp. 1481-90.

Stagljar, I.; Korostensky, C.; Johnsson, N. and te Heesen, S. (1998): A genetic system based on split-ubiquitin for the analysis of interactions between membrane proteins in vivo, Proc Natl Acad Sci U S A 95 [9], pp. 5187-92.

Stambolic, V.; Suzuki, A.; de la Pompa, J. L.; Brothers, G. M.; Mirtsos, C.; Sasaki, T.; Ruland, J.; Penninger, J. M.; Siderovski, D. P. and Mak, T. W. (1998): Negative regulation of PKB/Akt-dependent cell survival by the tumor suppressor PTEN, Cell 95 [1], pp. 29-39.

Stefan, E.; Aquin, S.; Berger, N.; Landry, C. R.; Nyfeler, B.; Bouvier, M. and Michnick, S. W. (2007): Quantification of dynamic protein complexes using Renilla luciferase fragment complementation applied to protein kinase A activities in vivo, Proc Natl Acad Sci U S A 104 [43], pp. 16916-21.

Steinacker, P.; Aitken, A. and Otto, M. (2011): 14-3-3 proteins in neurodegeneration, Semin Cell Dev Biol.

Stelzl, U. and Wanker, E. E. (2006): The value of high quality protein-protein interaction networks for systems biology, Curr Opin Chem Biol 10 [6], pp. 551-8.

Stelzl, U.; Worm, U.; Lalowski, M.; Haenig, C.; Brembeck, F. H.; Goehler, H.; Stroedicke, M.; Zenkner, M.; Schoenherr, A.; Koeppen, S.; Timm, J.; Mintzlaff, S.; Abraham, C.; Bock, N.; Kietzmann, S.; Goedde, A.; Toksoz, E.; Droege, A.; Krobitsch, S.; Korn, B.; Birchmeier, W.; Lehrach, H. and Wanker, E. E. (2005): A human protein-protein interaction network: a resource for annotating the proteome, Cell 122 [6], pp. 957-68.

Stewart, D. A.; Cooper, C. R. and Sikes, R. A. (2004): Changes in extracellular matrix (ECM) and ECM-associated proteins in the metastatic progression of prostate cancer, Reprod Biol Endocrinol 2, p. 2.

Stotz, A. and Linder, P. (1990): The ADE2 gene from Saccharomyces cerevisiae: sequence and new vectors, Gene 95 [1], pp. 91-8.

Strelkov, S. V.; Herrmann, H. and Aebi, U. (2003): Molecular architecture of intermediate filaments, Bioessays 25 [3], pp. 243-51.

Sun, X. J.; Rothenberg, P.; Kahn, C. R.; Backer, J. M.; Araki, E.; Wilden, P. A.; Cahill, D. A.; Goldstein, B. J. and White, M. F. (1991): Structure of the insulin receptor substrate IRS-1 defines a unique signal transduction protein, Nature 352 [6330], pp. 73-7.

Sunde, M.; Serpell, L. C.; Bartlam, M.; Fraser, P. E.; Pepys, M. B. and Blake, C. C. (1997): Common core structure of amyloid fibrils by synchrotron X-ray diffraction, J Mol Biol 273 [3], pp. 729-39.

Sussman, A.; Huss, K.; Chio, L. C.; Heidler, S.; Shaw, M.; Ma, D.; Zhu, G.; Campbell, R. M.; Park, T. S.; Kulanthaivel, P.; Scott, J. E.; Carpenter, J. W.; Strege, M. A.; Belvo, M. D.; Swartling, J. R.; Fischl, A.; Yeh, W. K.; Shih, C. and Ye, X. S. (2004): Discovery of cercosporamide, a known antifungal natural product, as a selective Pkc1 kinase inhibitor through high-throughput screening, Eukaryot Cell 3 [4], pp. 932-43.

Sylvester, M.; Kliche, S.; Lange, S.; Geithner, S.; Klemm, C.; Schlosser, A.; Grossmann, A.; Stelzl, U.; Schraven, B.; Krause, E. and Freund, C. (2010): Adhesion and degranulation promoting adapter protein (ADAP) is a central hub for phosphotyrosine-mediated interactions in T cells, PLoS One 5 [7], p. e11708.

Taira, T.; Iguchi-Ariga, S. M. and Ariga, H. (2004): Co-localization with DJ-1 is essential for the androgen receptor to exert its transcription activity that has been impaired by androgen antagonists, Biol Pharm Bull 27 [4], pp. 574-7.

Taira, T.; Saito, Y.; Niki, T.; Iguchi-Ariga, S. M.; Takahashi, K. and Ariga, H. (2004): DJ-1 has a role in antioxidative stress to prevent cell death, EMBO Rep 5 [2], pp. 213-8.

Takahashi, H.; Ohama, E.; Suzuki, S.; Horikawa, Y.; Ishikawa, A.; Morita, T.; Tsuji, S. and Ikuta, F. (1994): Familial juvenile parkinsonism: clinical and pathologic study in a family, Neurology 44 [3 Pt 1], pp. 437-41.

Takahashi, K.; Taira, T.; Niki, T.; Seino, C.; Iguchi-Ariga, S. M. and Ariga, H. (2001): DJ-1 positively regulates the androgen receptor by impairing the binding of PIASx alpha to the receptor, J Biol Chem 276 [40], pp. 37556-63.

Tang, X.; Jang, S. W.; Wang, X.; Liu, Z.; Bahr, S. M.; Sun, S. Y.; Brat, D.; Gutmann, D. H. and Ye, K. (2007): Akt phosphorylation regulates the tumour-suppressor merlin through ubiquitination and degradation, Nat Cell Biol 9 [10], pp. 1199-207.

Tao, X. and Tong, L. (2003): Crystal structure of human DJ-1, a protein associated with early onset Parkinson's disease, J Biol Chem 278 [33], pp. 31372-9.

Tarassov, K.; Messier, V.; Landry, C. R.; Radinovic, S.; Serna Molina, M. M.; Shames, I.; Malitskaya, Y.; Vogel, J.; Bussey, H. and Michnick, S. W. (2008): An in vivo map of the yeast protein interactome, Science 320 [5882], pp. 1465-70.

Tarrant, M. K. and Cole, P. A. (2009): The chemical biology of protein phosphorylation, Annu Rev Biochem 78, pp. 797-825.

Tatematsu, K.; Yoshimoto, N.; Koyanagi, T.; Tokunaga, C.; Tachibana, T.; Yoneda, Y.; Yoshida, M.; Okajima, T.; Tanizawa, K. and Kuroda, S. (2005): Nuclear-cytoplasmic shuttling of a RING-IBR protein RBCK1 and its functional interaction with nuclear body proteins, J Biol Chem 280 [24], pp. 22937-44.

Teplow, D. B. (1998): Structural and kinetic features of amyloid beta-protein fibrillogenesis, Amyloid 5 [2], pp. 121-42.

Thomas, B. and Beal, M. F. (2007): Parkinson's disease, Hum Mol Genet 16 Spec No. 2, pp. R183-94.

Tillman, J. E.; Yuan, J.; Gu, G.; Fazli, L.; Ghosh, R.; Flynt, A. S.; Gleave, M.; Rennie, P. S. and Kasper, S. (2007): DJ-1 binds androgen receptor directly and mediates its activity in hormonally treated prostate cancer cells, Cancer Res 67 [10], pp. 4630-7.

Tokunaga, F.; Nakagawa, T.; Nakahara, M.; Saeki, Y.; Taniguchi, M.; Sakata, S.; Tanaka, K.; Nakano, H. and Iwai, K. (2009): SHARPIN is a component of the NF-kappaB-activating linear ubiquitin chain assembly complex, Nature 471 [7340], pp. 633-6.

Trofatter, J. A.; MacCollin, M. M.; Rutter, J. L.; Murrell, J. R.; Duyao, M. P.; Parry, D. M.; Eldridge, R.; Kley, N.; Menon, A. G.; Pulaski, K. and et al. (1993): A novel moesin-, ezrin-, radixin-like gene is a candidate for the neurofibromatosis 2 tumor suppressor, Cell 75 [4], p. 826.

Uetz, P.; Giot, L.; Cagney, G.; Mansfield, T. A.; Judson, R. S.; Knight, J. R.; Lockshon, D.; Narayan, V.; Srinivasan, M.; Pochart, P.; Qureshi-Emili, A.; Li, Y.; Godwin, B.; Conover, D.; Kalbfleisch, T.; Vijayadamodar, G.; Yang, M.; Johnston, M.; Fields, S. and Rothberg, J. M. (2000): A comprehensive analysis of protein-protein interactions in Saccharomyces cerevisiae, Nature 403 [6770], pp. 623-7.

Uhlik, M. T.; Temple, B.; Bencharit, S.; Kimple, A. J.; Siderovski, D. P. and Johnson, G. L. (2005): Structural and evolutionary division of phosphotyrosine binding (PTB) domains, J Mol Biol 345 [1], pp. 1-20.

Ullrich, A. and Schlessinger, J. (1990): Signal transduction by receptors with tyrosine kinase activity, Cell 61 [2],

pp. 203-12.

Valente, E. M.; Abou-Sleiman, P. M.; Caputo, V.; Muqit, M. M.; Harvey, K.; Gispert, S.; Ali, Z.; Del Turco, D.; Bentivoglio, A. R.; Healy, D. G.; Albanese, A.; Nussbaum, R.; Gonzalez-Maldonado, R.; Deller, T.; Salvi, S.; Cortelli, P.; Gilks, W. P.; Latchman, D. S.; Harvey, R. J.; Dallapiccola, B.; Auburger, G. and Wood, N. W. (2004): Hereditary early-onset Parkinson's disease caused by mutations in PINK1, Science 304 [5674], pp. 1158-60.

van Wijk, S. J.; de Vries, S. J.; Kemmeren, P.; Huang, A.; Boelens, R.; Bonvin, A. M. and Timmers, H. T. (2009): A comprehensive framework of E2-RING E3 interactions of the human ubiquitin-proteasome system, Mol Syst Biol 5, p. 295.

Vanhaesebroeck, B. and Waterfield, M. D. (1999): Signaling by distinct classes of phosphoinositide 3-kinases, Exp Cell Res 253 [1], pp. 239-54.

Venkatesan, K.; Rual, J. F.; Vazquez, A.; Stelzl, U.; Lemmens, I.; Hirozane-Kishikawa, T.; Hao, T.; Zenkner, M.; Xin, X.; Goh, K. I.; Yildirim, M. A.; Simonis, N.; Heinzmann, K.; Gebreab, F.; Sahalie, J. M.; Cevik, S.; Simon, C.; de Smet, A. S.; Dann, E.; Smolyar, A.; Vinayagam, A.; Yu, H.; Szeto, D.; Borick, H.; Dricot, A.; Klitgord, N.; Murray, R. R.; Lin, C.; Lalowski, M.; Timm, J.; Rau, K.; Boone, C.; Braun, P.; Cusick, M. E.; Roth, F. P.; Hill, D. E.; Tavernier, J.; Wanker, E. E.; Barabasi, A. L. and Vidal, M. (2009): An empirical framework for binary interactome mapping, Nat Methods 6 [1], pp. 83-90.

Verdone, G.; Doliana, R.; Corazza, A.; Colebrooke, S. A.; Spessotto, P.; Bot, S.; Bucciotti, F.; Capuano, A.; Silvestri, A.; Viglino, P.; Campbell, I. D.; Colombatti, A. and Esposito, G. (2008): The solution structure of EMILIN1 globular C1q domain reveals a disordered insertion necessary for interaction with the alpha4beta1 integrin, J Biol Chem 283 [27], pp. 18947-56.

Vinayagam, A.; Stelzl, U.; Foulle, R.; Plassmann, S.; Zenkner, M.; Timm, J.; Assmus, H. E.; Andrade-Navarro, M. A. and Wanker, E. E. (2011): A directed protein interaction network for investigating intracellular signal transduction, Sci Signal 4 [189], p. rs8.

Vivanco, I. and Sawyers, C. L. (2002): The phosphatidylinositol 3-Kinase AKT pathway in human cancer, Nat Rev Cancer 2 [7], pp. 489-501.

Vogel, S. S.; Thaler, C. and Koushik, S. V. (2006): Fanciful FRET, Sci STKE 2006 [331], p. re2.

Wagenfeld, A.; Gromoll, J. and Cooper, T. G. (1998): Molecular cloning and expression of rat contraception associated protein 1 (CAP1), a protein putatively involved in fertilization, Biochem Biophys Res Commun 251 [2], pp. 545-9.

Wagenseil, J. E. and Mecham, R. P. (2007): New insights into elastic fiber assembly, Birth Defects Res C Embryo Today 81 [4], pp. 229-40.

Walhout, A. J. and Vidal, M. (1999): A genetic strategy to eliminate self-activator baits prior to high-throughput yeast two-hybrid screens, Genome Res 9 [11], pp. 1128-34.

Walsh, C. T. (2006): Posttranslational modification of proteins : Expanding nature's inventory., Roberts and Company Publishers.

Wang, E. T.; Sandberg, R.; Luo, S.; Khrebtukova, I.; Zhang, L.; Mayr, C.; Kingsmore, S. F.; Schroth, G. P. and Burge, C. B. (2008): Alternative isoform regulation in human tissue transcriptomes, Nature 456 [7221], pp. 470-6.

Wang, G. G.; Allis, C. D. and Chi, P. (2007): Chromatin remodeling and cancer, Part I: Covalent histone modifications, Trends Mol Med 13 [9], pp. 363-72.

Wang, J.; Hevi, S.; Kurash, J. K.; Lei, H.; Gay, F.; Bajko, J.; Su, H.; Sun, W.; Chang, H.; Xu, G.; Gaudet, F.; Li, E. and Chen, T. (2009): The lysine demethylase LSD1 (KDM1) is required for maintenance of global DNA methylation, Nat Genet 41 [1], pp. 125-9.

Wang, J.; Scully, K.; Zhu, X.; Cai, L.; Zhang, J.; Prefontaine, G. G.; Krones, A.; Ohgi, K. A.; Zhu, P.; Garcia-Bassets, I.; Liu, F.; Taylor, H.; Lozach, J.; Jayes, F. L.; Korach, K. S.; Glass, C. K.; Fu, X. D. and Rosenfeld, M. G. (2007): Opposing LSD1 complexes function in developmental gene activation and repression programmes, Nature 446 [7138], pp. 882-7.

Wang, L.; Yang, H. J.; Xia, Y. Y. and Feng, Z. W. (2010): Insulin-like growth factor 1 protects human neuroblastoma cells SH-EP1 against MPP+-induced apoptosis by AKT/GSK-3beta/JNK signaling, Apoptosis 15 [12], pp. 1470-9.

Wang, X.; McCullough, K. D.; Franke, T. F. and Holbrook, N. J. (2000): Epidermal growth factor receptor-dependent Akt activation by oxidative stress enhances cell survival, J Biol Chem 275 [19], pp. 14624-31.

Wang, Y. R.; Li, Z. G.; Fu, J. L.; Wang, Z. H.; Wen, Y. and Liu, P. (2010): TNFalpha-induced IP3R1 expression through TNFR1/PC-PLC/PKCalpha and TNFR2 signalling pathways in human mesangial cell, Nephrol Dial Transplant 26 [1], pp. 75-83.

Wang, Y.; Zhang, H.; Chen, Y.; Sun, Y.; Yang, F.; Yu, W.; Liang, J.; Sun, L.; Yang, X.; Shi, L.; Li, R.; Li, Y.; Zhang, Y.; Li, Q.; Yi, X. and Shang, Y. (2009): LSD1 is a subunit of the NuRD complex and targets the metastasis programs in breast cancer, Cell 138 [4], pp. 660-72.

Watanabe, M.; Chen, C. Y. and Levin, D. E. (1994): Saccharomyces cerevisiae PKC1 encodes a protein kinase C (PKC) homolog with a substrate specificity similar to that of mammalian PKC, J Biol Chem 269 [24], pp. 16829-36.

Wehr, M. C.; Reinecke, L.; Botvinnik, A. and Rossner, M. J. (2008): Analysis of transient phosphorylation-dependent protein-protein interactions in living mammalian cells using split-TEV, BMC Biotechnol 8, p. 55.

Welch, W. J. (2004): Role of quality control pathways in human diseases involving protein misfolding, Semin Cell Dev Biol 15 [1], pp. 31-8.

Wenzel, D. M.; Lissounov, A.; Brzovic, P. S. and Klevit, R. E. (2011): UBCH7 reactivity profile reveals parkin and HHARI to be RING/HECT hybrids, Nature 474 [7349], pp. 105-8.

Wenzel, D. M.; Stoll, K. E. and Klevit, R. E. (2011): E2s: structurally economical and functionally replete, Biochem J 433 [1], pp. 31-42.

Widmann, C.; Gibson, S.; Jarpe, M. B. and Johnson, G. L. (1999): Mitogen-activated protein kinase: conservation of a three-kinase module from yeast to human, Physiol Rev 79 [1], pp. 143-80.

Wilkes, M. C.; Repellin, C. E.; Hong, M.; Bracamonte, M.; Penheiter, S. G.; Borg, J. P. and Leof, E. B. (2009): Erbin and the NF2 tumor suppressor Merlin cooperatively regulate cell-type-specific activation of PAK2 by TGF-beta, Dev Cell 16 [3], pp. 433-44.

Wilm, M. (2009): Quantitative proteomics in biological research, Proteomics 9 [20], pp. 4590-605.

Wilson, M. A.; Collins, J. L.; Hod, Y.; Ringe, D. and Petsko, G. A. (2003): The 1.1-A resolution crystal structure of DJ-1, the protein mutated in autosomal recessive early onset Parkinson's disease, Proc Natl Acad Sci U S A 100 [16], pp. 9256-61.

Worseck, J.M.; Grossmann, A.; Weimann, M.; Hegele, A. and Stelzl, U. (2012): A Stringent Yeast Two-Hybrid Matrix Screening Approach for Protein-Protein Interaction Discovery, Bernhard Suter and Erich E. Wanker (eds.), Two Hybrid Technologies: Methods and Protocols, Methods in Molecular Biology, 812.

Xiao, G. H.; Beeser, A.; Chernoff, J. and Testa, J. R. (2002): p21-activated kinase links Rac/Cdc42 signaling to merlin, J Biol Chem 277 [2], pp. 883-6.

Xiong, H.; Wang, D.; Chen, L.; Choo, Y. S.; Ma, H.; Tang, C.; Xia, K.; Jiang, W.; Ronai, Z.; Zhuang, X. and Zhang, Z. (2009): Parkin, PINK1, and DJ-1 form a ubiquitin E3 ligase complex promoting unfolded protein degradation, J Clin Invest 119 [3], pp. 650-60.

Xiromerisiou, G.; Hadjigeorgiou, G. M.; Papadimitriou, A.; Katsarogiannis, E.; Gourbali, V. and Singleton, A. B. (2008): Association between AKT1 gene and Parkinson's disease: a protective haplotype, Neurosci Lett 436 [2], pp. 232-4.

Yaffe, M. B. (2002): Phosphotyrosine-binding domains in signal transduction, Nat Rev Mol Cell Biol 3 [3], pp. 177-86.

Yaffe, M. B. and Elia, A. E. (2001): Phosphoserine/threonine-binding domains, Curr Opin Cell Biol 13 [2], pp. 131-8.

Yaffe, M. B.; Rittinger, K.; Volinia, S.; Caron, P. R.; Aitken, A.; Leffers, H.; Gamblin, S. J.; Smerdon, S. J. and Cantley, L. C. (1997): The structural basis for 14-3-3:phosphopeptide binding specificity, Cell 91 [7], pp. 961-71.

Yamada, M.; Suzuki, K.; Mizutani, M.; Asada, A.; Matozaki, T.; Ikeuchi, T.; Koizumi, S. and Hatanaka, H. (2001): Analysis of tyrosine phosphorylation-dependent protein-protein interactions in TrkB-mediated intracellular signaling using modified yeast two-hybrid system, J Biochem 130 [1], pp. 157-65.

Yang, W. L.; Wang, J.; Chan, C. H.; Lee, S. W.; Campos, A. D.; Lamothe, B.; Hur, L.; Grabiner, B. C.; Lin, X.; Darnay, B. G. and Lin, H. K. (2009): The E3 ligase TRAF6 regulates Akt ubiquitination and activation, Science 325 [5944], pp. 1134-8.

Yang, W. L.; Wu, C. Y.; Wu, J. and Lin, H. K. (2010): Regulation of Akt signaling activation by ubiquitination, Cell Cycle 9 [3], pp. 487-97.

Yang, Y.; Gehrke, S.; Haque, M. E.; Imai, Y.; Kosek, J.; Yang, L.; Beal, M. F.; Nishimura, I.; Wakamatsu, K.; Ito, S.; Takahashi, R. and Lu, B. (2005): Inactivation of Drosophila DJ-1 leads to impairments of oxidative stress response and phosphatidylinositol 3-kinase/Akt signaling, Proc Natl Acad Sci U S A 102 [38], pp. 13670-5.

Yi, C.; Troutman, S.; Fera, D.; Stemmer-Rachamimov, A.; Avila, J. L.; Christian, N.; Persson, N. L.; Shimono, A.; Speicher, D. W.; Marmorstein, R.; Holmgren, L. and Kissil, J. L. (2011): A tight junction-associated

Merlin-angiomotin complex mediates Merlin's regulation of mitogenic signaling and tumor suppressive functions, Cancer Cell 19 [4], pp. 527-40.

Yonemura, S.; Hirao, M.; Doi, Y.; Takahashi, N.; Kondo, T. and Tsukita, S. (1998): Ezrin/radixin/moesin (ERM) proteins bind to a positively charged amino acid cluster in the juxta-membrane cytoplasmic domain of CD44, CD43, and ICAM-2, J Cell Biol 140 [4], pp. 885-95.

Yoshimoto, N.; Tatematsu, K.; Koyanagi, T.; Okajima, T.; Tanizawa, K. and Kuroda, S. (2005): Cytoplasmic tethering of a RING protein RBCK1 by its splice variant lacking the RING domain, Biochem Biophys Res Commun 335 [2], pp. 550-7.

You, A.; Tong, J. K.; Grozinger, C. M. and Schreiber, S. L. (2001): CoREST is an integral component of the CoREST- human histone deacetylase complex, Proc Natl Acad Sci U S A 98 [4], pp. 1454-8.

Yu, H.; Tardivo, L.; Tam, S.; Weiner, E.; Gebreab, F.; Fan, C.; Svrzikapa, N.; Hirozane-Kishikawa, T.; Rietman, E.; Yang, X.; Sahalie, J.; Salehi-Ashtiani, K.; Hao, T.; Cusick, M. E.; Hill, D. E.; Roth, F. P.; Braun, P. and Vidal, M. (2009): Next-generation sequencing to generate interactome datasets, Nat Methods 8 [6], pp. 478-80.

Yuan, J. and Yankner, B. A. (2000): Apoptosis in the nervous system, Nature 407 [6805], pp. 802-9.

Zacchigna, L.; Vecchione, C.; Notte, A.; Cordenonsi, M.; Dupont, S.; Maretto, S.; Cifelli, G.; Ferrari, A.; Maffei, A.; Fabbro, C.; Braghetta, P.; Marino, G.; Selvetella, G.; Aretini, A.; Colonnese, C.; Bettarini, U.; Russo, G.; Soligo, S.; Adorno, M.; Bonaldo, P.; Volpin, D.; Piccolo, S.; Lembo, G. and Bressan, G. M. (2006): Emilin1 links TGF-beta maturation to blood pressure homeostasis, Cell 124 [5], pp. 929-42.

Zanetti, M.; Braghetta, P.; Sabatelli, P.; Mura, I.; Doliana, R.; Colombatti, A.; Volpin, D.; Bonaldo, P. and Bressan, G. M. (2004): EMILIN-1 deficiency induces elastogenesis and vascular cell defects, Mol Cell Biol 24 [2], pp. 638-50.

Zhang, H.; Zha, X.; Tan, Y.; Hornbeck, P. V.; Mastrangelo, A. J.; Alessi, D. R.; Polakiewicz, R. D. and Comb, M. J. (2002): Phosphoprotein analysis using antibodies broadly reactive against phosphorylated motifs, J Biol Chem 277 [42], pp. 39379-87.

Zhang, N.; Bai, H.; David, K. K.; Dong, J.; Zheng, Y.; Cai, J.; Giovannini, M.; Liu, P.; Anders, R. A. and Pan, D. (2010): The Merlin/NF2 tumor suppressor functions through the YAP oncoprotein to regulate tissue homeostasis in mammals, Dev Cell 19 [1], pp. 27-38.

Zhou, M. M.; Ravichandran, K. S.; Olejniczak, E. F.; Petros, A. M.; Meadows, R. P.; Sattler, M.; Harlan, J. E.; Wade, W. S.; Burakoff, S. J. and Fesik, S. W. (1995): Structure and ligand recognition of the phosphotyrosine binding domain of Shc, Nature 378 [6557], pp. 584-92.

Zimek, A.; Stick, R. and Weber, K. (2003): Genes coding for intermediate filament proteins: common features and unexpected differences in the genomes of humans and the teleost fish Fugu rubripes, J Cell Sci 116 [Pt 11], pp. 2295-302.

Zucchelli, S.; Codrich, M.; Marcuzzi, F.; Pinto, M.; Vilotti, S.; Biagioli, M.; Ferrer, I. and Gustincich, S. (2010): TRAF6 promotes atypical ubiquitination of mutant DJ-1 and alpha-synuclein and is localized to Lewy bodies in sporadic Parkinson's disease brains, Hum Mol Genet 19 [19], pp. 3759-70.

# Appendix

| Symbol | GeneID | Description |
|---|---|---|
| ADAT3 | 113179 | adenosine deaminase, tRNA-specific 3, TAD3 homolog (S. cerevisiae) |
| AKR7A2 | 8574 | aldo-keto reductase family 7, member A2 (aflatoxin aldehyde reductase) |
| ALS2 | 57679 | amyotrophic lateral sclerosis 2 (juvenile) |
| ALS2CR8 | 79800 | amyotrophic lateral sclerosis 2 (juvenile) chromosome region, candidate 8 |
| AOF2 | 23028 | lysine (K)-specific demethylase 1A |
| ARFGAP1 | 55738 | ADP-ribosylation factor GTPase activating protein 1 |
| ARID5A | 10865 | AT rich interactive domain 5A (MRF1-like) |
| ASB3 | 51130 | ankyrin repeat and SOCS box containing 3 |
| ASB9 | 140462 | ankyrin repeat and SOCS box containing 9 |
| ATXN1 | 6310 | ataxin 1 |
| ATXN3 | 4287 | ataxin 3 |
| BECN1 | 8678 | beclin 1, autophagy related |
| C10orf18 | 54906 | chromosome 10 open reading frame 18 |
| C10orf2 | 56652 | chromosome 10 open reading frame 2 |
| C11orf16 | 56673 | chromosome 11 open reading frame 16 |
| C9orf150 | 286343 | chromosome 9 open reading frame 150 |
| CCDC33 | 80125 | coiled-coil domain containing 33 |
| CCNC | 892 | cyclin C |
| CDK6 | 1021 | cyclin-dependent kinase 6 |
| CREM | 1390 | cAMP responsive element modulator |
| DAPP1 | 27071 | dual adaptor of phosphotyrosine and 3-phosphoinositides |
| DCTN1 | 1639 | dynactin 1 |
| DUOXA1 | 90527 | dual oxidase maturation factor 1 |
| DYNC1I1 | 1780 | dynein, cytoplasmic 1, intermediate chain 1 |
| EMILIN1 | 11117 | elastin microfibril interfacer 1 |
| EPS8L2 | 64787 | EPS8-like 2 |
| ERCC8 | 1161 | excision repair cross-complementing rodent repair deficiency, complementation group 8 |
| EVL | 51466 | Enah/Vasp-like |
| FAM46A | 55603 | family with sequence similarity 46, member A |
| FRS3 | 10817 | fibroblast growth factor receptor substrate 3 |
| FTL | 2512 | ferritin, light polypeptide |
| FXN | 2395 | frataxin |
| GFAP | 2670 | glial fibrillary acidic protein |
| GLE1 | 2733 | GLE1 RNA export mediator homolog (yeast) |
| GRB10 | 2887 | growth factor receptor-bound protein 10 |
| GRN | 2896 | granulin |
| HSPB1 | 3315 | heat shock 27kDa protein 1 |
| HTRA2 | 27429 | HtrA serine peptidase 2 |
| HTT | 3064 | huntingtin |
| KRT19 | 3880 | keratin 19 |
| LASP1 | 3927 | LIM and SH3 protein 1 |
| LCK | 3932 | lymphocyte-specific protein tyrosine kinase |
| LITAF | 9516 | lipopolysaccharide-induced TNF factor |
| LMNA | 4000 | lamin A/C |
| MORN4 | 118812 | MORN repeat containing 4 |
| MRVI1 | 10335 | murine retrovirus integration site 1 homolog |
| NCALD | 83988 | neurocalcin delta |
| NCK2 | 8440 | NCK adaptor protein 2 |
| NDN | 4692 | necdin homolog (mouse) |
| NDUFV2 | 4729 | NADH dehydrogenase (ubiquinone) flavoprotein 2, 24kDa |
| NEBL | 10529 | nebulette |
| NEFL | 4747 | neurofilament, light polypeptide |
| NF2 | 4771 | neurofibromin 2 (merlin) |
| OLIG1 | 116448 | oligodendrocyte transcription factor 1 |
| PARK2 | 5071 | parkinson protein 2, E3 ubiquitin protein ligase (parkin) |
| PARK7 | 11315 | Parkinson disease (autosomal recessive, early onset) 7 |
| PIAS1 | 8554 | protein inhibitor of activated STAT, 1 |
| PIK3R1 | 5295 | phosphoinositide-3-kinase, regulatory subunit 1 (alpha) |
| PIK3R3 | 8503 | phosphoinositide-3-kinase, regulatory subunit 3 (gamma) |
| PINK1 | 65018 | PTEN induced putative kinase 1 |
| PRPH | 5630 | peripherin |
| PTGDS | 5730 | prostaglandin D2 synthase 21kDa (brain) |
| QSOX1 | 5768 | quiescin Q6 sulfhydryl oxidase 1 |
| RANBP3 | 8498 | RAN binding protein 3 |
| RNF11 | 26994 | ring finger protein 11 |
| RNF31 | 55072 | ring finger protein 31 |
| RYBP | 23429 | RING1 and YY1 binding protein |
| SEMA4G | 57715 | sema domain, immunoglobulin domain (Ig), transmembrane domain (TM) and short cytoplasmic domain, (semaphorin) 4G |
| SLC6A13 | 6540 | solute carrier family 6 (neurotransmitter transporter, GABA), member 13 |
| SMN2 | 6607 | survival of motor neuron 2, centromeric |
| SNCA | 6622 | synuclein, alpha (non A4 component of amyloid precursor) |
| SNCAIP | 153163 | hypothetical protein MGC32805 |
| SNCB | 6620 | synuclein, beta |
| SOD1 | 6647 | superoxide dismutase 1, soluble |
| TAGLN2 | 8407 | transgelin 2 |
| TARDBP | 23435 | TAR DNA binding protein |
| TMEM148 | 197196 | transmembrane protein 148 |
| ZDHHC17 | 23390 | zinc finger, DHHC-type containing 17 |
| ZNF655 | 442602 | zinc finger protein 655 |

**Figure 36: Additional information for proteins in the main network (Figure 13).**

Given are the official Symbol, the official full name and the EntrezGeneID.

| Symbol | GeneID | Description |
|---|---|---|
| APPL2 | 55198 | adaptor protein, phosphotyrosine interaction, PH domain and leucine zipper containing 2 |
| ATXN1 | 6310 | ataxin 1 |
| ATXN3 | 4287 | ataxin 3 |
| DAX1 | 190 | nuclear receptor subfamily 0, group B, member 1 |
| EGR2 | 1959 | early growth response 2 |
| HSH2D | 84941 | hematopoietic SH2 domain containing |
| NUMBL | 9253 | numb homolog (Drosophila)-like |
| RBCK1 | 10616 | RanBP-type and C3HC4-type zinc finger containing 1 |
| RNF112 | 7732 | ring finger protein 112 |
| SH2D2A | 9047 | SH2 domain containing 2A |
| SOCS4 | 122809 | suppressor of cytokine signaling 4 |
| STAT1 | 6772 | signal transducer and activator of transcription 1, 91kDa |
| STAT2 | 6773 | signal transducer and activator of transcription 2, 113kDa |
| STAT3 | 6774 | signal transducer and activator of transcription 3 (acute-phase response factor) |
| TNFR2 | 7133 | tumor necrosis factor receptor superfamily, member 1B |
| UBE2A | 7319 | ubiquitin-conjugating enzyme E2A (RAD6 homolog) |
| UBE2D4 | 51619 | ubiquitin-conjugating enzyme E2D 4 (putative) |
| UBE2E3 | 10477 | ubiquitin-conjugating enzyme E2E 3 (UBC4/5 homolog, yeast) |
| UBE2I | 7329 | ubiquitin-conjugating enzyme E2I (UBC9 homolog, yeast) |

**Figure 37: Additional information for proteins added in the extension step (Figure 14).**

Given are the official Symbol, the official full name and the EntrezGeneID.

| | Topic | SYMBOL Fire / ProteinA | OUTPUT [fold] Avg ± Stdev | Z-score | INPUT [RLU] Avg ± Stdev | min | OUTPUT [RLU] Avg ± Stdev | min | GeneID Fire / ProteinA |
|---|---|---|---|---|---|---|---|---|---|
| 1 | NEFL-KRT19-PRPH | KRT19 / neg. control (GPKOW) | 1,00 ± 0,09 | 0,00 | 1431 ± 51 | 1080 | 743 ± 67 | 743 | 3880 / 27238 |
| 2 | | KRT19 / KRT19 | 29,92 ± 10,14 | 2,85 | 1869 ± 508 | 1080 | 22232 ± 7535 | 743 | 3880 / 3880 |
| 3 | | KRT19 / NEFL 1-286 | 19,98 ± 0,62 | 30,78 | 1998 ± 680 | 1080 | 14842 ± 458 | 743 | 3880 / 4747 |
| 4 | | KRT19 / NEFL FL | 23,33 ± 0,73 | 30,78 | 1415 ± 945 | 1080 | 17337 ± 539 | 743 | 3880 / 4747 |
| 5 | | KRT19 / PRPH | 25,36 ± 3,91 | 6,24 | 1080 ± 123 | 1080 | 18844 ± 2901 | 743 | 3880 / 5630 |
| 6 | | NEFL 1-286 / neg. control (GPKOW) | 1,00 ± 0,13 | 0,00 | 2796 ± 316 | 2119 | 1293 ± 171 | 1293 | 4747 / 27238 |
| 7 | | NEFL 1-286 / KRT19 | 8,82 ± 0,77 | 10,17 | 2823 ± 257 | 2119 | 11407 ± 995 | 1293 | 4747 / 3880 |
| 8 | | NEFL 1-286 / NEFL 1-286 | 27,76 ± 2,86 | 9,35 | 2618 ± 86 | 2119 | 35893 ± 3701 | 1293 | 4747 / 4747 |
| 9 | | NEFL 1-286 / NEFL FL | 4,51 ± 0,40 | 8,77 | 2866 ± 102 | 2119 | 5831 ± 518 | 1293 | 4747 / 4747 |
| 10 | | NEFL 1-286 / PRPH | 0,82 ± 0,08 | -2,25 | 2560 ± 79 | 2119 | 1056 ± 106 | 1293 | 4747 / 5630 |
| 11 | | NEFL 1-286 / ASB3 | 4,86 ± 0,12 | 31,88 | 2258 ± 26 | 2119 | 6278 ± 156 | 1293 | 4747 / 51130 |
| 12 | | NEFL FL / neg. control (GPKOW) | 1,00 ± 0,10 | 0,00 | 2662 ± 249 | 2427 | 419 ± 43 | 419 | 4747 / 27238 |
| 13 | | NEFL FL / KRT19 | 26,42 ± 1,67 | 15,19 | 3303 ± 41 | 2427 | 11069 ± 701 | 419 | 4747 / 3880 |
| 14 | | NEFL FL / NEFL 1-286 | 5,72 ± 0,18 | 26,69 | 2818 ± 48 | 2427 | 2397 ± 74 | 419 | 4747 / 4747 |
| 15 | | NEFL FL / NEFL FL | 218,98 ± 14,88 | 14,65 | 4618 ± 392 | 2427 | 91753 ± 6237 | 419 | 4747 / 4747 |
| 16 | | NEFL FL / PRPH | 36,69 ± 0,81 | 43,97 | 3306 ± 166 | 2427 | 15374 ± 340 | 419 | 4747 / 5630 |
| 17 | | NEFL FL / ASB3 | 7,11 ± 0,39 | 15,53 | 2620 ± 138 | 2427 | 2979 ± 165 | 419 | 4747 / 51130 |
| 18 | | PRPH / neg. control (GPKOW) | 1,00 ± 0,24 | 0,00 | 4436 ± 997 | 2828 | 439 ± 104 | 439 | 5630 / 27238 |
| 19 | | PRPH / KRT19 | 19,61 ± 1,64 | 11,36 | 4078 ± 436 | 2828 | 8610 ± 719 | 439 | 5630 / 3880 |
| 20 | | PRPH / NEFL 1-286 | 3,25 ± 0,24 | 9,38 | 3628 ± 172 | 2828 | 1428 ± 105 | 439 | 5630 / 4747 |
| 21 | | PRPH / NEFL FL | 73,15 ± 3,27 | 22,05 | 4563 ± 81 | 2828 | 32113 ± 1436 | 439 | 5630 / 4747 |
| 22 | | PRPH / PRPH | 176,88 ± 35,05 | 5,02 | 6427 ± 5583 | 2828 | 77652 ± 15386 | 439 | 5630 / 4747 |
| 23 | PARK2 PPIs | PARK2 / neg. control (GPKOW) | 1 ± 0,042 | 0,00 | 1866 ± 115 | 1287 | 204 ± 9 | 204 | 5071 / 27238 |
| 24 | *PPI shown in network* | PARK2 / PARK7 | 10,59 ± 0,852 | 11,26 | 1930 ± 52 | 1287 | 2161 ± 174 | 204 | 5071 / 11315 |
| 25 | *PPI shown in network* | PARK2 / PINK1 | 4,21 ± 0,271 | 11,83 | 1378 ± 191 | 1287 | 859 ± 55 | 204 | 5071 / 65018 |
| 26 | ASB3 PPIs | ASB3 / neg. control (STAT1) | 1 ± 0,216 | 0,00 | 2123 ± 224 | 884 | 81 ± 18 | 81 | 51130 / 6772 |
| 27 | *PPI shown in network* | ASB3 / NEFL FL | 36,84 ± 0,938 | 38,19 | 1845 ± 40 | 884 | 2984 ± 76 | 81 | 51130 / 4747 |
| 28 | *PPI shown in network* | ASB3 / SH2D2A | 9,95 ± 1,597 | 5,60 | 1793 ± 401 | 884 | 806 ± 129 | 81 | 51130 / 9047 |
| 29 | SH2D2A PPIs | SH2D2A / neg. control (SOCS4) | 1 ± 0,108 | 0,00 | 2383 ± 84 | 1987 | 65 ± 7 | 65 | 9047 / 27238 |
| 30 | *PPI shown in network* | SH2D2A / ASB3 | 7,78 ± 0,974 | 6,96 | 1987 ± 391 | 1987 | 506 ± 63 | 65 | 9047 / 122809 |
| 31 | PIK3R3 PPIs | PIK3R3 / neg. control (GPKOW) | 1,00 ± 0,04 | 0,00 | 576 ± 40 | 364 | 350 ± 15 | 350 | 8503 / 27238 |
| 32 | *PPI shown in network* | PIK3R3 / SH2D2A | 5,64 ± 1,01 | 4,60 | 388 ± 18 | 364 | 1975 ± 353 | 350 | 8503 / 9047 |
| 33 | *PPI shown in network* | PIK3R3 / PIK3R3 | 29,08 ± 6,11 | 4,60 | 587 ± 90 | 364 | 10177 ± 2137 | 350 | 8503 / 8503 |
| 23 | RNF31 PPIs | RNF31(UBA) / neg. control (GPKOW) | 1,00 ± 0,03 | 0,00 | 5805 ± 1614 | 2091 | 653 ± 17 | 653 | 55072 / 27238 |
| 24 | | RNF31(UBA) / DAX1 | 2,24 ± 0,47 | 2,63 | 5016 ± 733 | 2091 | 1463 ± 308 | 653 | 55072 / 190 |
| 25 | | RNF31(UBA) / RBCK1 isoform 1 | 38,44 ± 1,44 | 26,04 | 4429 ± 409 | 2091 | 25100 ± 939 | 653 | 55072 / 10616 |
| 26 | | RNF31(UBA) / RBCK1 isoform 4 | 5,18 ± 0,25 | 16,56 | 4805 ± 374 | 2091 | 3380 ± 165 | 653 | 55072 / 10616 |
| 27 | | RNF31(UBA-IBR-IBR) / neg. control | 1,00 ± 0,09 | 0,00 | 2745 ± 161 | 720 | 1429 ± 126 | 1429 | 55072 / 27238 |
| 28 | | RNF31(UBA-IBR-IBR) / DAX1 | 2,86 ± 0,60 | 3,13 | 2528 ± 761 | 720 | 4092 ± 850 | 1429 | 55072 / 190 |
| 29 | | RNF31(UBA-IBR-IBR) / RBCK1 isoform 1 | 38,46 ± 1,89 | 19,86 | 953 ± 79 | 720 | 54964 ± 2695 | 1429 | 55072 / 10616 |
| 30 | | RNF31(UBA-IBR-IBR) / RBCK1 isoform 4 | 62,00 ± 6,92 | 8,81 | 1637 ± 174 | 720 | 88604 ± 9894 | 1429 | 55072 / 10616 |
| 31 | *PPI shown in network* | RBCK1 isoform 1 / neg. control (SOCS4) | 1,00 ± 0,17 | 0,00 | 1835 ± 417 | 973 | 59 ± 10 | 59 | 10616 / 122809 |
| 32 | *PPI shown in network* | RBCK1 isoform 1 / RNF31(UBA-IBR-IBR) | 652,15 ± 105,82 | 6,15 | 973 ± 325 | 973 | 38477 ± 6243 | 59 | 10616 / 55072 |
| 33 | *PPI shown in network* | RBCK1 isoform 4 / neg. control (SOCS4) | 1,00 ± 0,21 | 0,00 | 5154 ± 345 | 3529 | 68 ± 14 | 68 | 10616 / 122809 |
| 34 | *PPI shown in network* | RBCK1 isoform 4 / RNF31(UBA-IBR-IBR) | 396,74 ± 28,40 | 13,93 | 3529 ± 231 | 3529 | 26978 ± 1931 | 68 | 10616 / 55072 |
| 35 | *PPI shown in network* | DAX1 / neg. control (SOCS4) | 1 ± 0,135 | 0,00 | 1473 ± 300 | 1190 | 34 ± 5 | 34 | 190 / 122809 |
| 36 | *PPI shown in network* | DAX1 / RNF31(UBA-IBR-IBR) | 76,62 ± 22,563 | 3,35 | 2029 ± 650 | 1190 | 2605 ± 767 | 34 | 190 / 55072 |
| 37 | PARK7 - pS/T PPIs | ASB3 / neg. control (GPKOW) | 1,00 ± 0,02 | 0,00 | 1673 ± 33 | 790 | 358 ± 9 | 358 | 51130 / 27238 |
| 38 | | ASB3 / PARK7 | 10,67 ± 1,64 | 5,89 | 1079 ± 36 | 790 | 3819 ± 588 | 358 | 51130 / 11315 |
| 39 | | C11orf16 / neg. control (GPKOW) | 1,00 ± 0,21 | 0,00 | 5603 ± 564 | 2177 | 348 ± 72 | 348 | 56673 / 27238 |
| 40 | | C11orf16 / PARK7 | 7,53 ± 1,15 | 5,67 | 4318 ± 442 | 2177 | 2622 ± 401 | 348 | 56673 / 11315 |
| 41 | | RNF31(UBA) / neg. control (GPKOW) | 1,00 ± 0,03 | 0,00 | 5805 ± 1614 | 2091 | 653 ± 17 | 653 | 55072 / 27238 |
| 42 | | RNF31(UBA) / PARK7 | 1,33 ± 0,08 | 4,07 | 3905 ± 414 | 2091 | 866 ± 52 | 653 | 55072 / 11315 |
| 43 | | RNF31(UBA-IBR-IBR) / neg. control | 1,00 ± 0,09 | 0,00 | 2745 ± 161 | 720 | 1429 ± 126 | 1429 | 55072 / 27238 |
| 44 | | RNF31(UBA-IBR-IBR) / PARK7 | 4,26 ± 0,26 | 12,71 | 2059 ± 223 | 720 | 6083 ± 366 | 1429 | 55072 / 11315 |
| 45 | PARK7 - pY PPIs | PIK3R3 / neg. control (GPKOW) | 1,00 ± 0,12 | 0,00 | 1239 ± 119 | 830 | 301 ± 35 | 301 | 8503 / 27238 |
| 46 | | PIK3R3 / PARK7 | 8,18 ± 0,40 | 18,13 | 915 ± 103 | 830 | 2461 ± 119 | 301 | 8503 / 11315 |
| 47 | | PIK3R3_LL / neg. control (GPKOW) | 1,00 ± 0,12 | 0,00 | 3063 ± 89 | 2404 | 173 ± 21 | 173 | 8503 / 27238 |
| 48 | | PIK3R3_LL / PARK7 | 1,58 ± 0,40 | 1,46 | 2807 ± 118 | 2404 | 273 ± 69 | 173 | 8503 / 11315 |

**Figure 38: Co-IP raw data for chapter 3.2 and 3.3.**

Each experiment was performed as triplicate transfection and the measured relative luciferase units (RLU) before (INPUT) and after (OUTPUT) coimmunoprecipitation were averaged (Avg) and the standard deviation (Stdev) was determined. The fold change binding for each protein pair was then calculated from the relative luciferase intensities measured with the protein of interest and the negative control (OUTPUT [fold] Avg = OUTPUT [RLU] Avg/OUTPUT [RLU] min). The standard deviation (OUTPUT [fold] Stdev = OUTPUT [RLU] Stdev/OUTPUT [RLU] min) and the Z-score (OUTPUT [fold] Z-score = (OUTPUT [RLU] Avg-OUTPUT [RLU] min)/OUTPUT [RLU] Stdev) were also determined.

| | Topic | SYMBOL Fire / ProteinA | OUTPUT [fold] Avg ± Stdev | Z-score | INPUT [RLU] Avg ± Stdev | min | OUTPUT [RLU] Avg ± Stdev | min | GeneID Fire / ProteinA |
|---|---|---|---|---|---|---|---|---|---|
| 1 | NF2 dimer | NF2 isoform 1 / neg. control (DAX1 ) | 1,00 ± 0,19 | 0,00 | 9834 ± 992 | 8346 | 85 ± 16 | 85 | 4771 / 190 |
| 2 | | NF2 isoform 1 / NF2 isoform 7 | 7,94 ± 0,70 | 9,92 | 11602 ± 612 | 8346 | 675 ± 60 | 85 | 4771 / 4771 |
| 3 | | NF2 isoform 1 / NF2 isoform 1 | 90,60 ± 13,67 | 6,55 | 9644 ± 832 | 8346 | 7701 ± 1162 | 85 | 4771 / 4771 |
| 4 | | NF2 isoform 7 / neg. control (DAX1 ) | 1,00 ± 0,07 | 0,00 | 3999 ± 142 | 2888 | 658 ± 46 | 658 | 4771 / 190 |
| 5 | | NF2 isoform 7 / NF2 isoform 7 | 32,37 ± 6,99 | 4,49 | 3377 ± 639 | 2888 | 21302 ± 4597 | 658 | 4771 / 4771 |
| 6 | | NF2 isoform 7 / NF2 isoform 1 | 7,44 ± 0,94 | 6,83 | 3644 ± 255 | 2888 | 4898 ± 621 | 658 | 4771 / 4771 |
| 7 | NF2 PPIs | PIK3R3 / neg. control (GPKOW) | 1,00 ± 0,04 | 0,00 | 1228 ± 60 | 975 | 456 ± 19 | 456 | 8503 / 27238 |
| 8 | | PIK3R3 / NF2 isoform 7 | 5,13 ± 0,36 | 11,39 | 1034 ± 165 | 975 | 2341 ± 165 | 456 | 8503 / 4771 |
| 9 | | PIK3R3 / NF2 isoform 1 | 0,58 ± 0,10 | -4,03 | 1034 ± 140 | 975 | 265 ± 47 | 456 | 8503 / 4771 |
| 10 | | AOF2 / neg. control (GPKOW) | 1,00 ± 0,07 | 0,00 | 1534 ± 231 | 1534 | 1144 ± 79 | 1144 | 23028 / 27238 |
| 11 | | AOF2 / NF2 isoform 7 | 8,50 ± 0,77 | 9,78 | 1887 ± 163 | 1534 | 9729 ± 878 | 1144 | 23028 / 4771 |
| 12 | | AOF2 / NF2 isoform 1 | 2,02 ± 0,22 | 4,75 | 1874 ± 333 | 1534 | 2311 ± 246 | 1144 | 23028 / 4771 |
| 13 | | EMILIN1 / neg. control (GPKOW) | 1,00 ± 0,11 | 0,00 | 3879 ± 268 | 2844 | 1127 ± 129 | 1127 | 11117 / 27238 |
| 14 | | EMILIN1 / NF2 isoform 7 | 17,31 ± 1,42 | 11,52 | 2844 ± 57 | 2844 | 19514 ± 1596 | 1127 | 11117 / 4771 |
| 15 | | EMILIN1 / NF2 isoform 1 | 1,21 ± 0,23 | 0,93 | 3274 ± 615 | 2844 | 1367 ± 257 | 1127 | 11117 / 4771 |
| 16 | | NF2 isoform 7 / neg. control (DAX1 ) | 1,00 ± 0,07 | 0,00 | 3999 ± 142 | 2888 | 658 ± 46 | 658 | 4771 / 190 |
| 17 | | NF2 isoform 7 / AOF2 | 9,57 ± 2,06 | 4,17 | 3446 ± 758 | 2888 | 6294 ± 1352 | 658 | 4771 / 23028 |
| 18 | | NF2 isoform 7 / EMILIN1 | 37,29 ± 3,70 | 9,81 | 2888 ± 216 | 2888 | 24537 ± 2434 | 658 | 4771 / 11117 |
| 19 | | NF2 isoform 7 / PARK7 | 6,88 ± 0,80 | 7,31 | 3752 ± 226 | 2888 | 4526 ± 529 | 658 | 4771 / 11315 |
| 20 | | NF2 isoform 7 / PIK3R3 | 8,83 ± 0,55 | 14,24 | 3769 ± 259 | 2888 | 5811 ± 362 | 658 | 4771 / 8503 |
| 21 | | NF2 isoform 1 / neg. control (DAX1 ) | 1,00 ± 0,19 | 0,00 | 9834 ± 992 | 8346 | 85 ± 16 | 85 | 4771 / 190 |
| 22 | | NF2 isoform 1 / AOF2 | 4,82 ± 0,78 | 4,88 | 8346 ± 421 | 8346 | 410 ± 67 | 85 | 4771 / 23028 |
| 23 | | NF2 isoform 1 / EMILIN1 | 13,96 ± 1,37 | 9,47 | 9869 ± 300 | 8346 | 1187 ± 116 | 85 | 4771 / 11117 |
| 24 | | NF2 isoform 1 / PARK7 | 18,51 ± 0,74 | 23,65 | 9392 ± 602 | 8346 | 1573 ± 63 | 85 | 4771 / 11315 |
| 25 | | NF2 isoform 1 / PIK3R3 | 3,34 ± 1,12 | 2,08 | 11566 ± 549 | 8346 | 284 ± 96 | 85 | 4771 / 8503 |
| 26 | NF2 - PIK3R3 (MTs ProteinA) | NF2 isoform 7 / 2xneg. control (GPKOW) | 1,00 ± 0,12 | 0,00 | 4639 ± 266 | 2914 | 973 ± 113 | 973 | 4771 / 27238 |
| 27 | | NF2 isoform 7 / 2xPIK3R3 | 4,30 ± 0,14 | 23,79 | 3367 ± 229 | 2914 | 4183 ± 135 | 973 | 4771 / 8503 |
| 28 | | NF2 isoform 7 / 2xPIK3R3_KK | 2,27 ± 0,28 | 4,56 | 3976 ± 336 | 2914 | 2210 ± 271 | 973 | 4771 / 8503 |
| 29 | | NF2 isoform 7 / 2xPIK3R3_LL | 2,12 ± 0,14 | 8,15 | 3582 ± 297 | 2914 | 2058 ± 133 | 973 | 4771 / 8503 |
| 30 | | NF2 isoform 7 / 2xPIK3R3_Kwt | 2,97 ± 0,23 | 8,70 | 3432 ± 535 | 2914 | 2885 ± 220 | 973 | 4771 / 8503 |
| 31 | | NF2 isoform 7 / neg. control (GPKOW) | 1,00 ± 0,12 | 0,00 | 4389 ± 590 | 3114 | 749 ± 87 | 749 | 4771 / 27238 |
| 32 | | NF2 isoform 7 / PIK3R3 | 3,86 ± 0,39 | 7,33 | 3183 ± 663 | 3114 | 2889 ± 292 | 749 | 4771 / 8503 |
| 33 | | NF2 isoform 7 / PIK3R3_KK | 2,58 ± 0,49 | 3,20 | 3406 ± 232 | 3114 | 1931 ± 370 | 749 | 4771 / 8503 |
| 34 | | NF2 isoform 7 / PIK3R3_LL | 1,96 ± 0,24 | 4,09 | 3313 ± 460 | 3114 | 1471 ± 177 | 749 | 4771 / 8503 |
| 35 | | NF2 isoform 7 / PIK3R3_Kwt | 3,08 ± 0,23 | 9,02 | 3186 ± 193 | 3114 | 2310 ± 173 | 749 | 4771 / 8503 |
| 36 | NF2 - PIK3R3 (MTs Fire) | PIK3R3 / neg. control (GPKOW) | 1,00 ± 0,29 | 0,00 | 1320 ± 416 | 1096 | 596 ± 172 | 596 | 8503 / 27238 |
| 37 | | PIK3R3 / NF2 isoform 7 | 13,40 ± 4,21 | 2,95 | 1096 ± 301 | 1096 | 7988 ± 2506 | 596 | 8503 / 4771 |
| 38 | | PIK3R3_KK / neg. control (GPKOW) | 1,00 ± 0,07 | 0,00 | 1868 ± 417 | 1139 | 354 ± 24 | 354 | 8503 / 27238 |
| 39 | | PIK3R3_KK / NF2 isoform 7 | 11,42 ± 2,71 | 3,84 | 1139 ± 287 | 1139 | 4042 ± 960 | 354 | 8503 / 4771 |
| 40 | | PIK3R3_LL / neg. control (GPKOW) | 1,00 ± 0,15 | 0,00 | 1493 ± 55 | 1493 | 517 ± 79 | 517 | 8503 / 27238 |
| 41 | | PIK3R3_LL / NF2 isoform 7 | 8,07 ± 1,39 | 5,07 | 1598 ± 145 | 1493 | 4170 ± 721 | 517 | 8503 / 4771 |

**Figure 39: Co-IP raw data for NF2 interactions (3.5).**

Each experiment was performed as triplicate transfection and the measured relative luciferase units (RLU) before (INPUT) and after (OUTPUT) coimmunoprecipitation were averaged (Avg) and the standard deviation (Stdev) was determined. The fold change binding for each protein pair was then calculated from the relative luciferase intensities measured with the protein of interest and the negative control (OUTPUT [fold] Avg = OUTPUT [RLU] Avg/OUTPUT [RLU] min). The standard deviation (OUTPUT [fold] Stdev = OUTPUT [RLU] Stdev/OUTPUT [RLU] min) and the Z-score (OUTPUT [fold] Z-score = (OUTPUT [RLU] Avg-OUTPUT [RLU] min)/OUTPUT [RLU] Stdev) were also determined.

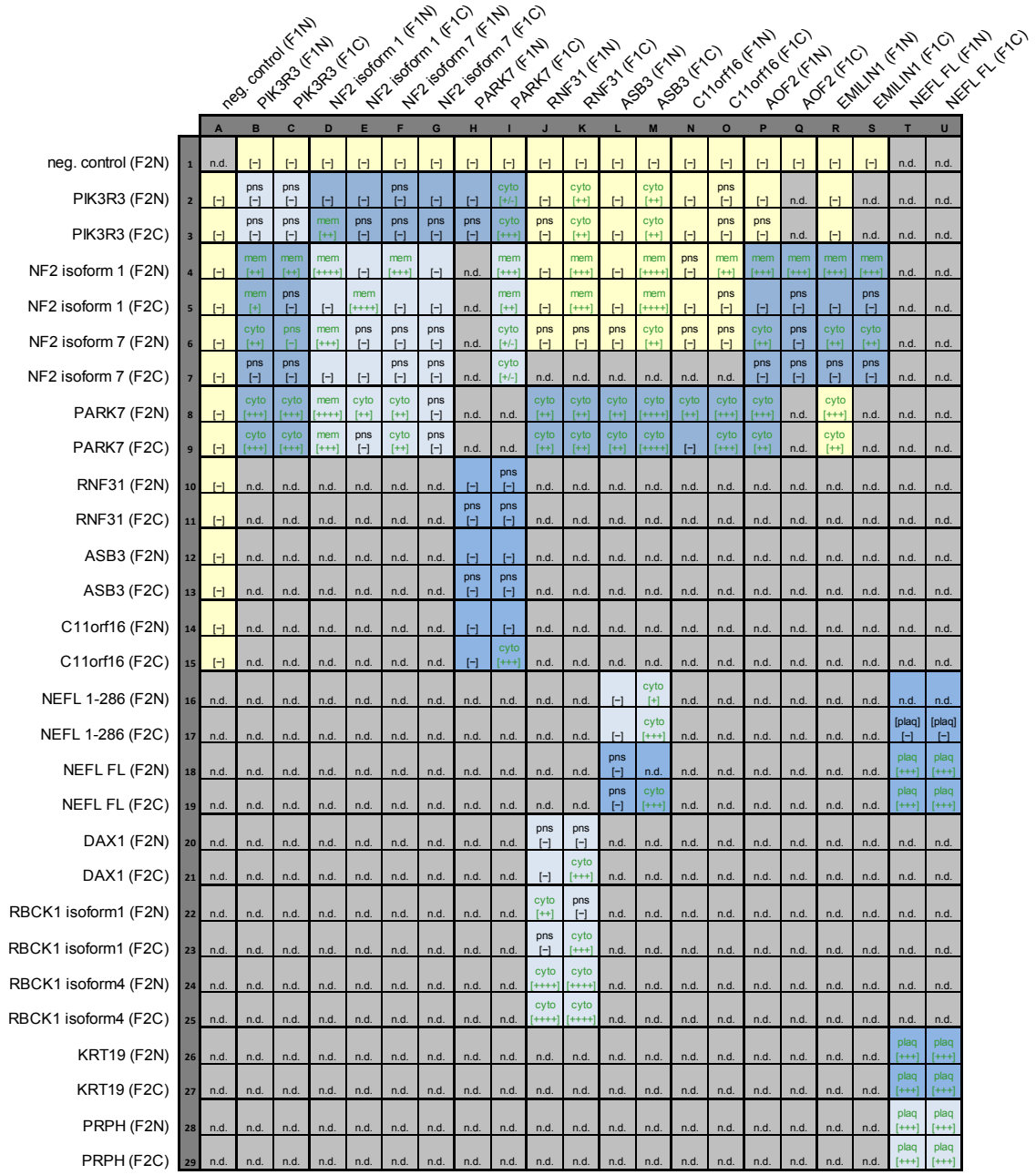


**Figure 40: Venus PCA results.**

Shown are combinations of Venus fusion protein pairs that were tested or not tested (n.d.) in Venus PCA experiments. Protein pairs depicted in dark blue have been found to interact in the Y2H screen and were already validated by co-IP experiments whereas pairs depicted in light blue were identified in co-IP experiments and pairs depicted in yellow and grey have not been tested in any of our systems before. Based on the strength of the obtained fluorescence signal the tested pairs were categorized as interacting (very weak [+/-], weak [+], medium [++], strong [+++], very strong [++++]) or not interacting ([-]). If fluorescent perinuclear structures without cytoplasmic fluorescence were observed the tested protein pair was regarded as non-interacting (pns [-]).The interacting pairs showed different subcellular localisations reaching from membranous (mem) to cytoplasmic (cyto). Sometimes the fluorescence signal was not homogenously distributed in the cell and plaques-like structures (plaq) were observed which clearly differed from perinuclear structures. Tested pairs depicted in yellow were not supposed to interact and were included to control the selectivity of the assay. Note that a very high fraction of these pairs fails to reconstitute a functional fluorescent Venus even if each partner of these control pairs was capable to interact with other partners.

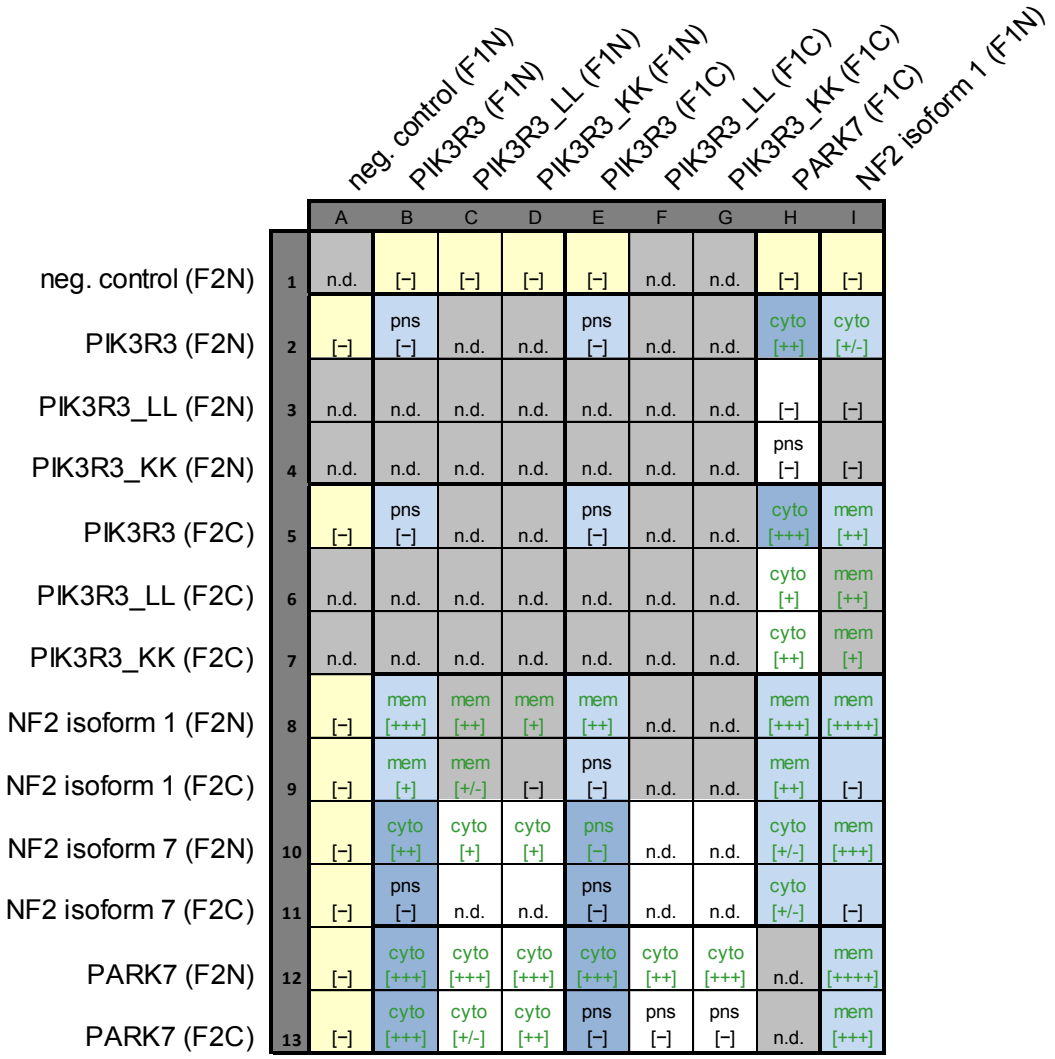


**Figure 41: Venus PCA results with mutant and wildtype PIK3R3.**

Shown are combinations of Venus fusion protein pairs that were tested or not tested (n.d.) in Venus PCA experiments. Protein pairs depicted in dark blue have been found to interact in the Y2H screen and were already validated by co-IP experiments whereas pairs depicted in light blue were identified in co-IP experiments and pairs depicted in yellow or grey have not been tested in any of our systems before. Tested pairs depicted in yellow were not supposed to interact and were included to control the selectivity of the assay. Pairs depicted in white include mutant PIK3R3 and showed a reduced co-IP interaction signal compared to wildtype PIK3R3. Based on the strength of the obtained fluorescence signal the tested pairs were categorized as interacting (very weak [+/-], weak [+], medium [++], strong [+++], very strong [++++]) or not interacting ([-]). If fluorescent perinuclear structures without cytoplasmic fluorescence were observed the tested protein pair was regarded as non-interacting (pns [-]).The interacting pairs showed different subcellular localisations reaching from membranous (mem) to cytoplasmic (cyto).

# Acknowledgements

An erster Stelle möchte ich mich bei meinem Supervisor Dr. Ulrich Stelzl für die hervorragenden Arbeitsbedingungen bedanken. Sein Enthusiasmus, seine Hilfsbereitschaft und seine Diskussionsbereitschaft haben wesentlich zum Gelingen dieser Arbeit beigetragen. Ich habe die angenehme Atmosphäre, die wertvollen Diskussionen und die produktive wissenschaftliche Zusammenarbeit am MPI für molekulare Genetik immer geschätzt und danke allen, die mich ein Stück weit auf dem Weg zur Promotion begleitet haben. Mein ganz besonderer Dank gilt allen ehemaligen und aktuellen Mitgliedern der Arbeitsgruppe Stelzl.

Ich danke Herrn Prof. Dr. Christian Spahn, Herrn Prof. Dr. Erich E. Wanker und Herrn Prof. Dr. Hans Lehrach für die Bereitschaft diese Arbeit zu begutachten. Ihnen sowie allen weiteren Teilnehmern des Promotionsausschuss gilt besonderer Respekt und Dank dafür, dass sie sich die Zeit genommen haben meine Arbeit zu evaluieren.

Bei Herrn Prof. Dr. Erich E. Wanker sowie den Mitgliedern seiner Arbeitsgruppe möchte ich mich für die erfolgreiche Kooperation im Rahmen des NeuroNet Projektes bedanken.

Von ganzem Herzen danke ich meiner Familie für ihre unermüdliche Unterstützung, ihre Liebe und Motivation. Ihr habt es mir ermöglicht diesen Lebensweg einzuschlagen, mich dabei unterstützt ihn zu gehen und gelehrt das Ziel nie aus den Augen zu verlieren, danke!